CURING OF POLY(ESTERIMIDE) ELECTROMAGNET-WIRE ENAMEL, ISOMID™:

A NULEAR MAGNETIC RESONANCE STUDY OF THE INFLUENCE OF CRESYLIC ACID ON THERMAL CURING

Emero BARONE B.Sc.
The Departments of Physical and Inorganic Chemistry
and Chemical Engineering,
The University of Adelaide,
Adelaide, South Australia,
Australia

Submitted in July, 1989

"Not Art and Science serve, alone;
Patience must in the work be shown.
A quiet spirit plods and plods at length;
Nothing but time can give the brew its strength."
-Johann Wolfgang Goethe,
from "Faust"

"Let us then be up and doing,
with a heart for any fate;
still achieving, still pursuing,
learn to labour and to wait."
-Longfellow

Preface

This thesis was completed under the aegis of Schenectady Chemicals Australia Pty. Ltd., and involves the industrial processing of poly(esterimide) electromagnet-wire enamel. Consequently, many technical terms are used to describe methods and phenomena found in the wire-enamelling industry. A glossary of terms has been included to provide a convenient reference, during the reading of this work.

Working for Schenectady Chemicals Aust. Pty. Ltd. over the last six years has been a rewarding experience, and because the work was instigated by this organisation in order to improve the processability of their product, Isomid 860™, efforts were concentrated toward that end. An understanding of the fundamental reactions, taking place during the thermal curing of Isomid™ varnishes onto copper wire, was considered to be necessary before any constructive changes to the solvent system of wire-varnishes can be undertaken. Hence, it is hoped that the work presented in this volume will contribute to an informed discourse on the functions of the wire-enamelling solvent, cresylic acid.

Adelaide, May 1989 Emero Barone

Table of Contents **Page**

Appendices

Abstract

Nuclear magnetic resonance (NMR) spectrometry has been used to characterise the proprietary poly(esterimide) resin (resin-SC) which is utilised as a varnish, in cresylic acid, to produce high quality dielectric coatings for electromagnet winding wires. These wires must be able to withstand high service temperatures (i.e., upto 180^0C, continuously). Although the resin is readily soluble in polar solvents and can easily be characterised by solution NMR techniques, the film that results from thermally curing the varnish is an insoluble and infusible, highly cross-linked polymer, requiring solid-state NMR methods for analysis. Unfortunately, these NMR techniques produce much broader peaks (≈100Hz in width) than the solution techniques, however, useful clues were obtained. Solid-state NMR methods were employed to characterise samples of industrially cured Isomid™ and Terebec™ wire-enamels.

Aromatic residues were detected in both wire-coatings, and were concluded to be aryl-ester derivatives of the polymers formed by reaction with the phenols present in cresylic acid, the varnish-solvent.

Solvent-extraction studies (using $CHCl_3$, DMSO, and EG) indicated that the residual solvents were structurally a part of the enamel-films, and are not released until the enamel is heated above 145 ± 2^0C, the **threshold** temperature. The **extra-resin** substances were thus extracted and detected by UV/visible spectroscopy on the extraction-solvent. Mass spectrometry of scrapings from an Isomid enamel-film also indicated a volatilisation of these substances as the temperature of the

ionising-chamber passed 144^{0}C.

Measurements of the water condensed during the esterification of benzoic acid (BA) with EG (in 10-fold excess) within the first 10 minutes of reaction has suggested that the phenols in cresylic acid can acid-catalyse the polycondensation of resin-SC. Two aryl titanate catalysts, tetraphenyl and tetra(**p**-nitrophenyl) titanates, were found to have a similar effect on the condensation-rate, whilst the use of tetra(2,4-dinitrophenyl) titanate greatly increased this rate. On the other hand, the proprietary alkyl titanate, "Tyzor TBT", showed little catalytic activity, possibly due to inhibition by BA. The greater thermodynamic stability of aryl and chelato-titanates suggests that "Tyzor TBT" reacts readily with functionalities of resin-SC and cresylic acid, in the wire-varnish prior to thermal curing. Aryl titanates are readily formed by exothermic ester exchange from "Tyzor TBT" when in solution with phenol, **p**-nitrophenol, and 2,4-dinitrophenol, at room temperature.

Broadband carbon NMR evidence for the chelation of 2-hydroxyethyl benzoate with titanium(IV) has suggested that coordination of the reactive hydroxyethyl chain end-groups of resin-SC can take place upon ester exchange with "Tyzor TBT". The postulated chelato-, or bischelato-, titanate is likely to be the seminal form of titanium in the coordiative catalysis of transesterification; the major polymerisation reaction.

In conclusion, the polycondensation dramaturgy, occurring during the thermal curing of Isomid wire-varnish, is

visualised as acid-catalysis by the phenols which also form aryl-ester derivatives with the poly(esterimide) resin. The aryl esters act as reactive intermediates in polymerisation; these esters are more amenable to nucleophilic substitution than are alkyl analogues such as the hydroxyethyl chain end-groups of resin-SC. The last traces of the phenols (i.e., residual), existing as esters, are released slowly during the late stages of thermal curing. Slow-release prevents nucleation of the volatile solvents, and thereby, blistering due to the formation of bubbles within the mostly cured, plastic enamel-film is avoided.

Therefore, cresylic acid (viz., the phenols) acts in tandem with the titanate catalyst (viz., "Tyzor TBT") to facilitate the polymerisation of the PEI resin (viz., resin-SC), so as to form a smooth, substantially void-free dielectric wire-coating.

Statement

This thesis does not contain material accepted for the award of any other degree or diploma in any university and, to the best of the author's knowledge an belief, contains no material previously written or published by another person, except where due reference is made in the text.

The author, Emero Barone, consents to the thesis being available for photocopying or loan if accepted for the award of the degree of Doctor of Philosophy in the Faculty of Science of the University of Adelaide.

Signed,

Emero Barone

Acknowledgements

The author wishes to thank the following individuals for rendering particular assistance.

Dr.P.E.M.Allen (supervisor) for advice and encouragement.

Dr.D.R.G.Williams (supervisor) for general advice.

Mr.M.F.Bray (former wire-industry colleague) for advice pertaining to the magnet-wire enamelling industry.

Mr.S.Hagias B.Sc(hons.) (research officer) for useful suggestions.

Mr.P.Kirkbride (Dept. of Services and Supply, Forensic Science Division), for the application of pyrolytic gas chromatography to wire-enamel scrapings from industrially cured Isomid wire-varnish.

Mr.F.P.Fonovic B.Sc.(hons.) and Ms.V.Macolino B.Sc.(hons.) for help with proof-reading the manuscript.

Mr.J.E.Pound (Technical Manager) and Mr.I.Gregory (Managing Director) of Schenectady Chemicals Australia Pty.Ltd.), for sponsoring this work.

Dr.E.H.Williams for running the Brüker CXP-300 nuclear magnetic resonance spectrometer.

Ms. Suzanne J. Brierley-Westall for help with proof-reading the final manuscript.

Index of tables

Index of figures

127 Figure 3.4(b) The expanded methylene region of figure 3.4(a). The diphenyl substituted methylene signal of the MDA radical, obscured by the DMSO signal of the inverse-gated, decoupled spectrum in figure 3.5, is clearly seen at 41.64ppm.

128 Figure 3.4(c) The expanded aromatic/carbonyl regions of figure 3.4(a).

129 Figure 3.5(a) The inverse-gated, decoupled ^{13}C-NMR spectrum (75.47MHz, DMSO, external lock: DMSO(d6), external reference: cyclohexane (26.84ppm against TMS)) of resin-SC with a 30 seconds delay between NMR pulses. The NOE is negligible, allowing the peak-integrals to reflect the nuclei-numbers.

130 Figure 3.5(b) The expanded methylene region of figure 3.5(a).

131 Figure 3.5(c) The expanded aromatic region of figure 3.5(a).

134 Figure 3.5(d) The assignments of the ^{13}C-NMR peaks to the approximate molecular structure of resin-SC (cf. table 3.3). Although a high field (i.e., 75.47MHz) spectrometer was used, many signals were not well resolved, and where peaks were found to be within 1.5ppm, specific assignments were not possible. Therefore, these structural features were assigned to groups of peaks.

144 Figure 3.6(a,i) The TOSS/PE-MASS ^{13}C-NMR spectrum (delrin; spinning rate: 3010Hz) of finely powdered resin-SC. The TOSS/PE-MASS experiment, described in §2.1.2, suppresses the spinning-sidebands, increasing markedly the spectral detail. (a,ii) The PE-MASS ^{13}C-NMR spectrum (delrin; spinning rate: 3010Hz) has been overlaid to accentuate the improvement in spectral detail. Note. Peaks 6,7, and 10 are small, and their intensities approach the baseline-noise, however, similar signals appear in an independent spectrum (cf. figure 3.6(b)) of resin-SC, suggesting that these peaks are real.

145 Figure 3.6(b) The TOSS/PE-MASS ^{13}C-NMR spectrum (delrin; spinning rate: 3010Hz) of powdered resin-SC which had been cured at 300^{0}C to a T_g of 102^{0}C (as measured by DSC). Note the significant relative decrease in the intensity of the HE-methylene peak, at 59.7ppm, as the HE-end-groups are esterified. Note. Peaks 5,6, and 8a appear at chemical shifts similar to peaks 6,7, and 10 in the solid-state spectrum of uncured resin-SC (cf. figure 3.6(a,ii)).

146 Figure 3.6(c) The TOSS/PE-MASS ^{13}C-NMR spectrum (delrin; spinning rate: 3010Hz) of scrapings from a cured model wire-enamel (i.e., a 10μm film cured from a varnish consisting of resin-SC (39.8wt.%), phenol (60.0wt.%), and "Tyzor TBT" (0.2wt.%) cured at 225^{0}C for 10 seconds). Comparison with figure 3.6(b) highlights an increased number of peaks in the aromatic region.

148 Figure 3.7 The PESOLIQ/PE-MASS ^{13}C-NMR spectrum (delrin; spinning rate: 3010Hz) of powdered, uncured resin-SC.

(a) The "solid-phase" spectrum highlights the resonances due to molecular moieties of low mobility. (b) The "liquid-phase" spectrum includes the remaining resin-spectrum, and shows the sample resonances due to highly mobile molecular moieties. The "liquid-phase" contains no sample peaks, suggesting that the resin contains no unreacted ethylene glycol (EG). Therefore, the "solid-phase" spectrum is similar to the PE-MASS spectrum in figure 3.6(a,ii).

150 Figure 3.8 The solid-state ^{13}C-NMR spectra (delrin; spinning rate: 3010Hz) of scrapings from Isomid wire-enamel coated onto 0.355mm copper wire. (a) The PE-MASS spectrum of untreated scrapings. The extraresin peaks have been highlighted by shading. Note the small peak at 29ppm.

151 Figure 3.8(b) The PE-MASS spectrum of the same scrapings, as used in experiment (a), after heating at 300^{0}C for one minute.

152 Figure 3.8(c) The TOSS/PE-MASS spectrum of the heat-treated scrapings of experiment (b). Aromatic peaks at: 116.8, 123.1, 130.0, and 131.9ppm, are evident; only the last two peaks are common to the resin (cf. figure 3.6(a,i)) in which the 129.5ppm peak, analogous to the 130.0ppm peak, here, is seen to reduce in its intensity upon curing (cf. figure 3.6(b)).

153 Figure 3.9(a) The TOSS/PE-MASS ^{13}C-NMR spectrum (delrin; spinning rate: 3010Hz) of scrapings taken from a 0.2mm diameter copper wire coated with Terebec PEI wire-enamel (courteously donated by Tycan (NZ) Pty.Ltd.). As for Isomid wire-enamel, extraresin peaks between 123.5 and 130.0ppm are apparent. Note the small peak at 30ppm which is also seen in figure 3.8(a).

154 Figure 3.9(b) The PE-MASS ^{13}C-NMR spectrum (delrin; spinning rate: 3010Hz) of the same Terebec enamel scrapings, as used in experiment (a), after being heated to 300^{0}C for one minute. The effective reduction of the intensities of the extraresin peaks is analogous to the effect of this heat-treatment on Isomid scrapings (cf. figure 3.8(b)).

158 Figure 3.10(a) The PE-MASS ^{13}C-NMR spectrum (delrin; spinning rate: 2470Hz) of scrapings from the cured film ($\approx$50μm in thickness) of the model-varnish #EM709 (cured at 300^{0}C for 15 seconds).

159 Figure 3.10(b) The BB^{13}C-NMR spectrum (20.1MHz, $CDCl_3$, TMS) of the resin modifier, Phenolic 709.

160 Figure 3.11(a) The PE-MASS ^{13}C-NMR spectrum (delrin; spinning rate: 2470Hz) of scrapings from the cured film ($\approx$50μm in thickness) of model-varnish #EMSH (cured at 300^{0}C for 15 seconds). N.B. No aromatic signals, attributable to the diisocyanate (i.e., Mondur SH), were detected. The peaks at 121.9, 125.4, and 129.7ppm, present in the solution spectrum of Mondur SH (cf. figure

1.0 Introduction

The enamelling of electromagnet-wire requires that a smooth, substantially defect-free insulating coating be applied to copper or aluminium wires of diameters in the range from 20μm to 1600μm. Highly polar solvents are used to apply resins onto the wire's surface prior to passing the wire through a thermal oven, either vertically of horizontally, so as to cure those resins into a hard, flexible, and continuous polymer-film. The solvents used are **cut** with **diluents** (i.e., non-solvents of lower boiling points) to reduce the unit cost of the varnishes.

The most popular varnish-solvent is cresylic acid; a blend of phenols, with the reputation of facilitating the formation of smooth enamel films. The reasons for this are unclear, but the work presented herein goes some of the way to understanding the role of cresylic acid during the curing process.

Schenectady Chemicals Australia Pty. Ltd. (SCA) markets a poly(esterimide) (PEI) varnish, Isomid™, which is the subject of this thesis. Isomid is a wire-enamelling varnish utilising cresylic acid as solvent, but requires slow enamelling speeds (viz., rates of curing) to yield acceptable enamelled wire, and is prone to giving unacceptable levels of surface defects. Improved processability is expected to increase the market-share of this product, and toward this end, SCA initiated the work presented.

The basis of Isomid is a PEI resin, **resin-SC**; a poly(ethylene terephthalate) with aromatic imide units interspersed randomly, and incorporating a trifunctional cross-linking unit. Reactive carboxyl and 2-hydroxyethyl (HE) ester groups (viz., chain ends) undergo polycondensation

reactions in the curing of resin-SC, and small molecules (i.e., water and ethylene glycol (EG)) are condensed which must rapidly travel out of the curing polymer-film; a film of ≈7μm can be cured within 4 seconds, a typical time spent in the curing-ovens. Consequently, any hinderance to this evaporation slows polycondensation, and requires longer oven-residence times which reduces the production-rate.

The main condensate is EG since the majority of curing reactions are ester exchanges. The molecules must pass through a polymer network before vaporising at the film-air interface, and dipolar interactions with the polymer slows the passage of EG. A highly polar solvent is needed to provide a continuous medium through which EG is carried out of the film, and in which the resin can polymerise.

Condensation is catalysed by protic acids (see §1.1), and the phenols of cresylic acid possess such protons; phenol and its homologues have pK_a's of about 10 in aqueous media. Therefore, in the early stages of curing cresylic acid is expected to acid-catalyse polycondensation.

Solvent-assisted curing would, however, go for nought if the solvent were too volatile to resist the high temperatures encountered in the ovens (i.e., 200 to 400^{0}C). Rapid vaporisation of the solvent causes severe blistering of the enamel-film. The solvent is the reaction-medium and cannot leave before the resin has formed a film about the wire since polymerisation would be retarded, and where substantial amounts leave after the film has cured, blistering is certain. Therefore, a successful enamelling-solvent must leave gradually, providing a favourable environment for polycondensation.

Cresylic acid is a reactive medium with the following properties:

(i) phenols, being protic acids, dissociate readily to release protons which catalyse polycondensation;

(ii) phenols esterify and transesterify polymer chains during the initial stages of curing, where cresylic acid is in excess, forming aryl-ester derivatives;

(iii) the aryl-esters, being more reactive than alkyl esters or carboxyl groups (see §1.1), are easily transesterified by the HE groups, providing a mechanism for more rapid polycondensation, and ensuring that the polymer film is established in the presence of the reaction-medium; and

(iv) the homogeneous alkoxyl titanium(IV) catalyst ("Tyzor TBT"; see §1.5) forms thermodynamically stable chelates with the HE chain end-groups which coordinatively catalyse polycondensation reactions (see appendix VI), and are likely to be the major form of the titanium in the wire-varnish.

A greater understanding of the action of this solvent system better equips the formulator of wire-varnishes to replace it with safer systems, or add compounds to improve the quality of the cured enamel-film.

The major portion of the work involved a characterisation of the poly(esterimide) resin by solution carbon nuclear magnetic resonance (NMR) spectrometry, allowing an interpretation of solid-state carbon NMR spectra of insoluble, infusible, and highly crosslinked Isomid enamel. Solid-state NMR is described in §2.1.2.

The remaining work has concentrated on simulating the curing process to determine the existence, if any, of solvent residues in the Isomid enamel, as well as to study the relative effect of catalytic quantities of phenols on a mod-

el reaction. Unfortunately, time and funding constraints precluded a rigorous treatment of the latter.

NMR chemical shifts are referred to tetramethyl silane (TMS), and infrared absorption band maxima are given in reciprocal wavenumbers.

1.1 Reactions and reactivities of carboxylic acid derivatives: polycondensation to polyesters

Generally, esterification and ester exchange reactions are considered to proceed through nucleophilic substitution on the carbonyl carbon, of a carboxylic acid or an ester functionality. The general reactions of this class are of the form

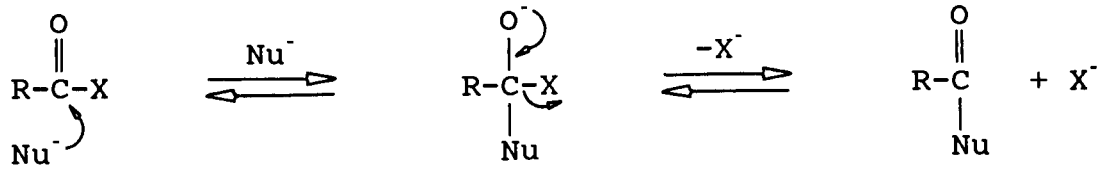

(Nu is any nucleophile) (I)

The reaction pathway is normally a nucleophilic addition/elimination involving a tetrahedral intermediate (I), followed by cleavage of the leaving group (X). The reactions of the carboxylic derivatives is distinguished from those of the simple carbonyl compounds (aldehydes and ketones) by a "good" leaving group attached to the carbonyl carbon atom.

The reactivity of the members of the carbonyl compounds toward substitution by a particular nucleophile is determined by the leaving group (X). Initially, electronic properties of X modifies the electron-density at the carbonyl group, thereby influencing its attractiveness to Nu. Once Nu has approached closely enough to form the transition-state (I), the ease of completion of substitution depends on the stability of the anion X^- in the reaction medium; the more stable the anion, the more readily it is eliminated. For example, aryloxy anions are better leaving groups than

alkoxyl anions and is explained by the greater stabilisation conferred by electromeric resonance. In other words, the stronger, harder bases are poor leaving groups; thus, groups such as HO^-, RO^-, and H_2N^-, which bond to carbon by small highly electronegative atoms of low polarisability, cannot normally be displaced easily by other nucleophiles. The best leaving groups found to be the anions of strong acids. Table 1.1 gives the order of reactivities for a series of carboxylates in which the acid strengths for the conjugate acids of the leaving groups decrease, a posteriori, down the table.

Table 1.1 The general order of reactivities for the carboxylate family of functional groups toward nucleophilic/elimination reactions. The order is given with respect to simple, monomeric esterification reactions, and not for polymeric ones, where the reactivity of chain end-groups depends on molecular weight and crosslinking density. The group reactivity decreases down the listing.

Substrate	Classification
RC(O)-Cl	acid chloride
RC(O)-OSR'	thiol ester
RC(O)-OC(O)R'	acid anhydride
RC(O)-OC_6H_5 (1)	phenyl ester
RC(O)-O$(CH_2)_2$OH (1)	2-hydroxyethyl ester
RC(O)-OC_2H_5 (1)	ethyl ester
RC(O)-OH	carboxylic acid
RC(O)-N(R')(R")	amide
RC(O)-O^-	carboxylate anion

Notes. (1) The ranking of these derivatives is based on measurements of reaction rates by Shevchenko et al.;[31,32,33] phenyl esters of terephthalic acid and benzoic acid were found to undergo transesterification with EG more readily than HE derivatives. The HE derviatives were, in turn, more reactive than the ethyl esters.

Esterification rates depend on both the acid and nucleophile concentrations, and are acid-catalysed. For a consideration of the kinetic aspects of esterification, it is convenient to discuss both acid-catalysis[2,3] and self-catalysis[2,4] of bifunctional polycondensations. Notwithstand-

ing, resin-SC forms a network-polymer since one monomer has a functionality of three; network-polymers are characterised macroscopically by a gel-point, defined as where each precursor molecule of monomer becomes bound to the rest. It is assumed, for the purpose of facilitating discussion, that condensation reactions are not significantly affected by crosslinking, at least not for low monomer-conversions.

Polycondensation reactions occur with monomer as well as between polymer end-groups, whereupon the molecular size increases considerably. There is little direct evidence to suggest that increasing the degree of polymerisation (DP) significantly affects reaction-kinetics as is the case for free-radical polymerisations,[5,6,7] however, at high conversions, where free monomer is virtually exhausted, reaction-rates for the end-groups become dependent on the mobility of their molecular environments. The diffusion coefficients of the condensation products may also become significant factors,[8] as the polymer network tightens, restricting movement.

The mechanisms of polycondensation reactions of dibasic acids (HOOC-R-COOH) with glycols (HO-R'-OH) are similar to those of simple condensations. The change in the concentration of the product-ester[2,4] depends on the molar concentrations of the carboxyl groups, hydroxyl groups (the nucleophiles), and protons (for protic-acid catalysed reactions),

$$d[\text{ester}]/dt = k[H^+][\text{COOH}][\text{OH}] \qquad (1.1)$$

The transition-state can be considered to contain a partially protonated leaving group, which forms a stable species upon cleavage.

In the absence of added protic-acid catalyst, carboxylic acid acts as the catalyst with the kinetics conforming to

a third-order law derived from equation (1.1),

$$d[ester]/dt = k[COOH]^2[OH] \qquad (1.2)$$

The third-order model is postulated for the esterification of diethylene glycol (DEG) with adipic acid, where the extent of reaction is above 80%. Between 50-80% conversion, the reaction tends towards second-order kinetics.

Reaction of the acid-catalyst with the polymer end-groups is generally responsible for deviations from equation (1.1) at high conversions (i.e., greater than 80%); the catalyst concentration becomes comparable with that of the carboxyl end-groups, when depleted by reaction with the hydroxyl end-groups. Therefore, the catalyst concentration and the rate of reaction diminish together.

Tang and Yao[9] propose an order of 2.5, and postulate that hydrogen ions, generated by the ionisation of the dibasic acid, protonate other hydroxyl groups to produce carbonium ion species, facilitating nucleophilic attack by the alcohols. However, they were selective in the data-points plotted, and the full plot departs considerably from linearity. The justification assumed proton-catalysis, and that the proton arose from ionisation of an acid end-group,

$$RC(=O)-OH \rightleftharpoons RC(=O)-O^- + H^+ \quad .$$

The dissociation constant (K_a) then gives

$$K_a[RCOOH] = [RCOO^-][H^+] = [H^+]^2$$

because, to maintain neutrality, the concentrations of protons and anions are identical. Therefore,

$$[H^+] = K_a^{0.5}[RCOOH]^{0.5} \quad .$$

The kinetic equation then becomes

$$d[ester]/dt = k[RCOOH]^{1.5}[Nu^-] \quad .$$

This kinetic equation fails to explain all of Tang and Yao's data, and is considered an inadequate model for the entire course of polycondensation.

For the near-equivalent esterifications (i.e., $OH_0/COOH_0=1.05$)[10] for 2,2-dimethyl-1,3-propanediol with maleic anhydride, sebacic acid, adipic acid, succinic acid and o-phthalic acid; Huang et al.[10] consider the reaction order to be 2.5 in the absence of any foreign catalyst. They propose that ionisation of the carboxylic acid end-groups is unlikely for the conditions found in polyesterifications and put forward a mechanism involving a complex series of acid-dimer interactions.

The complexity of the kinetics in bulk reactions has led to complex, non-integral reaction-orders, and may be a consequence of the changing polarity of the medium (also a reactant) during reaction. The initial reaction-mixture is a non-ideal solution; the reactants are highly concentrated, and thus, their activities are not equal to their mole fractions. During the later stages of polycondensation, however, the reactant concentration is much lower; the solution approaches ideality more closely, and the reactant species are much more polar. These conditions produce deviations from equations (1.1) and (1.2) for low monomer conversions less than 50%.

Thermodynamically, the system is far from ideal until the later stages of reaction where the reactants become dilute. As alluded to previously, uncatalysed polyesterification tends to third order kinetics above ≈80% conversion[11] which is similar to uncatalysed simple esterification reactions (i.e., between singly functional reactants) in dilute solution.[12]

Mares et al.[13] conclude for the reaction of terephthalic acid (TA) with EG in a medium of oligomeric PET that undissociated TA acting instead as catalyst. Transesterification, also known as ester interchange, ester exchange, or ester alcoholysis, is the most important of the reactions in the polymerisation of PEI wire-varnishes. These are the main reactions which the oligomerised resin undergoes during the curing process. It is convenient to consider transesterification as occurring in two ways: by ester exchange between HE end-groups, and between HE end-groups the monohydric alcohols of cresylic acid.

Cresylic acid is a common solvent for wire-enamelling, and consists of a blend of phenol and its homologues (see §1.5.2.1 for a description of the components); the hydroxyl protons being acidic. It is suggested that this solvent medium acid catalyses nucleophilic addition/elimination reactions and also partake in them as active nucleophiles. The mechanisms of these reactions are analogous to those already discussed. Since these reactions are equilibrium controlled, the large excess of reactive phenols ensures the formation of aryl ester derivatives of resin-SC, during the curing process. The reaction-order is expected to be greater than 2.0 since the catalyst is also a reactant. For example, the ester exchange of dimethylterephthalate (DMT) with EG appears to be a second-order reaction, neglecting the presence of any catalyst. Treating any catalyst as a reagent, the reaction instead follows third-order kinetics.[14]

Resin-SC is completely imidised[15] (see §3.1.1.2); the reactive chain end-groups being HE groups, with a small quantity of carboxyl groups (see table 3.5 for the acid and hydroxyl numbers). Therefore, the basic chemistry of poly-

(ethylene terephthalate) (PET) applies to the curing of PEI, with consideration of suitable reservations regarding the effect of the solvent medium and crosslinking on the overall reactivities of the end-groups.

1.1.1 Polycondensation by ester exchange in PET

1.1.1.1 Uncatalysed and protic-acid catalysed reactions

The equilibrium constant for the polymerisation of bis-(2-hydroxyethyl)terephthalate (BHET) and its oligomers to PET varies with the degree of conversion,[16,17] but only slightly with temperature. The reaction conformed to second-order kinetics[17] with an activation energy of about 92kJ/mole and the rate coefficient for the forward reaction increased with DP, whilst the rate of glycolysis (reverse reaction) was independent of DP.

The principle of equal reactivity of polymer end-groups was proposed by Flory.[2] However, the intrinsic chemical characteristics of a functional group can be altered by nearby substitution. When the point of substitution is more than six atoms distant and assuming no intervening conjugation, the effect is negligible. Challa[18] showed the reactions of the two end-groups of DMT to be the same, with equilibrium constants of 0.33 and 0.30, respectively, for the reactions

$$\text{EG} + \text{DMT} \longrightarrow \text{MHET} + \text{methanol}$$

and

$$\text{EG} + \text{MHET} \longrightarrow \text{BHET} + \text{methanol},$$

where MHET is 1,4-(2-hydroxyethylmethyl) terephthalate. These values were considered to be identical, within experimental error.

Thus, the end-groups of the terephthalate esters can be considered to be effectively equal. However, the reactivity of the trimellitimide ester endgroups may be affected by the

hyperconjugated imide ring,

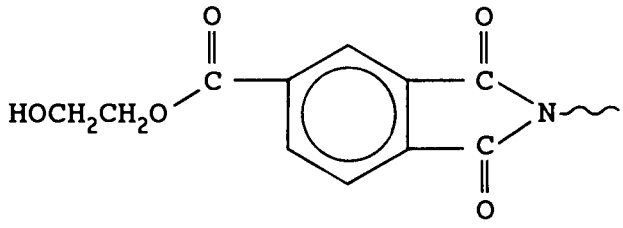

Donation of electrons into the reacting ester group would tend to reduce direct nucleophilic attack, but by the same token, such a contribution tends to stabilise any carbonium ion intermediates such as that postulated in the $A_{AC}2$ (acid-catalysed, acyl cleavage, bimolecular)[19] (cf. scheme 1) reaction mechanism

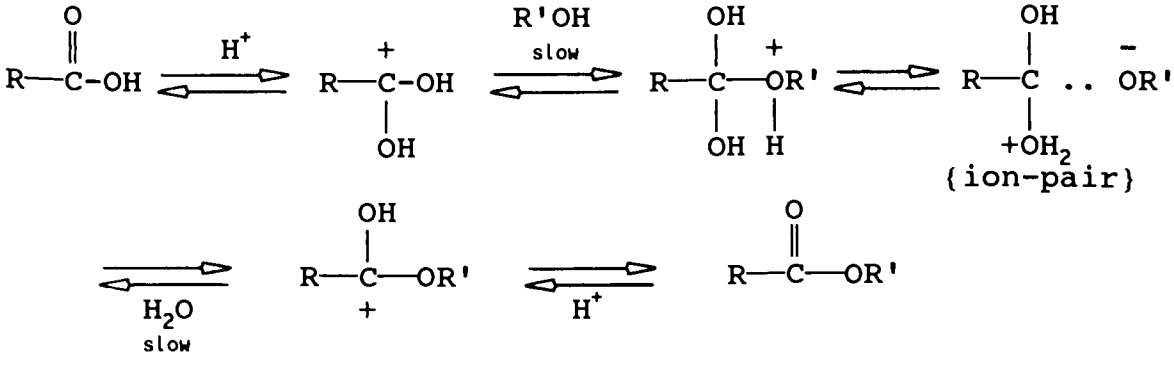

Scheme 1

Alternatively, the carbonium ion of the last step in the $A_{AL}1$ (acid-catalysed, alkyl cleavage, unimolecular)[19] (cf. scheme 2) mechanism may also be favoured by hyperconjugation with the imide substrate,

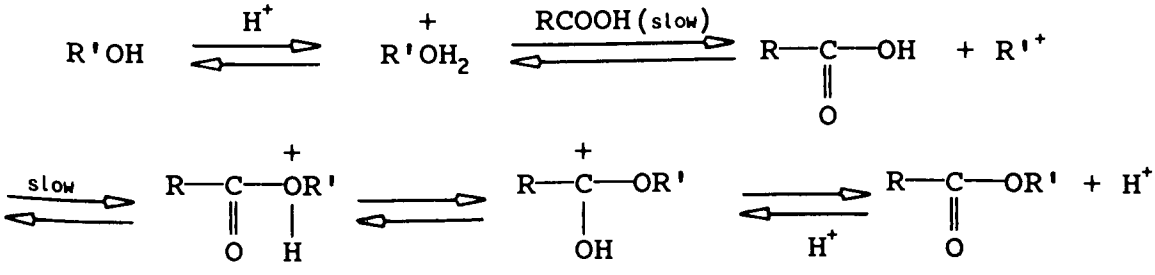

Scheme 2

Reaction by scheme 2 depends on protonation of the alcohol to form a stable carbonium ion (R'^{+}). The presence of these ions is favoured by a medium of high dielectric constant such as the cresylic acid solvent system used

widely in wire-enamelling. The rate-determining step in the $A_{AL}1$ mechanism is the electrophilic addition to the carbonyl group, and is therefore promoted by increased electron-density at that group.

Delocalisation of the imide-ring electrons across the trimellitic anhydride substrate to the carbonyl group opposite the imide-heterocycle (**vide supra**, p.11) is predicted by the canonical set of structural forms. Carbon nuclear magnetic resonance studies of the model compounds: 4,4'-methylene bis-(N-phenyltrimelliti-mide) (cf. §2.3.1) and terephthalic acid (cf. §2.2.1.5), indicate a small increase in the electron-shielding (i.e., a downfield shift of 8Hz) at this carbonyl carbon nucleus, supporting the proposed hyperconjugation of the imide substrate.

The unimolecular $A_{AC}1$ and $A_{AL}1$ (cf. scheme 1) mechanisms, classified by Ingold,[19] can, however, be discounted owing to the high reaction-orders generally encountered for condensation reactions, and because the reactants do not readily form carbonium or acylium ions. Of the two bimolecular mechanisms,[19] the $A_{AL}2$ has not been observed. Thus, the most likely mechanism, of the four reversible acid-catalysed ester-hydrolyses is the $A_{AC}2$ scheme; the rate-determining step is the nucleophilic substitution

$$R\text{-}C(=O)\text{-}OH_2^{+} + R'OH \rightleftharpoons R\text{-}C(=O)\text{-}O(H)R'^{+} + H_2O \quad .$$

In the absence of foreign acid-catalysts, self-catalysis by the carboxyl groups produces oxonium ions, and for reaction media of low dielectric constants, Hamann et al.[20] have proposed the formation of ion-pairs,

$$[R\text{-}C(=O)\text{-}O^{-} \ \ldots \ R\text{-}C(=O)\text{-}OH_2^{+}]_{\text{ion-pair}}$$

which then react with alcohol groups to release the nucleophilic oxyanions, RO^-.

The relatively high dielectric constants for the components of cresylic acid (e.g., phenol: $\epsilon = 9.78$ at 60^0C) suggests that oxonium ions and the conjugate carboxylate anions would be solvated, thereby obviating the formation of ion-pairs, at least during the early stages of varnish-curing when there is abundant cresylic acid available. The reactive ions may then tend to react preferentially with the solvating molecules. As the curing proceeds, and the solvent concentration is reduced by evaporation, the reducing dielectric constant of the medium may then tend to favour the formation of the ion-pairs proposed by Hamann et al.[20].

1.1.1.2 **Reactions catalysed by metal compounds**

Metal compounds are known to catalyse chemical reactions, a phenomenon believed to be due to the ionic nature of the central metal atom. The metal alkoxides constitute an important class of catalysts and are characterised by the metal-oxygen-carbon bonding system. The strongly electronegative oxygen atom induces considerable polarity in the $M^{\delta+}-O^{\delta-}$ bond, but this is partially offset by the electrophilic nature of the metal centre that are able to undergo covalency expansion by coordination with donor atoms. The characteristics of the titanate complexes have been reviewed later (see §1.2).

Yoda et al.[21] assumed that metal compounds induce a positive charge on the carbonyl carbon atom of the ester group of DMT, facilitating the attack of glycol and forming chelates,

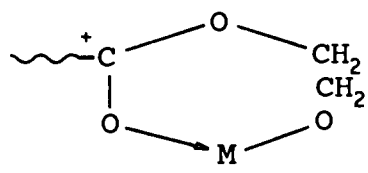

Although esterification and ester exchange reactions are fundamentally similar, their catalysts are not the same. Highly active transesterification catalysts have been distinguished by Hovenkamp,[22] who found manganese to be most active in the early stages of PET curing, where DMT and EG condense to form MHET and BHET, but manganese was poisoned by the small amounts of carboxylic acid groups formed by degradation.[23] The activity of antimony compounds, on the other hand, increased linearly with DP.

Salts of zinc, calcium and antimony were found to be active transesterification catalysts by Fontana.[14] Assuming that the active forms were the alkyl esters, such as polymer glycolates, rather than the acid salts, and that the fully active forms were the dialkyl esters (e.g., $Zn(OR)_2$), the mechanism for ester exchange or esterification may involved a six-membered (**aromatic**) transition-state,

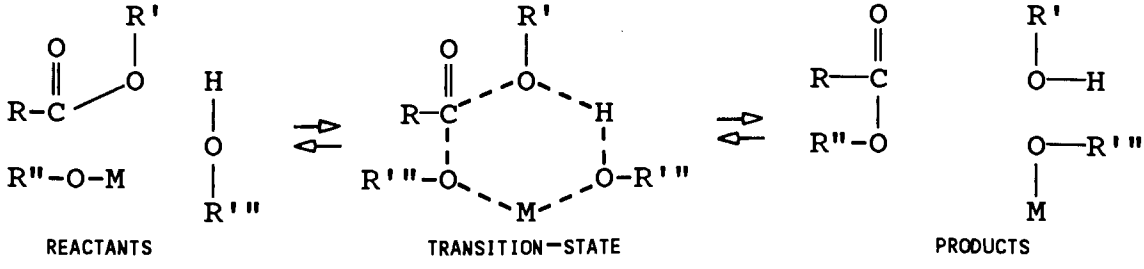

Scheme 3

The aromatic transition-state mechanism has been invoked to explain ionic, non-ionic, homogeneous, heterogeneous, as well as gas and liquid phase reactions.

Antimony compounds are found to enhance the catalytic activity of metals of less utility, possibly by binding more effectively to carboxyl groups, preventing them poisoning the lesser catalysts. Thus the antimony compounds may also have a catalytic effect on direct esterification. To the contrary, Stevenson and Nettleton's[24] study of the curing of low molecular-weight polymer in the presence of antimony

trioxide, parallelling Challa's[16,17,25] work on uncatalysed polymerisation, found the rate coefficient to be low, although the reaction rate was faster. They postulate that antimony trioxide (Sb_2O_3) does not effectively catalyse the polycondensation of the pure monomer (i.e., BHET) which tends to deactivate the catalyst.[26] Ester exchange reactions are commonly catalysed by Sb_2O_3 when used in tandem with zinc acetate ($Zn(OAc)_2.2H_2O$); in the reaction between PET and poly(ethylene sebacate)[27] by melt polycondensation.

Studies of bulk polycondensations, with regard to catalysis, are complicated by the diffusion of the small condensate molecules through the reaction medium since condensation reactions are equilibria; the presence of these condensates causes depolymerisation. Hence, the rate of polymerisation depends on the rate of diffusion[8] of the condensates through the polymer-bulk. In the cases where EG and water are condensed, as for PET, the order of diffusivities[28] is expected to be water >> phenol > EG, and has been assumed to be so for the curing of the PEI wire-varnishes.

Formation of azeotropic boiling mixtures with the solvent may also influence rate at which EG is removed from the sites of polycondensation. During experiments where a PEI wire-varnish was thermally cured under vacuum (≈10 torr), a mixture of condensates (i.e., EG and water) with solvent was isolated in a nitrogen trap. Further experiments, in which model varnishes (with phenol instead of cresylic acid) were cured, showed that a ternary azeotrope forms with phenol, having a boiling point of 101^{0}C (see appendix VII for the component-ratio). This boiling point is much lower than that for pure EG (i.e., 198^{0}C), therefore, similar azeotropic boiling-mixtures with cresylic acid can form during the

early stages of curing, facilitating the removal of EG by vaporisation from the reaction-sites.

Thin film polymerisation also facilitates the removal of condensation products. Thin films (≈1 to 3 μm) of adipic acid with propylene glycol have been cured by Campbell[29] using a continuous-film, rotating-cone, thin-film reactor. Film thickness, water concentration in the nitrogen atmosphere about the apparatus, and reaction temperature were the variables studied, and the basic assumption was that the reaction proceeded as a sequential process of esterification followed by diffusion of water through the gas/liquid interface which varied in area with film volume. Campbell implies that the film's surface area to volume ratio is a dependent variable for the rate of polyesterification, and that atmospheric water severely retards the forward reaction by encouraging the reverse; hydrolysis. Thus, diffusion rates of the condensates out from the film may not be a controlling factor in the rate of polyesterification unless the vapours are readily removed from the vicinity of the gas/liquid interface. To the contrary, Flory[30] found that in the bulk-polyesterification of diethylene glycol (DEG) with adipic acid, at 166^{0}C, the rate of reaction was not increased upon reducing the pressure to 200 torr. However, the condensates were required to travel across the reaction-bulk before vaporising, suggesting that the reaction-conditions in the depths of the bulk were not greatly altered. This is expected if the condensates are envisaged as hydrolysing ester-groups on their way out, before having reached the interface. Therefore, condensate diffusion-rates appear to be improved for polymerisation in thin films.

The rate of polycondensation is apparently improved by effective suppression of the reverse (depolymerisation) reactions, and this result can be further enhanced by increasing the intrinsic reactivities of the polymeric functional groups. The rate of bulk polymerisation of PET and the molecular weight of the resulting polymer have been found to increase[31,32,33] with the addition of small amounts of diphenyl terephthalate (DPT). The increased stability of the carbonium ion transition-state and the phenoxyl leaving group, due to resonance stabilisation through the aromatic ring, promotes nucleophilic addition at the carbonyl group. The model esterification reactions,

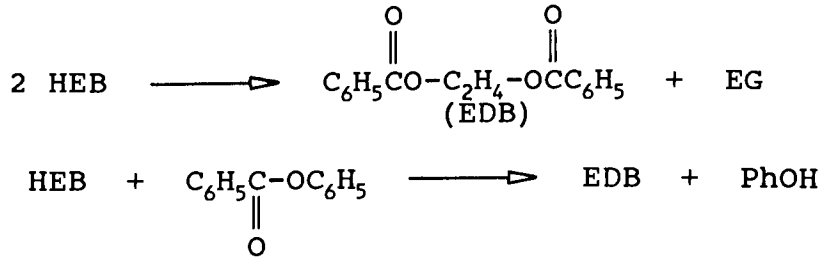

conducted by Shevchenko et al.[31] have given similar enthalpies of activation, whilst the rate of the second reaction was measured to be seven times that of the first reaction. A significant difference in the entropies of activation for the phenyl ester was proposed to explain the increase in reactivity instilled by the phenoxyl moiety.

In view of the uncertainty over polycondensation kinetics, curing of wire-varnishes is expected to be a complex affair. The varnish, containing a high concentration of oligomeric solute (i.e., 35-40wt.%) in a nonideal solution, is thinly coated onto a metal wire-surface. The coats are typically of the order of 5 microns thick. As the solvent is removed by vaporisation, the curing medium approaches those conditions found in a bulk polymerisation. During the last stages, when the solvents and diluents have been largely

vaporised, many of the reactive chain-ends having reacted, leaving a few reactive end-groups, which are dilute in the tightly crosslinked polymer network. The network creates a significantly immobile environment, and their reactions thereby become diffusionally restricted. The rate of diffusion of the condensation products away from the reaction-sites plays a role, as well, in the rate of curing. Therefore, the rate of polymerisation becomes dependent on the crosslink-density.[34]

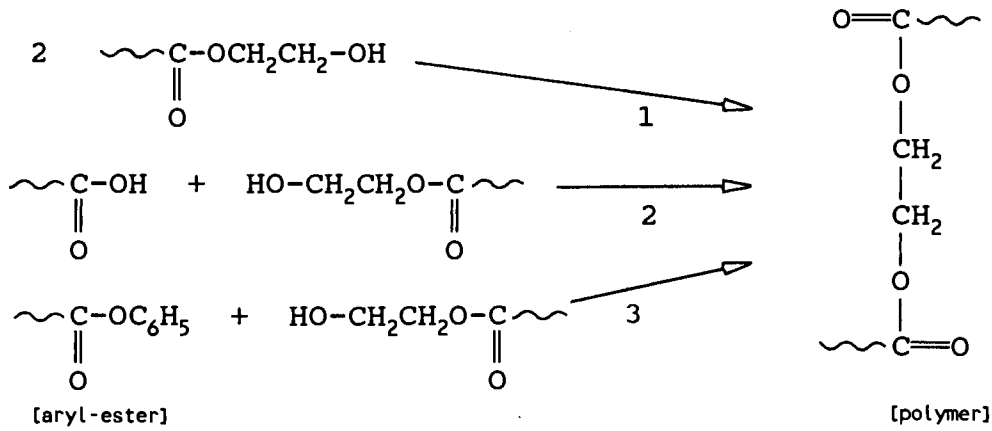

Scheme 4

The rates of the polycondensation reactions,[31,32,33] proceeding in the curing of PEI wire-varnishes based on the components given in table 1.6 (cf. §1.5.2), are expected to follow the order of reactions 1 and 2 << reaction 3, for those reactions given in scheme 4.

1.1.2 **Commercial polymers**

Commercially, PET's are manufactured from DMT and glycols catalysed by salts of manganese, zinc, calcium, cobalt, and other metals. In the later stages of conversion, when much of the methanol has been liberated, the catalyst is rendered catalytically inactive by reaction with a phosphorous compound such as triphenyl phosphate to a colourless form. The polymer is generated by heating with a transesterification catalyst such as cobalt acetate,[35] used either by itself or in combination with litharge (PbO) or antimony

trioxide; the ester exchange and polycondensation reactions are accelerated without discolorisation.

1.1.2.1 Poly(esterimide) (PEI) wire-coating systems

The PEI category of polymers has been available since 1966, and found wide usage as wire-enamels for those applications where high thermal resistance is required. The major commercial products available are: Imidex (General Electric); Teritherm (P.D.George & Co.); Isomid (Schenectady Chemicals, Inc.); Terebec (Dr.Beck & Co., a subsidiary of BASF); E3535 (Dr. Kurt Herberts, a subsidiary of Hoechst); and Cellatherm (Reinhold Chemie). These proprietary PEI's can be delivered as either hard resins, to be dissolved into the solvent-system of choice, or as ready-mixed varnish.

Many PEI's are synthesised from the following precursors. The imide-formers: **trimellitic anhydride** (TMA); pyromellitic anhydride; benzophenone tetraacid anhydride; **diaminodiphenyl methane** (MDA); **p**-phenyl diamine; **p**-aminobenzoic acid; aminoethanol; aminoacetic acid. The ester-formers: **terephthalic acid** (TA); itaconic acid; phenylindane diacid; benzophenone diacid; **ethylene glycol** (EG); glycerine; **tris(2-hydroxyethyl) isocyanurate** (THEIC).

The PEI resin upon which this thesis is founded is made up from TMA, MDA, TA, EG, and THEIC, the highlighted compounds, above (see §1.5.1), and the resin-forming reaction is performed without a foreign catalyst.

The enamel-film is formed by polycondensation in a cresylic acid solution along with a suitable transesterification catalyst (i.e., tetra-**n**-butyl titanate (TBT)). The catalyst must function in the presence of carboxyl end-groups without loss of activity, and therefore, antimony trioxide and zinc acetate have also been utilised[36] for the

manufacture of PEI's from N-(carboxyphenyl)trimellitimide, including the ortho-, meta-, and para-acids, and EG. Isomid also uses a proprietary TBT ("Tyzor TBT"), but although carboxyl end-groups exist in resin-SC, no other acid-insensitive catalyst is utilised in tandem.

1.1.3 Summary of polycondensation kinetics

The many attempts to understand the kinetics of uncatalysed polyesterification in the bulk, carried out since Carothers,[37] have made a general distinction between condensation and addition polymerisations, and have yielded a diversity of conclusions.[10,11,38] The conclusions have depended on the ranges for the extents of reaction studied; workers proposing second order rates with respect of the acid have concentrated on monomer-conversions below 80%,[38] whilst those advocating nonintegral orders have attempted to integrate over 0-95%.[10,11] As an example of the confusion that has prevailed, the reaction-order for the equimolar polymerisation of succinic acid with EG, based upon the results of Dostal and Raff,[39] has been proposed to be two,[39] three,[12] and 2.5.[10]

Tang and Yao[10] have also analysed Flory's[30] results for the polymerisation of DEG with adipic acid and caproic acid over 0-92% conversion, and propose that these conform to a 2.5-order. Their kinetic model is a simple approach to the problem, in that it did not concede that such bulk-reactions are complex affairs. Under bulk conditions, the reactants act as solvents; at low extents of reaction (below 80%) they are highly concentrated, suggesting a significant departure from thermodynamic ideality, and the effect on reaction rate is not well understood. Ideality is approached most closely above 80% conversion where the reactants become very dilute.

Flory's[30] own analysis of the polymerisation of PET is

more realistic: no significant dissimilarity in the reaction-rates of polyesterification and simple esterification were found, and above 80% conversion, the rate was third-order. Below 80%, no lower rate-orders were appropriate. Solomon[40] has affirmed the third-order rate for 80-92.7% of reaction, and an examination of the results for lower conversions revealed a good agreement with second-order kinetics between 50-80% conversion, a feature previously ignored by Flory.

Later, Hamann et al.[20] proposed that third-order kinetics is the most consistent with experimental results for the esterification of lauryl alcohol with lauric acid, at varying concentrations in lauryl laurate. They postulate the formation of reactive ion-pairs in low polarity media for both uncatalysed and catalysed reactions.

The confusion has arisen from a lack of general appreciation for the relationship between the reaction time and the extent of reaction.

Estimates for the activation energy of polyesterification fall into two groups. For solution polymerisation, the values are found to be similar to simple esterifications: 54.4kJ/mole[41] for acetic acid with methanol, 63(±)kJ/mole[10] for various dibasic acids with 2,2-dimethyl-1,3-propanediol, and 59(±4)kJ/mole[9] for the bulk-polymerisation of succinic and adipic acids with EG, and adipic acid with DEG have been reported. In bulk-polymerisations, however, Flory[11] finds a value of 105(±8)kJ/mole for the reaction of succinic acid with EG conducted in the absence of solvent, in dioxane, and in excess glycol. Kienle and Hovey[42] also report a higher value of 95kJ/mole for the polycondensation of phthalic anhydride with oligomeric PET.

Campbell's[29] polyesterification of adipic acid with propylene glycol in thin films yielded an activation energy of 95kJ/mole, a significantly higher value than that found for bulk-polymerisation (i.e., 53kJ/mole). Campbell explained this as a change in the rate-determining step, or controlling rate, from polymerisations in the bulk to the films due to alignment of reactive groups at the surface, or the orientation of water molecules at the gas/liquid interface, in film-polymerisation. These values are similar to those for bulk and solution reactions, respectively, and may reflect the greater ease of condensate-diffusion from reaction-sites in solution and thin-film polycondensations, thereby manifesting a lower activation energy.

Campbell proposes that, at moderate DP's (i.e., ≈60% monomer conversion), the reactive groups in the thin-film experience a rapid decrease in mobility. The reaction is effectively constrained within two dimensions of free movement, and the reaction-rate becomes dependent on the rate of diffusion of reactive groups into a state of encounter rather than on the rate of encounters between them. Therefore implying for wire-enamelling, that more energy is needed to cure PEI as a film beyond a moderate degree of conversion; a lower DP than that found for the linear polymer system used by Campbell, since crosslinking tends to more effectively immobilise the pendant reactive groups.

1.2 **Titanium(IV) esters**

Titanium esters are also widely known as titanates, and these terms are used interchangably in this review. These compounds are widely used as reagents in organic syntheses.

A cursory overview of the topic is presented, giving a very brief summary of the immature field of titanium chem-

istry; the correlations between structure and reactivity are poorly understood. As recently as 1980[43], it was discovered that titanation of classical carbanions with $ClTiX_3$ (**II**) leads to species of reduced basicity and reactivity, increasing the regio-, chemo- and stereoselectivity in reactions with compounds such as aldehydes, ketones and allyl halides. Since the ligand X in compound **II** can be varied widely, the electronic and steric nature of the titanium reagents are easily changed. This helps in predicting the stereochemical outcome of C-C bond forming reactions, but the trial and error method remains necessary in other applications.

Generally, transition metals have long been recognised as active catalysts for many reactions. In an isolated atom, completely filled d-orbitals result in a spherically symmetrical charge distribution. The partially filled d-orbitals of titanium, however, lead to localisation of the charge, and permits electronic overlap with ligands and incoming reactant molecules.

Correspondence between d-orbital energies and the molecular orbital energies of a ligand makes for a strong interaction,[44] providing a mechanism for electron-transfer within a titanium complex; electrons are exchanged between ligands and the central metal atom as well as between the d-orbitals themselves. These characteristics can promote normally symmetry-forbidden processes by lowering activation energy barriers, and contribute, if not determine, the catalytic activity of the transition metals. However, geometric and electronic factors must also be considered, as they strongly influence reaction-rates.

The electronic configuration of titanium is $[Ar]3d^2 4s^2$ (i.e., a d^0 species), and possesses free coordination sites.[43] The distribution of electrons in the molecular orbitals of the titanium compounds depends on the ligands attached to the central atom. $TiCl_4$, for example, has a formal electron-count of eight, ignoring the lone-pairs of the chloride ligands, but these eight lone-pairs may combine[45] to form e_2, t_1 and t_2 orbital combinations. Thus, with effective electron donation to the titanium centre, $TiCl_4$ may be considered an eighteen-electron molecule.[43] Notwithstanding, $TiCl_4$ is a strong Lewis acid with the ability to expand its coordination to six. Such octahedral compounds of titanium are also d^0-species, as is $Ti(CH_3)$. 2pyridine which is a 12-electron system.

The chemical properties of titanium(IV) esters are largely influenced by their ability to easily expand from a tetrahedral conformation, consistent with its maximum valence, to its maximum coordination of six; a phenomenon not unique to titanium.

1.2.1 **The Ti-O bond**

Homolytic bond cleavage of ligands in the transition metal complexes depends on the strength of the Ti-O bond. From a range of calorimetric experiments, Bradley and Hillyer[44] have estimated the mean energy of this bond to be 431kJ/mole.

The bond strengths for the titanium subfamily (i.e., group IVB) decrease[45] in the order M-O > M-Cl > M-N > M-C, and monotonically increase with the atomic mass of M. The Ti-C bond strength is similar to many involving the main group metals.[46] The TI-O bond, however, is markedly stronger than the Ti-C bond, suggesting that its formation is thermodynamically favourable.

1.2.2 Hydrolysis, alcoholysis and acidolysis of titanium(IV) esters

Titanium alkoxides, of which "Tyzor TBT" is one, have several unique properties which are useful in the catalysis of organic reactions such as asymmetric epoxidation,[47] and these are:

(i) the exchange of monodentate ligands occurs rapidly in solution;

(ii) titanium(IV) easily expands its coordination, rendering it a flexible reaction site;

(iii) they are Lewis acids, able to modify the electronic characteristics of electron-rich ligands such as alkyl peroxyl and carboxyl adducts, activating them towards nucleophilic attack.

Hydrolysis. The reactive nature of titanates is shown by their tendency to rapidly hydrolyse. From such hydrolyses, Boyd[48] has proposed that partially hydrolysed titanates readily react with tetraalkyl titanates to produce compounds with varying degrees of polymerisation. Condensation of these compounds to TiO_2 was considered to be the slow step,[49] whilst the fourth, and final, butoxide ligand resisted displacement by water.

Minami et al.[50] has hydrolysed TBT and concluded that hydrolysis occurs in two stages: an initial, rapid reaction is followed by a slow approach to a temperature-dependent equilibrium over 7-12 hours. A small amount of polymerisation was found to occur upon boiling TBT in butanol with water, suggesting that Ti-OH bonds are more thermodynamically stable than the $Ti-OC_3H_7$ bonds.

The rapidity and completeness of hydrolysis depends on the size of the alkoxide ligand; the rate of hydrolysis slows with increasing length of the alkyl substituent. The

decrease in the hydrolysis rate is most noticeable after three out of the four ligands have been substituted. Bistan and Gomory[49] have confirmed the difficulty of complete ligand displacement, and further propose that the difficulty is increased by bulkier ligands. The ligand-effect on the hydrolysis of tetrahedral titanates was given as follows: phenyl, **m**-cresyl < benzyl, cetyl, **n**-heptyl < **n**-butyl.

The reasons for this behaviour are unclear, but Bradley[51] has proposed that an equilibrium is established between hydrolysis and esterification in alcoholic solutions, assuming that Ti-OH bonds are relatively stable. If ligand-ligand steric factors are considered, ligand repulsion leads to lengthening of the Ti-O bonds. The steric repulsion diminishes as the bulky ligands are hydrolysed; the Ti-O bonds of the remaining alkoxide ligands strengthen, and further displacement becomes more difficult.

A likely hydrolysis mechanism involves nucleophilic attack by water through an octahedral transition-state[52] which accommodates the non-bonding electrons of the water molecule. Ebulliometric (i.e., boiling point depression) measurements have suggested that traces of foreign protic acids have the effect of increasing the hydrolysis rate, perhaps by protonating the alkoxide ligands,

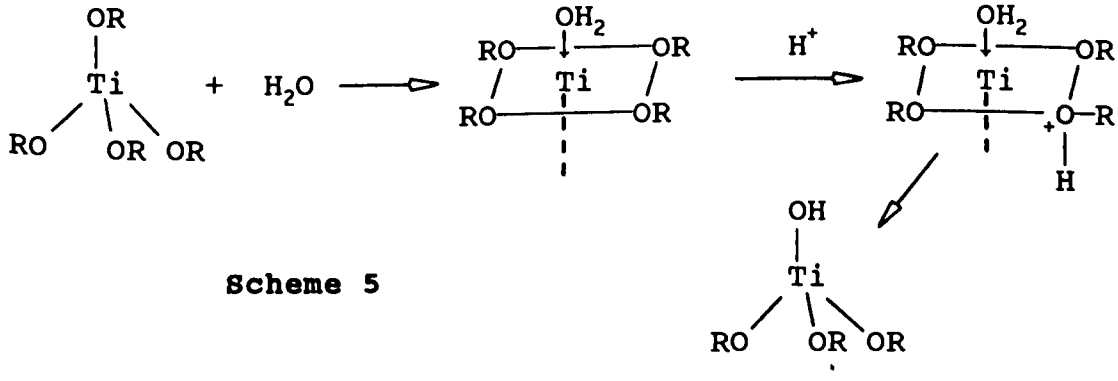

Scheme 5

Traces of alkali have the opposite effect, that is, decreasing the rate of hydrolysis. The incoming hydroxide ion

may be sterically hindered by the butoxide ligands, effectively opposing nucleophilic attack, while the protonated ligand, being a better leaving group, moves away prior to, or in concert with, the approach of the nucleophile.

Isotopic-labelling studies[53] of the hydrolysis of tetraneopentyl titanate indicate preferential breakage of the Ti-O bond, rather than the C-O bond. Therefore, the ligands leave intact, supporting the displacement mechanism (see scheme 5).

Aggregation of the titanates can also occur upon hydrolysis. Condensation has been postulated by Winter[54] to explain the evolution of butanol and butene during the hydrolysis of TBT with heating, and the amounts of condensation products suggest a dimer is formed. Organic acids had the effect of increasing the rate of condensation at low temperatures, again suggesting that protonation of the ligands (cf. scheme 5) facilitates substitution.

Acidolysis. Titanium(IV) esters react readily with organic acids according to the series of reactions

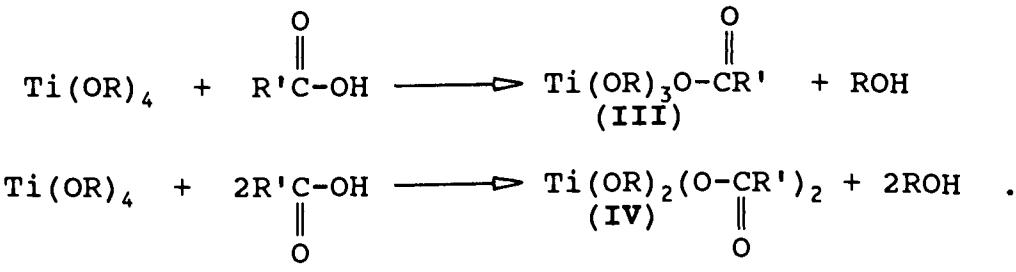

Displacement of more than two alkoxide groups is difficult, perhaps due to chelation of the carboxyl groups through the octahedral positions of the expanded form, and thereby preventing further nucleophilic substitution through the octahedral transition-state mechanism (cf. scheme 5). Although chelation suggests that titanium acylates should be stable, the postulated heterocyclic interaction forms a strained four-membered ring, rendering the trialkoxy tit-

anium acylates (**III**) and the dialkoxy titanium diacylates (**IV**) unstable; they decompose slowly at room temperature, and rapidly at 75^{0}C to produce a simple ester and a condensed ester (e.g., a poly(alkoxytitanyl acylate)),

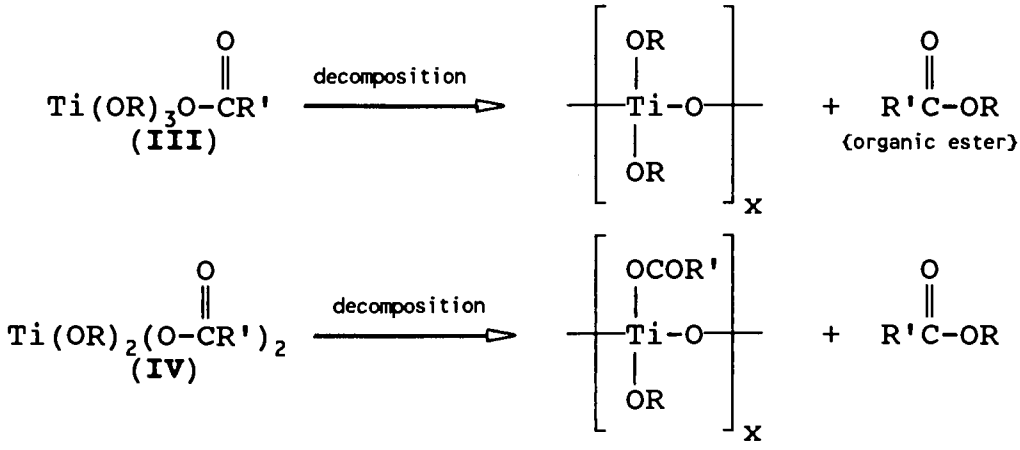

Scheme 6

As well as rapid hydrolysis, titanium esters are characterised by undergoing rapid ester exchange with organic esters at high temperatures.

Bidentate ligands which form five and six-membered chelate rings result in the most stable titanium complexes; dichelates are formed readily by the substitution of tetra-isopropyl titanate, and have enthalpies of formation between 62 and 84kJ/mole. Based on the physical properties of α and β-amino acid salts of transition-metals,[55] a cyclic covalent structure is postulated, for instance,

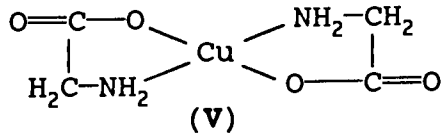

(**V**)

The cyclic structure of dichelate (**V**) explains its colour and low electrical conductance; the colour is given to resemble that of the $Cu(NH_3)_4^{2+}$ complex, differing widely from the usual green colour of copper salts such as copper(II) acetate. The low electrical conductance indicated not only that the salt is very stable, but also that the chelate itself had zero ionic charge.

Boeseken[56] demonstrated that the strongest chelates formed between boric acid and glycols are those of the α, β-dihydroxy compounds to giving five-membered rings of the type

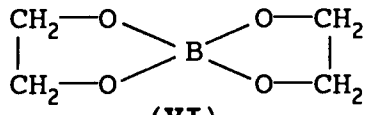

(VI)

The properties demonstrating chelation (i.e., decreased acidity and electrical conductance) indicated weaker chelation when the hydroxyl groups were further apart. Other metals show a similar preference for complexes with 1,2-diols, for example, arsenic[57] and iron[58] form stable chelate-complexes with o-diphenols such as pyrocatechol. Titanium, too, is expected to form stable chelates with EG; a condensation product of the curing of Isomid wire-varnish, and is characteristic of the generally greater stability of five and six-membered heterocyclic rings. Thus, a variety of relatively stable metal chelates form with ethylenediamine, diethylene-triamine, triethylene tetramine, triaminotriethylamine, o-hydroxy acids, β-dioxime, 2-hydroxyazo compounds, 8-hydroxy-quinoline, 1-hydroxyanthraquinone, and many other structures too numerous to mention here; all forming chelate-rings of five or six atoms.

Chelated complexes can also be formed by monohydroxylic alcohols containing one or more additional, suitable functionality such as carbonyl, keto, amido, or other electron-rich groups. Aqueous solutions of titanium oxalate,[59] and glyceryl titanate,[60] were patented in the 1940's, and many chelates have since been characterised by X-ray crystallography,[61] for example, the adduct formed upon the treatment of the acrylate of ethyllactate with $TiCl_4$ prior to a Diels-Alder reaction with cyclopentadiene,

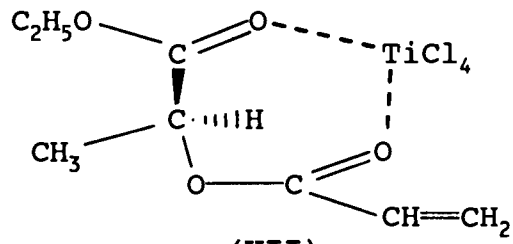

(VII)

and the diphosphine chelate,[62]

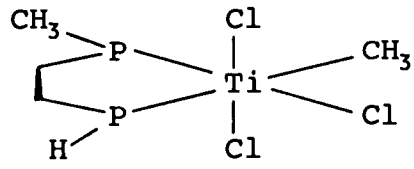

(VIII)

The latter example exists in a distorted octahedral geometry; a proton of the methyl group finds itself in unusually close proximity to the titanium atom. The proton may act in much the same way as a lone-pair, donating electrons into empty titanium orbitals.

Chelation of titanates renders them water soluble and resistant to hydrolysis. For example, Suvorov et al.[63] have reported esters of the type

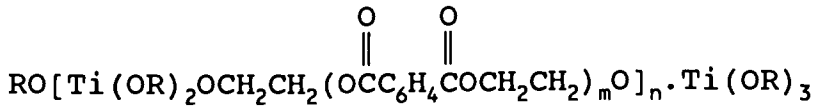

(R = isopropyl or butyl) which hydrolyse slowly in atmospheric moisture. Another example is titanium lactate,

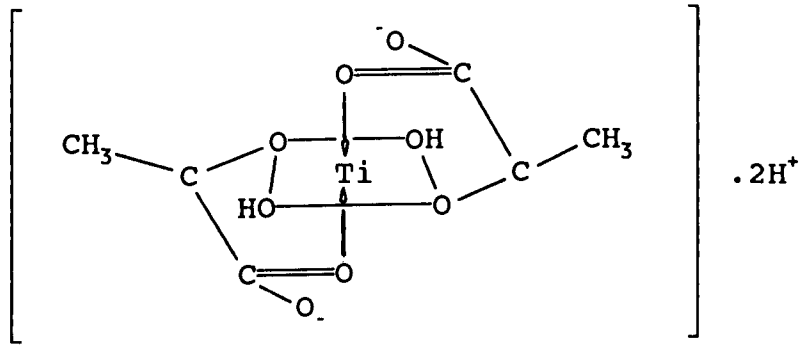

(IX)

a white, water-soluble solid which forms a stable, strongly acidic aqueous solution, even after prolonged boiling.

Alcoholysis of alkyl titanates by glycols in chloroform[63] solution at 60-90^{0}C and reduced pressure yields

inhomogeneous, viscous, transparent, colourless liquids or solid yellow resins soluble in organic solvents. Upon esterification at 130-170^0, solid crosslinked substances were formed. Such is also the case for the high-temperature **reesterification**[64] of hydroxyl terminated oligoesters with TBT or tetraisopropyl titanate to give insoluble, non-melting polymeric titanium glycolates $[Ti(O_2R')_2]$**polymer**, where R' represents the alkyl portion of the hydroxyl chain-ends. The temperature at which the glycolate forms decreases in the order: 2,3-butanediol glycol oligo-esters > phthalic oligo-esters > fumaric oligo-esters.

Hydroxyl containing polymers, such as nitrocellulose, epoxy resins, polyesters, alkyds, and acrylics, react rapidly with alkyl titanates to form crosslinked polymers. The reactions are employed in very fast drying paints and inks;[65] a coat of titanate-solution is applied immediately over fresh paint or ink which then dries in times of the order of one second.

1.2.3 Catalysis by titanium(IV) esters

1.2.3.1 General

Catalysis by titanates had received little industrial attention until Kraitzer et al.[66] used TBT in temperature-resistant paint formulations. During the 1950's, alkyl titanates were utilised as ester exchange catalysts in the preparation of polyester resins.[67] In PEI wire-varnishes, TBT is commonly incorporated in the formulation (see §1.5.2) for this same purpose.

Titanates are excellent ester exchange catalysts for reactions between esters and alcohols, and between esters. The comparative rates of ethanol production in the reaction of ethyl benzoate with butanol (cf. table 1.2), and in the

presence of various metal-esters[51] show that the titanate ester is much more effective than the esters of main-period elements and other group IVB elements (e.g., zirconium).

Table 1.2 The rates of ester exchange (expressed as the amount of ethanol removed) of ethyl benzoate with butanol in the presence of a number of organometallic compounds.

Catalyst	Concentration (wt.%)	Rate of ethanol removed (cm^3/hour)
Tetraisopropyl titanate	5	>280
Aluminium triisopropoxide	5	70
Sodium ethylate	5	50
Tetraethyl silicate	5	10
Tetrabutyl zirconate	5	0
Tributyl borate	5	0

Recently, the kinetics and mechanism for the catalysis of the polycondensation of poly(butylene terephthalate),[68,69] and the esterifications of polyester plasticisers[70] and mono(2-ethylhexyl) phthalate[71] have received considerable attention in the literature.

Fradet and Marechal[68] adopted a coordinative model to explain the catalytic activity of TBT on the polyesterification of difunctional oligomers, using the esterification of octadecanoic acid with 1-octadecanol as a model. They proposed catalysis to be mediated by two reactant/catalyst complexes either through chelation of the carboxyl group (cf. complex **A**, scheme 7, **vide infra**) or via intramolecular hydrogen-bonding (cf. complex **D**) between proximal carboxyl and alkoxyl ligands. The first adduct (i.e., **A**) sees an increase in the electrophilicity of the carbonyl group, facilitating nucleophilic attack by a hydroxyl-group-containing species at the carbonyl-carbon atom. The second mechanism shown in scheme 7 instigates intramolecular reaction by a molecular rearrangement, about the titanium centre.

Interaction of TBT with the carbonyl functionality was supported by the infrared (IR) spectrophotometry of tributyloctadecanoyl titanate, where the carbonyl band of octadecanoic acid (expected at 1710cm^{-1}) was replaced by two peaks at 1560 and 1450cm^{-1}, characteristic of carbonyl complexes.[72]

The model reaction-rate was determined to be second-order with respect to the reactants in the presence of a protic catalyst, and first-order in the presence of TBT.

Barshtein and Sorokina[70] have also postulated a coordinative transition-state similar to **A** (cf. scheme 7), to explain the catalysis of the esterification of polyester plasticisers from dicarboxylic acids, or their anhydrides, with glycols by titanates.

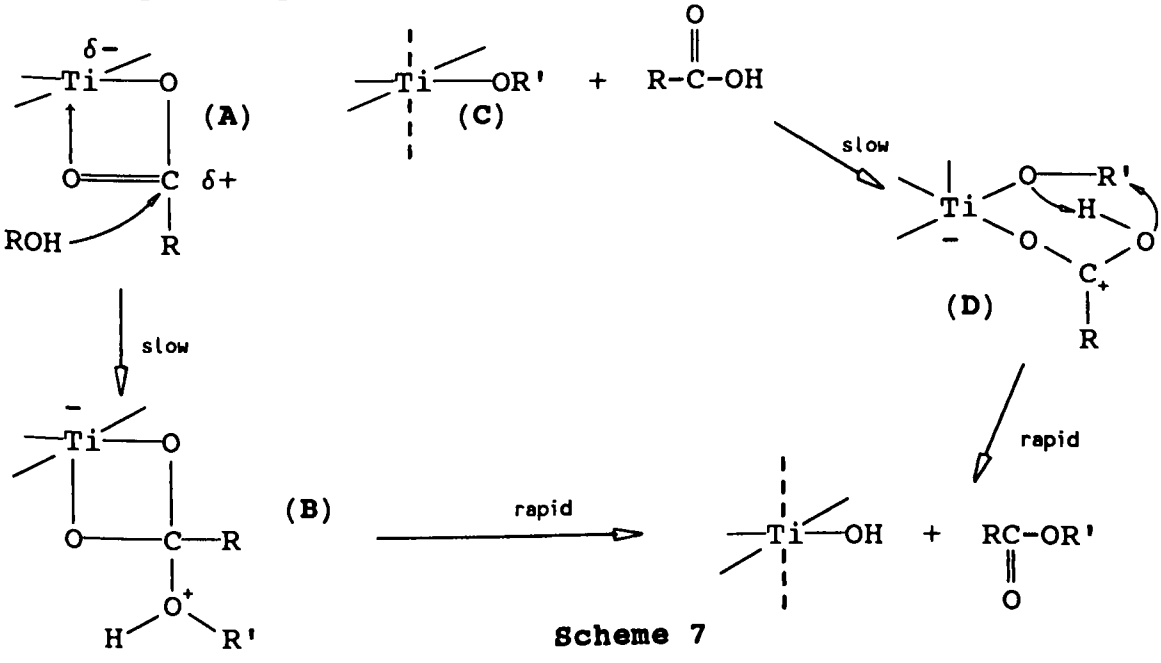

Scheme 7

In alcoholic solution, dissociation of hexaalkoxy titanate, of the form $H_2Ti(OR)_6$, has also been postulated to effect esterification by a protic acid-catalysis[19] mechanism. However, little influence[71] of the dielectric constant of the reaction medium on the rate of the TBT-catalysed esterification of mono-(2-ethylhexyl) phthalate with 2-ethylhexanol has been reported. The degree of ionisation of protic acids depends substantially on the polarity of the reaction

medium, and therefore, the hypothesis of a protic-type titanate catalyst seems unlikely.

Since 1981, F. Pilati[69] and coworkers have studied the TBT-catalysed reactions involved in the formation of poly(butylene terephthalate). During their early investigations,[69(a,b)] they tentatively discounted the notion of basic catalysis which requires the breakage of Ti-O bonds of titanate-complexes, forming active nucleophiles (viz., alkoxide ions),

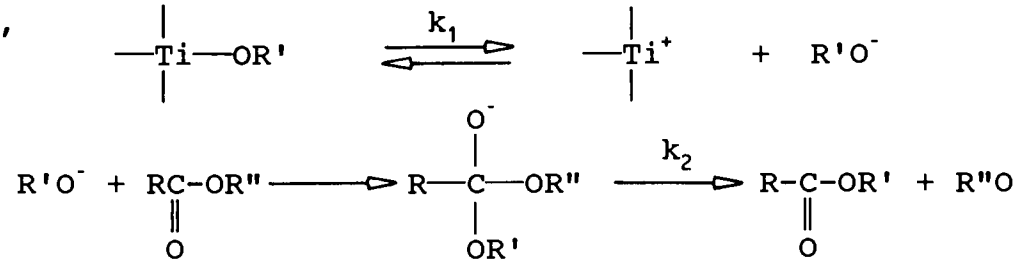

Benzoic acid (BA) is found to inhibit the catalytic action of TBT, a phenomenon which can be explained by both basic-catalysis and the alternative coordinative reaction mechanisms. In the former, a dramatic decrease in alkoxide ion concentration can be expected, and in the latter, stable Ti/BA adducts[69(c)] are formed which prevent the coordination of either ester or alcohol reactant species. However, at high concentrations of BA, TBT shows a measurable catalytic effect, favouring the coordinative mechanism, although basic catalysis cannot be discounted.

A stable Ti/BA adduct was observed[69(c)] to form at room temperature in chloroform solution (viz., a broad IR absorption band at 1550cm^{-1}); the strong carbonyl band of BA disappeared at BA/Ti mole ratios less than unity. Similar IR bands for Ti/ester adducts were not observed, reflecting a greater interaction between the carbonyl group of the 4-hydroxybutyl (HB) esters and the Ti centre.

Ester exchange of the butoxide ligands with HB chain-ends led to the postulation of the reactive intermediate

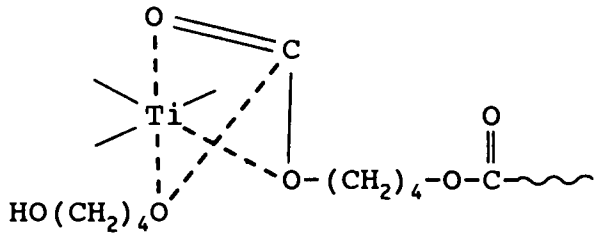

The condensation products, water and 1,4-butanediol, were found to inhibit the catalyst;[69(e)] catalytically inactive titanium compounds are formed such as TiO_2 and titanium hydroxides with water, and glycolysis produces titanium chelates which are less reactive than TBT, but usually undergo the same reactions at high temperatures.

Six-membered (**aromatic**) ring intermediates were postulated by Fontana and Osborne[73] in 1960 to explain the stereospecific polymerisation of 1-olefins by Ziegler-Natta catalyst systems, and Fontana[74(a)] later applied the notion to the uncatalysed polycondensation of PET (cf. scheme 3) as well as to its thermal decomposition (**vide infra**, scheme 8). The concept of the intrinsic stability of six-membered rings was also invoked by Siling et al.[71] to explain the catalysis of both esterification and ester exchange. Proposed intramolecular hydrogen bonding provides the bridge between reactants, completing six-membered transition-states (**vide infra**, scheme 9). The reactants, now brought into juxtaposition about the titanium centre, react by an intramolecular rearrangement, yielding the desired products.

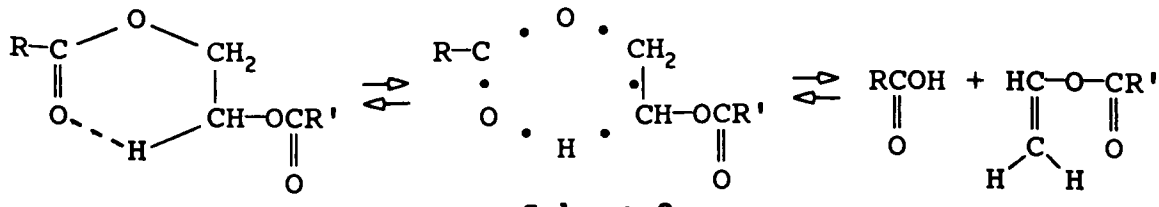

Scheme 8

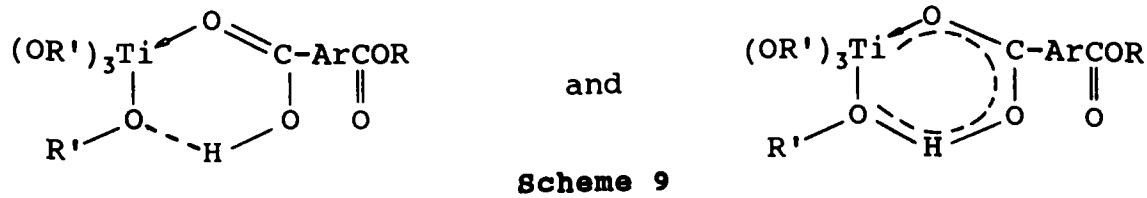

Scheme 9

Fortunato et al.[69(f)] found the catalytic activity of TBT to decrease as the concentration of TBT increases; in the model ester exchange reaction of 4-hydroxybutyl benzoate with 1,4-butylene dibenzoate, the reaction order with respect to TBT was also found to decrease. These observations were explained by **aggregation** (or autoassociation) of the catalyst molecules, leading to octahedral coordination about each titanium centre, and thereby deactivation. Aggregation is the formation of **n**-mers, instead of monomeric titanates. For example, Holloway [74(b)] has detected aggregation in various alkyl titanates by signal broadening in carbon nuclear magnetic resonance spectrometry at low temperatures, and **n**-alkyl ligands seemed to encourage the formation of trimers and higher aggregates. Tomita and Ida[75] propose a similar effect to explain a drop in the catalytic activity of TBT in the polycondensation of DMT with EG as the reactant concentrations diminish.

1.2.3.2 **Ligand effects - aryl esters of titanium(IV)**

The physical properties as well as the catalytic activities of titanates are affected by the nature of the ligands attached to the titanium atom. For instance, the boiling points, densities, and viscosities of **tert**-butyl and **sec**-butyl titanates are very much lower than for **n**-butyl titanates; the former, bulky ligands shield the titanium centre to attack through the octrahedral site, preventing aggregation through Ti-O-Ti bridging, thereby reducing the possibility of extensive molecular association. Again, the octahedral aryl titanates are coloured[76] from white ($TiCl_2(OPh)_2$.2benzophenone) and yellow ($TiCl_3(OPh)$.2benzopheneone) to red ($TiCl(OPh)_3$.2acetophenone) and brown ($Ti(OPh)_4$.2acetophenone; $Ti(OPh)_4$.2benzophenone), with the tetrahedral aryl tit-

anates[77] tending to orange or red. By comparison, benzyl and allyl titanates, in which back-coordination (viz., conjugation of the Ti-O bond, **vide infra**) is unlikely to take place, are colourless; all titanium compounds absorb in the near ultraviolet, but aryl titanates show a marked shift into the visible region.[78] Phenyl titanates, based on $TiCl_4$ in **n**-hexane, exhibit a distinctive bathochromic shift (a **"blue"** shift) from the spectra of $TiCl_4$ and phenol. The concept of back-coordination was proposed by Haslam[79] to explain the spectral shift,

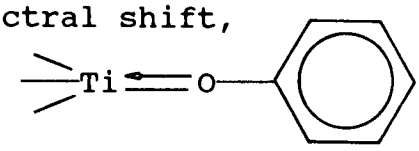

yielding hyperconjugation of the ligands with the titanium atom.

The effect of resonance with the phenyl ring, through dative-type bonding to titanium, explains the greater thermodynamic stability of aryl titanates. For example, the tetraphenyl titanate (TPT) was found to form exothermically when phenol was mixed with TBT at room temperature, both in $CHCl_3$ solution and neat (see appendix V for the formation of TPT from "Tyzor TBT").

The acceptor properties of the metal phenoxides, which are Lewis acids, are better than the corresponding halides such as $TiCl_4$, possibly because of aggregation[80,81] whereby the titanium centre achieves its maximum coordination, but it seems more likely that the fundamental electronic character of these complexes is such as to increase the positive nature of the titanium centre by delocalisation of electrons into the phenyl ligands. TPT is considered, from cryoscopic measurements,[80] to be monomeric in $CHCl_3$ solution. However, octahedral coordination of unesterified phenol molecules was noted in TPT synthesised with an excess of phenol since upon

standing for a few months in an air-tight container, phenol was found to condense onto the vessel walls, whilst no change in the orange coloured, solid TPT was discerned, suggesting that residual phenol is bound by secondary forces. Note that TPT had been washed copiously with $CHCl_3$ to remove unreacted phenol.

The effects of ligands on the catalytic activity of titanate(IV) esters in condensation reactions has not been addressed at all in the literature. However, for the purpose of completing this discussion, a brief summary of the published work for the polymerisation of olefins is presented; the implications are useful in attempting further understanding of the catalytic action of aryl titanates.

Nowakowska et al.[82] has found that increasing the electron donating capacity of the ligands tends to decrease the overall catalytic activity towards olefin polymerisations. The aryl ligands reduce the positive charge on the titanium atom, thereby hindering coordination to the olefinic π-electrons. The presence of phenoxyl ligands causes a rearrangement[83] of the molecular energy levels, due to π-coupling of the oxygen lone-pairs, and lowers the energy barrier to the insertion reaction of the propagation step.

Zucchini et al.[84] proposes a general increase in catalytic activity with decreasing electron donation, or polarity, of the ligand; increasing the positive character of the titanium atom. Catalytic activity increases in the ligand-series: $N(C_2H_5)_2 < O(CH_2)_3CH_3 < OC_6H_5 < Cl$, implying that the catalytic activity of the aryl titanates increases as the pK_a of the conjugate acid of the ligand decreases. A similar effect has been observed for the esterification of BA with EG (see §3.2.3) with a range of tetraaryl titanates.

Steric interaction between the aryl ligands also has an effect on catalytic activity. Taft[85] has correlated increasing activity with decreasing steric repulsion between alkyl ligands. The catalytic activity of titanates with 2,4,6-substituted phenoxyl ligands has been reported to follow the order, CH_3 < Cl < H,[84] where the **ortho**-substituents generate more steric repulsion than **para**-substituents. Increasing ligand-ligand repulsion tends to lengthen the Ti-O bond, reducing the contribution of π-electrons to the central atom, having the effect of increasing the positive character of the titanium atom, and thereby increasing the catalytic activity of the complex. The catalytic activity was noted[84] to decrease with increasing bulk of the phenyl-substituents. On the other hand, the bulkier ligands discourage the approach of electron-rich reactants which enter into the titanium's sphere of influence through octahedral sites, so the observed trend in catalytic activity may also be due to an increase in the ease of displacement of the bulkier ligands, or perhaps readiness to dissociate from titanium, resulting in a relatively stable cationic complex species and the conjugate phenoxyanion,

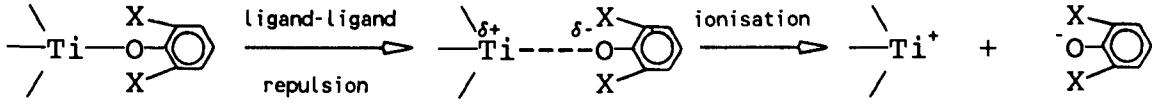

Ionisation is, of course, favoured in highly polar solvents where solvation stabilises the ions.

The overall activity is thus a result of two opposing effects: the steric repulsion between the ligands, and the electronic effects of the aryl substituents.[86] The yield of polyethylene, by olefinic polymerisation, depends on the nature of the $-OC_6H_4X$ ligands and is found to increase in the series for the substituent X: **p**-methoxy < **p**-methyl < **m**-

methyl < **m**-methoxy < **p**-bromo ≤ **p**-chloro < **m**-chloro. The series directly correlates with ascending electron-accepting character of the aryloxy ligands, with ligand-ligand repulsion being similar in the range. Therefore, the rate of olefinic polymerisation is a function of the pK_a of the conjugate alcohols of the ligands (viz., ArOH); increasing with acidity,[84] that is, electrons are drawn away from titanium, thereby increasing the partial positive charge residing there. This suggests that phenyl titanates are able to expand their coordination to accomodate incoming nucleophiles, and that the positive nature of the central atom is an important factor in catalyses by organotitanium compounds.

Titanium alkoxides do not combine with mercaptans[87] to form the mercaptides, although the thiol hydrogen atom is more acidic than the hydroxylic proton of an alkanol; the electron-donating power of the atom adjacent to the active proton is important in these exchange reactions, implying substitution occurs by a coordination mechanism involving that atom (cf. scheme 5). The implication is that ineffective coordination occurs between the sulphur of the mercaptans and the titanium centre.

Titanium alkoxides containing unshielded oxygen atoms are largely associated, exhibiting high boiling points, densities, viscosities, and refractive indices. Compatibility with polar solvents, too, is attributable to association, and such solvents exhibit high surface activity where titanates are present, suggesting an increased polarity of those already polarised solvent-bonds which associate with titanium.

Chelating ligands block the vacant octahedral coordination-sites through which reactants are proposed to coordinate. Such titanium chelates are much less reactive than titanium alkoxides, but usually undergo the same reactions at high temperatures (i.e., >300^{0}C), breaking the weaker coordinative bond and liberating the octahedral coordination-sites for the entry of reactants. Compounds which can be transformed into their alcoholic derivatives by enolisation react readily with titanium alkoxides, forming five-membered chelates. For example, vigorous reaction with β-ketones results in octahedral bischelated dialkyl titanates. The increased thermodynamic stability of chelated titanates is an important property to note for further reference, when the likely forms of titanium in Isomid wire-varnish are considered, later.

Where the ligands contain many hydroxyl groups, bridging between titanium centres can easily occur, and this behaviour is utilised effectively in crosslinking suitable polymers, that is, those containing reactive, pendant groups. Chelation stabilises solutions of paint-resins, yielding long shelf-lives and rapid crosslinking upon baking.

On a final note, it serves to reiterate that aryl and vinyl titanates (orange to red in colour) tend to be more thermodynamically stable than the alkoxyl analogues, and that this is attributed to hyperconjugation of the Ti-O bond. In contrast, benzyl and allyl titanates cannot partake of hyperconjugation, and therefore, are colourless.

1.3 **The copper wire surface**

Drawn copper wire to be enamelled, is cleaned and annealed in a reducing atmosphere of steam, immediately prior to being coated with wire-varnish (see §1.4.3 for a des-

cription of the enamelling process). Therefore, the wire surface is made up of large-grained metallic copper with little copper oxide. The effect of a copper substrate on polycondensation reactions undertaken on the wire-surface is a possible source of catalysis or retardation of the curing of wire-varnishes, and is therefore considered in this section.

Melchiore and Mills[88] propose that copper oxide (Cu_2O) can react with carboxylic acid groups (RCOOH) to form a reactive salt, that is,

$$2RCOOH + Cu_2O \longrightarrow 2Cu^{+}(OOR)^{-} + H_2O$$

Thus, copper oxide can be converted into a form which is soluble in polar solvents such as the wire-enamelling solvent; cresylic acid. Extensive solubilisation of highly conductive copper, can conceivably contribute to breakdown of the dielectric (i.e., cured enamel) when subjected to high-voltage stresses, and as such is a highly undesirable contaminant since the wire-coating is primarily an electrical insulator. As well, salt formation with the carboxylic acid chain end-groups in the PEI resin may influence their reactions with HE end-groups (viz., esterification) and the polymeric ester groups (viz., ester exchange).

Rogers[89] reports an interaction between impregnants (i.e., unsaturated polyester varnishes) and bare copper, resulting in jelly-like, undercured polymer. The implication is that copper-substrates deactivate olefinic functional groups by coordination, rendering them unreactive.

1.3.1 **The metal-wire surface**

The surface-atoms of transition metals are known sites of catalysis, having capacities for bonding[89] through **d**-orbitals which are available to neither free atoms nor those

deep within the solid. Whereas the free, unoccupied orbitals of surface-atoms can bond with adsorbate molecules,[90] such orbitals are normally saturated about atoms within the bulk, and may not be present at all in free atoms. However, correlation of catalytic activity[91,92] with the electronic occupancy of the **d**-orbitals is tenuous.

1.3.2 Catalysis of polycondensation by metallic copper

Increased rates of polycondensation have been reported for thin-film **melt** reactions of PET on stainless-steel surfaces,[93] and have been attributed to catalysis at the surface.[94] However, it is not clear whether the main active site is on dissolved metal (in the form of salts) or the metal/**melt** interface.

Stevenson[95] has considered the effect of metal-surfaces on the rate of **melt**-polycondensation for 1 to 5mm films of PET catalysed by antimony trioxide, assuming the reaction kinetics to be second-order,[97] the rate constant was compared for a range of metals. The nondissolving metals (i.e., molybdenum, rhodium, silver, passivated stainless-steel, and tantalum), as determined by X-ray fluorescence spectroscopy of the prepolymer, produced no appreciable increase in the reaction-rate. Dissolved copper (520ppm), however, yielded a small increase in the rate of polycondensation, while titanium (50ppm dissolved in the molten prepolymer) gave a rate constant twice that on copper, and on iron (>1500ppm dissolved) the rate constant was five times that on copper. Although those metals which dissolved were better catalysts, for similar amounts of dissolved metal, copper had a comparatively low catalytic activity.

Considering that under ideal industrial conditions, that is, given a clean copper-wire surface free of oxide,

and a very short curing time of the order of a few seconds, the polymerisation rate for wire-varnishes is expected to be substantially unaffected by the copper-surface since dissolution of copper into the wire-varnish is not expected to be rapid, and the activity of such copper is likely to be lower than "Tyzor TBT".

1.4 Magnet-wire enamels: production and properties

The background to magnet-wire insulating systems and their application are discussed herein, followed by a brief discussion of the classification of electromagnet-wire enamels, placing PEI into its marketing context. Testing procedures for the finished wire are also reviewed with reference to the physical properties required of the PEI coatings, in particular. Finally, a review of the literature concerning PEI wire-varnishes and enamels is presented, emphasising the lack of published work which deals with the curing-chemistry of wire-coatings.

PEI forms a heat-resistant wire-enamel used widely for stator-wound induction motors, transformers, direct-current field coils and armatures, and solenoids. This enamel-type is especially suited to motors designed for high operating temperatures (i.e., up to 180^0C). This is achieved with the thinnest coating of polymer possible so as to maximise the packing-efficiency, or **filling-factor**, of magnet-coils wound from the wire; the greater the filling-factor the greater is the magnetic flux density generated by a given electrical current.

The thin polymeric film is expected to resist severe service conditions which include high-voltage stresses and high operating temperatures, remaining unaffected by solvents and oils (also refrigerants, in some applications),

and withstand mechanical abuse during high-speed winding, where the wire is asked to twist, bend, and be abraded on its journey from the **pay-off** spool into a tightly wound magnet-coil.

1.4.1 Development of magnet-wire insulation

The development of magnet-wire was a necessity instigated by the harnessing of electromagnetism to do useful work. Electromagnetism was discovered by a Danish physicist, Hans Christian Oersted, who in 1820 showed that a wire carrying an electric current deflects a magnetised needle. A year later, the British scientist, William Sturgeon, constructed the first electromagnet. He used a "horseshoe" shaped piece of iron, insulated with paper or cotton, around which was wound a coil of copper wire. William Henry (1828), working in the United States of America, increased the number of turns per unit length of coil using cotton or silk insulated copper wire on an iron rod, generating a greater magnetic field flux. Ultimately, he built a sixty pound unit in 1832 capable of lifting almost a ton.

The most important application of this phenomenon was devised by the English scientist Michael Faraday. Investigating the principles of electromagnetic induction in 1831, at the Royal Institution (London), he was led to the invention of the electric motor and the dynamo. The salient experiment involved the rotation of a copper disc between the poles of a permanent horseshoe-magnet, generating a direct current between the periphery of the disc and the spindle.

The crude dynamo encouraged Hippolyte Pixii (1832) to devise a generator using permanent magnets and a wire-wound armature, in place of the copper disc. The electromotive force generated in this way was found to alternate in pol-

arity so a commutator was employed to rectify the current. Later, Charles Wheatstone (1845) replaced the permanent magnets with electromagnets excited by electrochemical cells. In 1857 they were made to self-excite, that is, the field coils received current from the armature terminals. The development of the "ring" windings of Antonio Panciotti (1860) and Zénobe Théophile Gramme (1870) made it possible to add the outputs of many armature windings in a multipolar generator, and thus obtain higher voltages. Ring windings, bound to the surface of the revolving armature, were improved by the barrel, or drum-type windings of Frederich von Hefner-Alteneck (1872). These evolved from the shuttle-type windings of Ernst Werner von Siemens (1856). Recessing the armature coils into slots, as proposed by Panciotti (1860), reduced the air-gap between stator and armature, reduced the hysteresis losses, and increased the magnetic field strength for a given field coil. Modern electrical generators and motors are constructed in a similar manner.

Along with power transformers, developed commercially by George Westinghouse (1886), generators began to be used widely for the supply of electricity to a growing market. However, the development of efficient field coils was hampered by the insulation technology available. Throughout this period, lapped cotton tape was used as both a separator between the iron core laminations and an insulator; the disadvantage of this material was its high cost and low **filling-factor**. In spite of these disadvantages, cotton tape is still used in tandem with paper, fibre-glass, and plastic foil as wrapping for very large rectangular conductors, used in high voltage machines. Once lapped, the modern version of the covering is usually impregnated with varnish and cured

to yield an insulator of very good mechanical and electrical endurance.

Clear and black asphaltic (for improved flexibility) air-dried oleoresinous enamels were used as wire insulation around the turn of the century, but the short service life of this material ensured the wide-spread use of lapped insulation until the post-World War II (WWII) epoch.

Poly(vinyl formal), known by its brand-name, Formvar, was introduced in 1938, followed by the polyamide, Nylon-6. Increased coating thickness and good edge coverage became possible with these enamels and a variety of coating thicknesses were offered by wire-makers. The varnishing of square and rectangular wires became viable and proved suitable for service in machines operating below 4kV.

Immediately after WWII, due directly to war-time research efforts into new polymer systems, the types of enamels available proliferated into the hundreds, and the high temperature materials were yet far in the future (ca. 1965). During this period the concept of using two different coatings (**dual-coating**) was developed; the first **dual-coating** was made available in 1953 when a polyamide film was applied over Formvar, polyester, polyurethane, and acrylic films to lower surface friction, improving resistance to mechanical damage during high-speed winding.

During the early 1960s, polyester coated wire became a popular product in high-temperature applications until the aromatic polyimides, poly(aramidimide)'s, and the PEI's provided extended thermal endurance at service temperatures $\geq 180^{0}$C. By 1965, PEI insulation systems had achieved market domination due to low overall cost, good storage-stability, where polyimides do not store well for long periods, and a

high Temperature-Index (TI) of 180^{0}C (see §1.4.2), making it suitable for all commercial applications. The PEI wire-varnish, Isomid, which is the subject of this report, was patented[97] and introduced in the late 1960s by Schenectady Chemicals, Inc.

1.4.2 **Heat classification**

Before WWII, electrical motor operating temperatures were confined to 90^{0}C and below, accomodating the oleoresinous wire-enamels and natural-fibre lapped insulators which were then current. As the war approached, the operating temperatures increased to 105^{0}C with asphaltic and phenolic polymers. Silicone rubber was first used in 1945 and led to heat-resistance far above contemporary limits, allowing smaller more compact motor designs capable of enduring much higher field-generating voltages. Ulimately, applications were designed to operate at temperatures up to 180^{0}C, and thus, there developed a need for a thermal rating of individual insulating materials (i.e., Temperature Index (TI)) and total insulating systems (Thermal Class). The latter includes the encapsulant and impregnating enamels. The thermal classifications given in table 1.3 were in universal use by the end of the 1950's.

Table 1.3 System classification and temperature-indices for electrical systems and wire/coil insulation materials.

Classification for insulation systems	Temperature Index (TI) for insulation materials (^{0}C)
O(1)	90
A	105
E(2)	120
B	130
F	155
H	180
C	220

Notes. (1) Obsolete classification. (2) Seen only in Europe.

Thermal Class corresponds directly to TI which in turn represents the maximum allowable operating temperature when the application is in a clean, dry, vibration-free environment for normal working conditions (i.e., continuous running during the ordinary industrial working hours). Thus, for a class F winding, for instance, the maximum allowable hot-spot temperature is 155^{0}C. The hot-spot temperature is that which will be achieved deep within the winding when operating at thermal equilibrium.

1.4.3 **Magnet-wire enamelling, general**

Compared with other forms of wire insulation systems, such as plasticised poly(vinyl chloride), wire-enamels increase least the cross-sectional dimensions of the conductor, thereby affording the greatest filling-factor.

The enamel is applied to the wire surface immediately prior to passing through a baking oven (cf. figure 1.1, **vide infra**) organised in either a horizontal or vertical configuration. The latter oven-orientation is used with **heavy** wires due to excessive wire-catenaries (viz., the curve assumed when hung horizontally between two supports; cf. figure 1.1), therefore horizontal arrangement are limited to wire-diameters below ≈0.5mm.

Six to eight coats of enamel are applied, with individual coats of the order of 0.02 to 0.05mm in thickness. These films cure quickly during the oven-residence time (≈4secs). Multiple coating also ensures that tiny **blow-holes** and **bare-spots**, caused by rapid solvent vaporisation and poor wetting, respectively, are covered by subsequent coats; a critical requirement since the electrical integrity of the film, under constant high-voltage stresses, must be of a very high order to fulfil the requirements of the magnet-winding processes and applications of the magnet-wire (cf. §1.4.4.4).

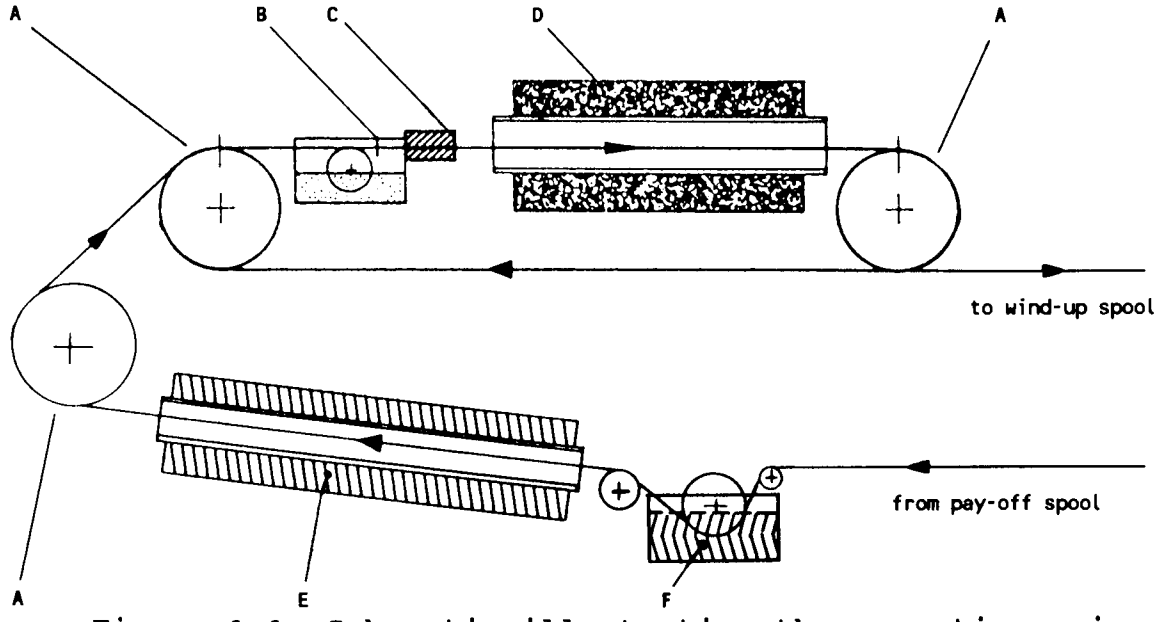

Figure 1.1 Schematic illustrating the operating principles of horizontal wire-enamelling.
LEGEND A : guiding sheaves D : enamel-curing oven
B : varnish-bath E : wire-annealing oven
C : coating thickness regulator F : water bath

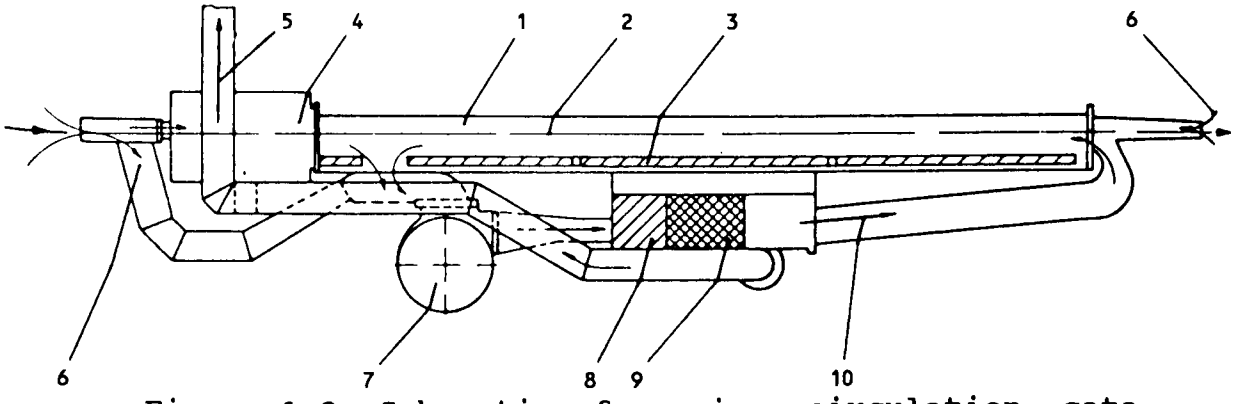

Figure 1.2 Schematic of an air-recirculation, catalytic-conversion enamel curing oven.
LEGEND 1. Oven cavity 6. Inlet air
2. Wire path 7. Air blower
3. Heating elements, oven 8. Oxidation catalyst heater
4. Heat exchanger 9. Tantalum catalyst unit
5. Exhaust 10. Hot CO_2 and steam

Figure 1.2 shows the air-recirculation system used on **catalytic ovens** which are designed to oxidise solvent vapours (**out-gases**) to CO_2 and steam. The out-gases from the curing varnish are passed over heated (to $\approx 600^0C$) tantalum mesh, and the exhaust is recirculated to the oven inlet, providing added heat for curing. These ovens are most energy efficient and reduce the levels of noxious fumes ultimately exhausted into the atmosphere.

Wire-varnish is applied to wire by either **dipping** or **wiping**. Dipping involves passing the wire vertically through the varnish-bath; the excess running back into the bath prior to baking. The desired film thickness, or **build**, is obtained by adjustment of the varnish application rate, the solids content, and the viscosity of the varnish. Wiping, on the other hand, is accomplished by either felt-pads or by metal-dies. Felt-wiping is accomplished by passing the wire between two varnish-soaked felt-pads which are pressed together. The desired build is controlled by the solids content and the viscosity of the varnish, as well as by the grade of the felt used; felt porosity, pressure applied to the felt-pads, and varnish-pump pressure determine the rate of varnish-application to the wire. Together with these variables, the thicknesses of the pads, and the length of the wiping-path are used to fine-tune process. Alternatively, die-wiping employs metal dies sized to apply a thin coat of varnish. The tuning of this method is simpler since the only variable, apart from the die-size, are the solids content and the viscosity of the varnish. Although die-wiping is best suited to vertical application, the method has been successfully used with horizontal oven-configurations for wires above $\approx 300\mu m$.

Concentricity - the evenness of the cured polymer-film around the wire - is determined by the alignment of the dies, and depends on the wire-catenary, although some self-adjustment is possible, due to the hydrostatic pressure caused by varnish flowing through the dies.

The oven-temperature profile is readily adjusted by switching a number of electrical heating elements along the oven-shaft, and by adjusting the inlet, recirculation, and

exhaust gas-flows. However, the stoving conditions are altered by the enamelling-speed (i.e., the rate of passage through the oven), and the heats of vaporisation of varnish-solvents. The rate of solvent-evaporation affects the temperature of the varnish during the early stages of curing, where the solvent is abundant, and for this reason, some ovens are designed with very hot ($\approx 400^{0}C$) inlets.

1.4.4 **Test procedures**

Wire-enamels are required to be flexible enough to withstand the bending and stretching which occurs during high-speed coil-winding. Electromagnet-wires are typically able to resist being wound onto their own diameters (viz., 1x **mandrel-wrap**) without breaking of the enamel-film or loss of adhesion to the metal substrate.

1.4.4.1 **Windability**

Windability is tested by twisting and stretching the wire, and then examining it for mechanical damage. A good wire-enamel is expected to stretch to the point where the wire snaps. Withstanding 20% elongation followed by winding onto a 1x mandrel-wrap, producing a total elongation of 70% at the outerlayers, will be sufficient for almost any winding procedure encountered in the manufacture of magnet-coils. However, this alone does not ensure successful winding; the wire-coating must also withstand abrasion, as the wire must pass over many guiding sheaves at high-speed, without tearing. The abrasion resistance has been improved by **dual-coating**; top-coat being one which has a high tolerance to abrasion. For example, poly(aramidimide) top-coats increase the abrasion resistance of polyamide enamel with little sacrifice in the TI.

Previously, a repeated abrasion test was employed in which the number of strokes of a weighted blade needed to strip the enamel away from the metal-wire, indicated the enamel's relative resistance to abrasion. However, polyamide coatings gave unusually low values by this test, albeit excellent windability. Thus, a single scrape test is now used in which the blade loading required to instigate failure is quoted, instead. The performance of polyamide coatings suggests that a low coefficient of friction is desirable to minimise damage.

Absolute measurement of the coefficient of friction for a polymeric surface is difficult. A relative value can be determined as a function of the tension along the wire while running it over a friction contact surface (e.g., a 20mm rod) and comparing that with a free-running wire (i.e., where the rod is driven).

Although polyamide enamels give the lowest surface friction of the currently available products, lubrication by oils and waxes is also used extensively. Generally, waxes are preferred since they do not interfere with the adhesion of encapsulants and trickle varnishes, used to bind rigidly the magnet-coils of motors, transformers, and chokes.

1.4.4.2 **Heat shock and solvent crazing**

Heat shock performance is tested by applying a rapid elongation followed by a mandrel-wrap (1x or 2x) after which the coil is heated to a given temperature for a specified time and cooled. The coil is then inspected for **beaks**; orthogonal splits on the outside of the coil. Such failure is indicative of undercured polymer, but where this is not the case, increasing the crosslink density and/or introducing heat-resistant chain-units into the polymer improved

resistance to heat shock.

Resistance to **solvent-crazing** is desirable to prevent electical breakdown of the film caused by the absorption of solvents. Susceptibility to crazing is assessed by immersing a loose coil of enamelled wire into the varnishes or solvents used for encapsulation or trickling. The wire is then wiped and inspected microscopically for cracking.

1.4.4.3 **Adhesion**

A very important property of wire-enamels is their key, or adhesion, to the wire-surface. Poorly prepared copper wire, with excessive oxide coating or greasy deposits, instigates low adhesion, and subsequently, the enamel tends to blister during thermal curing. Where the wire has survived curing and winding, service operating temperatures of 200^0C or above lead to unsatisfactory enamel adhesion, that is, bubbling or peeling may occur due to the formation of a non-adherant oxide at the metal-film interface.

Adhesion can be tested in a similar manner to abrasion resistance: after partially removing the enamel by scraping, a torsional deformation is applied to the scraped segment of wire. Where adhesion is inadequate, the damaged film flakes away from the wire.

1.4.4.4 **Electrical properties**

Winding of magnet-wire causes preferential thinning of the enamel at the sites of bending, rather than presenting fractures. Of course, thinning reduces the amount of dielectric material available for insulation, and therefore, the insulating properties depend on the mechanical loads applied during winding as well as the initial thickness of the film. However, the latter is somewhat variable since coatings on round wire lack perfect concentricity, and on rectangular

wire, coverage over the edges is not constant.

The procedure used for measuring dielectric strength attempts to simulate the thinning by tightly twisting segments of wire together, producing **twisted-pair** specimens. The predominant damaging effect of exposing such specimens to a continual voltage-stress is the mechanical erosion of the film due to corona (i.e., partial discharge). Corona is seen as an electrical discharge over the film-surface. The partial discharge-inception voltage (PDIV) for high enamel thicknesses[98] is about 200 volts per metre at 25^{0}C, decreasing with temperature. Heat-aging reduces this value, and increasing the voltage-stress above the PDIV reduces the useful life of various enamels, as indicated by the data of table 1.4 for the endurance of enamels subjected to a range of voltage-stresses.

Table 1.4 Voltage endurance at room temperature of various magnet-wire enamels, above the PDIV.[98]

Enamel Temperature Index (TI)	Endurance (hours) against the electrical stress (V)			
	300	600	900	1200
105	100	22	9	5
130	75	15	6.7	2.4
155	311	45	9.5	1.5
200	590	84	20	9
220	193	34	12	6

The capacitance of the insulating film is another property used to judge the suitability of a wire-sample for a particular purpose. The dissipation factor, or dielectric-loss factor, for a coating is a function of the DP, the crosslink density, and the concentration of polar groups; all of these factors may change with the extent of cure. Therefore, the state of cure can be readily monitored by %-dissipation. The sensitivity of this technique is increased

by measuring this property with temperature; a sharp decrease in %-dissipation is observed at a particular temperature, this inflection (viz., **knee-point**) correlates with the TI of the enamel being tested.

1.4.4.5 **Burn-out**

The capacity of the magnet-wire to withstand bursts of high temperatures, simulating current surges and overloads, is also tested using twisted-pair specimens. A high current is applied to the wire and the temperature monitored until **burn-out**; seen as smoking and charring. Resistance to burn-out tends to correlate with TI.

1.4.4.6 **Environmental factors**

The service environment of a magnet-wire significantly influences its performance and service-life. For instance, the burn-out temperatures for polyimide coatings are lowered by 150^0C when the test is conducted in refrigerant. Therefore, testing procedures should simulate, as nearly as practicable, the service conditions.

With the exception of refrigerant-immersed motors, and perhaps a few specialised machines operating while immersed in liquids or gases, industrial motors do not rely on the magnet-wire enamel for environmental resistance. Rather, the trickle-varnishes and encapsulants are applied to the coils, and provide a significant measure of protection.

1.4.5 **Poly(esterimide) wire-enamel**

Several investigators have published syntheses for, and characteristics of, novel PEI resins. Loncrini[99] describes the preparation of many arylene bistrimellitate dianhydrides by the acidolysis of TMA with aromatic diacetoxy compounds, and by the esterification of trimellitic acid monoacid chloride with diphenols. These were, in turn, condensed with

a variety of aromatic diamines, in polar solvents, to produce the imides. Maiti and Das[36] describe a synthesis of a dicarboxylic acid, containing an internal imide group, with EG. The three isomers (i.e., ortho, meta, and para) were obtained by the condensation of each respective aminobenzoic acid with TMA in N,N-dimethylformamide. The solubilities, solution viscosities, crystallinity and thermal stabilities of the products were evaluated. Whilst the ortho and meta isomers were found to be amorphous, the para isomer was crystalline. Thermal stability was qualitatively evaluated from the flexibility of polymer films left at 325^{0}C for 100 hours, and found to follow the order, para ≥ meta > ortho. The aromatic PEI's, especially those prepared from **p**-phenylene bis(trimellitate) dianhydride, were found to exceed the thermal performance of poly(amideimide)'s and polyesters. Maros and DeAbajo[100] have prepared a homologous series of PEI's by the polycondensation of the imide diacids with propylene glycol. The imide diacids were synthesised from TMA and aliphatic **omega**-amino acids ranging in length from one to five methylene groups. The softening temperatures of the PEI's were found to increase with the number of imide groups per unit mass of resin, but only for dicarboxylic imide components containing few methylene groups since increased chain flexibilty concurrently decreases the softening point. Yamada and Ikeda[101] have found 38μm films of PEI compounded with polyamide and polyimide gave better heat shock, heat resistance, abrasion resistance, and resistance to solvent-crazing than PEI only. Koenig et al.[102] has characterised poly-(N,N'-bis(phenoxyphenyl) pyromellitimide) with UV/visible Raman-IR, and Fourier transform IF spectrometries.

The published work has concentrated heavily on synthesis and characterisation, and only three papers have appeared,[103,104,105] concerning PEI's similar formulations to resin-SC (see §1.5.1). There is no literature concerned with curing-chemistry of PEI wire-varnishes.

1.4.5.1 **Formulation objectives**

Wound magnet-wire is normally encapsulated or impregnated with binding varnishes, therefore, the materials must be compatible. The solvents used in electrical varnishes should not attack other components of the insulation, the film should not contain ingredients that will migrate out and into associated insulation, degrading it, nor should degradation products attack other insulation materials. Compatability is established by accelerated aging tests for samples of the materials in question in contact with twisted-pair specimens, the electrical integrity of which is measured by the PDIV and the burn-out resistance (cf. §1.4.4.4 and §1.4.4.5).

The selected varnish-solvents must provide the proper evaporation rates, satisfying the temperature-profile of the curing oven employed and the enamelling speed desired, giving smooth, regular films. Optimally, the solvents should be of low cost, and the **solids-content** of the wire-varnish ought to be in the range of 30 to 50wt.%. Solids-content reflects the concentration of resins in a varnish.

Most resin systems can be made to achieve the desired results with cheap hydrocarbon-solvents. The higher TI resins need expensive, highly polar solvents such as dimethyl acetamide, dimethyl formamide, dimethyl sulphoxide, N-methyl pyrrolidone, or cresylic acid. The resulting varnishes are diluted with hydrocarbons which are generally the byproducts

of petroleum fractionation, and include ethyl acetate, acetone, cyclohexanone, and acetamide. Examples of extensively used proprietary diluents are Shellsol™ (Shell Chemical (Australia) Pty.Ltd.) and Pegasol™ (Amoco Chemicals Corporation).

Diluents are poor resin solvents, but at levels of ≈40vol.% of the "varnish" (i.e., resin in a polar solvent), they do not lower the overall solubility parameter sufficiently to precipitate the resin. The diluents are chosen to satisfy two criteria, to minimise the unit cost of the varnish, and to have a boiling range suitable for the curing oven, but lower than the solvent to avoid precipitation of the resin, during thermal curing. For example, a commonly employed diluent for ovens with hot inlets is Shellsol 1552™ which has a boiling range of 140 to 200^{0}C.

1.4.5.2 **Curing of magnet-wire varnish**

Macroscopically, the curing of wire-varnishes occurs in two fundamental processes; the removal of diluents and solvents, and the formation of a polymer network by polycondensation. Of course, these are simultaneous.

Where the rate of solvent evaporation is too rapid, **blistering** and **cratering** of the polymer film occurs; these are the major common film-defects. Where hot, dessicated air is blown across the varnish film, the solvent molecules at the surface are stripped quickly, leaving a solid semicured film riding on a cooler solvent pool. When solvents begin to leave this pool, expanding with increasing temperature, the film lifts and bubbles - blistering. Alternatively, where oven hot-spots boil-off the solvents prematurely, leaving undercured polymer behind, craters result.

Suppose further, that polycondensation proceeds too quickly, trapping the more polar solvent-molecules in the network, and that insufficient solvent remains to entrain the condensation byproducts (i.e, water and EG), then these byproducts are unable to escape readily, and in effect, retards curing. Where the solvents volatilise in the wrong order,[107] little **blow-holes**, or **pinholes**, appear over the cured film. Evaporation of solvents before diluents causes precipitation of undercured polymer, and pinholes result at the sites of such events. The undercured precipitate forms a spot of material which carbonises at the high temperatures encountered, leaving a hole in the enamel-film. It is imperative that solvent-removal be controlled so as to minimise film-defects. To this end, the temperature-profile of the enamelling oven used, and the evaporation of solvents/diluents must be compatible, with due consideration for the size of the wire to be enamelled, therefore, the enamelling-speed is chosen to maximised the energy-input to production-volume ratio. Plainly, a number of simultaneous processes occur. In practice, formation of the ideal thin, continuous film may not develop at all, and for this reason the varnish is applied in several coats, each covering the shortcomings of previous ones.

Fine-tuning the many variables, with due regard for the curing characteristics of the varnish and the continuously changing atmospheric conditions, is a "black art" requiring years of apprenticeship.

The testing procedures described in this section are destructive and time-consuming to apply, and therefore are only used in random-checking quality-control of the final product. However, the operator requires a quick, easily app-

lied method to judge coating-quality during production; the the **jerk-test** and the colour of the cured enamel. The jerk-test is a simple method of checking the extent of cure; a length of wire is snapped. A well-cured sample exhibits a single concentric break, leaving behind a smooth film adhering to the metal substrate, but an undercured sample results in multiple breaks with a loss of film adhesion, and is detected by running a finger-nail along the wire. The colour of the cured enamel is another indicator of the state of cure; for PEI's, a light straw colour generally suggests insufficient baking, while pale brown is considered ideal. A dark brown colour, however, indicates over-baking, whence the enamel becomes too brittle, and cannot withstand a 1x mandrel-wrap, which can also be readily applied.

1.5 **The PEI wire-varnish**

The PEI wire-varnish is made-up of a resin, resin-SC, which is the film-former, two modifying resins, added to improve the flow and wetting properties of the varnish, those being, Phenolic 709™ and Mondur SH™, a transesterification catalyst, and the solvent system.

1.5.1 **The PEI resin (resin-SC)**

Resin-SC was synthesised according to a patented formulation[107(a)] (cf. table 1.5), and resulted in an amber-coloured, brittle solid, melting at about 53(±4)^{0}C. The incorporation of THEIC, as a high temperature crosslinker, compromises the flexibility of the basic polymer[2] (cf. figure 1.3), and the resultant wire-enamel is found to be less flexible than other proprietary PEI enamels. However, by the same token, the resultant Isomid coating has better resistance to high temperatures.

The monomers, or **resin-precursors**, are mixed together and refluxed at 220^{0}C until the distillate has an acid value between 6 and 8mgKOH/g_{resin} (see appendix I for the standard test method used in determining acid numbers).

Table 1.5 The formulation[107(a)] for the PEI oligomer, resin-SC. The information presented here has been patented by Schenectady Chemicals, Inc.; the parent company of SCA.

Component	Ratio, wt.%	Moles/(gram of resin)
Ethylene Glycol (EG)	14.6	2.280×10^{-3}
THEIC	35.0	1.342×10^{-3}
Trimellitic Anhydride (TMA)	21.7	1.290×10^{-3}
Methylene Dianiline (MDA)	9.9	4.989×10^{-4}
Terephthalic Acid (TA)	18.8	1.133×10^{-3}

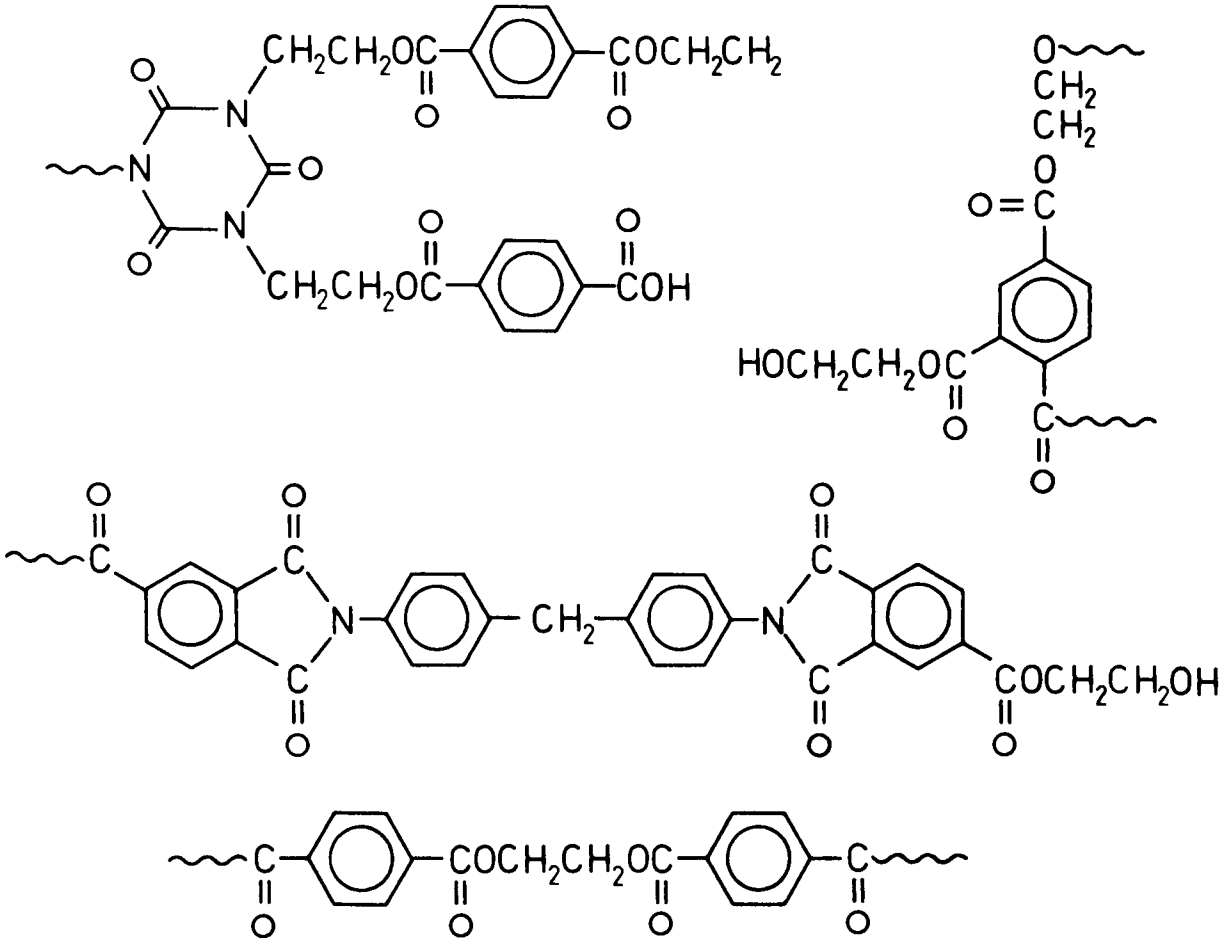

Figure 1.3 The approximate structure of resin-SC; assumed from the expected esterification and imidisation reactions. The latter results in the formation of the more stable imide heterocycle, rather than the alternative amide functions (cf. §2.3.1).

1.5.2 Formulation for Isomid* wire-varnish

The patented formulation[107(b)] for Isomid was used to produce the wire-enamel coating which is the subject of this thesis is given in table 1.6, and will be referred to by the tradename, Isomid. Isomid wire-varnish is manufactured by dissolving the resin in (B), (C), and (D), and then heating the mixture to 120^{0}C, with agitation, until completely dissolved. The solution is allowed to cool to 88^{0}C, and then (E), (G), and (H) are added, before again heating to 120^{0}C for 2 hours. The Gardner-Holdt viscosity of the resulting wire-varnish should be V3/4, and the solids-content about 39.2%. The resin modifiers and the catalyst are premixed into a little cresylic acid prior to addition to the bulk of the resin/solvent/diluent mixture, avoiding the precipitation of any of the resin ingredients.

Table 1.6 A typical formulation[107(b)] for PEI wire-varnish which was patented by Schenectady Chemicals, Inc., and is wire-varnish is marketed under the name, Isomid.

Components	Ratio (wt.%)
A. PEI resin	41.5
B. Cresylic acid, CA-43	13.6
C. Phenol	10.2
D. Solvesso 100	19.4
E. Tetraalkyl titanate, catalyst	1.4
F. Ethylene glycol	1.9
Resin modifiers	
G. Blocked isocyanate (Mondur SH™: a triisocyanate cyclised from toluene diisocyanate (Mobay Chemicals, Inc.) -wt.% dissolved in CA-43 and Solvesso 100)	7.9
H. Phenolic resin (Phenolic 709™: a m,p-cresol/formaldehyde resin (SCA) -wt.% dissolved in CA-43)	4.1

Note. The cresylic acid cited, CA-43 is a product of Merichem Co., and has the following composition (wt.%): 6-8 phenol, 9-10 o-cresol, 15-20 m-cresol, 8-11 p-cresol, 1-3 o-ethylphenol, 9-11 m-ethylphenol, 3-5 p-ethylphenol, 1 of 2,6-dimethylphenol, 11-17 of 2,4- & 2,5-dimethylphenol, 10-13 of 2,3- & 3,5-dimethylphenol, 5-8 of 3,4-dimethylphenol, and 1 of 2,4,6-trimethylphenol.

*Isomid is a trademark of Schenectady Chemicals, Inc., and denotes their range of poly(esterimide) wire-varnishes.

The diluent, Solvesso 100™ (Exxon Chemicals, Inc.) is a mixture of tetramethyl benzene with dialkyl and trialkyl benzene having a boiling range of 182-204°C.

The aim of the Isomid formulation is to yield a wire-enamel of outstanding thermal properties; capable of withstanding a heat-shock of 260°C, usually 200°C, and a burn-out exceeding 400 secs.

1.5.2.1 **The solvent system**

The solvent system consists of two components, one which dissolves the resins (viz., solvents), and another dilutes the solvent (viz., diluents) and modifies the boiling characteristics of the system. Commonly, the diluent is made up of aromatic hydrocarbons with boiling ranges ensuring that these evaporate before the solvent, during the thermal curing of the varnish. This prevents resin-precipitation during the early stages of curing, where the polymer-film has not yet formed. Evaporation also cools the reaction mixture, preventing undesirable crusting at the surfaces of varnish pools (see §1.4.5.2) which lead to blistering of the film.

Table 1.7 Typical components of cresylic acid.

Fraction	Boiling Range (°C)	Components
phenol	182	-
o-cresol	191	-
m,p-cresol	200-203	m,p-cresol;2,6-xylenol;2,4-;
xylenols	207-222	2,5-;2,3-;3,5-xylenols;o,m,p-ethylphenols;2,4,6-trimethyl-phenol;o-propylphenol
"high boilers"	223-240	3,4-xylenol;ethylmethylphenols ;other trimethylphenols and propylphenols

Note. Cresylic acids are coloured pale yellow (straw-coloured) to brown.

The solvent provides a medium for the curing reaction, and as such, any chemical reactions between the solutes and

solvents influence the rate of film-curing. Cresylic acid is a coal distillate composed of phenol and many of its homologues. Table 1.7 lists the main components of common commercial cresylic acids. The hydroxyl groups of cresylic acid can partake of condensation reactions with resin-SC, and this issue is discussed extensively in chapter 3.0.

Table 1.8 The gas chromatographic analyses of two cresylic acid samples.

Compnonent	Ratio (wt.%) Supplier (a)	Supplier (b)
phenol	5.9	19.5
o-cresol	6.3	13.8
m,p-cresol	70.5	45.7
low boilers	11.4	16.1
high boilers	5.9	4.9

Note. Supplier (a) is Kono Chemical Co. Ltd., and supplier (b) is Dr.Kurt Herberts & Co. verm. Otto Louis Herberts.

Cresylic acids vary widely in formulation, depending on the supplier. Table 1.8 gives the gas chromatographic analyses of two proprietary cresylic acids. Generally, the desirable level of phenol is ≈10wt.% which has been determined empirically by the industry, and supply (a), of table 1.8, is expected to be troublesome in wire-enamelling; the curing-characteristics of varnishes are greatly affected[108] by the amounts of each of the phenols. Whenever pin-holes and blistering of the film cannot be suppressed by oven-tuning, a common "trick" is to boost the phenol-level of the varnish by ≈2wt.%. It is believed that the presence of phenols maintains relatively slow, even vaporisation of solvents, helping condensed water and EG to leave the film, minimising disturbances to, and irregularities, in either the surface or the integrity of the polymer-film.

The component-ratios can be determined by either the source of the acid or by blending pure phenols. Table 1.9

lists the constituents of cresylic acids obtained from the coal tar and petroleum, and compared with two blended acids.

Table 1.9 The component ratios[109] (wt.%) of two cresylic acids derived from natural sources, compared with two synthetic examples.

Component	Coal Tar Distillate	Petroleum Distillate	Synthetics I	Synthetics II
phenol	45	24	33	40
cresol	12	18	19	20
m,p-cresol	30	28	32	31
low boilers	12	24	16	9
high boilers	1	6	-	-

1.5.2.2 **Enamel modifying resins**

Additional resins are incorporated into the wire-varnish to improve flow and adhesion to the metal-wire substrate, as well as the previous enamel coating (cf. §1.4.3). The addition of small amounts of epoxides, polyisocyanates, polyamides, and phenolic resins are used to achieve these ends.

Isomid contains two such modifiers: Phenolic 709, a resole-phenolic resin based on **m**- and **p**-cresols; and Mondur SH, a phenol-blocked* triisocyanate produced by cyclising toluene diisocyanate. These reactive resins copolymerise with resin-SC, but since they are incorporated in only small amounts (≈3wt.%; cf. table 1.6), do not significantly modify the physical properties of the finished polymer-film.

1.5.2.3 **The proprietary catalyst, "Tyzor TBT"**

"Tyzor TBT" is a partially polymerised tetrabutyl titanate supplied by E.I. du Pont de Nemours & Co. (Inc.). The specification of the properties of this product are quoted from du Pont's technical information (cf. table 1.10).

---

*Phenol-blocking is widely used to protect the highly reactive isocyanate groups in commercial polyurethane prepolymers: $-NH-C(O)-OC_6H_5$.

Carbon NMR of neat "Tyzor TBT" (see §2.3.9) showed the presence of a contaminant, probably ethoxyl ligands,[110] with signals at 19 (methyl) and 71ppm (methylene), in addition to the four butoxyl-ligand signals[110] at 14.3(methyl), 19.6(gamma-methylene), 36.1(β-methylene), and 74.8ppm(α-methylene). The contaminant is not likely to interfere with the functioning of the catalyst since, when mixed into the varnish, all alkoxyl ligands are expected to be substituted by either aroxyl ligands, by ester exchange with the phenols of cresylic acid, forming the more stable aryl titanates, or HE (2-hydroxyethyl) chain end-groups of resin-SC to form most stable chelates (cf. appendix VI). The condensed alkyl alcohols, butanol and possibly ethanol, are easily evaporated from the wire-varnish.

Table 1.10 The properties of the proprietary tetrabutyl titanate, "Tyzor TBT".

Property	Value
Molecular weight (g/mole)	340
Ratio of titanium (wt.%)	14.1
Ratio of titanium dioxide (wt.%)	23.5
Appearance	pale yellow
Specific gravity (at 25^{0}C)	0.99
Viscosity (centipoise, at 25^{0}C)	65
Flash point (Pensky-Martens Closed Cup Tester) (^{0}C)	47
Effect of water	rapid hydrolysis

Note. The catalyst was supplied by E.I.du Pont de Nemours & Co.(Inc.)

2.0 Experimental techniques and materials

2.1 Characterisation methods

The experimental techniques used to synthesise model compounds, and to characterise them, as well as the resin, are described and discussed in this chapter. It was deemed most efficacious to adopt the format of listing the spectrometric analyses along with the experimental procedures and yields, allowing the discussion of results (in chapter 3.0) pertaining to the resin, its varnish, and its enamel, to develop smoothly, without unnecessary disruptions to describe incidental data. Therefore, many important facts are presented in this chapter, laying a foundation for an exposition of the resin's nature, and the curing electromagnet-wire coatings.

The characterisation techniques are presented first since data yielded by them is quoted in the compound descriptions following. The fundamental techniques employed were proton and carbon-13 solution, as well as solid-state NMR spectrometries; the last technique is described in some detail, due to its comparative novelty. Where well known techniques are described (viz., solution NMR, mass spectrometry, differential scanning calorimetry (DSC), infrared spectroscopy (IR), and gas chromatography (GC)), only the instruments and instrumental conditions are presented. The only chemical analytical method adopted was the acid/base titrations used to determine the concentrations of the reactive chain ends-groups; the standard test procedures of SCA were adopted.

2.1.1 High resolution fourier transform nuclear magnetic resonance spectroscopy of solutions

High resolution spectra were measured with two instru-

ments: a Brüker WP80, at a static field frequency of 80MHz for ^{1}H spectra, and 20.1MHz for broadband decoupled (BB) ^{13}C spectra; and a Brüker CXP300 for ^{1}H (at 300.13MHz), and ^{13}C (at 75.47MHz) spectra. Sample concentrations were about 10 mg/cm^3, and tetramethyl silane (TMS) was used as internal chemical-shift reference except where solvent signals (having been referenced to TMS) were more convenient references. Chloroform(d1), benzene(d6), and DMSO (d6) were used as internal locking solvents, but where they were not compatible with the sample solution an external lock of D_2O, sealed in a capillary tube, was used instead. Wherever NMR data is quoted, the dissolution and locking solvents as well as the field frequency are specified in brackets. Where only a locking solvent is declared, the samples had been made-up in perdeuterated spectroscopic-grade solvents, acting as both dissolution and locking solvents.

All NMR experiments were performed at ambient temperature (297±3K). Both spectrometers used a phase alternating pulse sequence (PAPS) in quadrature signal detection mode. Where NMR data is quoted for experiments performed at some other temperature, that has been given along with the other experimental parameters.

The BB^{13}C-NMR spectra were acquired using the following parameters: a 3.5μsec/45^{0} carbon pulse; ^{1}H broadband decoupling at 2W with a resonant frequency offset of 5800Hz; spectral width of 5000Hz; analytical offset frequency of 10500 Hz; and an 8k data table. To improve signal resolution a Lorentz-Gaussian multiplication of the free induction decay (f.i.d.) was applied, yielding a line broadening of 1Hz.

Before describing the gated resonance technique used to suppress the nuclear Overhauser effect (NOE), which disallows the use of peak integrals to count the numbers of carbons atoms in the molecules of the sample, it is necessary to mention the measurement of T_1 values. These values are the longitudinal or spin-lattice relaxation rates[110] upon which gating relies. The value of T_1 is determined from the rate of equlibration of the macroscopic magnetisation vector ($M_{z'}$), for the nuclear spin ensemble, to the value of the unperturbed magnetisation vector M_0; aligned with the static magnetic field (B_0), following perturbation into the -z' direction of the rotating frame. The method used to measure T_1 was the inversion recovery technique[111] (cf. figure 2.1) in which a 180^0 pulse inverts the macroscopic magnetisation (i.e., $M_{z'} = -M_0$) followed by a delay time (τ) between pulses. This time is the experimental variable. The residual magnetisation, after decaying toward M_0 during τ, is then measured by triggering a 90^0 B_1 pulse to bring $M_{z'}$ into the x-y plane where the f.i.d. can be scanned. The initial amplitude of the f.i.d. is directly related to the magnitude of the residual $M_{z'}$ vector, and is in turn related to T_1 by the Bloch equations for the condition, $M_{x'} = M_{y'} = 0$. Hence,

$$dM_{z'}/dt = -(M_{z'} - M_0)/T_1 \quad .$$

Integrating this equation for the condition, $M_{z'} = -M_0$ at time (t) = 0 leads to

$$M_{z'} = M_0(1-2\exp(-t/T_1)). \qquad (2.1)$$

According to this relationship, no signal can be observed when $M_{z'} = 0$. For this condition, equation (2.1) becomes

$$\tau_0 = T_1 \ln 2 = 0.693T_1 \quad , \qquad (2.2)$$

and from this, T_1 can be determined. However, this null method is not accurate due to inhomogeneity in the static magnetic field (B_0), in which case the spin ensemble is not completely inverted from M_0 by the 180^0 pulse. The slope of a semilogarithmic plot of the f.i.d. intensity ($M_{z'}$ - M_0) against τ yields a more accurate value for T_1. Notwithstanding this error, the null method was utilised to estimate the T_1 of resin-SC; a τ_0 of about 100msec was obtained, giving a T_1 of about 0.14 seconds from equation (2.2).

Having established the value of T_1, an inverse-gated, decoupled ^{13}C-NMR experiment on the proprietary resin was performed in order to suppress NOE. The pulse sequence for this experiment is illustrated in figure 2.2. A recycle time of 30 seconds was used, yielding $M_{z'} = (1 - 1.7x10^{-93}.M_0)$ (cf. equation (2.1)); the spin ensemble had sufficient time for more than 99% to equilibrate to M_0. Effective suppression of the NOE permitted integration of carbon signals.

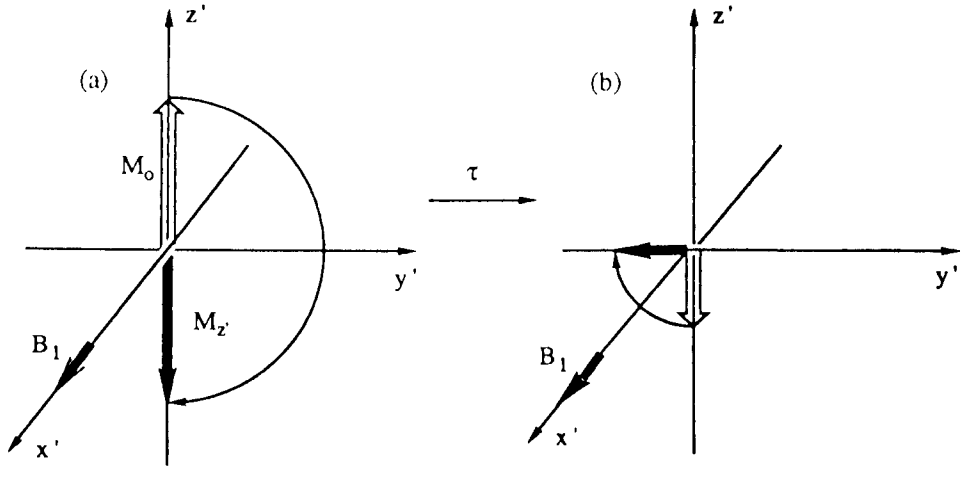

Figure 2.1 Determination of T_1 by 180^0, τ, 90^0 sequences. (a) **M** is inverted by a 180^0 pulse at time 0. (b) After time τ, a 90^0 pulse rotates it to the y (or -y) axis. The initial amplitude of the f.i.d., after the 90^0 pulse, is proportional to the value of M_z at time τ. Thus, the magnitude of **M** is negative at small τ (as for (b)), increasing exponentially (viz. eq. (2.1)) towards a positive asymptote (**M** = M_0).

Another technique utilised in the assignment of carbon signals was off-resonance proton decoupling. Irradiating the sample with a ^1H decoupling field that is just off the resonant frequency achieves partial decoupling; nuclei experiencing first-order (caused by one-bond) and second-order (long range) coupling give broadened carbon signals, while quaterary nuclei exhibit no substantial change in peak width. Peak broadening behaviour characterises the respective carbon nuclei, of the sample molecule, with respect to the direct attachment of protons. A decoupling frequency offset of 4500Hz was used.

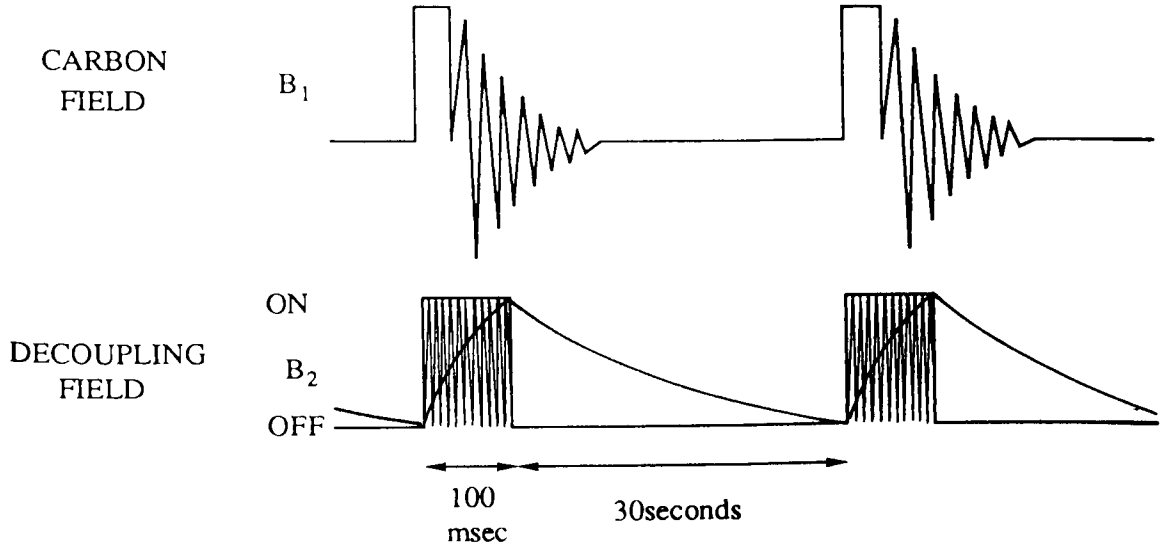

Figure 2.2 Pulse sequence for inverse-gated, decoupling experiments.[113] The decoupler is switched on during data acquisition; the NOE is suppressed, while the protons are decoupled. The red trace signifies the magnitude of the NOE.

^1H-NMR spectra were obtained on the Brüker CXP300 with a spectral width of 4000Hz, a 45^0 proton pulse of 12μsec, and a 16k data table. The Brüker WP80 was also used for ^1H-NMR spectra, in these cases a spectral width of 1000Hz, a pulse of 10μsec, and a 4k data table were used. TMS was used as the internal reference and the error in peak integration was found, by duplicating NMR spectra, to be better than

0.03 proton units.

2.1.2 Proton enhanced, cross-polarised magic-angle spinning carbon NMR

A Brüker CXP300 NMR spectrometer was used to obtain ^{13}C solid-state spectra of samples of cured wire-enamel and solid resin.

NMR spectra of solids obtained by conventional means show peak broadening of the order of 20kHz because of strong dipolar coupling (^{13}C-^{1}H; ^{13}C-^{13}C) and chemical shift anisotropy (CSA). In order to produce high resolution spectra, for structural (viz., chemical shift) information to be extracted, the line broadening needs to be reduced. The techniques required to achieve this have been reviewed extensively by Schaefer and Stejskal,[114] Havens and Koenig,[115] and O'Donnell.[116] Since these are not yet widely familiar, a brief summary follows.

The resonant frequency of a ^{13}C nucleus depends on the magnetic field which it experiences. In addition to this static magnetic field (B_0, defined to be in the z'-direction), local fields (B_{loc}) arising from neighbouring nuclei with non-zero quantum numbers are present, generating local magnetic dipole moments (μ) opposed to B_0. The z'-component of a local field at nucleus **1**, generated by a neighbouring nucleus **2**, is given by the relationship,

$$B_{loc} \approx \pm\mu(3\cos^2\theta - 1)/r_{1,2} \quad ,$$

where $r_{1,2}$ is the distance between the two nuclei and θ is the angle between B_0 and a vector joining the nuclei. The sign describes the two possibilities for the neighbouring spin; either parallel or antiparallel to the external field. We can now see that the effective magnetic field observed at nucleus 1 is $B_0 \pm B_{loc}$.

The major source of the static dipolar interaction is between carbons and protons in a solid sample, wherein there may exist many pairs of spins with different r and θ, and therefore different B_{loc}, producing an envelope of characteristic line splittings manifested as a broad Gaussian lineshape of width 10-40kHz. To reduce this heteronuclear coupling, a decoupling field of 100W or more is applied, producing a considerable sharpening of the solid-state resonances (peakwidths $\approx$5kHz), and thereby an improvement in signal-to-noise ratio.

The residual broadness is attributed to CSA and dipolar interactions (homonuclear). The principal cause is the anisotropy of the electron density surrounding carbon nuclei. Generally, the Larmor frequency of a spinning carbon nucleus is a function of its molecular orientation in B_0, and thus, the observed chemical shift is dependent upon the orientation of the atomic and molecular electron clouds with respect to B_0. Whereas in a liquid the averaging effect of rapid molecular motions yields observable isotropic chemical shifts, the anisotropy of the immobile molecules in amorphous solids or crystal powders results in a complicated lineshape which represents the sum of all the similar chemical shifts.[117]

Line broadening due to CSA can be reduced by mechanically spinning the sample[118,119] since the time-averaged dipolar Hamiltonian scalar is proportional to $3\cos^2\beta-1$,[118] where β is the angle between the bond axis and B_0, and since the magnitude of CSA can conveniently be expressed in terms of a mechanical rotation angle,[120] the effect of CSA is reduced to zero when the solid sample is spun at 54.7^0 (the

magic angle) to B_0. However, the sample spinning rate must be comparable to the frequency bandwidth of the CSA (≈1-5 kHz). This method has been demonstated to be valuable in the characterisation of solid polymers[121] as the peakwidths are reduced to the order of 100Hz. Since the dipole-dipole interactions cause wide, structureless line shapes, of ≈20kHz in breadth, where no line-narrowing techniques are employed, it has been suggested that total suppression of CSA might be achieved by magic-angle, sample spinning (MASS) when the sample is spun at a similar frequency.[116] However, this is not attainable with contemporary instumental technology and so cannot be demonstrated. Excellent review articles have been written on this subject by Andrew.[122,123]

The Brüker CXP300 was used to obtain MASS^{13}C spectra of solids with spinning rates of 2 to 3kHz along with high-powered dipolar decoupling.

Although combining dipolar decoupling and MASS techniques allows high resolution ^{13}CNMR spectra of solids to be obtained, Fourier transform (FT) experiments on such samples suffer from three additional problems, inherent to ^{13}C nuclei: first, the magnetic moment of such a nucleus is low, about 1/4th that of the proton, resulting in a low net magnetization; also, the natural abundance of this isotope is only 1.1%, lowering signal strength; and finally, T_1's of the ^{13}C spin system are 10-100 times longer than for the protons in the same molecule. These problems can be overcome by using the technique known as cross polarisation (CP), or proton enhancement (PE),[124] where magnetisation is transferred from the proton spins to the carbon spins. The rate of such transfer is characterized by a contact time; the

length of time the carbon magnetisation is allowed to interact with the carbon radio frequency (r.f.) field while the proton r.f. field is removed (T_{cp}). Schaefer and Stejskal[114] have used this parameter to study the spin-spin contribution in T_1.

Sensitivity enhancement by CP was introduced by Hartmann and Hahn[124] and applied to ^{13}C-NMR by Pines et al.[125] Under normal conditions, transfer of polarisation from protons to carbons in B_0 is slow due to the mismatch of their Larmor frequencies, meaning that the mutual ^1H-^{13}C spin flips required for a CP transfer are not energetically favourable. The Boltzmann population distribution in the two spin systems may be defined in terms of their **spin temperatures** (T_s), and for two energy levels, their population ratio (n_1/n_2) is given by Boltzmann's law,

$$n_1/n_2 = \exp(-\Delta E/RT_s) \quad ,$$

where ΔE is the energy difference between the two levels. From this equation, small population differences mean high T_s, and large differences mean low T_s; the latter is synonymous with a large spin polarisation, and thereby an increased NMR signal intensity. Through dipolar coupling, the rare, **hot** ^{13}C spin system can be brought into **thermal** contact with the larger, **cold** ^1H spin system. A large **temperature** decrease in the ^{13}C system can occur while the **temperature** of the ^1H system increases only slightly due to its high **heat capacity**. Hartmann and Hahn[124] found that this condition could be achieved by letting the two spin systems precess in their respective rotating-frames at a common frequency; a double rotating-frame spin-lock experiment. The spin-flip energies (i.e., the Zeeman levels) in the rotat-

ing-frame of the ^{1}H and ^{13}C spin systems are matched, and the spin systems are effectively coupled through dipolar interactions. For transfer of spin magnetisation between these nuclei to take place, some of the precessional components of the two spin systems must have the same angular frequency (ω). This cannot be so as long as they both precess about B_0. However, **thermal** contact is possible in the rotating-frame if the Hartmann-Hahn condition is fulfilled, that is,

$$\omega_C = \gamma_C . B^1_C = \gamma_H . B^1_H = \omega_H \quad ,$$

where the ω_C and ω_H are the carbon and proton precessional frequencies; γ_C and γ_H are the ^{13}C and ^{1}H gyromagnetic ratios, and B^1_C and B^1_H are the magnitudes of the carbon and proton r.f. fields, which are applied simultaneously. The theoretical upper limit to the signal enhancement, over a conventional 90^0 Bloch decay, is given by the ratio, $\gamma_H / \gamma_C \approx 4$. By adjusting the ^{13}C r.f. field, the Hartmann-Hahn condition is attained by polarisation of **hot** carbon nuclei by **cold** proton nuclei, which are spin-locked onto an r.f. field at 90^0 to B_0. A significant advantage of the CP technique is that it allows the use of recycle times of the order of the spin-lattice relaxation time of the protons, $T_1(H)$, rather than the spin-lattice relaxation time of the carbons, $T_1(C)$. Practically, $T_1(H)$ is generally much shorter than T1(C), therefore the carbon pulse repetition rate is much greater with CP than with conventional 90^0 carbon-spin pulses; in solid polymers $T_1(H)$ requires no more than 100μsec. Once the protons are allowed to repolarise in the z-direction the carbons may be pulsed again to accumulate more data. Although for polymers at room temperature, the recycle time can be less than 0.5 seconds,[114] it is usual to set a pulse

cycle time of $5.T_1(H)$ to ensure that most (about 99%) of the nuclei equilibrate.[126]

The application of CP can go beyond the accumulation of structural information,[125] to the study of molecules absorbed on surfaces,[127] the characterisation of mobility and phase transitions of macromolecules,[128,129] and to the study of liquid crystals.[130] In addition to accessing well resolved spectra, studying the FT line resonance amplitudes as a function of CP contact time, yields valuable dynamic information for determining relative group mobilities.

Application of both CP and MASS techniques reduces peakwidths to about 500Hz, and spectra can be obtained in times comparable to solution NMR.

A particularly cogent aspect of the CP technique is its efficiency. For efficient CP, $T_1^C > T_1^H$; the repetition rate being limited by T_1^H (usually less than one second for polymers), and not the former (of the order of 10 to 4000sec). Improvement in the signal-to-noise ratio by accumulation of f.i.d.'s is only observed for those cases where CP is an efficient process, that is, where there exists a substantial static dipolar interaction. Even so, sharp lines, although at reduced intensities, are common for polymers with substantial chain-segmental freedom, as in the spectra of solid elastomers above their glass transition temperatures. The reduced intensity is due to microscopic rotational motions which compromise the near static dipolar interactions, needed for the transfer of polarisation during the carbon-proton CP contact period. The dipolar Hamiltonian[114] for the doubly-rotating frame, depends on both the distance between the two coupled spin-systems, and the angle between this macroscopic

vector and B_0. For highly mobile spin-systems, the magnitudes of these independent variables will vacillate, occasioning uncertainty in the static interaction component; the dipolar Hamiltonian scalar is reduced in magnitude, and the signal intensity diminishes. A significant implication is that unreacted substances, existing within polymer matrices as isolated free molecules, are not likely to give rise to strong signals during CP NMR experiments. Therefore, additives such as lubricants, plasticisers, and solvents; materials used in industrial processing of polymers, can be assumed to be virtually invisible by solid-state NMR.

The high-power, decoupled CP-MASS ^{13}C-NMR spectra were acquired with a Brüker CXP300 spectrometer using the following instrumental parameters: a ^{13}C field-frequency of 75.47 MHz with a 6kHz offset and a 20kHz sweep-width; the ^{1}H and ^{13}C r.f. fields were approximately 1.4 and 5.6G, respectively, for a precessional frequency of 63kHz; a recycle time of 5 seconds; a 90^0 carbon pulse size of 4.2μsec; a contact time of 1 msecond; and a probe temperature of 297±3K. Where spinning side-bands were suppressed, this was achieved using the TOSS pulse sequence.[131] The samples were packed into hollow Andrew-Beams rotors[120,132] which were machined from Kel-F with mushroom caps made of delrin, providing a prominent resonance at 88.5ppm used as a reference. The solid samples were either in the form of a fine powder, as with the resin, or as fine scrapings, with the cured wire-enamels.

Molecular regions of greatly differring mobilities were distinguished as either **liquid-like** (regions of relatively short relaxation times), or **solid-like** (the complimentary

regions of longer relaxation times) using PESOLIQ*, a novel pulse sequence. Details of PESOLIQ are not available to be described. For alternative reference, a short discussion of such discrimination techniques is given by Harris.[133] Notwithstanding the above reservation, the pulse sequence differentiates between molecules which are constrained in their motions and those which are relatively mobile; the distinction is made on the basis of a difference in susceptibility to cross polarisation, which in turn depends on static, dipolar interactions; as we have seen, this property differs between the constrained and the very mobile molecular portions.

2.1.3 **Infrared (IR) spectroscopy**

Infrared spectra were obtained with a dispersive Perkin-Elmer instrument; model 683. Each spectrum was calibrated against the 1602cm^{-1} band of polystyrene. The infrared samples were prepared as nujol mulls on NaCl discs, and where spectra below 800cm^{-1} were needed KBr discs were preferred.

The IR bands are characterised by broadness and sharpness with the codes: V (very), S (strong), B (broad), W (weak), and sh (sharp). The spectra were obtained at room temperature.

2.1.4 **Gas chromatography (GC)**

A Carle Instruments, Inc. analytical chromatograph, model 311, was utilised. A standard polar Carbowax 20M column with a poly(ethylene glycol) liquid phase was used at 210^{0}C. An inlet temperature of 230^{0}C was selected, and the carrier gas was high purity helium. The elutants were de-

*PESOLIQ is an NMR pulse sequence designed by Dr.E.H.Williams, in the early 1980's, at the University of Adelaide, NMR Centre, and is presently yet to be patented.

tected with referenced dual thermistors by monitoring the thermal conductivity of the carrier gas at the column outlets.

Analyses of the relative molar ratios of the components in distillates from esterification reactions were achieved by GC. The component fractions were approximated with respect to the total area under each chromatogram, ignoring the small differences in molar thermal conductivity of each component on detector response. Duplicate measurements of peak areas were obtained by cutting out and weighing each peak in the chromatograms.

The relative standard deviation for this integration method was estimated by cutting-and-weighing five photocopies of a chromatogram of a three-component mixture (water, EG, phenol); the result was 2.46% which is close to McNair's[134] estimation (i.e., 1.79%) for ten runs of an eight-component mixture.

2.1.5 **Differential scanning calorimetry (DSC)**

The use of DSC in the study of condensation polymerisation was found to be limited by the vaporisation of condensation products, which tend to escape from the sample pans, blocking the purge gas line-filters. Such events may lead to overheating of the sample holders, resulting in fusion of the heating elements. Where this method was used, the experiments were conducted on a Perkin-Elmer instrument, model DSC-2, fitted with an Auto Scan-Recorder Chart Controller accessory. Samples of 5.5mg were weighed and hermetically sealed into aluminium pans, referenced against an empty pan. High purity nitrogen was used to purge the sample holders, at a pressure of 240-260kPa. A heating rate of 20deg./min.,

a cooling rate of 320deg./min., over a temperature range of 330K to 750K, and a scanning sensitivity of 5 mcalories/second were the experimental parameters used.

The temperature of second-order changes in the heat capacity of the sample (i.e., glass transition temperature) were defined to be the temperature at which the initial deviation from the baseline occurs (i.e., the low-temperature inflection), and was measured to be the intersection of the projections from the baseline and the riser, the knee-point.

2.1.6 **Acid number determination**

The acid number of resin-SC (i.e., the number of carboxyl groups per gram of resin) was determined by titrating with a standardised 0.845M methanolic solution of potassium hydroxide (KOH). Three samples of resin (0.8-5g) were dissolved into 100cm^3 of a non-acidic solvent mixture; 50 vol.% propan-2-ol(AR) and 50vol.% DMSO. The solvent mixture was first neutralised by titrating with standard KOH, against phenolphthalein.

The method was validated by titrating known masses of benzoic acid(LR); of four titres, for titrations on masses between 0.0549 to 0.2613g, the standard deviation for the differences with the calculated titres was found to be 0.4 ml of standard KOH. However, the error is likely to be greater than that indicated by the techniques reproducibility, as the end-point is indistinct (given, in the test method, as the persistence of a pink colour for 15 seconds).

Four samples of the resin were similarly titrated according to the standard SCA procedure (cf. appendix I), giving an acid content of $1.91(\pm0.05)\times10^{-4}$moles/gram of resin; corresponding to an acid number of $10.5(\pm0.5)$mgKOH/g_{resin}.

The hydroxide ion is a very reactive species, able to hydrolyse ester as well as the carboxyl groups; a side-reaction which generates new carboxyl groups which consumes still further quantities of hydroxide ions. Since ester hydrolysis is slower than acid hydrolysis, the speed of titration is also a variable affecting the final titre volume.

Notwithstanding this shortcoming, the titres obtained were within the scatter expected, that is, the overall variation was within 0.4ml.

2.1.7 **Hydroxyl number determination**

The concentration of the resin's hydroxyl chain end-groups in resin-SC was estimated by titration with standard methanolic KOH. Prior to titration, the OH ends were esterified with an excess of acetic anhydride in pyridine. The unreacted acetic anhydride was hydrolysed to acetic acid which was titrated. The difference between this and a parallel blank titre (i.e., without resin) gave the amount of acetic anhydride consumed by esterification with the resinous OH groups.

Table 2.1 The triplicate results for the titration of the excess acid anhydride in the hydroxyl number determination for the PEI resin, resin-SC. The method is given in appendix I.

Sample mass (g)	Blank titre (ml)	Sample titre (ml)	Hydroxyl number[(1)] ($mgKOH/g_{resin}$)
1.4541	29.34	17.23	173
1.4926	29.34	16.76	175
2.0354	29.34	11.58	181

Notes. The standard methanolic KOH concentration was $3.76(\pm0.02)\times10^{-1} mol.dm^{-3}$, being standardised against benzoic acid.

The averaged hydroxyl number is $176(\pm4) mgKOH/g_{resin}$.

The corrected average hydroxyl number (calculated by subtracting the acid number from the hydroxyl number) is $165(\pm5) mgKOH/g_{resin}$.

The hydroxyl number was expressed as the milligrams of KOH equivalent to one gram of the resin sample. Since the

titre determined includes the titration of the acid ends along with acetic acid, the titre was adjusted accordingly with respect to the acid number calculated in §2.1.6. The results are given in the notes accompanying table 2.1.

The standard SCA test procedure was used to determine the hydroxyl number (see appendix I).

2.1.8 **Mass spectrometry**

In mass spectrometry, gas phase ions are formed from the sample under consideration, and those ions are then separated according to their mass to charge ratio (m/e). The greatest advantage of this technique is that it can give detailed information about chemical composition with only a few micrograms of sample, and was used to study scrapings of Isomid wire-enamel.

The instrument employed was a ZAB 2HF double-focussing spectrometer, using 70eV electron-impact ionisation with a direct insertion probe; the sample being introduced directly into the ionisation chamber on the tip of a ceramic tube.

The method was used to study the non-resinous residues present in the proprietary Isomid wire-coating. For this purpose, the sample was gradually heated from ambient temperature to 283^{0}C; the first traces of volatilised residues were detected at an ionisation-chamber temperature of 144^{0}C. The mass spectrum is presented in appendix IX.

2.1.9 **Ultraviolet/Visible spectrophotometry**

Ultraviolet (UV) spectra were obtained with a Varian DMS-100 instrument. Matched cuvettes were used with differential subtraction of the solvent spectrum, that is, a digitised solvent spectrum was used as a reference for zeroing of the baseline.

2.2 Materials

2.2.1 The resin: resin-SC

Samples of the poly(esterimide) resin, resin-SC, which is the film-former utilised in Isomid wire-enamel, were synthesised according to the formulation (cf. table 1.5) and the procedure given in §1.5.1. The resin is based on a terephthalate polyester, modified to produce a resin with higher thermal endurance, whilst retaining sufficient film-flexibility for use as a wire-coating. These properties were accomplished by the incorporation of imide functionalities[135] and a triazine crosslinker forming a network polymer. However, the use of crosslinking markedly compromises the attainable film flexibility;[136] the stress increasing monotonically with the degree of crosslinking for any given strain. Therefore, the amount of triazine crosslinker was therefore chosen to give a workable compromise.

Samples of the industrial grade resin-precursors were supplied by SCA, and characterized by their melting points and by spectroscopic techniques. The latter were also used to characterise a series of model compounds which were used to help describe the resin's ^{13}C-NMR spectrum.

2.2.1.1 EG: ethylene glycol (1,2-ethanediol); $HOCH_2CH_2OH$

A slightly viscous, clear, and very hygroscopic liquid found to contain water by a broad IR stretching band at 3400 cm^{-1}, and was therefore distilled (b.pt., 198^{0}C) and stored over molecular sieves (type 3A): **^{1}H-NMR**(neat, external $CDCl_3$ and TMS, 80MHz) δ(ppm) 3.86(CH_2, singlet), and 5.59(OH, broad singlet, halfwidth = 20Hz); **IR**(cm^{-1}) 3350VSVB(OH, stretching), 2950VS, 2890VS(CH, stretching), 1415 and 1460SB(CH_2, bending), 1330 and 1360sh(CH_2, wagging), 1250S, 1205S (CH_2,

twisting), 1080 and 1020VS(C-O, stretching), 880 and 860 Ssh(CH_2, rocking); **^{13}C-NMR**(DMSO, $CDCl_3$, 20.1MHz) δ(ppm) 63.2 (methylene).

The position of the hydroxyl proton, in the ^{1}H-NMR spectrum, was found to shift dramatically upfield, with the decreasing concentration of EG in $CDCl_3$, to a broad peak at 2.6ppm, when at 8mg/ml. The dependence of chemical shift on concentration is typical of intermolecularly hydrogen-bonded substances; ethanol[137] exhibits a similar upfield shift, from 5.1ppm to 2.3ppm, at 5vol.% in carbon tetrachloride.

2.2.1.2 THEIC: 1,3,5-tris-(2-hydroxyethyl)-1,3,5-triazine-2,4,6-trione

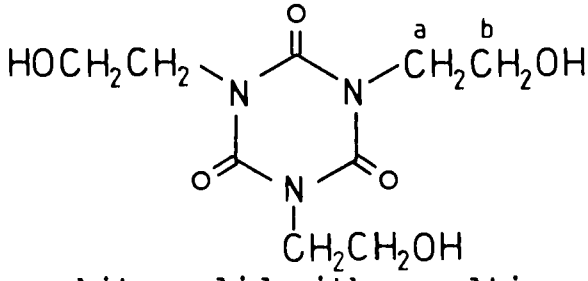

THEIC is a white solid with a melting point range of 136-137^{0}C, and is sparingly soluble in solvents of low polarity. The sample, provided by SCA, was purified by recrystallisation from an azeotropic mixture of methyl ethyl ketone (AR, 30%v/v) and methanol(AR, 70%v/v).[138] The melting point rose to 137-139^{0}C, agreeing with the literature values: 137.5-139.5^{0}C[139]; 138-142^{0}C[140]; 134-136^{0}C.[141] **^{1}H-NMR**(35mg/ml of DMSO(d6), 80MHz) 4.58(<u>triplet</u>, ^{3}J=5.9Hz, OH), 3.55(quartet, ^{3}J=5.6Hz, methylene-**b**), 3.85(triplet, ^{3}J=5.6Hz, methylene-**a**); **^{1}H-NMR**(47mg/ml in D_2O, 80MHz) 4.65(<u>singlet</u>, OH), 3.60 (triplet, ^{3}J=5.58Hz, methylene-**b**), 3.87(triplet, ^{3}J=5.58Hz, methylene-**a**); **IR** 1680VSVB(C=O), 1460VSVB(ring),[142] 3490VS (OH), 3360VS, 3250VS(OCH_2, CH_2), 1360S, 1340S, 1320S, 1275S, 1260S, 1155S, 1055VS, 1035VS, 990S(CH_2, bending), 910S, 890

S, 790S, 765S (CH_2, CCH, CN, OCH, CO, NCN), 620S, 560S(CNC), 540W(NCN); **^{13}C-NMR**(75mg/ml in DMSO, external D_2O, 20.1MHz) 43.8(methylene-**a**), 57.3(methylene-**b**), 148.9(carbonyl). The IR spectrum was similar to that examined by Vorotyntseva et al.[140], and is notable in that the O-H stretching band is split (viz., 3400 and 3505cm^{-1}); a phenomenon attributed to either intermolecular hydrogen-bonding, or Fermi-resonance. The band is also similarly located to that in EG; some 400 cm^{-1} higher than the OH band in HEB (cf. §2.3.6) at 3000cm^{-1}, in which intramolecular H-bonding prevails.[147]

The lack of coupling of the hydroxyl proton (underlined peaks; **vide supra**) when dissolved in water, as opposed to DMSO, is due to a more rapid proton exchange; the proton position fluctuating at a greater frequency than that of the NMR experiment.

2.2.1.3 **TMA: trimellitic anhydride**

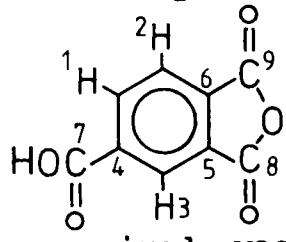

The material, as received, was a white solid, sparingly soluble in nonpolar solvents, with a melting point range of 221 to 235^{0}C, indicating the presence of impurity: **^{1}H-NMR** (DMSO(d6), 80MHz) 7.70 and 7.78(H_2, second-order splitting, $^3J_{H,H}$=7Hz), 8.12 and 8.20(H_3, second order splitting, $^3J_{H,H}$=7 Hz), 8.48(H_1, singlet), 13.2(OH, singlet), 8.28 and 8.39(trimellitic acid impurity, doublet); **IR** (impurity bands) 1165 W, 1140W, 1070S, 860W, 770S, and 660W. These IR bands coincided with those for trimellitic acid.[144] The presence of **TMA** was confirmed by bands at 1780(VS) and 1840(S)cm^{-1}, due to stretching modes of the anhydride ring.[145] TMA was purified

by recrystallisation from dimethyl formamide (DMF), giving a melting point range of 163-165^{0}C (literature value: 161-163.5^{0}C).[146] The **^{13}C-NMR**(DMSO, external D_2O, 20.1MHz) spectrum of this product was: 132.2(C_1), 129.0(C_2), 129.8 (C_3), 132.6 (C_4), 133.0(C_5), 137.7(C_6), 166.4(C_7), 167.9(C_8), 168.8(C_9). The proton and carbon NMR assignments were made with the aid of Bruck's[146] assignments for trimellitic acid and calculated values for the chemical shifts.[148]

2.2.1.4 **MDA: methylene dianiline**

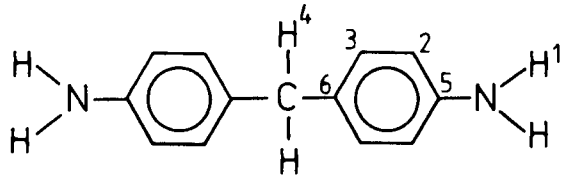

MDA is a yellow solid, soluble in most solvents, with a melting point of 92-94^{0}C (literature value: 91-93^{0}C),[146] indicating that the proprietary sample was quite pure: **^{1}H-NMR** ($CDCl_3$, 80MHz) 6.90 and 6.99(H_2, second-order splitting, $^3J_{H,H}$ =7.2Hz), 6.53 and 6.62(H_3, second-order splitting, $^3J_{H,H}$=7.2 Hz), 3.41(H_1, singlet), 3.75(H_4, singlet); **IR** 3450W, 3420W, 3340W(NH_2, stretch), 1630SB(NH_2, bending), 1515S, 1290S, 1120W(ring), 1180W, 810S(CH_2); **^{13}C-NMR**($CDCl_3$, 20.1MHz) 129.8 (C_2), 115.4(C_3), 40.2(C_4), 144.5(C_5), 132.2(C_6). Assignments were consistent with those quoted for MDA by Havens et al.[149] and Martinez et al.[150]

2.2.1.5 **TA: terephthalic acid**

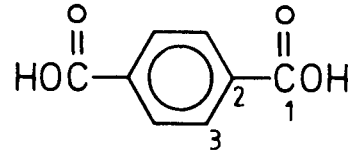

The sample of TA was as a white solid found to sublime at temperatures greater than 320^{0}C, and to dissolve only in

highly polar solvents such as DMSO and DMF. A slight impurity was detected by NMR spectrometry, so the sample was recrystallised from DMF: **^{1}H-NMR**(DMSO, $CDCl_3$, 80MHz) 8.05 (aromatic); **IR** 1690VS(C=O), 1575S, 1510S, 1290VSB, 1140W, and 1110W(ring), 1020S(CH, in-plane bending); **^{13}C-NMR**(DMSO, $CDCl_3$, 20.1MHz) 166.9(C_1), 134.7(C_2), 129.6(C_3).

2.2.2 Other reactants and solvents

DMSO, a dipolar aprotic solvent, was chosen to be the main solvent since TA and its derivatives are only sparingly soluble in chlorinated or aromatic solvents. Thus, to combine functions, perdeuterated DMSO was used as the static-field frequency locking solvent for NMR spectrometry, and as the sample solvent medium.

The analytical (BDH Chemicals Ltd.) and spectroscopic (ICN Biomedicals Inc.) grades of DMSO were stored over molecular sieves to avoid absorption of atmospheric moisture. Any other solvents used were of analytical grade (BDH Chemicals Ltd.).

Reactants of suspect purity were treated prior to use. **P**-nitrophenol (NP) and 2,4-dinitrophenol (DNP) were purified by recrystallisation from DMSO. The other reactants: phenol (PhOH), benzoic acid (BA), and 98% sulphuric acid were all of analytical grade, while $SOCl_2$ was freshly distilled before use. Titanium tetrachloride, used as a shift reagent, aiding NMR peak assignments as well as to study the formation of Ti(IV) complexes with 2-hydroxyethyl benzoate, was also of analytical grade. "Tyzor TBT" was used as a precursor in the synthesis of aryl titanates. Spectroscopic grades of benzene(d6) and chloroform(d3) were used as supplied by CEA (France) and Stohler Isotope Chemicals (USA),

respectively.

2.3 Synthesis of model compounds and catalysts

The following synthetic methods were employed to produce samples of model compounds and Ti(IV) catalysts. Analytical data is quoted to identify the compounds, including IR, proton NMR, and carbon NMR spectrometric information.

2.3.1 MBPT: 4,4'-methylene bis-(N-phenyltrimellitimide)

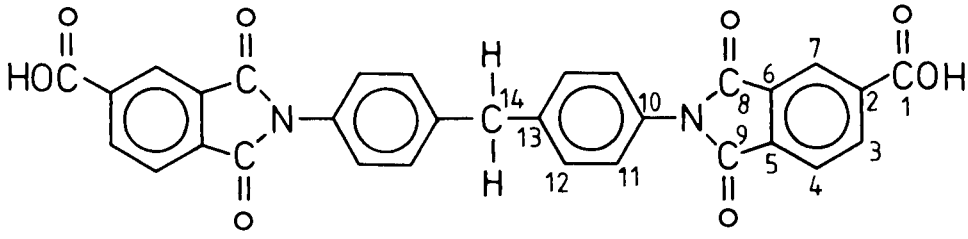

In the synthesis of this imide, DMSO was chosen as the reaction medium since polar solvents have the property of strongly associating with both reactants, TMA and MDA, and tend to accelerate the imidisation reaction.[151]

The synthesis was performed in two stages: first, the amide was produced at room temperature; then, the solution was heated to cyclise the amide into its imide form. MDA (5.00g, 0.025mmol) and TMA(10.00g, 0.060mol) were dissolved in DMSO(100ml) and allowed to stand for one hour. The characteristic IR bands, for the amide (also referred to as **amic acid**), were found at 1550 and 1240cm^{-1}.[135,152] The solution was then refluxed at 165(±5)^{0}C for an additional two hours. On cooling, a white precipitate separated which was washed with acetone before drying in air. The yield was 12.3g, 37mol%. The imide was identified by the evolution of an IR band at 1780cm^{-1};[152,153] an imide stretching band at 735cm^{-1} was also found. The melting point of the product was found to be 386^{0}C, with a glass transition temperature (by DSC) of 209^{0}C: **^{1}H-NMR**($CDCl_3$, 80MHz) 8.39 and 8.41(H_3, second-order

splitting, $^{3}J_{H,H}$=7.8Hz), 8.72 and 8.75 (H_4, second-order splitting, $^{3}J_{H,H}$=7.8Hz), 7.76 and 7.79(H_{11}, second-order splitting, $^{3}J_{H,H}$=11Hz), 7.70 and 7.74(H_{12}, second-order splitting, $^{3}J_{H,H}$=11Hz), 4.42(OH, singlet), 8.6(H_7, singlet), 2.86(H_{14}, singlet); **^{13}C-NMR**(DMSO, $CDCl_3$, 20.1MHz) 166.5(C_1), 135.0(C_2), 136.8(C_3), 123.5(C_4), 136.6(C_5), 132.2(C_6), 123.9 (C_7), 165.9(C_8), 166.0(C_9), 141.3(C_{10}), 129.4(C_{11}), 127.5 (C_{12}), 129.9(C_{13}), 40.2(C_{14}). The trimellitimide assignments were based on those given for a diglycidyl ester of 1,3-bis-(N-trimellitimide) propane, and its derivative with MDA.[150] The carbonyl assignments were based on those for TMA (cf. §2.2.1.3), while the methylene carbon was assigned from MDA (cf. §2.2.1.4).

NMR assignments for the aromatic carbon nuclei of the MDA-radical were contradicted by those of White et al.[154] for the model imides, bis-3-nitrophthalimide and bis-4-nitrophthalimide, of MDA, obtained on a Varian XL100 spectrometer in DMSO(d6). Although the chemical shifts were similar, and within 0.1ppm in magnitude, White et al. have assigned them in the reverse order to that expected from the spectra of MDA (cf. §2.1.4), acetanilide,[154] and N-phenylphthalimide.[154] Furthermore, electron density calculations based on a linear combination of atomic orbitals,[156] and using Pople's[155] CNDO/INDO computational method (cf. appendix VIII) for the chemical prototype molecule N-(4-methylphenyl) maleimide, indicate that the N-substituted carbon has the least electronic shielding, supporting its assignment to the largest chemical shift, that is, 141.3ppm. The other chemical shifts were assigned according to the previously mentioned model compounds.

2.3.2 MBPA: 4,4'-methylene bis-(N-phenylterephthalamic acid)

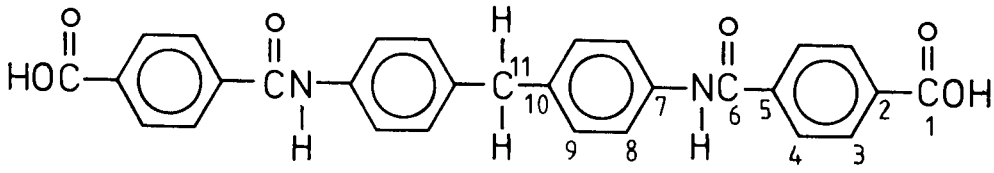

Into 200ml of DMSO were dissolved 10.00g(0.060mol) of TA and 5.90g(0.030mol) of MDA. The solution was refluxed at 150-155^{0}C for 2 hours and then cooled, yielding a white precipitate. The product was isolated by vacuum filtration and washed with cold acetone to remove any unreacted MDA; the washings were pale yellow due to unreacted MDA. The product was air dried and the yield was 9.6g, 48mol%: **IR** 3440Ssh (amide stretching band); **^{13}C-NMR**(DMSO, $CDCl_3$, 20.1MHz) 167.1 (C_1), 134.8(C_2, C_5), 129.5(C_3,C_4,C_8 & C_{10}), 167.1 (C_6), 145.3 (C_7), 127.9(C_9), 40.2(C_{11}). The assignments for the carbon signals are tentative because only five resonances were obtained, rather than the expected eleven.

2.3.3 THET: tris-(2-hydroxyethyl) trimellitate

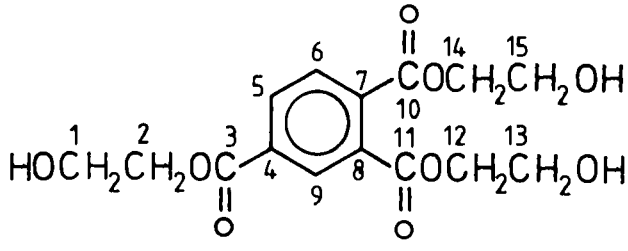

An acid-catalysed esterification was used to produce the 2-hydroxyethyl triester of TMA. Thus, a solution of 30.00g(0.483mol) of EG and 61.80g(0.322mol) of TMA in 200ml of benzene was acidified with 1.0ml of H_2SO_4, and then refluxed at 120-125^{0}C through a Dean and Stark apparatus for 8 hours. The condensed water (6ml) was trapped in the receiver. The solvent (benzene) was removed from the reaction solution by vacuum distillation, leaving a pale yellow oily liquid. To this liquid was added 50ml of water which diss-

olved any unreacted EG, and precipitated of the triester which was then filtered-off, washed with cold water, and dried in a dessicator. The yield of triester was 42.2g, 38 mol%: **^{1}H-NMR**($CDCl_3$, 80MHz) 3.6(groups **1**, **13**, **15**; triplet), 4.2(groups **2**, **12**, **14**; triplet), 4.5(OH, singlet), 7.7(H_9, complex), 8.1 (H_5 & H_6, complex); **^{13}C-NMR**(DMSO, $CDCl_3$, 20.1 MHz) 60.0, 60.8, 61.3(C_1, C_{13}, C_{15}), 67.6, 69.7, 71.9 (C_2, C_{12}, C_{14}), 132.4(C_4), 131.4(C_5), 129.4(C_6), 136.1(C_7), 132.7(C_8), 129.9(C_9), 165.1, 167.5, 166.8(C_3, C_{10}, C_{11}).

2.3.4 PET: polyethylene terephthalate

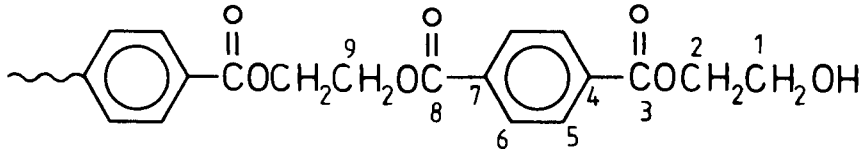

The synthetic method outlined in §2.3.3 for THET was repeated for PET; with 20.00g(0.322mol) of EG, 26.80g(0.161 mol) of TA, and 4ml of H_2SO_4. Condensed water (8ml) was collected in the Dean and Stark receiver. The yield was 82wt.% (i.e., 33.4g): **^{1}H-NMR**($CDCl_3$, 80MHz) 3.7(H_1, triplet), 4.3(H_2, triplet), 4.7(H_9, singlet), 8.1(aromatic protons, singlet); **^{13}C-NMR**(DMSO, $CDCl_3$, 20.1MHz) 59.2(C_1), 66.4(C_2), 165.2(C_3), 134.8(C_4), 129.7(C_5, C_6), 130.9(C_7), 164.5(C_8), 64.5(C_9).

A polymerisation byproduct was extracted by washing with ethanol (AR) and precipitating with water: **^{13}C-NMR** ($CDCl_3$, 20.1MHz) 165.2 (C_a), 133.6(C_b), 129.7(C_c), 129.6(C_d), 135.3(C_e), 165.9(C_f), 67.0(C_g), 59.4(C_h). The probable identity of the byproduct is the singly esterified derivative of TA,

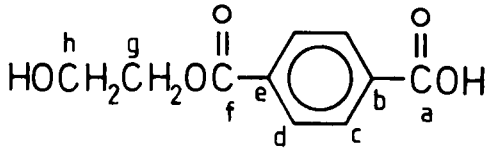

The IR spectrum of the major product was found to be similar to that published by Serboli[157] or PET.

2.3.5 **DET: diethyl terephthalate**

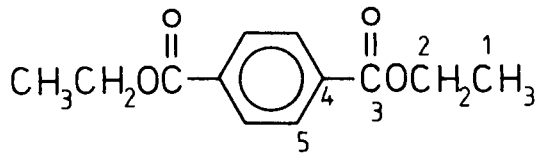

The synthetic method of §2.3.3 was used; the reaction medium was ethanol instead of benzene, with refluxing. The reactant quantities were: 26.80g(0.161mol) of TA, 200ml of ethanol, and 4ml of H_2SO_4. The large excess of ethanol provided a forward impetus for the equilibrium controlled esterification;[1] The precipitated product was filtered, washed with cold acetone, and air dried. The product yield was 18.6g, 52mol%: **^{13}C-NMR**(DMSO, $CDCl_3$, 20.1MHz) 14.1(C_1), 61.2(C_2), 166.9(C_3), 134.7(C_4), 129.6(C_5). The assignments for the methylene carbons were made by comparison with the carbon chemical shifts for ethanol (57.8ppm, methylene; 18.5, methyl). The electron shielding is therefore seen to increase (upfield shift) for the hydroxyl methylene, and decrease (downfield shift) for the carboxylate methylene group.

2.3.6 **HEB: 2-hydroxyethyl benzoate**

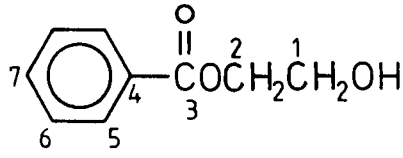

This compound was synthesised from benzoyl chloride (BC), a similar method to that used by Miyake[158] to synthesise the TA analogue. Formation of the side-product, ethylene dibenzoate (EDB), was discouraged by dilution and vigorous agitation of the reacting mixture. Therefore, a

benzene (50ml) solution of BC (43.042g; 0.409mol) was slowly added, drop-wise, to a benzene (100ml) solution of EG (24.554g; 0.396mol), with vigorous stirring. The resulting solution was neutralised with 2vol% $NaHCO_3$ (aqueous) and the benzene removed under reduced pressure. The white product was recrystallised from benzene, yielding 28.510g, 42mol% of HEB, having a melting point range of 43-44^{0}C. EDB was separated from the supernatant benzene by slow evaporation, yielding 6.33g, 5.7mol% of the white solid EDB with a melting point range of 71-72^{0}C. Both melting points were similar to those quoted in the CRC Handbook of Chemistry and Physics (64th edition) for HEB.

The characteristics of this model compound are expected to be close to those of the HE chain end-groups of resin-SC. The proposition of intramolecular H-bonding occurring was advanced by Challa[25] in 1960, and by Shevchenko et al.[32] in 1979, to explain discrepencies in the rates of model condensation reactions involving HEB and bis(2-hydroxyethyl) terephthalate.

HEB is characterised, and the results discussed at length, in appendix II; the presence of an intramolecular H-bond having an average heat of formation of 1.7(±0.4)kJ/mole corresponds closely to Challa's proposal (i.e., 1.7kJ/mole),[25] and to the value calculated from Shevchenko's data, by taking the difference in the activation energies for the esterification reactions of EG and HEB with BA (i.e., 2.1kJ/mole). Dependence of the H-bond on the dielectric strength and H-bonding ability of the solvent medium has been demonstrated by carbon NMR conducted in a range of media (cf. appendix II), such as a relationship is significant when

interpreting the role of solvent during wire-enamel curing.

2.3.7 **PB: phenyl benzoate**

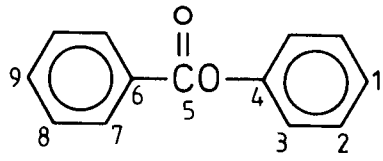

The method of §2.3.5 was repeated in the synthesis of PB; reactant quantities were: 12.0g (0.098mol) of BA, 153.6g (1.632mol), and 1.0ml of H_2SO_4. The white, solid product was purified by recrystallisation from ethanol, yielding 9.5g, 48.9mol%. The melting point range was 69-70^{0}C (literature value: 69^{0}C[158]): **^{13}C-NMR**(DMSO, $CDCl_3$, 20.1 MHz) 125.8(C_1), 129.9 or 129.4(C_2), 121.7(C_3), 150.8(C_4), 164.6(C_5), 133.7 (C_6), 129.4 or 129.8(C_7), 129.4 or 129.8(C_8), 128.7(C_9).

2.3.8 **DPT: diphenyl terephthalate**

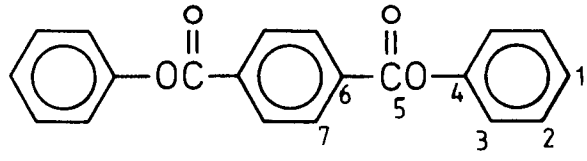

Refluxing 29.99g(0.181mol) of TA with 110ml of freshly distilled $SOCl_2$ for 2 hours. The excess thionyl chloride was removed by vacuum distillation, leaving the cooled acid chloride as a pale yellow liquid; to this was added a solution of 34.27g(0.364mol) of phenol in 100ml of 10% aqueous NaOH with stirring for 20 minutes.[159] The product precipitated as a white solid and was isolated by vacuum filtration, washed with cold water, and purified by recrystallisation from DMF.[160] The yield was 31.2g, 54mol%: **^{13}C-NMR**(DMSO, $CDCl_3$, 20.1 MHz) 126.3(C_1), 129.7(C_2), 121.8(C_3), 150.8(C_4), 209.8 (C_5), 133.8(C_6), 130.3(C_7); **IR** 3000S(OH stretching), 1740S and 1370S(characteristic phenyl ester stretching bands[157]).

2.3.9 **Titanate(IV) Catalysts**

Three aryl titanates, ranging in ligand polarities were synthesised to study their effectiveness as catalysts in the model esterification of BA with EG (cf. §2.4.2).

The starting material for the synthesis of these catalysts was proprietary "Tyzor TBT" which, according to du Pont's specification (cf. §1.5.2.3), contained about 76.5 wt.% of TBT, with the remaining titanium in the form of TiO_2. Tetraaryl titanates were found to be readily formed; an exothermic alcoholysis reaction occurred with TBT at room temperature. Bistan and Gomory[49] found that the butyl ligands of TBT are more labile than similar aryl ligands; the relative rapidity and completeness of the hydrolysis of butyl ligands was found to be greater than for phenyl or cresyl ligands. Further, Boyd[48] found that higher homologues easily displace lower alkoxyl ligands, probably via nucleophilic attack at the titanium centre,[161] and this was suggested as a convenient route for the production of the higher titanates. "Tyzor TBT" is no exception and undergoes rapid ligand exchange at room temparature, under anhydrous conditions. Haslam[161] postulated that this proceeds by a mechanism analogous to that postulated for hydrolysis, involving an octahedral intermediate complex.[52] The nucleophilic alcoholic oxygen of the incoming ligand attacks the tetrahedral titanium centre through an octahedral site, occasioning ligand substitution.

The required titanates were synthesised by the addition of a stoichiometric amount of an aryl alcohol (i.e., each of phenol, NP, and DNP), and the condensed butanol distilled. In each synthesis, 16.94g of "Tyzor TBT" (≈0.038mol of TBT)

was reacted with 0.2mol of aryl alcohol by heating to 120-130^{0}C for 30 minutes. Upon cooling the resultant titanates were washed with three portions of cold ethanol (25ml), removing any unreacted aryl alcohol, recrystallised from $CHCl_3$, and dried in a dessicator. Tetraphenyl titanate (TPT) was orange in colour, while the two nitrophenyl titanates: tetra(**p**-nitrophenyl) titanate (TNPT) and tetra(2,4-dinitrophenyl) tiatanate (TDNPT), were reddish-brown.

The aryl titanates were considered to be tetrahedral since Ti(IV) is a d^0 transition metal, therefore, three IR active stretching modes, for the Ti-O bonds, were tentatively assigned to weak bands below 700cm^{-1} (cf. table 2.2). Although literature reference to IR data for aryl titanates is not available, Kriegsmann and Licht[162] have made tentative assignments for the Ti-O bond in a series of alkyl titanates, ranging from 556-619cm^{-1}.

Table 2.2 Tentative assignments for the degenerate IR active, Ti-O bond stretching modes of the aryl titanates, below 700cm^{-1}. All of the bands were weak.

Titanate	Ti-O IR bands (cm^{-1})
"Tyzor TBT"	600(sh), 545(sh), 505(sh)
TPT	575(sh), 510(sh), 490(sh)
TNPT	630(sh), 540(sh), 500(sh)
TDNPT	640(B), 580(B), 520(B)

Table 2.3 The aromatic BB^{13}CNMR(DMSO, $CDCl_3$) chemical shifts for the phenoxyl ligands on Ti(IV) against the extent of ligand substitution. The source of titanium was proprietary "Tyzor TBT". The aromatic resonances of phenol have been included for the purpose of comparison.

Molar Ratio of phenol to titanium	Aromatic Carbon Chemical Shifts (δ,ppm)			
	ipso	ortho	meta	para
1.0	165.7	119.5	129.4	120.5
3.0	160.7	117.4	129.9	121.2
5.0	157.2	116.8	130.7	121.8
6.5	156.4	115.7	129.7	120.9
phenol	157.8	115.7	129.6	119.7

BB^{13}C-NMR was used to monitor the synthesis of TPT. The aromatic resonances of phenol were found to drift toward lower fields with increased substitution; the effect was greatest for the carbons closest to the Ti-O bond. Increasing ligand substitution (cf. table 2.3) increased the electron density (decreased chemical shift) at the **ipso** aromatic carbon, indicating that the Ti-O bond strength decreases as the steric repulsion between the bulky ligands increases with greater substitution by phenol. The carbon NMR spectrum of the saturated titanate were found to have resonances at similar shifts to phenol.

An elemental analysis of TPT (see appendix V) indicates that it is monomeric,[163] and it was assumed that the aryl titanates examined here are both monomeric, with Ti-O bond orders between 1 and 2 due to "back-coordination"[79] (see §1.2.5.2) of the oxygen lone-paired electrons.

Peak assignments for the carbon NMR (in DMSO; benzene (d6); 20.1MHz) spectra of the three titanates synthesised were made by following the high field shift in the resonances of the precursory aryl alcohols. In the case of TDNPT, due to low solubility in DMSO, the signals were not easily distinguishable from the baseline noise, therefore, the peak assignments given (**vide infra**) are tentative. The carbon NMR assignments for the aryl titanium(IV) esters are listed below along with the chemical shifts for the corresponding aryl alcohol form of the ligands (in brackets).

"Tyzor TBT"

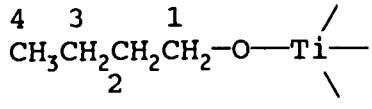

δ(ppm) 74.8(C_1, **63.7**), 36.1(C_2, **35.2**), 19.6(C_3, **19.8**), 14.3 (C_4, **14.5**);

TPT 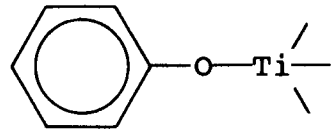

δ(ppm) 156.3(ipso, **157.8**), 116.8(ortho, **115.7**), 130.7 (meta, **129.6**), 121.8(para, **119.7**);

TNPT 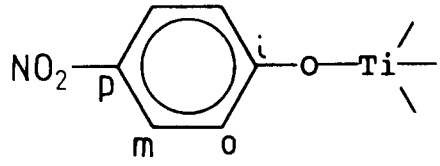

δ(ppm) 164.6(ipso, **161.8**), 115.9(ortho, **115.9**), 126.2 (meta, **126.4**), 140.3(para,**141.7**);

TDNPT 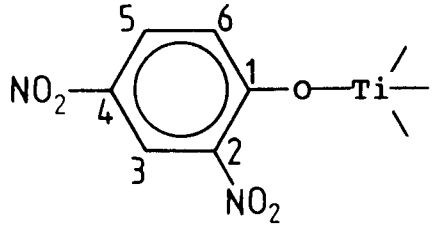

δ(ppm) 163.8(C_1, **176.5**), 129.8 or 127.3(C_2, **157.9**), 125.6 (C_3, **121.7**), 139.9(C_4, **143.9**), 127.3 or 129.8(C_5, **129.3**), 115.4(C_6, **120.2**).

2.3.10 **Resin made with phenol, instead of EG**

The synthesis of a model PEI resin in which EG was replaced with phenol was based upon the formulation for resin-SC (cf. table 1.5, §1.5.1). Into a round bottomed reaction vessel (1L) was placed: 17.552g(0.1865mol) phenol; 27.690g (0.1060mol) THEIC; 17.196g (0.0895mol) TMA; and 14.918g (0.0898mol) TA. The reaction mixture was refluxed at 230^{0}C, under a nitrogen atmosphere, for 1.5 hours.

The resin produced was amber coloured (similar to resin-SC) with a melting point of 190.5(±0.5)^{0}C.

2.3.11 **Resin made with phenol, instead of EG and THEIC**

The procedure described in §2.3.10 was adopted in the synthesis of a model PEI resin in which the hydroxylic pre-

cursor-compounds of resin-SC, EG and THEIC (cf. §1.5.1) were replaced with a mole-equivalence of phenol.

The reaction charge consisted of: 7.90g(0.039mol) of MDA; 14.80g(0.089mol) of TA; 17.30g(0.089mol) of TMA; and 25.62g(0.272mol) of phenol, condensing 4.52g of water and 0.39g of phenol, to yield a reddish-brown powder having no melting point below 300^{0}C.

The BB ^{13}C-NMR spectrum (in DMSO(d6), 20.1MHz, at 25^{0}C) of the product showed the expected the carbonyl signals at 165.98 and 166.40ppm for the imide rings, as well as a carbonyl signal at 167.98ppm which was assigned to unreacted carboxylic acid groups. The presence of unreacted phenol was deduced by aromatic signals at 115.45, 118.96, and 157.60ppm. No evidence of phenyl-esters was discernable.

2.3.12 **A polymer from THEIC and TMA**

THEIC (5.0g; 0.019mol) was esterified with TMA (9.6g; 0.057mol) in refluxing DMSO at 210^{0}C, under atmospheric conditions, for 2.5hours. The product was an orange gel, suggesting that a three-dimensional polymer had formed which was swelled by the reaction-solvent, DMSO.

The ^{1}H-NMR spectrum (in DMSO, 20.1MHz, at 25^{0}C) of the gel was difficult to interpret due to signal broadening caused by crosslinking, however, two signals were well resolved, those arising from the methylene protons. The methylene proton-signals were assigned as

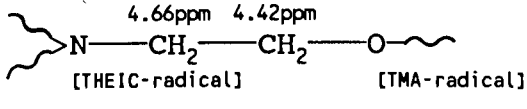

2.4 **Relative rates of polycondensation reactions**

The rates of mass lost during the curing of catalysed and uncatalysed model enamels, as well as model condensation

reactions, were dealt with in two ways: in the first, the masses of enamel samples were followed during thermal curing. In the second, the quantity of water distilled with respect to reaction time was determined.

2.4.1 Thermogravimetric analysis of the curing of model enamels

Two model enamels were mixed to represent the wire-enamel, Isomid. Resin-SC was dissolved into phenol, representing the solvent system. The enamel formulations, as listed in table 2.4, contained 40wt.% resin, simulating the solids content of Isomid (35wt.%) when measured by heating a 2g sample at 200^{0}C for 2 hours. The amount of catalyst, "Tyzor TBT", used was approximately 1wt.%, again similar to that used in Isomid. The enamels were thoroughly mixed until homogeneous, clear, reddish solutions ("varnish") were obtained.

Table 2.4 The formulations for the catalysed and uncatalysed model enamels used in mass-loss experiments.

Component	Catalysed		Uncatalysed	
	Mass (g)	wt.%	Mass (g)	wt.%
resin-SC	5.0011	39.38	5.0011	40.00
phenol	7.5008	59.80	7.5008	59.99
"Tyzor TBT"	0.1025	0.82	——	——

The temperature of the electric furnace used was 300 (±10)^{0}C, simulating the enamelling ovens, which operate from about 250^{0}C at their entrances to above 400^{0}C at their exits. In tared pyrex crucibles as curing-vessels, three varnish samples of 0.5(±0.01)g were heated in the electric furnace. Curing was monitored by interrupting the heating, cooling to room temperature in a dessicator, then weighing the crucibles. The following standard regimen was used:

(i) initially, the furnace temperature was allowed to

equilibrate (0.5 hour);

(ii) the loaded crucibles were placed onto fire-bricks, in the furnace, such that they were not in contact with any of the walls;

(iii) after about 10 minutes the crucibles were removed and placed into a dessicator to cool;

(iv) they were then weighed;

(v) steps (ii), (iii), and (iv) were repeated for the additional approximate stoving times of; 20, 40, 80, and 160 minutes.

The relative standard deviation of the sample masses, for the three matched samples, was found to be 3.3%.

2.4.2 **Model condensation reactions**

The rates of model esterification reactions were determined by measuring the amount of distilled condensation product against reaction time. Microdistillation apparatus was used to collect the distillate for a reaction temperature of $220(\pm 15)^{0}C$ and GC was employed, by peak integration, to determine the amount of condensate in the distillate.

The condensation reaction was carried out by the following procedure:

(i) a silicone oil bath was heated to the reaction temperature ($220\pm 15^{0}C$);

(ii) the assembled microdistillation apparatus was then loaded with the reaction mixture and lowered into the oil bath;

(iii) as each distilled sample was collected, the time, the still-head temperature, and the bath temperature were recorded.

Six distillations for each of the uncatalysed and catalysed varnishes were performed to ascertain the experimental uncertainty. The maximum experimental variation in the amount of water distilled was typically of the order of 10 wt.% (i.e., ±0.009mol) for the "Tyzor TBT" catalysed reactions, and 2wt.% for the uncatalysed esterifications of BA with EG. The larger error, associated with the catalysed reactions, was due to the increased rate of condensate distillation, and the difficulty of replicating the reaction temperatures during the early stages of the experiments. Variablity in the still-head temperature, as the apparatus warms up to reaction temperatures upon immersion, generated inconsistencies in the quantities of distillate reaching the condenser column, preferring to run back into the reaction mixture, instead. Although the uncertainty is unacceptable for a rigorous analysis of the rates of the water condensation, reflecting the intrinsic rate of esterification, the procedure was sufficiently accurate to highlight large differences in reaction rates, and is useful for a broad comparison of the catalytic effects of phenol, NP, DNP, TPT, TNPT, and TDNPT.

3.0 Results and discussion

3.1 Spectroscopic studies

The predominant emphasis in PEI research[32,164,165] has been on syntheses and physical properties. Many PEI resin formulations, similar to that of Schenectady Chemicals, Inc.(i.e., resin-SC; cf. §1.5.1), have appeared in the patent literature,[166,25] but the effects of solvents on the curing of the wire-varnishes have not been discussed.

The only fundamental spectrometric research available in the public domain has been undertaken by Dr.Penczek's group at the Instytut Chemii Przemyslowej in Warsaw, Poland. One of the PEI resin investigated by this group is similar to resin-SC, varying only slightly in the ratio of the precursor components (i.e., TMA, TA, THEIC, MDA, and EG), and was examined in detail by IR and proton NMR.[105] A number of such resins, designated **PEI-T** ("T" indicates the presence of THEIC), were examined, and although formulations were not given, the ratios for the hydroxyl-to-carboxyl group (i.e., 17.2:1.0 to 48.5:1.0)[104,105] were much higher than for resin-SC (i.e., 1.3:1.0). The latter ratio was determined by integrating relevant carbon peaks in the inverse-gated, decoupled NMR spectrum (discussed later in §3.1.1.3). The PEI-T resins were formulated using stoichiometric ratios of the imide components (i.e., TMA:MDA = 2.0:1.0) whereas resin-SC contains an excess of TMA with respect to MDA (i.e., 2.6:1.0, respectively), allowing the TMA excess to form cross-links in the PEI network. Lastly, the acid number of resin-SC was found, by titration with methanolic KOH, to be similar to those of the PEI-T resins.

Despite these differences, the published spectrometric (i.e., IR and proton NMR) characteristics of the PEI-T resins were noticed to be similar to resin-SC. Resin-SC was further characterised by BB^{13}C-NMR (cf. §2.1.1), enabling MASS ^{13}C-NMR (see §2.1.2 for a description of this technique) to be used in a study of solid, cured Isomid wire-enamel (see §1.5.2 for the formulation of Isomid wire-varnish, §1.4.3 for a description of its processing into wire-enamel). Peak assignments for resin-SC were based on similar assignments established for the model compounds discussed in §2.2 and §2.3 for the same spectrometrical solvents (i.e., $CHCl_3$ and DMSO, and their perdeuterated forms).

Proton NMR is hampered by signal broadening and peak-overlap with increasing crosslink-density. The greater range of carbon chemical shifts, and the elimination of multiplicity by proton decoupling of the carbon atoms in ^{13}C-NMR has permitted a more detailed structural analysis of resin-SC.

3.1.1 **Spectrometric study of resin-SC**

3.1.1.1 **Infrared spectrometry**

As mentioned above, the formulation of resin-SC (cf. §1.5.1) provides for an excess of TMA with respect to MDA. Since the imide groups resulting from their condensation are resonance stabilised, all the MDA is expected to be converted. The weak stretching-mode absorption band for imide-carbonyl bonds is observed at 1780cm^{-1} [164,165,167] (cf. figure 3.1), along with one of the characteristic imide-ring deformation bands at 730cm^{-1}. The other, expected at 600cm^{-1},[168] was not observable due to the NaCl absorption in that region.

The IR spectrum (cf. figure 3.1) shows no sign of the presence of amide groups produced by the condensation of MDA

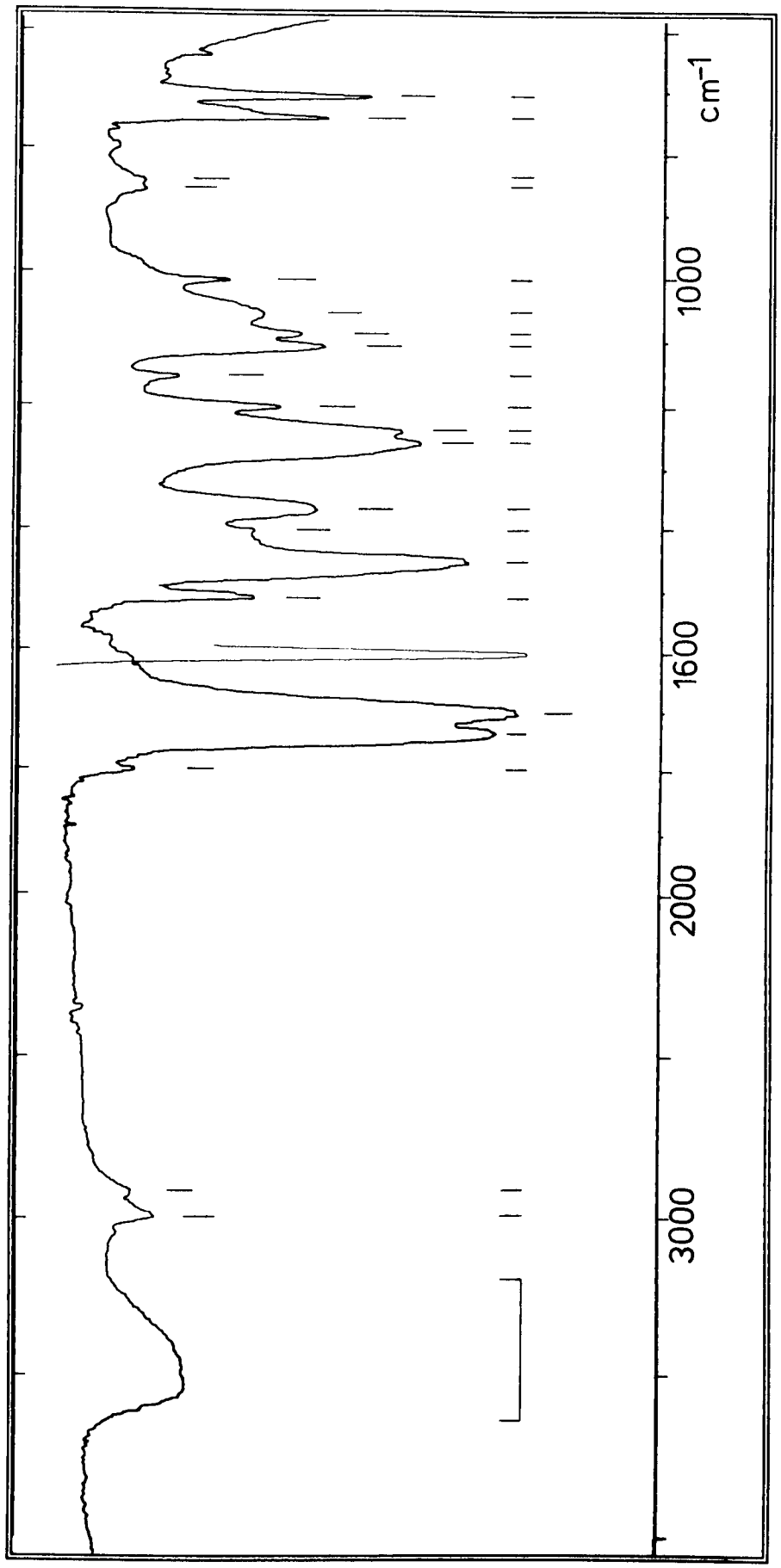

Figure 3.1 The IR spectrum of the PEI resin, resin-SC, in a nujol mull between NaCl windows. The spectral assignments are presented in table 3.1.

with carboxylate functionalities other than anhydride. The spectrum exhibits a very broad stretching band between 2700 and 3600cm^{-1} which can include an amide stretching band (viz., at 3440cm^{-1}; cf. §2.3.2). However, the presence of amide groups is expected to be detected by a carbonyl stretching band at 1550cm^{-1}; this band was not observed (cf. figure 3.1 and table 3.1), and therefore such functionalities are absent from the structure of resin-SC.

Cynkowska et al.[105] claim that their PEI-T resins showed incomplete imide cyclisation when synthesised below 230^{0}C. In contrast to this claim, although resin-SC is made at 220^{0}C, no evidence of amide groups has been discerned by either IR, proton NMR (viz., no signals were found below 3.0 ppm; cf. §3.2), or BB^{13}C-NMR (viz., no signals at or about 145.3ppm, expected for aromatic carbon nuclei adjacent to an amide substituent, according with model compound MBPA; cf. §2.3.2 and figure 3.4). Furthermore, no amine signals for the precursor MDA were observed by proton NMR (viz., at 3.41 ppm; cf. §2.2.1.4). Therefore, resin-SC contains no partially cyclised imide groups, and the MDA is fully reacted, although resin-SC is synthesised below 230^{0}C.

A quantitative estimation of the imide content of resin-SC was calculated from the ring deformation band at 730 cm^{-1} [105] by referencing against the acid and the ester C-O stretching bands at 1275 and 1220cm^{-1}, respectively (cf. table 3.1). Thus, the integral ratio (as measured by the cut-and-weigh method) of imide to acid plus ester C-O was found to be 1.0:4.1.

The same imide to (acid + ester) C-O integral-ratio was estimated from the resin formulation (cf. §1.5.1) by consid-

ering the total number of moles of amine groups (i.e., $2.n_{MDA}$; **A**) against the total number of moles of carboxyl groups expected to remain after the complete imidisation of MDA (i.e., $2.n_{TA}+ n_{TMA}+ (2.n_{TMA}- 4.n_{MDA})$; **B**). The result of this summation gives a molar ratio for **A:B** of 1.0:4.1, and equals the integral-ratio derived from the IR spectrum, confirming that all the MDA has in fact been converted during resin-production.

Table 3.1 Summary of the IR bands, and their assignments, for the proprietary PEI resin, resin-SC. The spectrum is illustrated in figure 3.1.

Absorption Bands cm^{-1}	band-shape	Band Assignments
730	S,sh	imide-ring deformation
765	S,sh	-C-H rocking (methylenes); C-N bending
785	W,sh	-C-H rocking
810	W,B	
860	B	para- and unsymmetrical ring-
875	W,B	stretching; -NCN-, $-CH_2-$, and
890	W,B	-C-O- stretching
915	VW,sh	-C-N- stretching (THEIC)
990	W,sh	
1020	sh	-C-H in-plane bending (aromatic)
1040-1080		-C(O)-O- str.;-C-H in-plane ben.
1105	sh	-C-N stretching (imide)
1125	S,sh	1,4-disubstituted ring str.
1155	VW,sh	-C-H in-plane ben. (aromatic)
1170	B	-C-N str. (imide); -C-H in-plane bending
1220	sh	-C-O-C- str. (1,4-disubstituted ester)
1255	S,VB	
1275	S,B	-C-O(H) and -C(O)-O- stretching
1380	B	
1415	W	-C-H bending (alkyl)
1465	sh	aromatic ring stretching
1695	VS,B	-C=O stretching (THEIC)
1730	VS,B	-C=O asymmetrical str. (ester)
1780	W,sh	-C=O symmetrical str. (imide)
2890	S	-C-H stretching (MDA)
2970	S	-C-H stretching (THEIC)
3010	W,B	-C-H stretching (aromatic)
2800-3700	S,VB	-O-H stretching

Notes. Where resin precursors are cited in brackets, the bands were assigned to those polymer fragments. Assignments have also been assisted by data given in references 33, 105, and 140.

3.1.1.2 **Proton NMR spectrometry**

The proton NMR spectrum of resin-SC (cf. figure 3.2) was found to be complicated by overlapping of the peaks. Generally, the spectrum is composed of two clusters of signals: one cluster of methylenes between 3.6 and 4.5ppm, and another of aromatic peaks between 6.5 and 8.7ppm.

Contrary to the opinion of Cynkowska et al.,[105] assignment of the aromatic signals for the TMA radicals was considered to be made difficult by the close proximity, in terms of chemical shifts, of the signals. The chemical shift region between 8.0 and 8.3ppm, for the spectra of a sample dissolved in DMSO(d6) and $CDCl_3$ (cf. figure 3.2(d) and 3.2(b), respectively), show overlapping of the signals attributable to TA and TMA radicals. However, when the most intense peak (viz., at 8.30ppm) is assigned to TMA, the integral ratio of TMA to TA to MDA (viz., the chemical shift regions, 8.29-8.7:8.0-8.29: 7.4-7.7ppm, respectively) is calculated to be 1.0:1.5:1.2. The numerical value of this integral-ratio is close to the molar ratio determined from the resin formulation, that is, 1.0: 1.2:1.1, respectively.

During a synthesis of resin-SC (cf. §1.5.1), samples of the reacting mixture were drawn out at intervals and the ^1H-NMR spectrum taken in DMSO(d6). A broad cluster of peaks was seen to evolve between 4.0 and 4.5ppm (cf. figure 3.2(e)), and is attributed to the formation of glycolic esters. Assuming that esterification and ester exchange reactions occur exclusively during much of the synthesis, the broadness of the methylene region may be explained by the presence of the species: -Ar-C(O)O-CH_2CH_2-OC(O)-Ar- , -Ar-C(O)O-CH_2CH_2-OH, >N-CH_2CH_2-OH , and >N-CH_2CH_2-OC(O)-Ar- (Ar represents

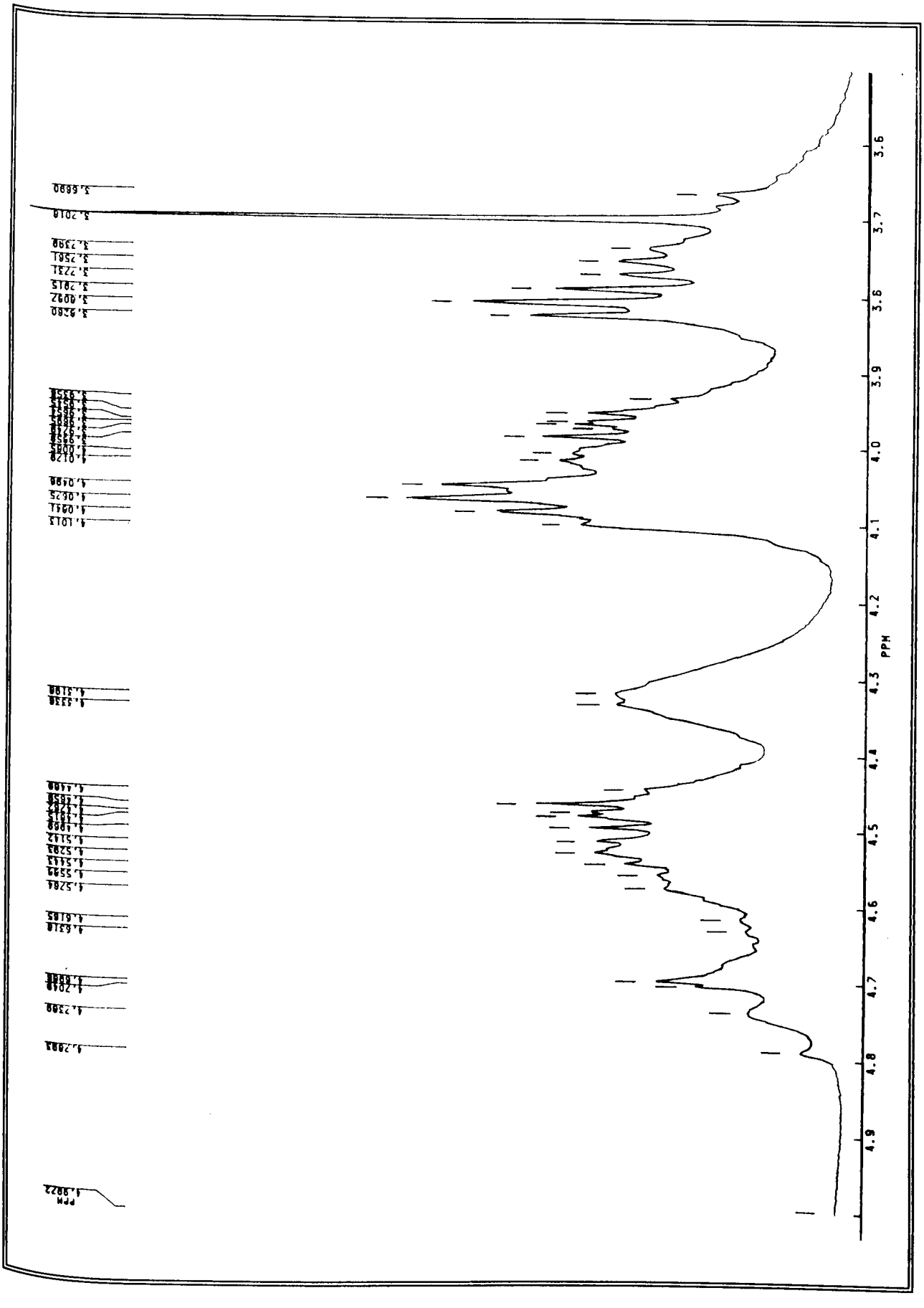

Figure 3.2(a) The methylene region of the ^{1}H-NMR spectrum (300.13MHz, $CDCl_3$, at 25^{0}C) of the proprietary PEI resin, resin-SC.

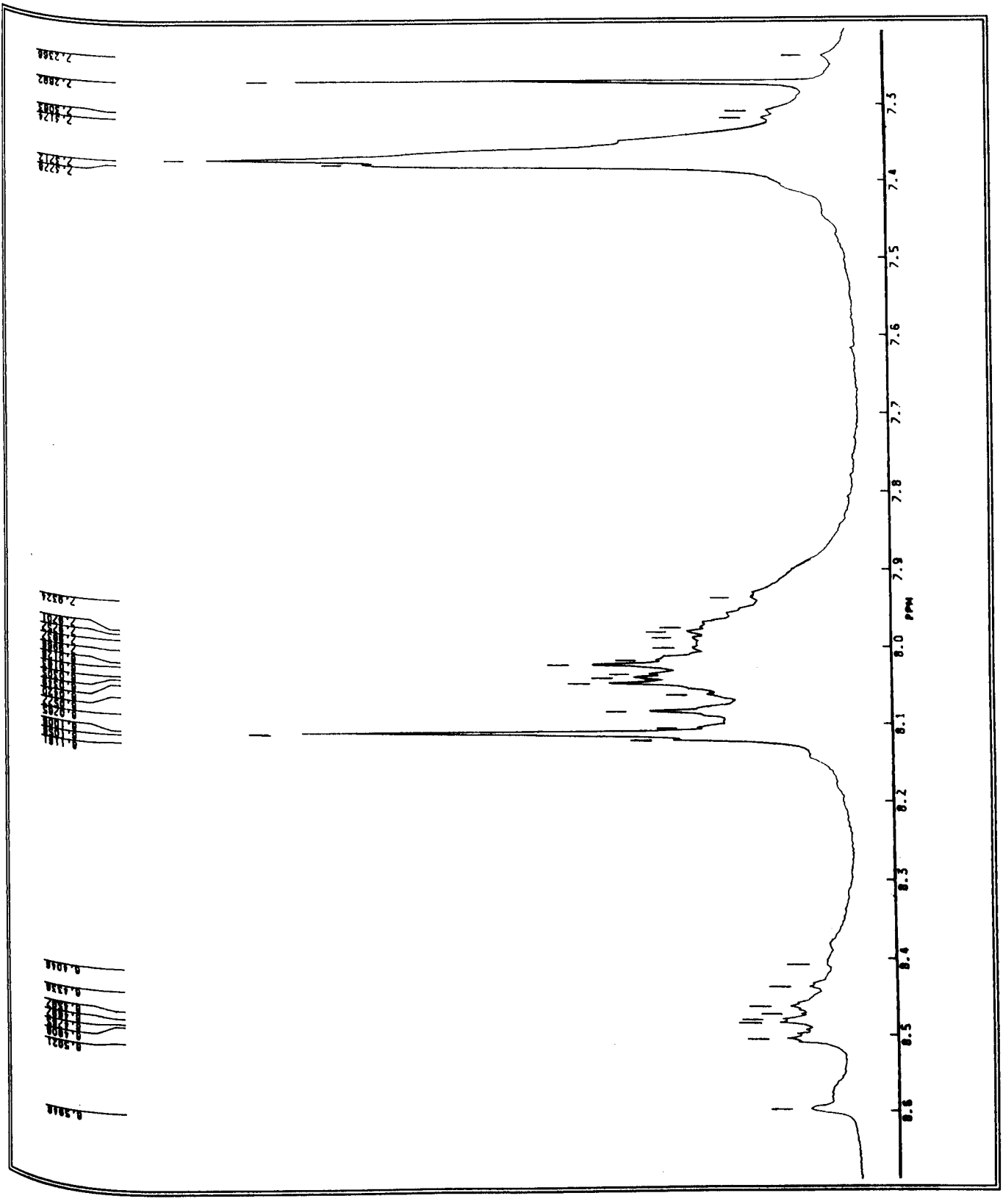

Figure 3.2(b) The aromatic region of the ^{1}H-NMR spectrum (300.13MHz, $CDCl_3$, at 25^{0}C) of resin-SC.

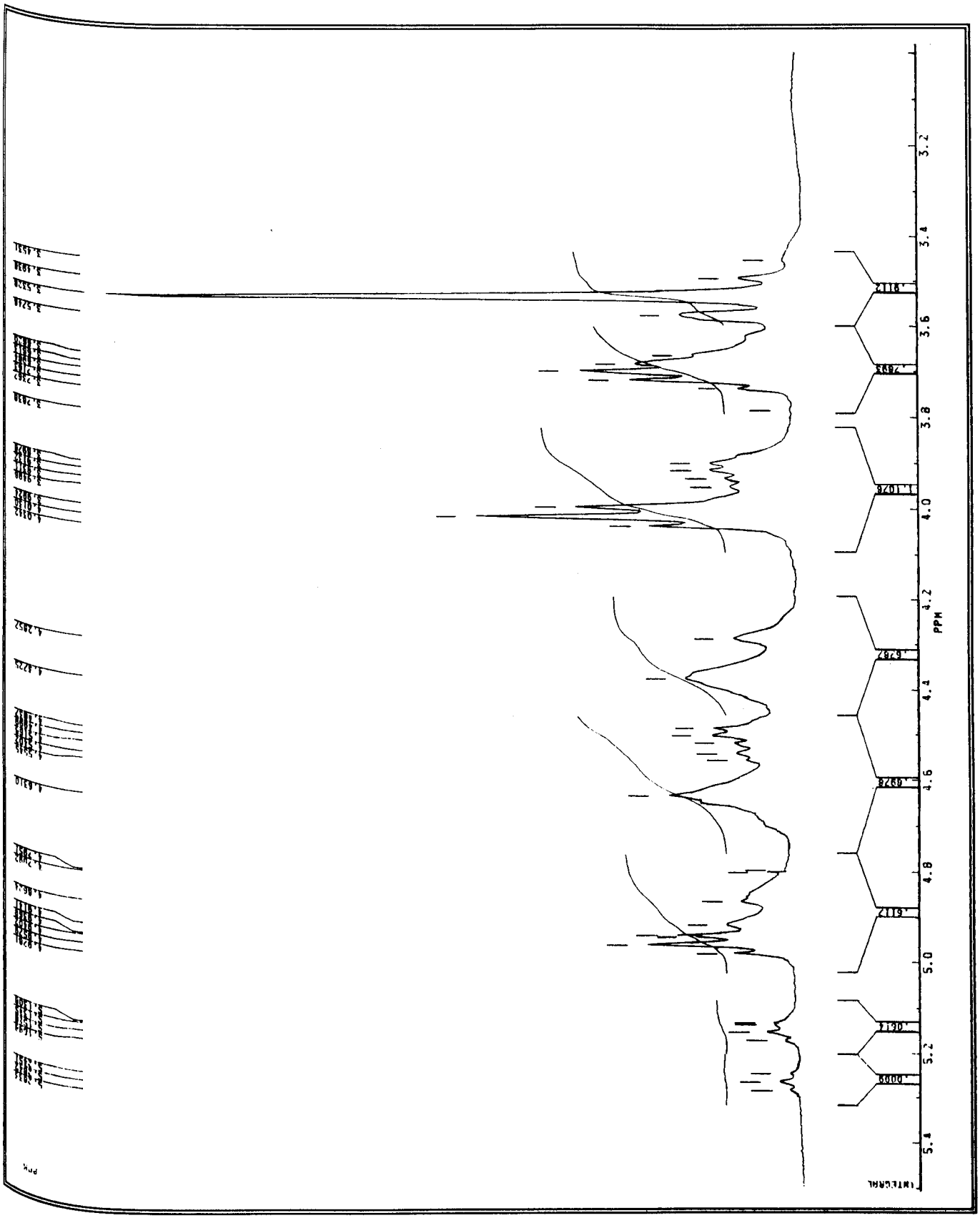

Figure 3.2(c) The methylene region of the ^{1}H-NMR spectrum (300.13MHz, DMSO(d6), at 25^{0}C) of resin-SC.

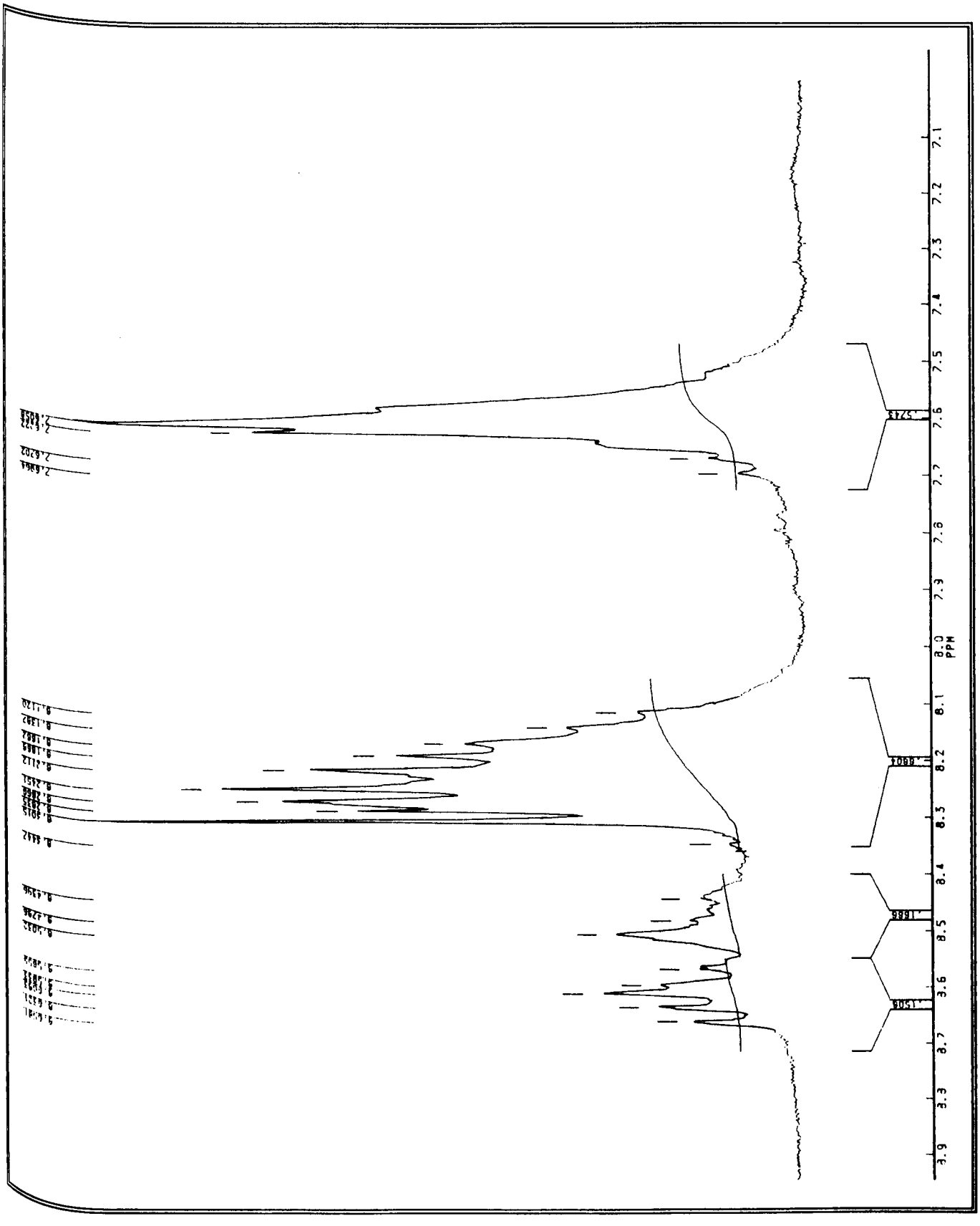

Figure 3.2(d) The aromatic region of the ^{1}H-NMR spectrum (300.13MHz, DMSO(d6), at 25^{0}C) of resin-SC.

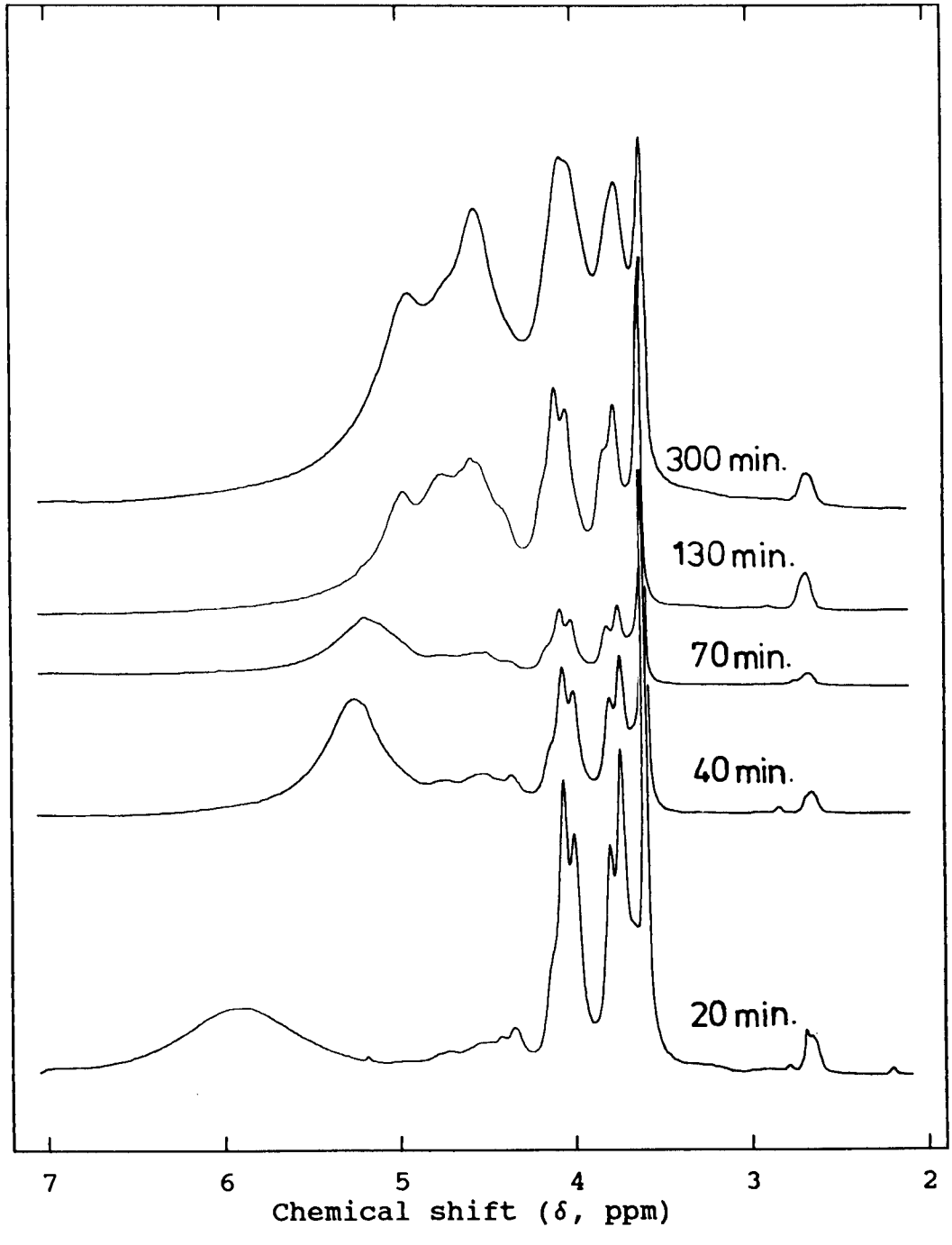

Figure 3.2(e) A series of ^{1}H-NMR spectra (80MHz, DMSO(d6), at 25^{0}C) arranged to show the changes occurring during the synthesis of resin-SC. The proprietary PEI resin formulation (cf. table 1.5) was used with refluxing at a reaction temperature of 220^{0}C. The times at which reaction samples were taken are given alongside the respective spectra.

either TMA or TA phenyl groups). Therefore, the resin contains twelve distinct and slightly different methylene groups, although the number is greater when the side-reaction, etherification, is also taken into account.

Glycolic ethers are products of nucleophilic substitution between alcoholic groups, but since hydroxylic carbons are not highly polarised, as are the carbonyl carbons of the carboxylate groups, these reactions occur less readily in the absence of a strong protic acid catalyst.[169] Such a promoter is not included in the resin formulation. In any case, at 220^{0}C, catalysis by foreign protic acids are likely to preferentially produce alkenes. Thus, the amounts of ethers formed are assumed to be negligible.

Division of the ^{1}H-NMR spectrum into an aromatic region (between 7.0 and 8.7ppm) and a methylene region (between 3.0 and 5.5ppm) permits a quantitative comparison of these molecular radicals. Here, unlike the integration of individual peaks, the total area of peak-clusters can easily be determined owing to the large chemical shift separation. The spectrum of a sample of resin-SC in DMSO, shown in figures 3.2 (c) and 3.2(d), yields an aromatic to alkyl proton ratio of 1.0:2.4, respectively, which is similar to the calculated molar ratio of 1.0:2.1, respectively. In this determination, the three triplets between 4.8 and 5.3ppm were discounted as they arise from hydroxyl protons (cf. table 3.2).

The good agreement found for the peak integrals with the calculated molar ratios confirms that the major products of resin-synthesis are those esters discussed above (cf. pages 110 and 116).

Table 3.2 Analysis of the ^{1}H-NMR spectra (300.13 MHz at 25^{0}C) of the resin, shown in figure 3.2, for the two spectrometrical solvents: $CDCl_3$ and DMSO(d6). Peak assignments were based on the ^{1}H-NMR assignments for the model compounds (cf. §2.2 and §2.3).

Molecular fragment	Chemical shifts, δ ppm in DMSO(d6)	in chloroform(d1)
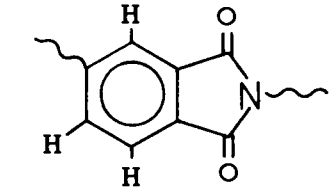	8.0 - 8.7	7.8 - 8.6
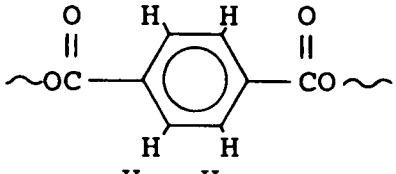		
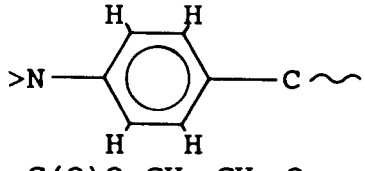	7.45 - 7.7	7.3 - 7.45
-C(O)O-C$\underline{H}_2$-C$\underline{H}_2$-O-		
>N-C-C$\underline{H}_2$-OH	4.37[2] 4.2-5.0[1]	4.2 - 4.7
>N-C$\underline{H}_2$-C-O-	4.63[2]	
-C(O)O-C-C$\underline{H}_2$-OH	3.55 - 3.75	3.6 - 3.85
>N-C-C$\underline{H}_2$-OH		
-C(O)O-C$\underline{H}_2$-C-OH	3.85 - 4.05	3.87 - 4.15
>N-C$\underline{H}_2$-C-OH		
-Ar-CH_2-Ar-	3.53	3.70
-OH	variable[3]	variable[3]

Notes. (1) Spectra for ethyl diethanoate (in DMSO(d6)) and $CDCl_3$ were also used as models. The data were taken from "The Aldrich Library of Proton NMR Spectra" (1974).
(2) The proton NMR (DMSO, 20.1MHz) assignments for a network polymer of THEIC condensed with TMA was used as a model for these assignments (cf. §2.3.12)
(3) The position of the OH proton peak varies with sample concentration, and the proton/acceptor properties of the NMR solvent. In DMSO (cf. figure 3.2(c)), triplets between 4.8 to 5.3ppm could be due to OH groups; these peaks are not observed in chloroform (cf. figure 3.2(a)).
(4) In chloroform, TA gives rise to an aromatic singlet at 8.05ppm (cf. §2.2.1.5). Such a signal is also observed in the spectrum of the resin: at 8.106ppm in chloroform, and at 8.302ppm in DMSO.

Assignments for the ^{1}H-NMR peaks are presented in table 3.2 for solutions of resin-SC in both DMSO(d6) and $CDCl_3$. The spectrum of the sample in DMSO(d6) is less congested, exhibiting substantial downfield shifting of the hydroxyl

signals than in $CDCl_3$. Although the OH signals are expected between 3.8 and 5.7ppm,[170] their positions are strongly dependent on the nature of the solvent, the concentration[171] of the subject molecular substituents, and the temperature at which the NMR experiment is performed. For instance, the formation of hydrogen-bonds with traces of water can lead to significant downfield shifts[171] as the hydroxyl proton is deshielded by secondary bonding.

Other chemical shift differences between the spectra in the two spectrometrical solvents used are also apparent. Comparing these shifts with respect to $CDCl_3$, the aromatic peaks are shifted downfield whilst the alkyl proton signals exhibit some upfield shifts. For example, the bisphenyl substituted methylene signal of the MDA radical has a chemical shift of 3.70ppm in $CDCl_3$ and 3.53ppm in DMSO(d6), an upfield shift of 0.17ppm.

The spectrum in DMSO(d6) (cf. figures 3.2(c) and 3.2 (d)) shows better differentiation of the low field triplets at 4.96($^3J_{H,H}$= 6.0Hz), 5.15($^3J_{H,H}$= 5.7Hz), and 5.26ppm ($^3J_{H,H}$= 5.4Hz), and are seen to be significantly shifted downfield from the spectrum in $CDCl_3$ (cf. figures 3.2(a) and 3.2(c)). The strong solvent interaction indicates that these peaks arise from the hydroxyl protons of the HE chain end-groups. This conclusion is consistent with the coupling constants which are seen to be similar to those found for HEB (cf. appendix II for a detailed spectrometrical exposition for HEB in both solvents) and THEIC (cf. §2.2.1.2).

Utilising the chemical shift of the OH-proton of HEB in $CDCl_3$ (cf. appendix II), the triplet at 4.96ppm ($^3J_{H,H}$ = 6.2 Hz; integral defined to be 1 proton unit) is attributable to

the OH-protons of the HE chain end-groups. The peak intensity and multiplicity correlates with the triplet at 4.01ppm ($^3J_{H,H}$= 6.2Hz; relative integral = 2 proton units) and the quartet at 3.96ppm ($^3J_{H,H}$= 5.9Hz; relative integral = 2 proton units) such that the following are plausible assignments for the HA end-groups associated with the TA-radicals of resin-SC,

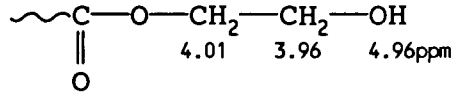

No other clear prominent triplets are observed, suggesting that the HE groups of THEIC-radicals, expected to generate triplets at 3.55 and 3.85ppm in a DMSO solution (cf. §2.2.1.2), have been substantially esterified during the synthesis of resin-SC.

The identity of the small triplets at 5.15 and 5.26ppm, seen for resin-SC in DMSO(d6) solution (cf. figure 3.2(c)), are not easily determined since none of the model compounds for which ^{1}H-NMR spectra were obtained showed similar peaks. For example, in THEIC, the OH-proton signal was observed at 4.58ppm (in a DMSO solution; cf. §2.2.1.2), and for HEB, this proton was seen at 4.41ppm (in acetone (d6); cf. table A.2, appendix II); at higher fields than the two unassigned signals. Alternatively, the ^{1}H-NMR spectrum of PET (in $CDCl_3$ solution; cf. §2.3.4) shows the chain-methylene protons at 4.7ppm; also seen in resin-SC at 4.6986ppm (cf. figure 3.2 (a). Hence, in view of insufficient facts, the low-field triplets at 5.15 and 5.26ppm cannot be assigned, but since there is a significant downfield shift in the spectra, from resin-SC in $CDCl_3$ to DMSO(d6) solutions, the protons responsible for these signals are expected to interact strongly

with the more polar solvent.

Presuming that the OH-protons for the HE end-groups can be assigned to the peaks between 4.4 and 5.3ppm in figure 3.2(c), the sum of the integrals for these peaks was used to calculate a hydroxyl number for resin-SC by calibrating the integral against the MDA-methylene peak at 3.53 ppm in figure 3.2(c). The assumption is that this calibrant peak represents a proton concentration of 9.978×10^{-4} moles/g_{resin}, according to the formulation of resin-SC; the hydroxyl number thus calculated is 78mgKOH/g_{resin}. However, owing to the difficulties encountered in assigning peaks, this value is not considered to be very reliable. The value is far below the hydroxyl number determined by titration (i.e., 165(±5) mgKOH/g_{resin}; §2.1.7).

Resin-SC also contains carboxyl chain end-groups, according to its acid number (i.e., 10.5(±0.5)mgKOH/g_{resin}). However, the ^{1}H-NMR spectra of figure 3.2 have not showed acid proton peaks between 9 and 13ppm[170] due to the low concentration of these nuclei.

Based on the ^{1}H-NMR evidence, resin-SC is considered to be a ramified oligomer with a predominance of HE chain end-groups, affirming the approximate structure illustrated in figure 1.3 (cf. §1.5.1).

The application of ^{1}H-NMR spectrometry has yielded useful information about the composition of resin-SC, although a detailed analysis is obviated by the poor peak-resolution, even at high static field strengths (i.e., 300.13MHz). Hence, a more detailed exposition requires the use of more techniques which provide increased resolution.

3.1.1.3 **Carbon NMR spectrometry**

The carbon spectra of resin-SC are presented in figures 3.3 through 3.5. Figure 3.3 shows the BB^{13}C-NMR spectrum in DMSO(d6) with an expansion of the methylene region (i.e., 40 to 70ppm; cf. figure 3.3(b)). Figure 3.4 shows the spectrum of a sample resin in $CDCl_3$ with expansions of the methylene (cf. figure 3.4(b)) and aromatic (i.e., 110 to 140ppm; cf. figure 3.4(c)) region. Figure 3.5 represents the inverse-gated, decoupled carbon NMR spectrum in DMSO(d6) for a 30 second delay (τ), rendering the sample near to fully relaxed (via spin-lattice relaxation) according to the relation[172]

$$\ln(M_o - M_z) = \ln 2.M_o - \tau/T_1 \qquad (3.1)$$

for M_o, the equilibrium magnetisation, defined to be unity; M_z representing the z-component of the macroscopic magnetisation; and T_1 standing for the spin-lattice relaxation time for the sample (see appendix III for further details); this value was determined to be 0.14 seconds. Therefore, the magnitude of M_z (x) after a τ of 30 seconds is given by substitution into equation (3.1); $\ln(1 - x) = \ln 2(1) - 30/0.14$, which implies that $x = 1 - 2.15 \times 10^{-13} \approx 1$. Hence, after this delay-time, any NOE contribution to the peak intensities can be neglected (i.e., the magnitude of M_z is very close to that of M_o), and the peak integrals reflect adequately the numbers of carbon nuclei bringing them about. Due to the much wider chemical shift range than for the protons, and the decoupling of protons, the spectra consist of singlets having a greater effective chemical shift dispersion; peak-overlap is therefore rare, even for quite large molecules.

The carbon chemical shifts for resin-SC were found to be slightly different to the model compounds, for similar

carbon nuclei. The error for the correlation of signals between resin-SC and the model compounds, in the same spectrometrical solvents, was estimated to be 1.3ppm by considering three well resolved peaks: the methylene signals for the THEIC and MDA radicals (cf. §2.2.1.2, §2.2.1.4, §2.3.1, and §2.3.2). Table 3.3 presents the chemical shifts for these peaks in resin-SC (for a solution in DMSO(d6)), comparing them with the analogous peaks for the model compounds, also in DMSO(d6).

Therefore, it was not possible to assign with certainty individual peaks in the spectra of resin-SC which were not resolved from other peaks by ±1.3ppm. Hence, the peaks were considered as divided into clusters, including the peaks falling within this range about the analogous peaks in the model compounds. Figure 3.5(d) shows the assignments to the approximate molecular structure for resin-SC according to this criterion.

The ^{13}C-NMR spectrum of resin-SC in DMSO(d6) (cf. figure 3.3) contains fewer resolved carbonyl peaks than the spectrum of resin-SC in $CDCl_3$, shown in figure 3.4. Three THEIC-carbonyl peaks at 149.5ppm, and seven ester/acid-carbonyl peaks between 164.47 and 166.32ppm are apparent in the latter, whereas the former consists of one THEIC-carbonyl and four ester/acid-carbonyl peaks. In contrast, the methylene region shows no more detail in $CDCl_3$ than in DMSO(d6); this highly polar solvent interacts strongly with carbonyl moieties, as was found for HEB (cf. appendix II, fig. A.2), tending to mask the differences in electronic environments.

The chemical shifts for the BB^{13}C-NMR spectra as well as the inverse-gated, decoupled carbon NMR spectrum (cf.

figure 3.5(a)) are listed in table 3.4(a), and the structural assignments are shown in figure 3.5(d). Table 3.3(b) lists the model compounds used to aid each assignment.

Table 3.3 The chemical shifts for the MDA and THEIC radcals of resin-SC in DMSO (cf. figure 3.3(b)) compared with similar signals for those model compounds (in DMSO solution) listed; the differences are given as X-Y.

Carbon type (-methylene)	Resin-SC chemical shift (δ, ppm) (X)	Model chemical shift (δ, ppm) (Y)	Reference model (cf. §2.2 & §2.3)	X-Y (ppm)
MDA-	41.493	40.2	MDA; MBPT; MBPA	+1.3
THEIC-(1)			THEIC	
a	44.679	43.8		+0.9
	44.761			+1.0
b	57.920	57.3		+0.6

Notes. (1) The labels used in §2.2.1.2 for the methylene groups are used; nitrous methylene group is labelled "a", and the hydroxylic methylene group is labelled "b".
The largest difference between the model and resin peaks (i.e., X-Y) is 1.3ppm, and indicates the magnitude of the uncertainty in the chemical shifts of the peaks of ^{13}C-NMR spectrum of resin-SC.

More detail may be yielded by alternative pulsed-NMR experiments. Two-dimensional spectra is a possible direction for further investigation into the chemical structure of resin-SC; the two basic experiments of two-dimensional NMR are heteronuclear shift correlation (HSC) and COSY, preferably in the form of phase-sensitive DQF-COSY. Detailed descriptions of such experiments are well reviewed by Derome,[173] and will not be discussed here. Further, spectrum editing, pulsed NMR techniques are also suggested, for instance, INEPT and DEPT may prove worthy since separate spectra are generated for CH, CH_2, and CH_3 groups; yielding similar information to off-resonance decoupling, but because the polarisation transfer spectra can be acquired with BB decoupling, both sensitivity and resolution are greatly improved.

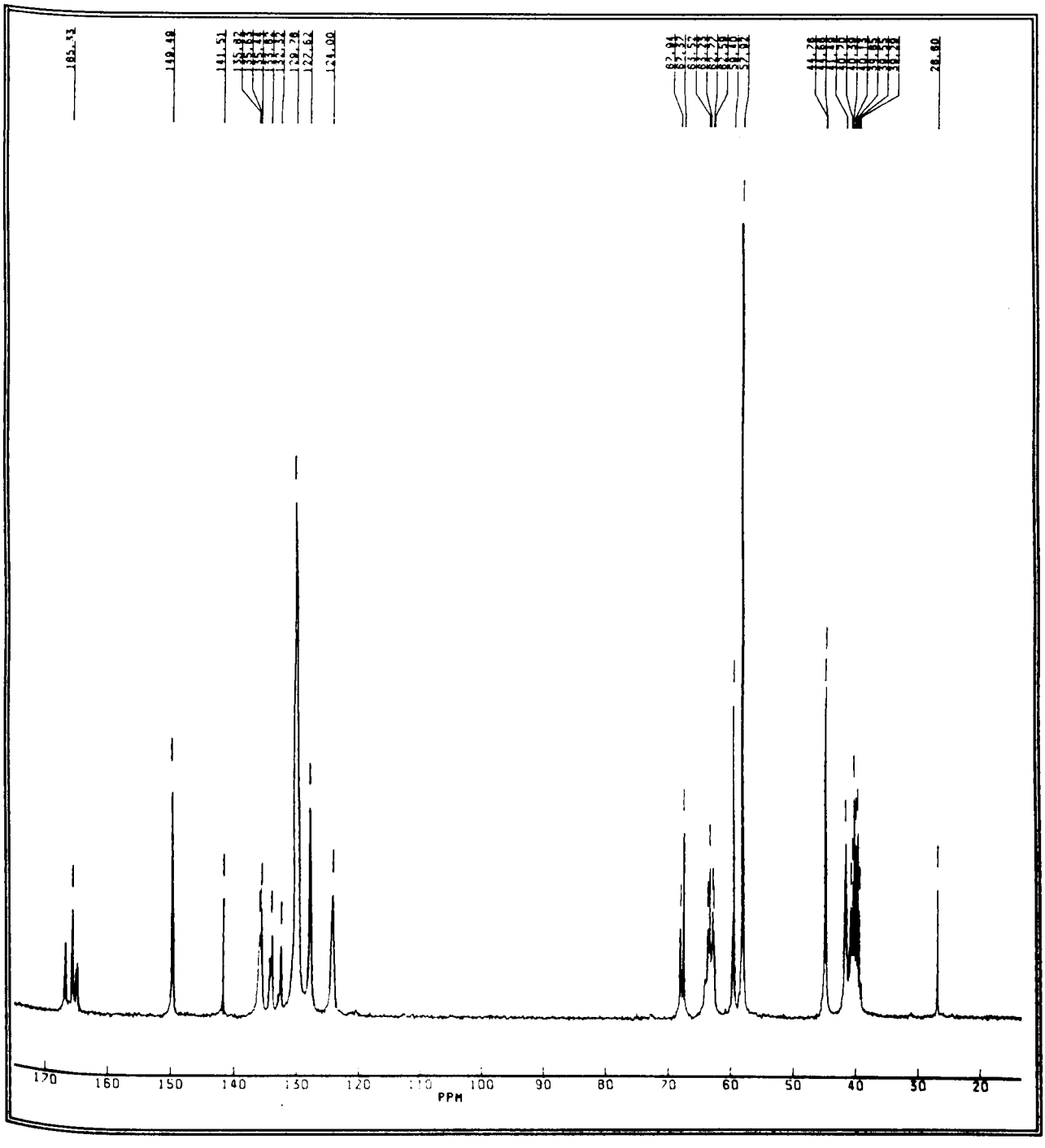

Figure 3.3(a) The broadband decoupled ^{13}C-NMR spectrum (75.47MHz, DMSO(d6), external reference: cyclohexane(26.84ppm against TMS) of resin-SC.

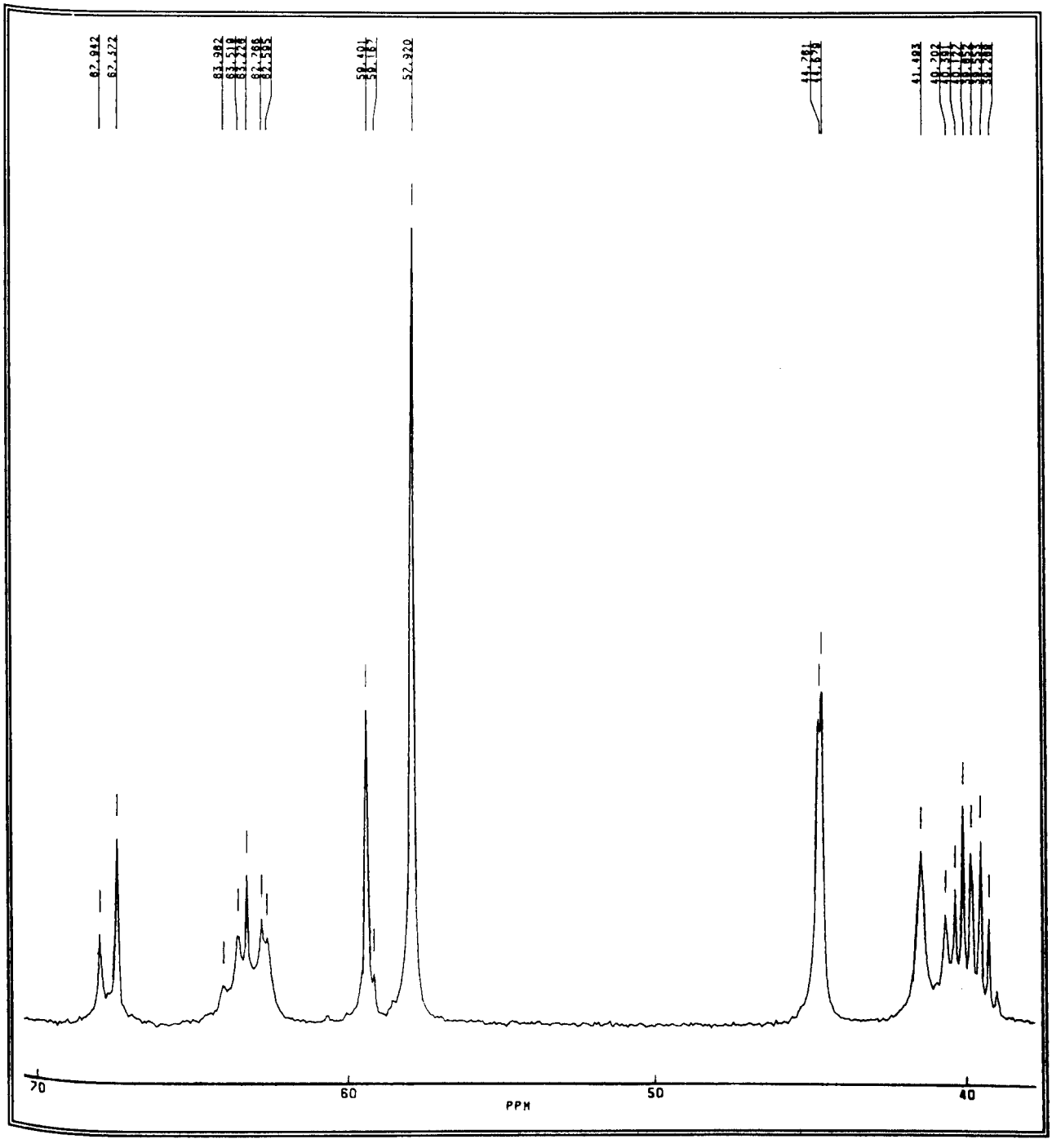

Figure 3.3(b) The expanded methylene region of the spectrum given in figure 3.3(a).

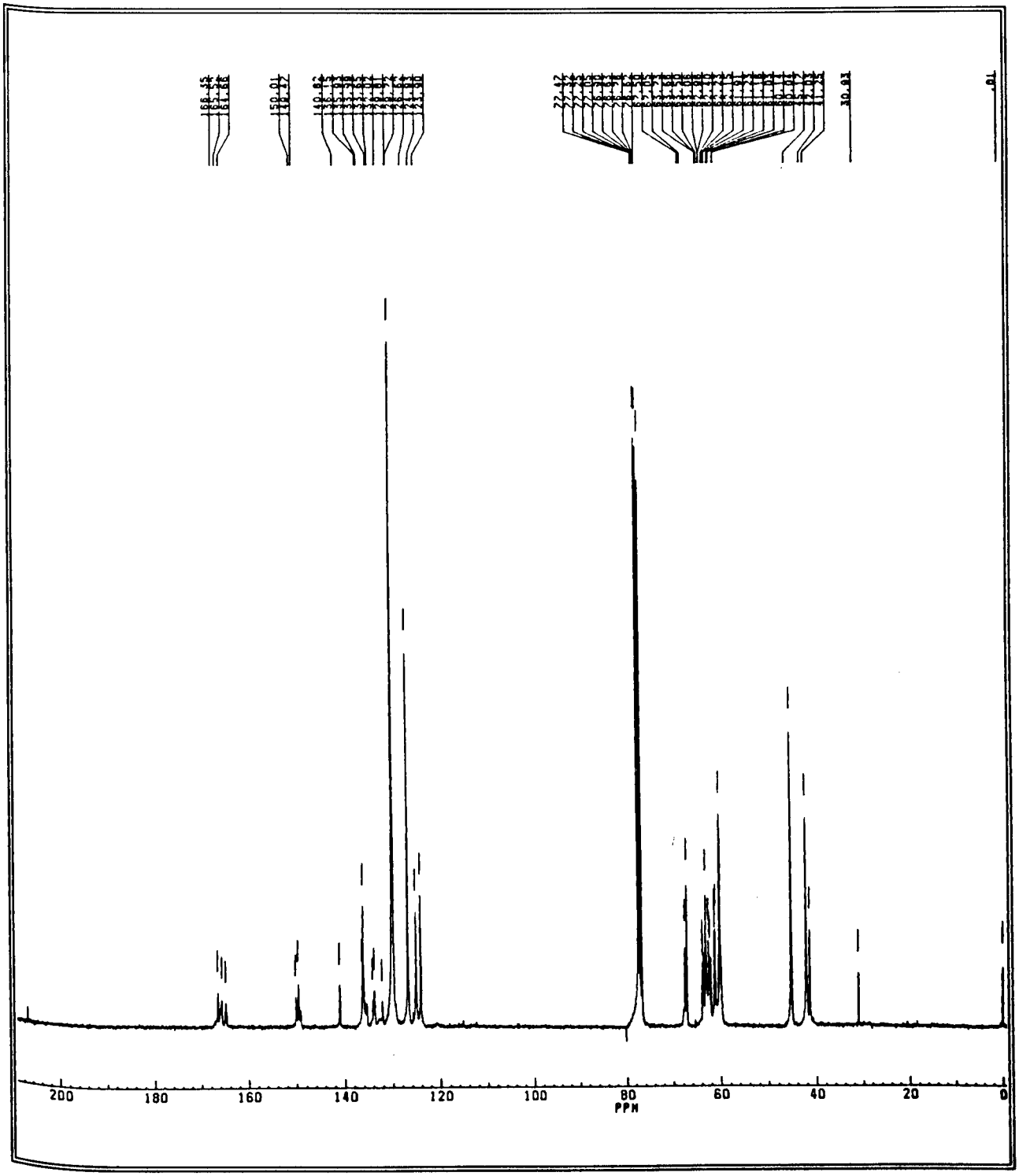

Figure 3.4(a) The broadband decoupled ^{13}C-NMR spectrum (75.47MHz, $CDCl_3$, TMS) of resin-SC.

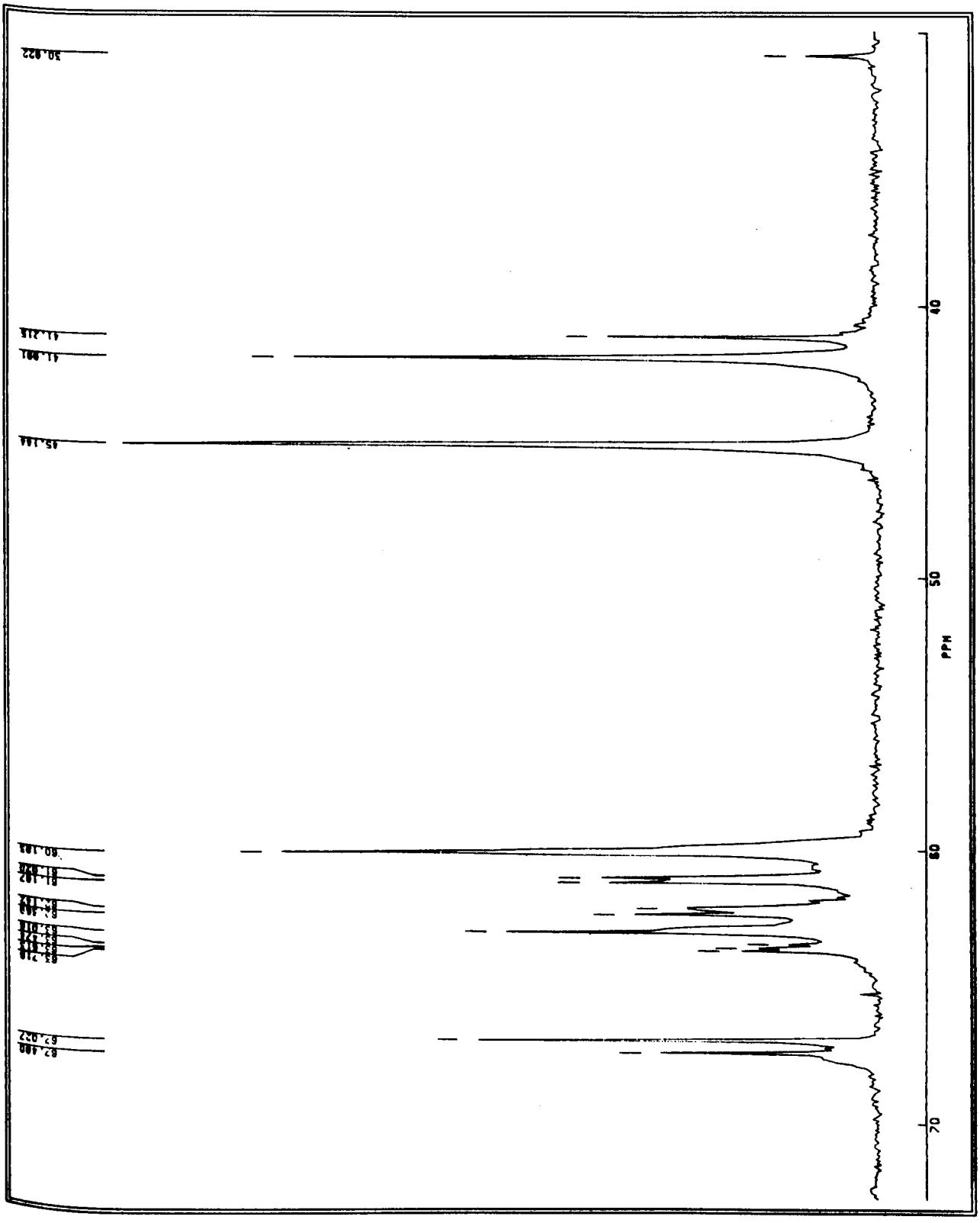

Figure 3.4(b) The expanded methylene region of figure 3.4(a). The diphenyl substituted methylene signal of the MDA radical, obscured by the DMSO signal of the inverse-gated, decoupled spectrum in figure 3.5, is clearly seen at 41.64ppm.

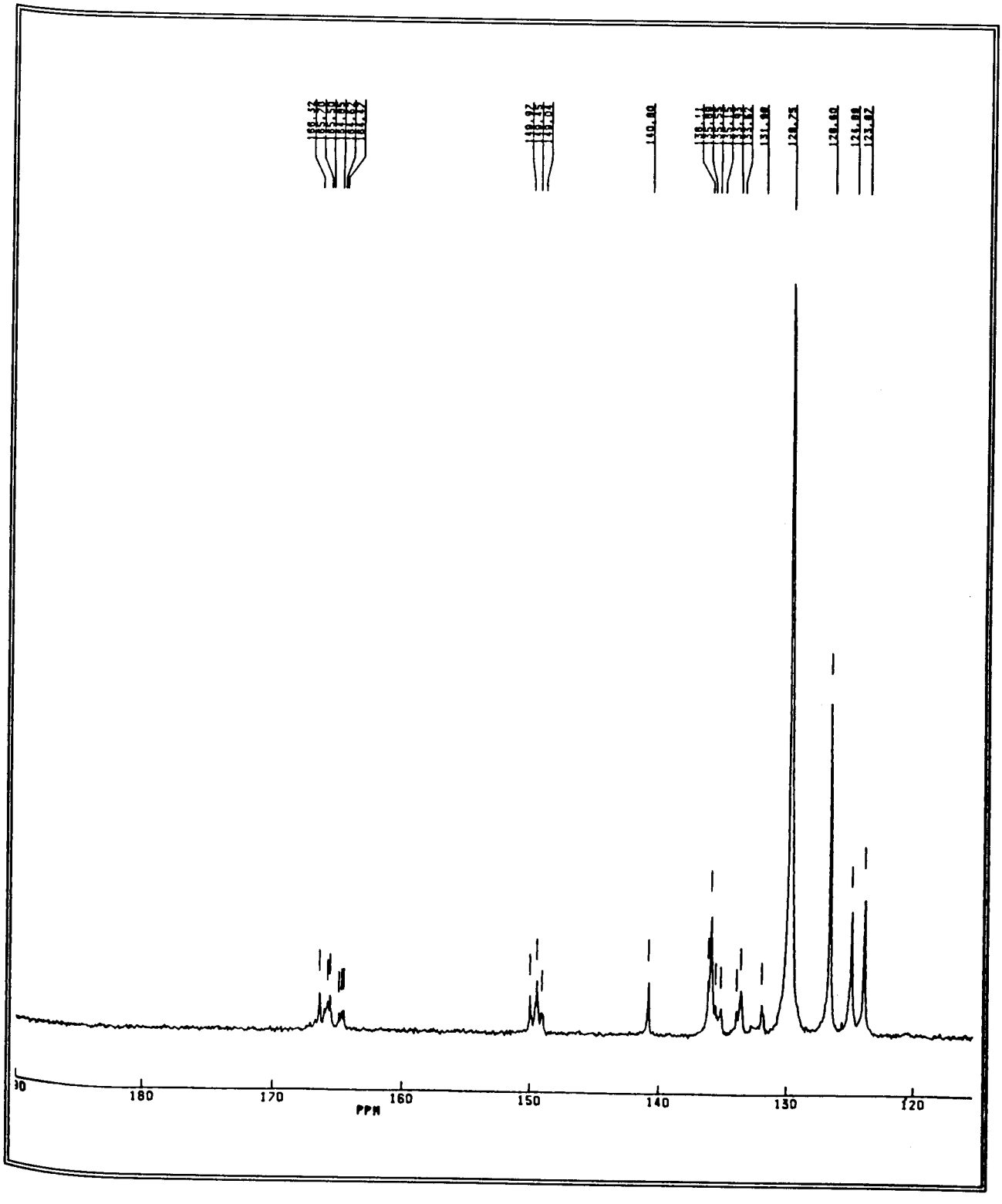

Figure 3.4(c) The expanded aromatic/carbonyl regions of figure 3.4(a).

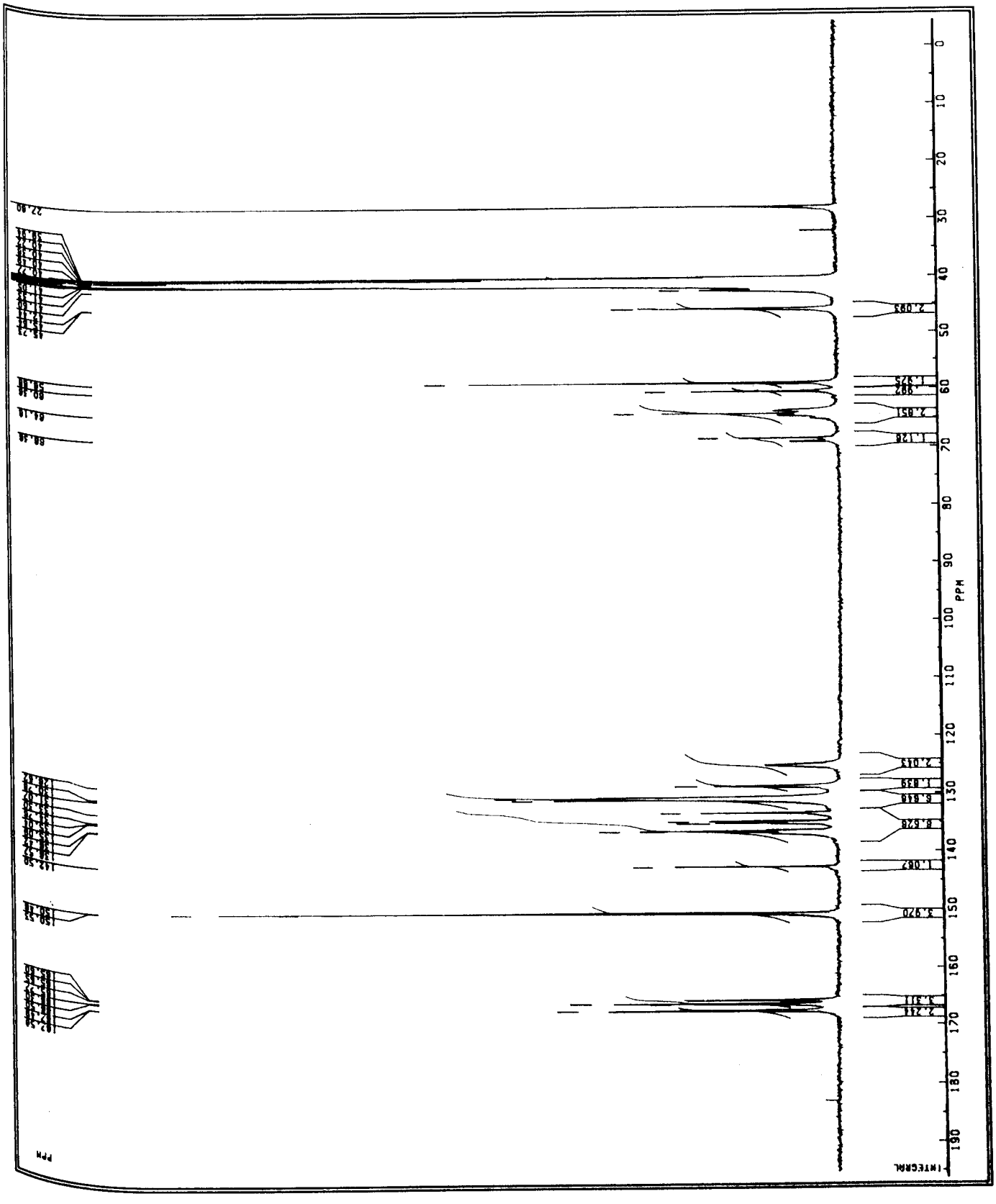

Figure 3.5(a) The inverse-gated, decoupled ^{13}C-NMR spectrum (75.47MHz, DMSO, external lock: DMSO (d6), external reference: cyclohexane (26.84ppm against TMS) of resin-SC with a 30 second delay (viz., τ) between NMR pulses. The NOE is negligible, allowing the peaks to reflect the relative numbers of carbon nuclei.

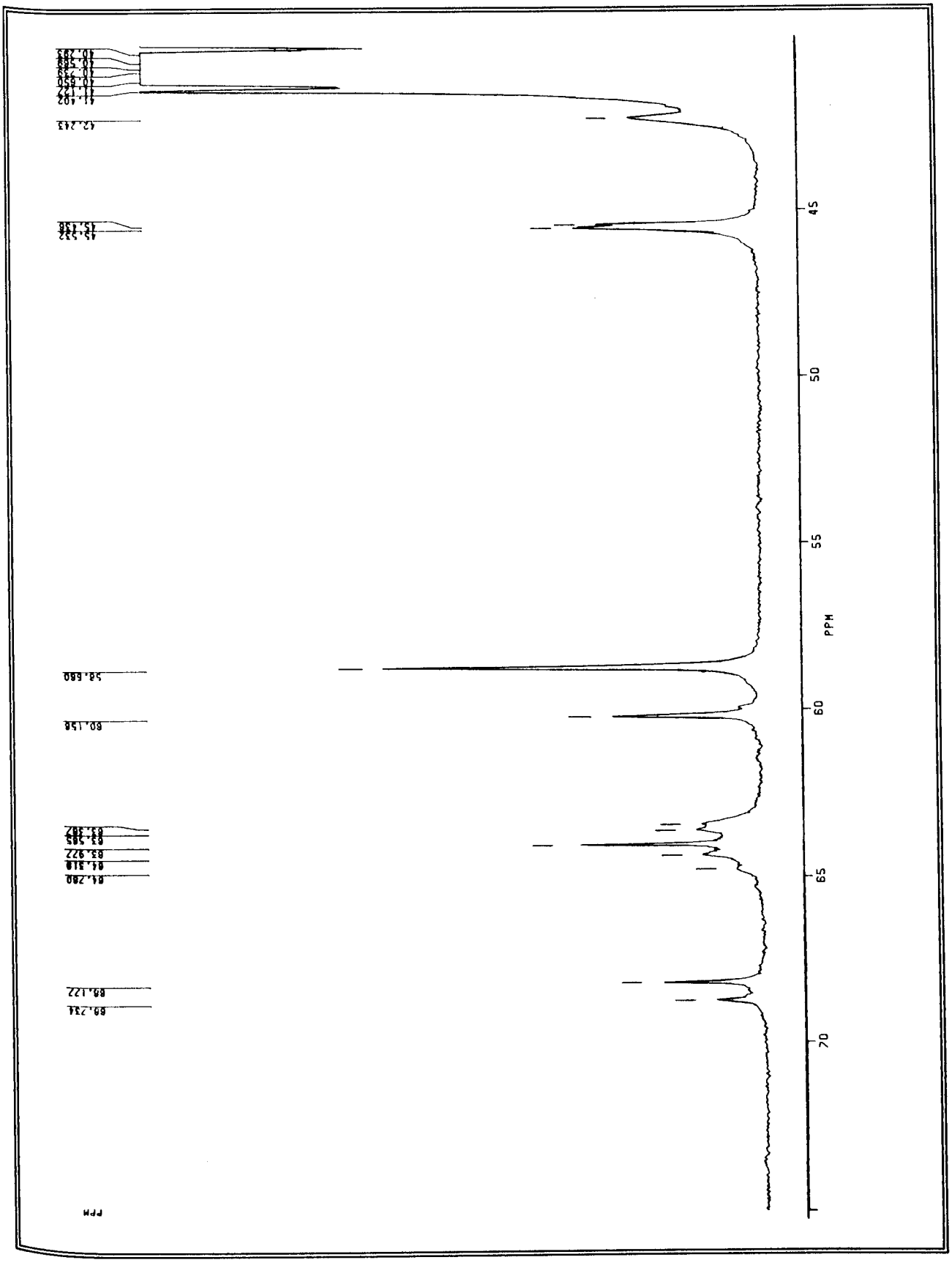

Figure 3.5(b) The expanded methylene region of figure 3.5(a).

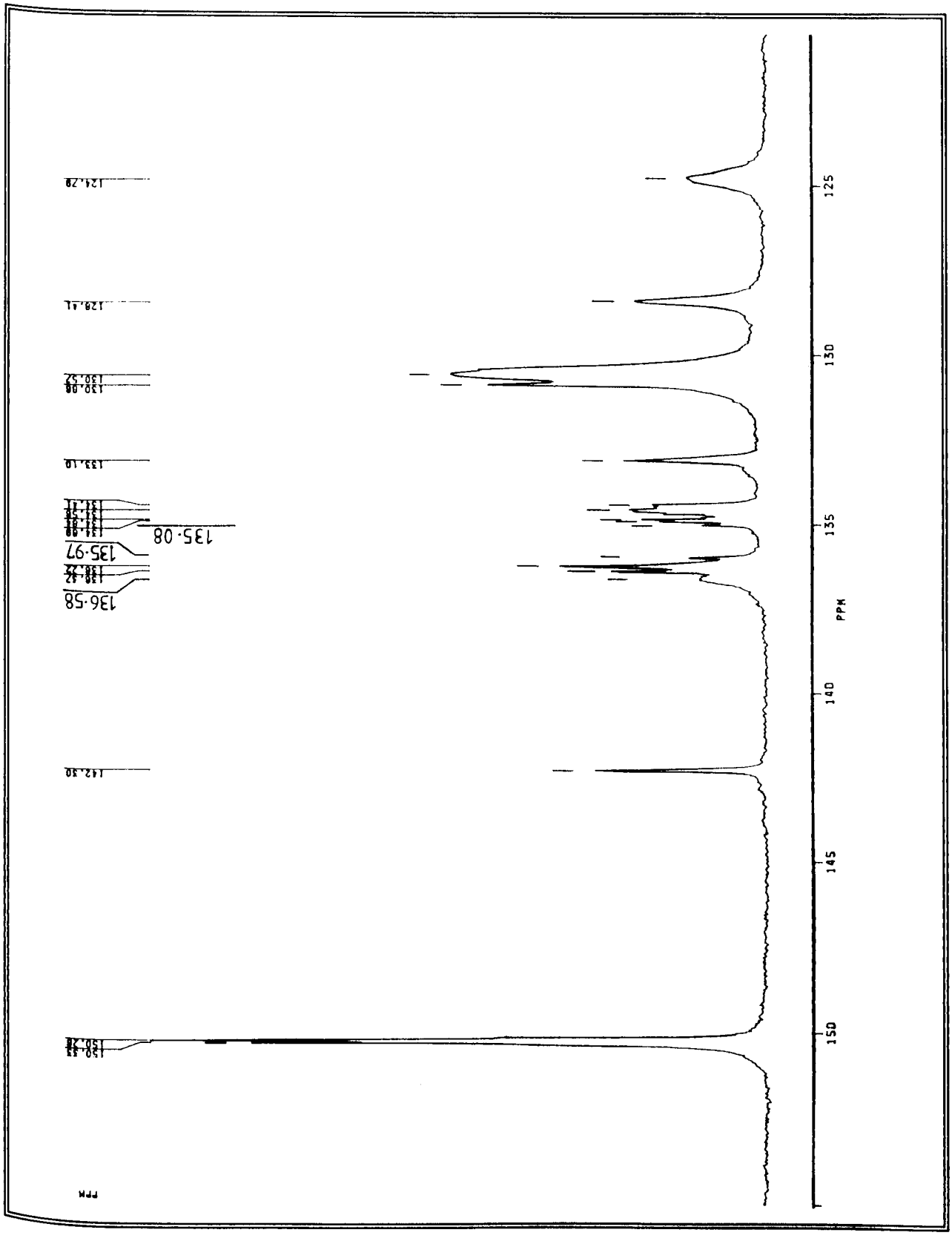

Figure 3.5(c) The expanded aromatic region of figure 3.5(a).

Table 3.4(a) The ^{13}C-NMR peaks for resin-SC, taken from the spectra presented figures 3.3 to 3.5.

Peak number	Chemical Shifts (δ, ppm) in DMSO(d6)[1]	in $CDCl_3$	in DMSO[2]	Integrals[3] (units)
METHYLENES				
1	41.73	41.99	41.47	——
2,2'	44.92,45.00	45.14	44.67,44.76	2.093
3	58.16	60.10	57.89	1.975
4,4'	59.41,59.64	61.02,61.19	59.39	0.992
5	62.83	62.14	62.66	} 2.851
6	63.01	62.37	62.80	
7	63.47	63.02	63.21	
8	63.76	63.47	63.55	
9	——	63.61	——	
10	64.22	63.72	63.99	
11	67.61	67.03	67.41	} 1.126
12	68.18	67.48	67.96	
AROMATICS				
13	124.24	123.87,124.89	124.02	2.043
14	127.86	126.60	127.64	1.839
15	130.02	129.75	129.80,130.09	6.648
16	132.56	131.98	132.33	} 6.626
17	132.94	133.62	133.64,133.79	
18	134.06	133.93	134.07,134.12	
			134.25	
19	134.44	135.15	135.20	
20	135.68	135.55	135.45	
21	135.87	135.89	135.60	
22	136.06	136.11	135.81	
23	141.75	140.80	141.53	1.067
CARBONYLS				
24	——	149.04	——	} 3.970
	149.73	149.45	149.49	
	——	149.97	149.96	
25	164.7	164.47	164.83	} 1.033
26	164.9	164.62	164.88	
27	——	164.85	165.00	
28	165.57	165.50	165.53	} 2.279
29	——	165.70	165.63	
30	——	165.90	165.73	
31,31'	166.8	166.32	166.72,166.81	2.244

Notes. Assignments of peaks were made from the BB ^{13}C-NMR assignments for the model compounds described in §2.2 and §2.3 (cf.table 3.4(b)). Due to an uncertainty of 1.5ppm in the chemical shifts of similar carbon nuclei, it was not always possible to assign individual peaks. Hence, groups of peaks are assigned to the structural features of the resin (cf.figure 3.5(d)) where ambiguity exists, e.g., the group of peaks 5-10 includes all of the methylene signals for methylenes adjacent to ester groups.

(1) The chemical shifts are adjusted by +0.24ppm for the error found in the assignment of the external reference (viz., cyclohexane) in the spectrum given in figure 3.3.

(2) The chemical shifts are adjusted by -0.77ppm for the error in the assignment of the external reference (viz., cyclohexane) in the spectrum given in figure 3.5.

(3) The spectrometer generated peak-integrals are quoted from the inverse-gated, decoupled ^{13}C-NMR spectrum given in figure 3.5.

The spectrum for resin in $CDCl_3$ solution was referred to internal TMS, and the others were referred to neat cyclohexane (at 26.875ppm; 20.1MHz, $CDCl_3$, 3vol.% TMS, 25^{0}C) sealed in a capillary-tube.

Table 3.4(b) The model compounds (cf. §2.2 and §2.3) utilised for assigning the ^{13}C-NMR peaks listed in table 3.4(a) to the approximate structure of resin-SC, in figure 3.5(d).

Peak number	Model compound(s)	Remarks
METHYLENES		
1	MDA(§2.2.1.4)	bisphenyl methylene group
2,2'	THEIC(§2.2.1.2)	nitrous methylenes
3	THET(§2.3.3)	hydroxylic methylenes of unesterified THEIC ends
4,4'	THET; PET(§2.3.4)	hydroxylic methylenes of the HE chain end-groups
5-10	PET	methylenes of the glycolic chain units
11-12	PET; THET	methylenes adjacent to the ester groups in the HE chain end-groups
AROMATICS		
13	MBPT(§2.3.1)	TMA-radicals in the imide chain units
14	MBPT	MDA-radicals of imide-units (meta to the nitrogen atom)
15	MBPT	MDA-radicals of imide-units (ortho and para to nitrogen)
16,17	MBPT; THET; TMA (§2.2.1.3); TA (§2.2.1.5); MBPA (§2.3.2)	
18,19	PET; THET; TA; MBPT	TMA-radicals: ipso and ortho to esterified carboxyl groups
20-22	THET; MBPT	ipso carbon of TMA-radicals
23	MBPT	MDA-radicals: ipso to nitrogen in imide-units
CARBONYLS		
24	THEIC	
25-27	PET	esterified TA-radicals
28-30	MBPT; THET	
31,31'	MBPT; TA; TMA; THET	

Notes. Assignments were referred to the similar carbon atoms of the model compounds. Therefore, the assignments given in figure 3.5(d) are easily compared with the model compounds by noting the type of carbon atom to be considered; the atomic labelling used in figure 3.5(d) is not related the labels used to assign NMR signals to the model compounds.

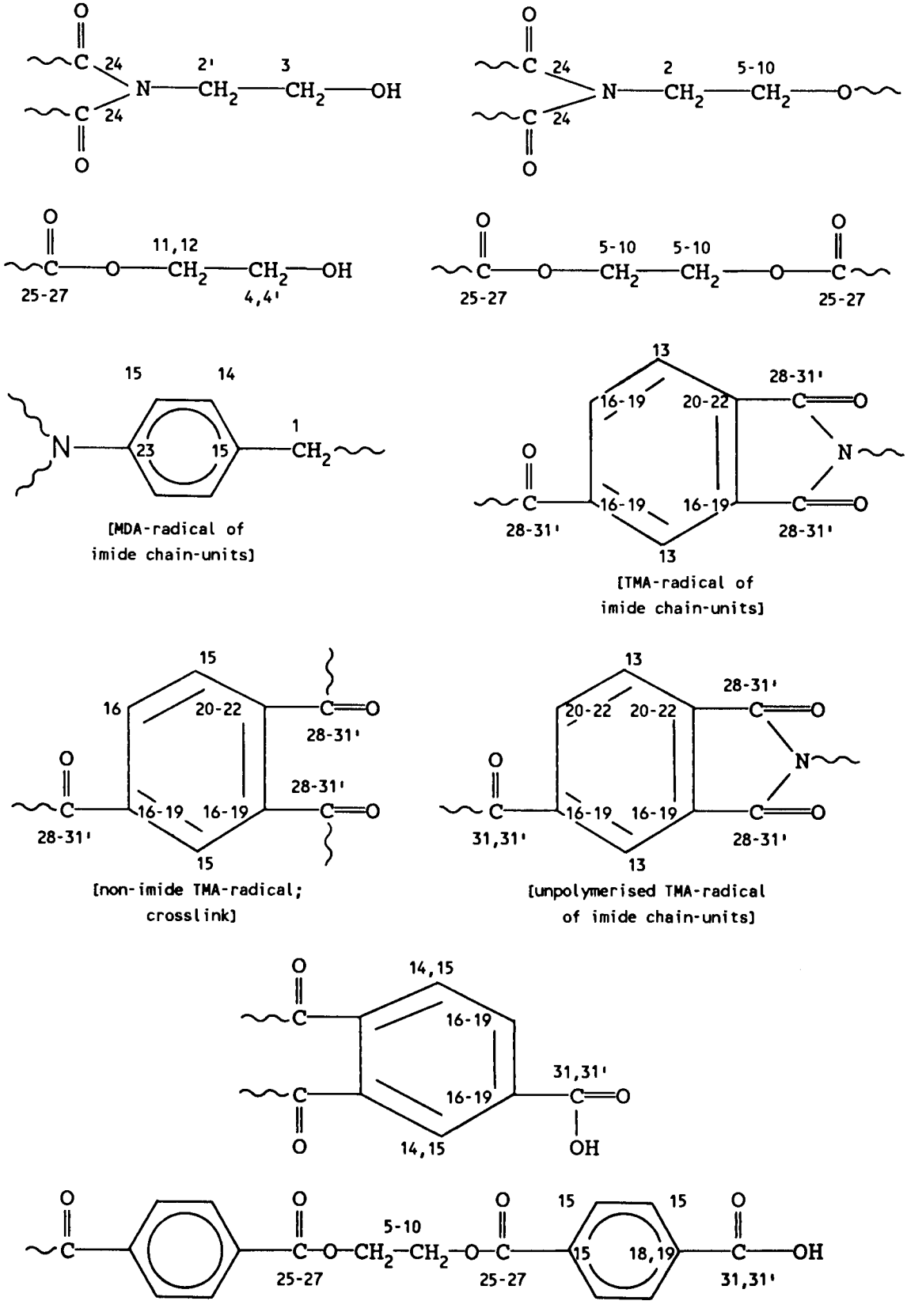

Figure 3.5(d) The assignments of the ^{13}C-NMR peaks to the approximate molecular structure of resin-SC (cf. table 3.3). Although a high field (i.e., 75.47MHz) spectrometer was used, many signals were not well resolved, and where peaks were found to be within 1.5ppm, specific assignments were not possible. Therefore, these structural features were assigned to groups of peaks.

The relative numbers of carboxyl and HE chain end-groups in resin-SC were determined by integration of the appropriate peaks in the inverse-gated, decoupled ^{13}C-NMR spectrum (see the assignments given in figure 3.5). The computed integrals (by the Brüker CXP-300 spectrometer) for the methylene peaks between 45 and 70ppm were totalled, and calibrated against the integral for the nitrous-methylene signals (at 44.67 and 44.76ppm) of the THEIC radicals, yielding a ratio of 3.2:1.0, respectively. The same ratio was calculated by the cut-and-weigh method of these peaks, and was found to be 3.3:1.0, respectively; a variation of 3.8%. The magnitude of this variation is similar to the estimated error for the latter method (i.e., 2.46%; cf. §2.1.4). The former method gave an error of 1.3% greater than the latter method, therefore, this difference was attributed to the error inherent in the integral-computation performed by the CXP-300. Hence, the peak-integrals generated by the CXP-300 were considered to represent reasonably the peak-areas of the NOE-suppressed spectrum (cf. figure 3.5(a)), and were thus used in the discussion following.

Comparison of the integral-ratio for the carbonyl (between 149-167ppm) and aromatic peaks (between 124-142ppm), referred to the THEIC-carbonyl peak (at 150.46/150.53ppm) as a calibrant, with the same ratio calculated from the resin formulation (cf. table 1.5) yields a discrepency of 9%. Therefore, the peak-integrals are sufficiently accurate to give useful carbon counts to within an estimated uncertainty of 9 + 1.3%, or ≈10%. A factor for calibration is needed to relate peak-integrals to structural features, and thus, peaks within the spectrum were chosen to act as references.

Calibration peaks were chosen in accordance with two criteria: first, that the carbon nuclei which generate the peaks are structurally remote (i.e., more than four bonds) from the polymer propagation-sites; such nuclei are not subject to vast changes in chemical environment during resin-synthesis, and thereby have similar NMR signals to the resin-precursors (cf. §2.2). Assignments can therefore be made confidently. The other criterion was that the peak of choice be spectrally well resolved, allowing its integral to be calculated easily. Thus, the peaks selected were those arising from the **ipso**-aromatic carbon nucleus to the imide nitrogen atom (i.e., peak 23; cf. figure 3.5(d)), and the THEIC-carbonyl carbon atom (i.e., peak 4). These are referred to as the "calibrants". Integral-calibration factors were calculated for each calibrant nucleus from their molar concentrations, determined using the resin formulation, such that the factors have the units of mol/(g_{resin}.integral-unit). The factors thus calculated are listed in table 3.5 together with the averaged integral-calibration factor. The standard deviation of this average is 5% of the value, and well within the uncertainty quoted earlier for the comparison of the integrals of peak-clusters with the sum of the molar concentrations for the relevant nuclei (i.e., 9%). The assignment of a larger number of reference peaks is expected to improve the accuracy of the factor, but no other peaks comply with the selection criteria.

The integral-calibration factor was used to estimate the numbers of reactive chain end-groups from figure 3.5. The hydroxyl number was estimated directly from the sum of

the integrals for peaks 3 and 4, which are due to the methylene nuclei adjacent to OH end-groups, yielding a value of $2.9(\pm0.3)\times10^{-3}$mol/g_{resin} (i.e., $158(\pm16)$mgKOH/g_{resin}). This value is similar to that determined titrimetrically (viz., $165(\pm5)$mgKOH/g_{resin}; cf. table 2.1) and that published for PEI-T[104] (i.e., 164mgKOH/g_{resin}). In comparison, the value determined from the ^{1}H-NMR spectrum (i.e., 78mgKOH/g_{resin}; cf. §3.1.1.2) is very low, suggesting that the latter is inaccurate (assignments were difficult; cf. §3.1.1.2).

Table 3.5 The integral-calibration factors for the inverse-gated, decoupled ^{13}C-NMR spectrum (cf. fig. 3.5(a)) of resin-SC.

Carbon Nucleus(1)	Chemical Shift (δ, ppm)	Computed Integral(2) (integral-units)	Formulation Concentration (mol/g)	Calibration Factor (mol/(g.integral-unit))
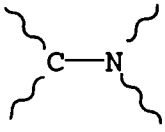	141.53	1.1±0.1	9.8×10^{-4}	$9.2(\pm0.9)\times10^{-4}$
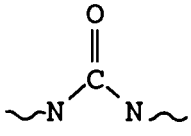	149.49, 149.96	4.0±0.4	4.0×10^{-3}	$1.0(\pm0.1)\times10^{-3}$

Notes. (1) Reference peaks were selected for their remoteness from propagation-sites; the ipso-aromatic signals selected were shown by ^{1}H-NMR to be the only form of MDA-radicals present in resin-SC.

(2) The integrals quoted are those computed by the Brüker CXP-300 spectrometer used to obtain the inverse-gated, decoupled ^{13}C-NMR spectrum shown in figure 3.5(a).
The averaged value for the calibration-factor is $9.7(\pm0.5)\times10^{-4}$mol/g_{resin}.

The acid number cannot be derived as easily as the hydroxyl number since the individual carbonyl peaks could not be assigned confidently (cf. figure 3.5(d); table 3.4). The cluster of peaks designated as peaks 28 to 31' are assigned to the HE-ester, the imide, and the carboxyl carbonyl groups. Hence, in order to extract the number of carboxyl carbonyls (and thereby the acid number) a differential calculation was performed to eliminate the integrals of the

first two carbonyl-types. Thus, the number of imide carbonyls was estimated from peak 23 (i.e., twice the integral of the peak due to the **ipso**-aromatic carbon from the nitrogen atom) to be 1.1(±0.1)integral-units, and the number of HE-ester carbonyls was estimated from peaks 3 and 4 (i.e., the same as the number of hydroxyl groups); 3.0(±0.3) integral-units. Addition of these values (i.e., 4.1(±0.4) integral-units), followed by subtraction of this sum from the totalled integral of the carbonyl peak-cluster (i.e., peaks 28 to 31'; 4.5(±0.5) integral-units) yields an integral associated with the carboxyl end-groups, that is, 0.4(±0.12) integral-units.

Table 3.6 The numbers of -COOH and -OH chain end-groups of resin-SC, deduced from the inverse-gated, decoupled NMR peak integrals (cf. figure 3.5). The acid and hydroxyl numbers, determined by titration, are compared with values derived from proton and carbon NMR spectra, and the values for the literature resin PEI-T. The values are given in milligrams of KOH equivalent to one gram of resin sample.

Source	Acid Number ($mgKOH/g_{resin}$)	Hydroxyl Number ($mgKOH/g_{resin}$)
PEI-T[1]	9.6	164
Titration[2]	10.5(±0.5)	165(±5)
Proton NMR[3]	——	78
Carbon NMR[4]	22(±8)	158(±16)

Notes. (1) See Penczek et al.[104] (2) Details of the titrimetrical acid and hydroxyl number determination methods are presented in appendix I. (3) Due to peak overlap, difficulty was met in assigning peaks within the clustered methylene region, therefore, the hydroxyl number deduced from the ^{1}H-NMR spectrum (cf. §3.1.1.2) is tentative. No carboxylic acid hydroxylic proton was observed, obviating calculation of the acid number from the ^{1}H-NMR spectrum of resin-SC; Cynkowska et al.[105] has also not detected this proton-signal for PEI-T. (4) Inverse-gated, decoupled ^{13}C-NMR spectrometry was used to suppress the NOE (cf. figure 3.5(a) and §2.1.1).

Converting the carbonyl group-integral to a molar concentration, using the integral-calibration factor, yields the value $3.9(\pm1.4)\times10^{-4}mol/g_{resin}$, or an acid number of $22(\pm8)mgKOH/g_{resin}$ which is similar to the titrimetrically determined value (i.e., $10.5(\pm0.2)mgKOH/g_{resin}$; cf. §2.1.6).

The difference is 11.5mgKOH/g_{resin}, or 47% of the value derived by integration, suggesting that the method used is not particularly accurate; this discrepency is of a similar order to the cumulative relative error for the calculation of the carboxyl-integral (i.e., 30.2%).

Table 3.6 compares the acid and hydroxyl numbers determined by the two NMR methods with the titrimetric values for both resin-SC and PEI-T.[104] Apparently, ^{13}C-NMR is the more useful method for the counting of reactive chain end-groups as well as the detailed characterisation of such polymeric systems. The NOE-suppressed ^{13}C-NMR spectrum has yielded data which correlates quite well with the wet-chemical methods used throughout the varnish industry, taking into account the errors, and is therefore a viable alternative method for the characterisation of the structural components of industrially important, albeit complex, resins.

A notable feature of the ^{13}C-NMR spectrum in $CDCl_3$ (cf. figure 3.4) is the absence of any peaks which can be assigned to intramolecularly hydrogen-bonded HE end-groups. The existence of such secondary bonding is expected to give rise to a carbonyl peak, or peaks, at ≈172ppm (172.47ppm in HEB; cf. appendix II, table A.3), but the spectrum exhibits no such signal downfield of 166.81ppm. Therefore, since there are sufficient HE end-groups to generate such a signal, it must be concluded that they do not partake of intramolecular hydrogen-bonding, at all. Disruption of such secondary interactions by the carbonyl groups of the resin (i.e., the ester and carboxyl groups) is a likely explanation for the absence. Perhaps this causes the three THEIC-carbonyl peaks observed for resin-SC in chloroform solution (149.04,

149.45, and 149.97ppm; peak 24; cf. figure 3.4(c)) which are seen as a single peak at 149.49ppm in DMSO solution (cf. figure 3.3(a)). Polar solvents such as DMSO perturb any hydrogen-bonding, solvating all of the carbonyl groups of the THEIC-radicals in resin-SC.

The absence of intramolecular hydrogen-bonding, of the sort found in HEB in $CDCl_3$ solution, is not relevant to the curing of Isomid wire-varnish since cresylic acid (a strong proton donor) disrupts effectively any such interactions, solvating the reactive end-groups.

Solution ^{13}C-NMR spectrometry has provided useful confirmation of the concentrations of the reactive chain end-groups as well as an insight into the overall chemical structure of resin-SC. However, these techniques are unsuitable for the study of the highly crosslinked wire-enamels formed by thermally curing Isomid wire-varnish. The enamel is an infusible, insoluble, tightly crosslinked polymer film, which can neither be dissolved nor swollen by highly polar solvents. Hence, solid-state ^{13}C-NMR spectrometric techniques were used to study the cured state; Isomid wire-coating.

3.1.1.4 **Solid-state NMR spectrometry of resin-SC**

The first consideration in the solid-state NMR analysis of Isomid wire-enamel (viz., the cured wire-varnish) is to establish the solid-state NMR characteristics of resin-SC.

The spinning-sideband suppressed (i.e., the TOSS/PE-MASS) solid-state ^{13}C-NMR spectrum of resin-SC is given in figure 3.6, exhibiting five broad peaks which are seen at similar chemical shifts as in the BB^{13}C-NMR spectra (cf. figures 3.3 to 3.5). Table 3.7 compares the TOSS/PE-MASS

spectrum of a finely ground sample of resin with the BB^{13}C-NMR spectrum of the same sample. The aromatic peak (at ≈131.2ppm) is resolved into two major peaks at 129.5 and 132.5ppm (cf. figure 3.6(a,ii)). Such detail is lost in PE-MASS spectra (using CP only; cf. §2.1.2) which are without sideband suppression, resulting in a featureless single, broad aromatic peak. Furthermore, three smaller peaks are noticed at 122.9, 124.1, and 141.5ppm, and again in figure 3.6(b) (the TOSS/PE-MASS spectrum for resin-SC cured thermally to a T_g of 102^{0}C), these latter peaks are seen a little more prominently at 122.9, 124.6, and 141.7ppm. The smaller peaks approach the intensity of the baseline-noise, but since they appear in independent spectra and correlate with peaks in the BB^{13}C-NMR spectra of resin-SC (cf. table 3.7), these peaks are confidently considered to be present.

Curing a sample (4.3g) of resin-SC to a glass transition temperature (T_g) of 102^{0}C by heating at 300^{0}C under vacuum produced a significant reduction in the intensity of the HE-methylene signals (at 59.0 and 66.8ppm; cf. figure 3.6(b)). Upon polycondensation, the HE end-groups are converted to ethylene diesters with the loss of condensed EG by vaporisation; EG and water were found to have condensed (0.02g) in a nitrogen-trap. Analysis by ^{1}H-NMR (80MHz, DMSO (d6), 25^{0}C) yielded two distinct singlets at 2.9ppm (i.e., EG-methylene groups), defined to be 1.0 proton-unit in area, and at 3.6 ppm (i.e., water) with a relative area of 3.3 proton-units. Absence of the OH-proton signal of EG was due to hydrogen-bonding with water; the water signal therefore, includes this resonance; the difference gives the proportion of water-protons present, that is, 3.3-(1.0/2)=2.8 proton-

units. Therefore, the molar ratio of water ((2.8 units)/(2 protons)) to EG ((1.0 unit)/(4 protons)) is 5.6:1.0, and thus, the material that had distilled into the nitrogen-trap contained 85mol% water and 15mol% EG, that is, 62wt.% water and 38wt.% EG, which is equivalent to 0.012g of water and 0.0074g of EG. Therefore, the mass lost from the resin was 0.28wt.% water and 0.17wt.% EG. The ^{1}H-NMR spectrum exhibited no other resonances, indicating that in the absence of solvents and catalysts the resin cures through esterification rather than ester exchange in the initial stages of curing, although both reactions are significant. Based on the acid number of resin-SC (§2.1.6), of the 8.05×10^{-4}moles of the carboxyl end-groups available, 6.67×10^{-4}moles have apparently esterified.

Esterification of carboxyl with HE end-groups condensed water, and ester exchange[33,104,174] between HE end-groups condensed EG. Ester exchange is the only source of EG since the resin contains no free EG, according to the PESOLIQ/PE-MASS spectrum of resin-SC (cf. figure 3.7); the "liquid-like" spectrum is devoid of any sample signals, including an EG signal expected at ≈63ppm. The conclusion was further confirmed by washing a sample of powdered resin in water; the extraction showed no trace of EG by either ^{1}H- or ^{13}C-NMR spectrometry.

Table 3.7 Analysis of the TOSS/PE-MASS ^{13}C-NMR spectrum (delrin; spinning rate: 3010Hz) of a powdered sample of resin-SC. The peaks are compared with the BB^{13}C-NMR spectra of the resin given in figures 3.2 to 3.5.

Group Number[1]	Chemical Shifts (δ,ppm) Solid-State NMR[2]	Solution NMR[3]
METHYLENES		
1	40.9	41.47
2, 3	43.7	44.67, 44.76
4, 4'	59.0	57.89 - 59.39
5 - 10	63.0	62.66 - 63.99
11, 12	66.8	67.41, 67.96
AROMATICS		
13	122.9, 124.1	124.02
14, 15	129.5	127.64 - 130.09
16	131.2	132.33
17 - 22	133.3	133.79 - 135.81
23	141.5	141.53
CARBONYLS		
24	149.4	149.49, 149.96
25 - 31'	165.1	164.83 - 166.81

Notes. (1) Structural groups are numbered in figure 3.5(d).
(2) The TOSS/PE-MASS ^{13}C-NMR spectrum is shown in figure 3.6(a,i), and differs from the PE-MASS spectrum (cf. figure 3.6(a,ii)) by the absence of spinning-sidebands, revealing more detail.
(3) The solution NMR (i.e., BB^{13}C-NMR) peaks were taken from the spectrum in solution with DMSO(d6); shown in figure 3.5(a).
Peaks 13 and 23 have intensities similar to the baseline-noise, but are resolved in two independent TOSS/PE-MASS spectra (viz., figures 3.6(a,i) and 3.6(b))), both of which exhibit these peaks at sim-ilar chemical shifts. As well, similar peaks are observed in the BB^{13}C-NMR spectrum of resin-SC.

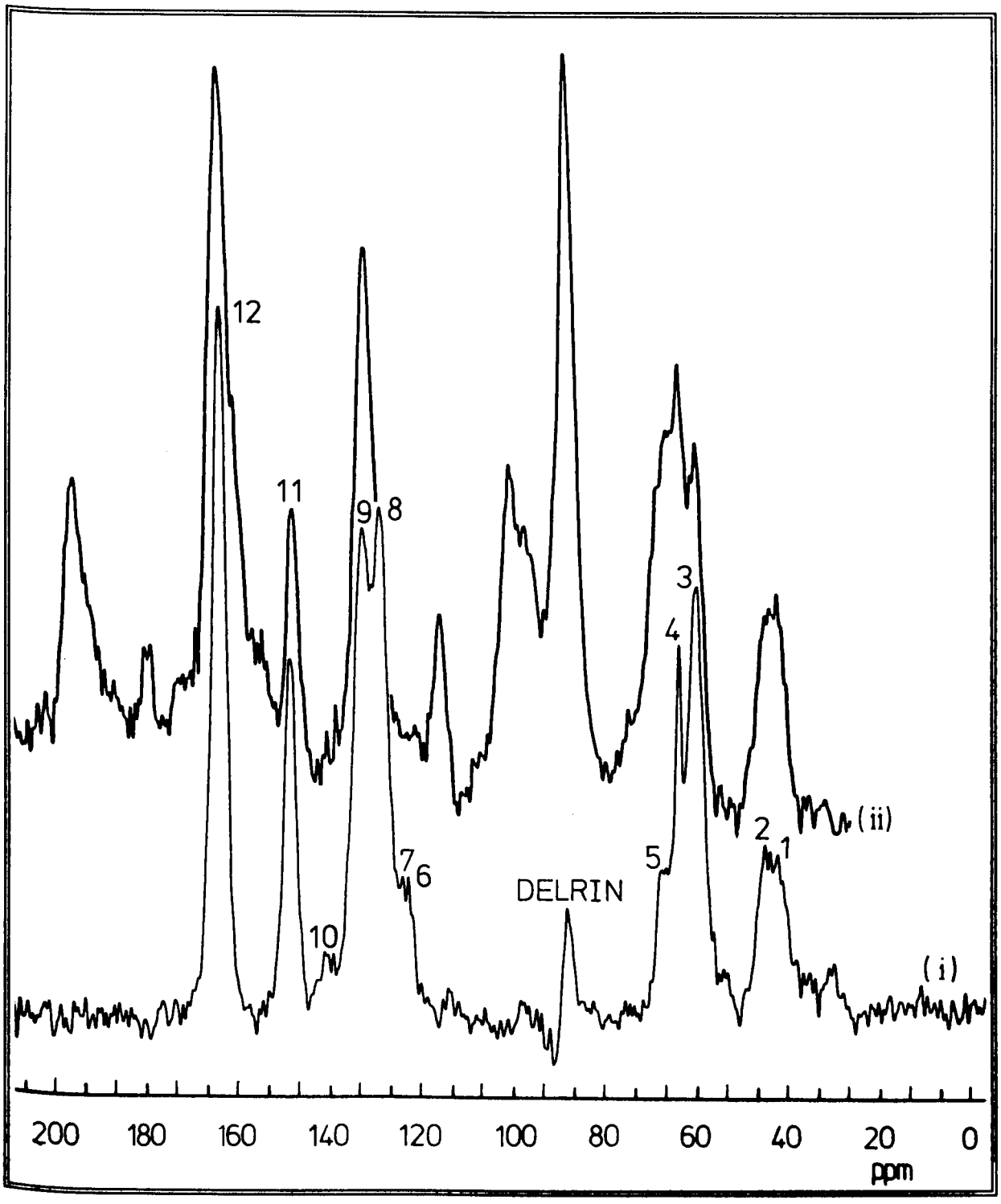

Legend

1. 40.9	3. 59.0	6. 122.9	9. 133.3	11. 149.4
2. 43.7	4. 63.0	7. 124.1	10. 141.5	12. 165.1
	5. 66.8	8. 129.5	Delrin: 87.3ppm	

Figure 3.6(a,i) The TOSS/PE-MASS ^{13}C-NMR spectrum (delrin; spinnind rate: 3010Hz) of finely powdered resin-SC. The TOSS/PE-MASS experiment, described in §2.1.2, suppresses the spinning-sidebands, increasing markedly the spectral detail. (a,ii) The PE-MASS ^{13}C-NMR spectrum (delrin; spinning rate: 3010Hz) has been overlaid to accentuate the improvement in spectral detail.

Note. Peaks 6, 7, and 10 are small, and their intensities approach the baseline-noise, however, similar signals appear in an independent spectrum (cf. figure 3.6(b)) of resin-SC, suggesting that these peaks are real.

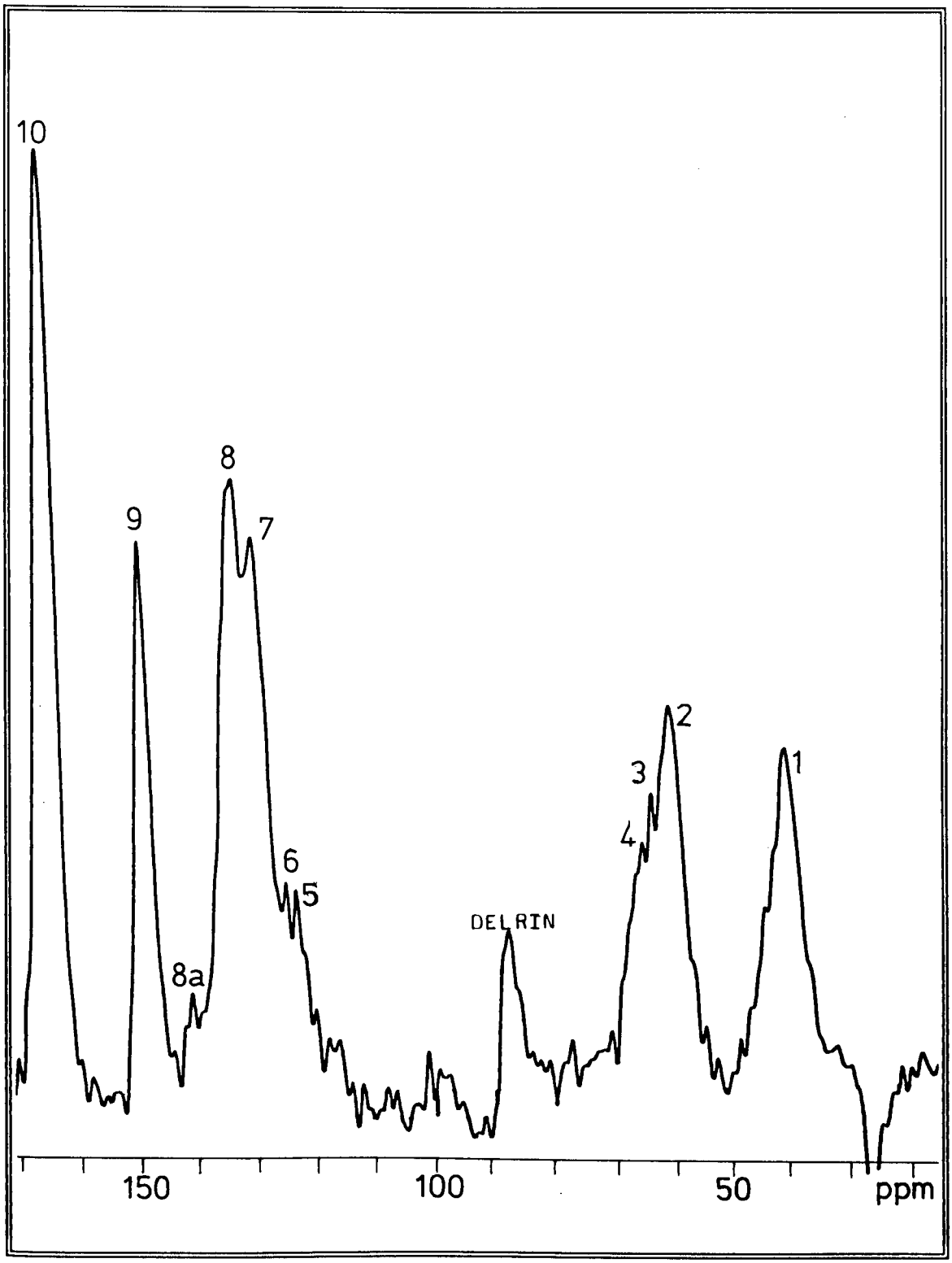

Legend			
1. 40.5	3. 62.9	6. 124.6	8a. 141.7
2. 59.7	4. 64.5	7. 129.4	9. 148.7
	5. 122.9	8. 132.5	10. 164.8

Figure 3.6(b) The TOSS/PE-MASS ^{13}C-NMR spectrum (delrin; spinning rate: 3010Hz) of powdered resin-SC which had been cured at 300^{0}C to a T_g of 102^{0}C (as measured by DSC). Note the significant relative decrease in the intensity of the HE-methylene peak, at 59.7ppm, as the HE end-groups are esterified.

Note. Peaks 5, 6, and 8a appear at chemical shifts similar to peaks 6,7, and 10 in the solid-state spectrum of uncured resin-SC (cf. figure 3.6(a,i)).

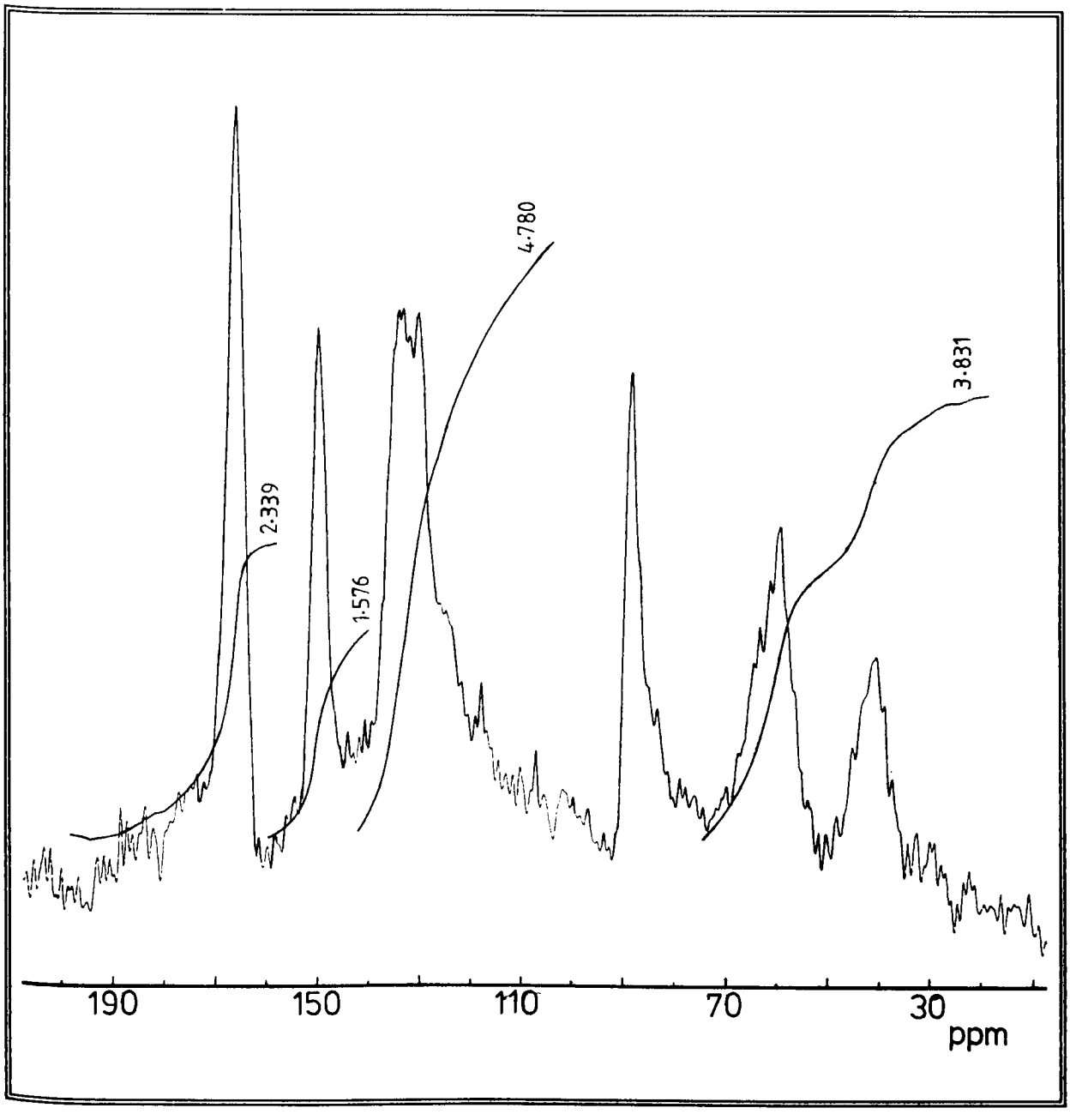

Figure 3.6(c) The TOSS/PE-MASS ^{13}C-NMR spectrum (delrin; spinning rate: 3010Hz) of scrapings from a cured model wire-enamel (i.e., a 10μm film cured from a varnish consisting of resin-SC (39.8wt.%), phenol (60.0wt.%), and "Tyzor TBT" (0.2wt.%) cured at 225^{0}C for 10 seconds). Comparison with figure 3.6(b) highlights an increased number of peaks in the aromatic region.

3.1.2 The chemical composition of industrially cured PEI wire-enamel film

Two proprietary PEI wire-enamels were analysed by MASS ^{13}C-NMR; scrapings from Isomid and Terebec* wire-coatings were analysed by PE-MASS and TOSS/PE-MASS ^{13}C-NMR spectrometry. Terebec produced a TOSS/PE-MASS spectrum (cf. figure 3.9(a)) which was remarkably similar to that of Isomid (cf. figure 3.8); both show aromatic peaks which cannot be explained as a part of the fundamental polymer system (viz., resin-SC) by comparing with the spectra of resin-SC.

The lack of high resolution in PE-MASS experiments, as compared with solution NMR, prevents a detailed structural analysis of the solid-state. Nonetheless, the PE-MASS and TOSS/PE-MASS spectra of scrapings of the wire-enamels (cf. figures 3.8 and 3.9) show marked discrepencies from the resin spectrum of figure 3.7 in the aromatc region. The additional, significant peaks at 124.9 and 128.9ppm suggest the presence of aromatic species which are not derived from the polycondensation of the resin. Those peaks not attributable to the resin will, for the purposes of simplifying the discussion, be referred to as **extraresin** peaks.

The TOSS/PE-MASS spectrum of resin-SC (cf. figure 3.6 (a,i)) shows more detail than the PE-MASS spectrum in (cf. figure 3.6(a,ii)), and peaks similar to the extraresin peaks are observed. However, the resin peaks do not diminish in their intensity upon thermal curing (cf. figure 3.6(b); the TOSS/PE-MASS spectrum of resin-SC cured to a T_g of 102^{0}C).

On the other hand, heating scrapings from Isomid wire-

---

*Terebec is a trademark of Dr.Beck & Co., a subsidiary of BASF (cf. §1.1.2.1), for a PEI wire-enameling varnish which is similar to Isomid. The sample used was kindly donated by Tycan Pty.Ltd., Auckland, New Zealand.

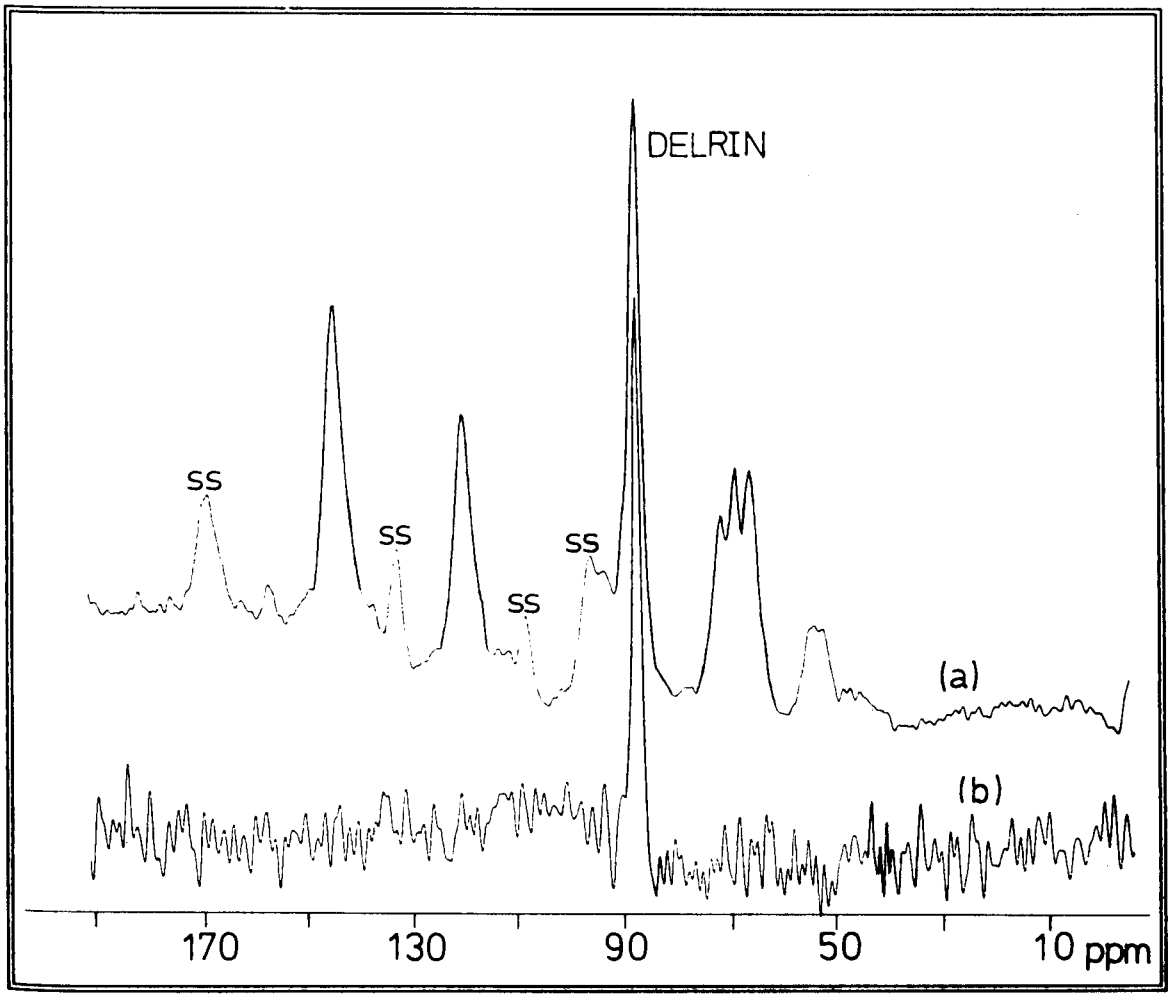

Figure 3.7 The PESOLIQ/PE-MASS ^{13}C-NMR spectrum (delrin; spinning rate: 3010Hz) of powdered, uncured resin-SC. (a) The "solid-phase" spectrum highlights the resonances due to molecular moieties of low mobility. (b) The "liquid-phase" spectrum includes the remaining resin-spectrum, and shows the sample resonances due to highly mobile molecular moieties. The "liquid-phase" contains no sample peaks, suggesting that the resin contains no unreacted ethylene glycol (EG). Therefore, the "solid-phase" spectrum is similar to the PE-MASS spectrum in figure 3.6(a,ii).

enamel at 300^{0}C for one minute produces a marked decrease in the intensities of the extraresin peaks (cf. figure 3.8(b)). Hence, the extraresin species, giving rise to the these peaks, do not originate from resin-SC, and are easily removed by the application of heat. The identity of the chemical species responsible is a key to an improved understanding of the enamel-curing process.

Before considering the physical properties of the wire-enamel scrapings with respect to the extraresin species, it is useful to eliminate the more unlikely possibilities.

Thermal degradation of the HE chain end-groups, at the common varnish-curing temperatures of near 500^{0}C, could lead to the formation of vinyl esters,[74,175,176,177] $CH_2{=}{=}CH{-}O{-}C(O){\sim}$. The ^{13}C-NMR resonances of the methylene and methine groups are expected to appear at 96 and 141.6ppm,[178] respectively, but do not correlate with the extraresin peaks. Thus, the subject species are not accounted for degradation of the chain end-groups. This also eliminates the formation of ethylene by cleavage of the ester linkage.

Alternative side-reactions include nucleophilic substitution of the aromatic rings in the polymer network by HE-oxyanions (i.e., ${\sim}CH_2{-}CH_2{-}O^-$). These reactions are postulated by Hamann et al.[20] to occur through self-catalysis by the carboxyl end-groups; ion-pairs are generated by reversible acid-catalysed hydrolyses of esters by an $A_{AC}2$ mechanism (see §1.1.1.1). The formation of such aromatic ethers are expected to produce **ipso**-aromatic carbon resonances at about 160ppm,[36,148] of which no evidence has been found.

Further aromatic substitution reactions are possible with electrophilic agents such as carbonium ions (e.g.,

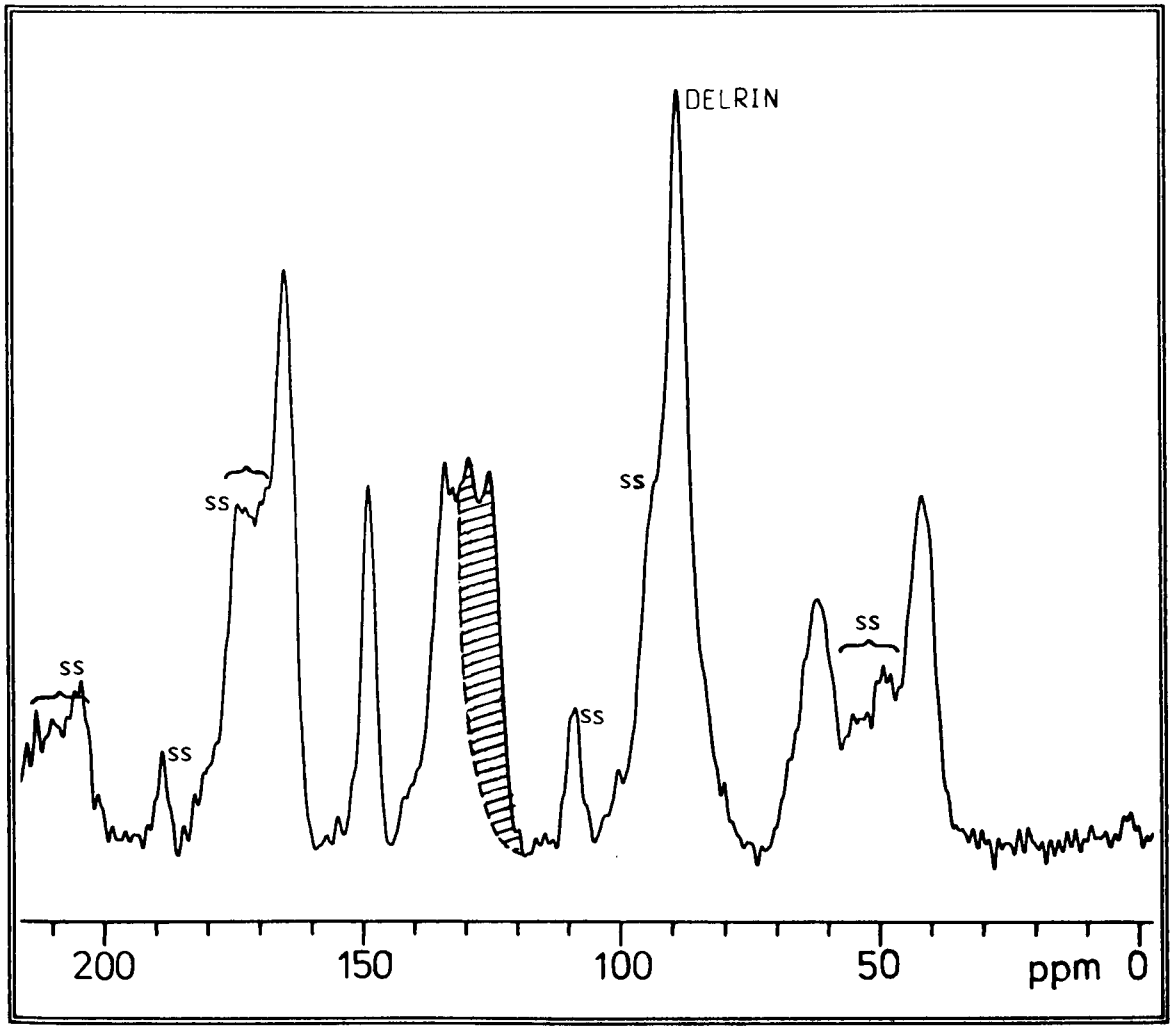

Figure 3.8 The solid-state ^{13}C-NMR spectra (delrin; spinning rate: 3010Hz) of scrapings from Isomid wire-enamel coated onto 0.355mm diameter copper wire. (a) The PE-MASS spectrum of untreated scrapings. The extraresin peaks have been highlighted by shading.

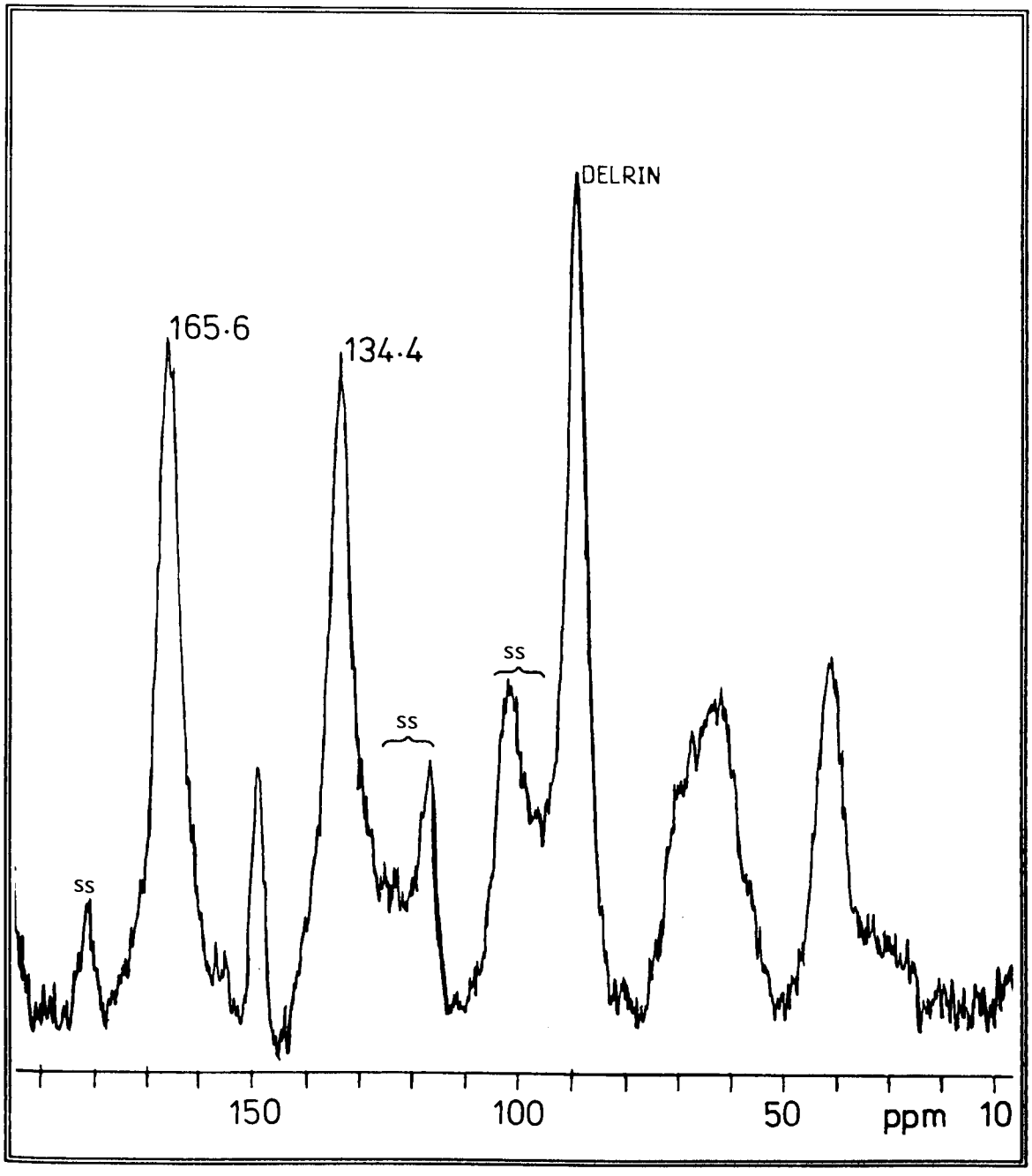

Figure 3.8(b) The PE-MASS spectrum of the same scrapings, as used in experiment (a), after heating at 300°C for one minute.

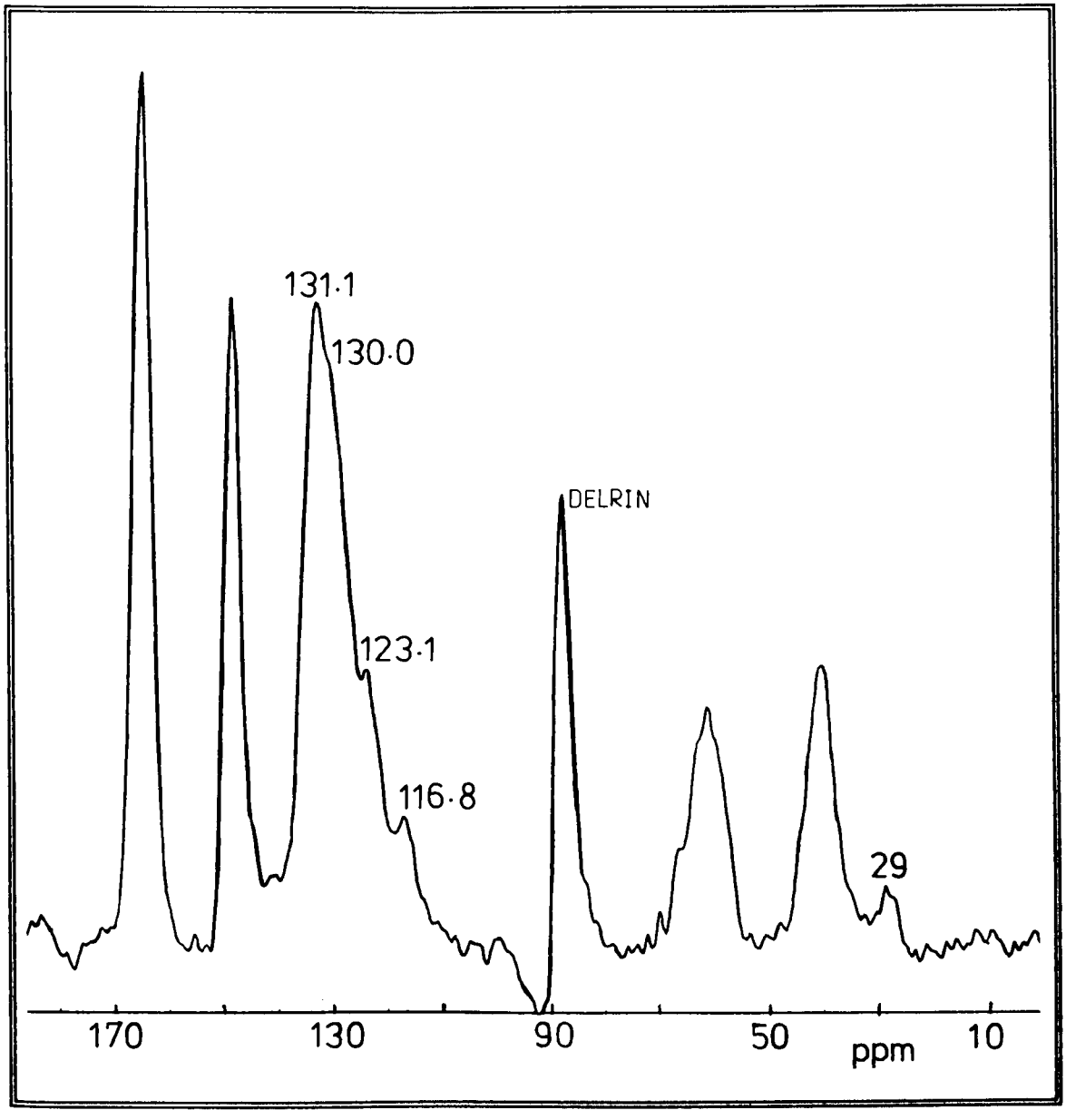

Figure 3.8(c) The TOSS/PE-MASS spectrum of the heat-treated scrapings of experiment (b). Aromatic peaks at: 116.8, 123.1, 130.0, and 131.9ppm, are evident; only the last two peaks are common to the resin (cf. figure 3.6(a,i) in which the 129.5ppm peak, analogous to the 130.0ppm peak, here, is seen to reduce in its intensity upon curing (cf. figure 3.6(b)). Note the small peak at 29ppm.

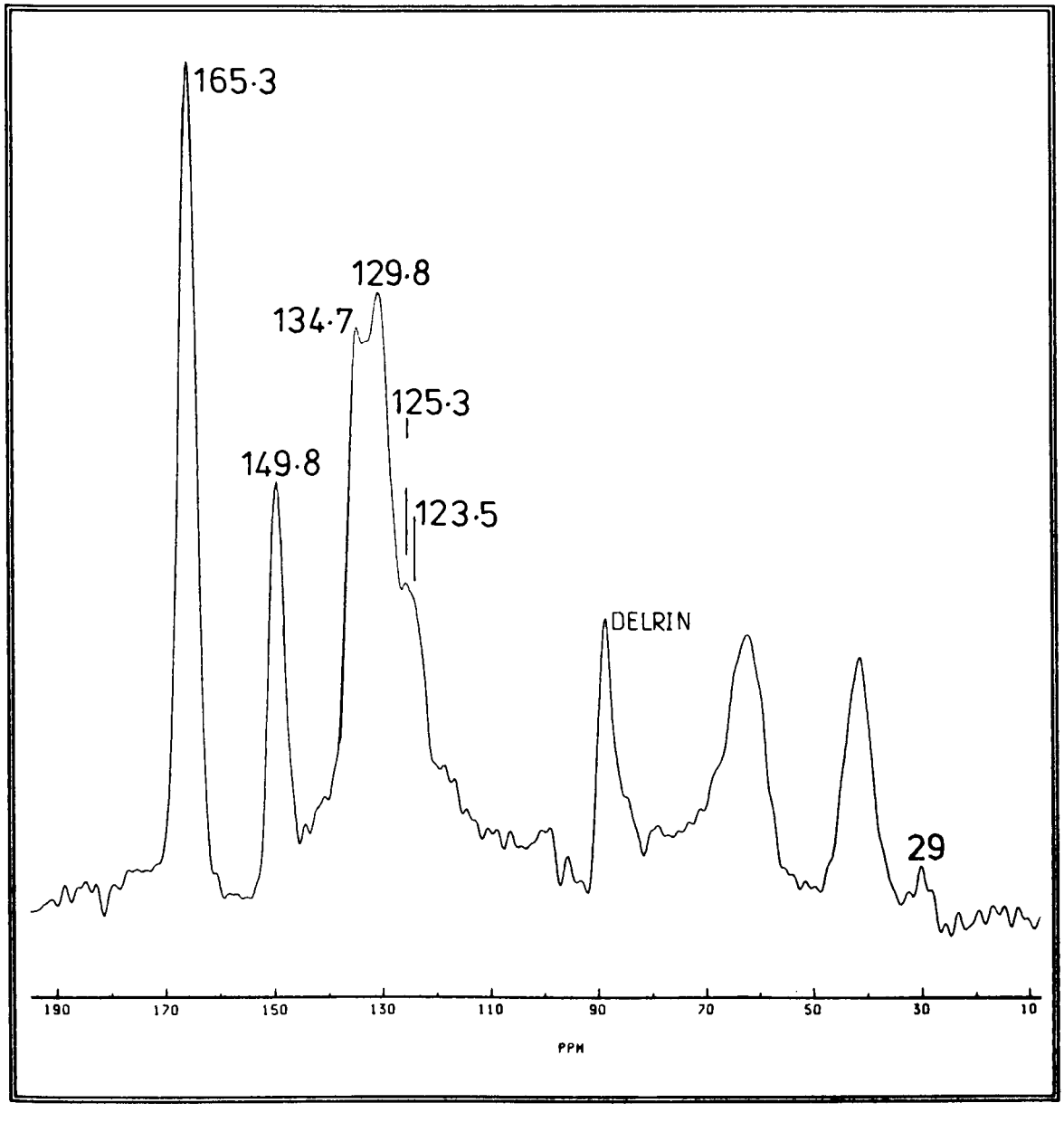

Figure 3.9(a) The TOSS/PE-MASS ^{13}C-NMR spectrum (delrin; spinning rate: 3010Hz) of scrapings taken from a 0.2mm diameter copper wire coated with Terebec PEI wire-enamel (courteously donated by Tycan(NZ) Pty.Ltd.). As for Isomid wire-enamel, extraresin peaks between 123.5 and 130.0 ppm are apparent. Note the small peak at 29ppm which is also seen in figure 3.8(a).

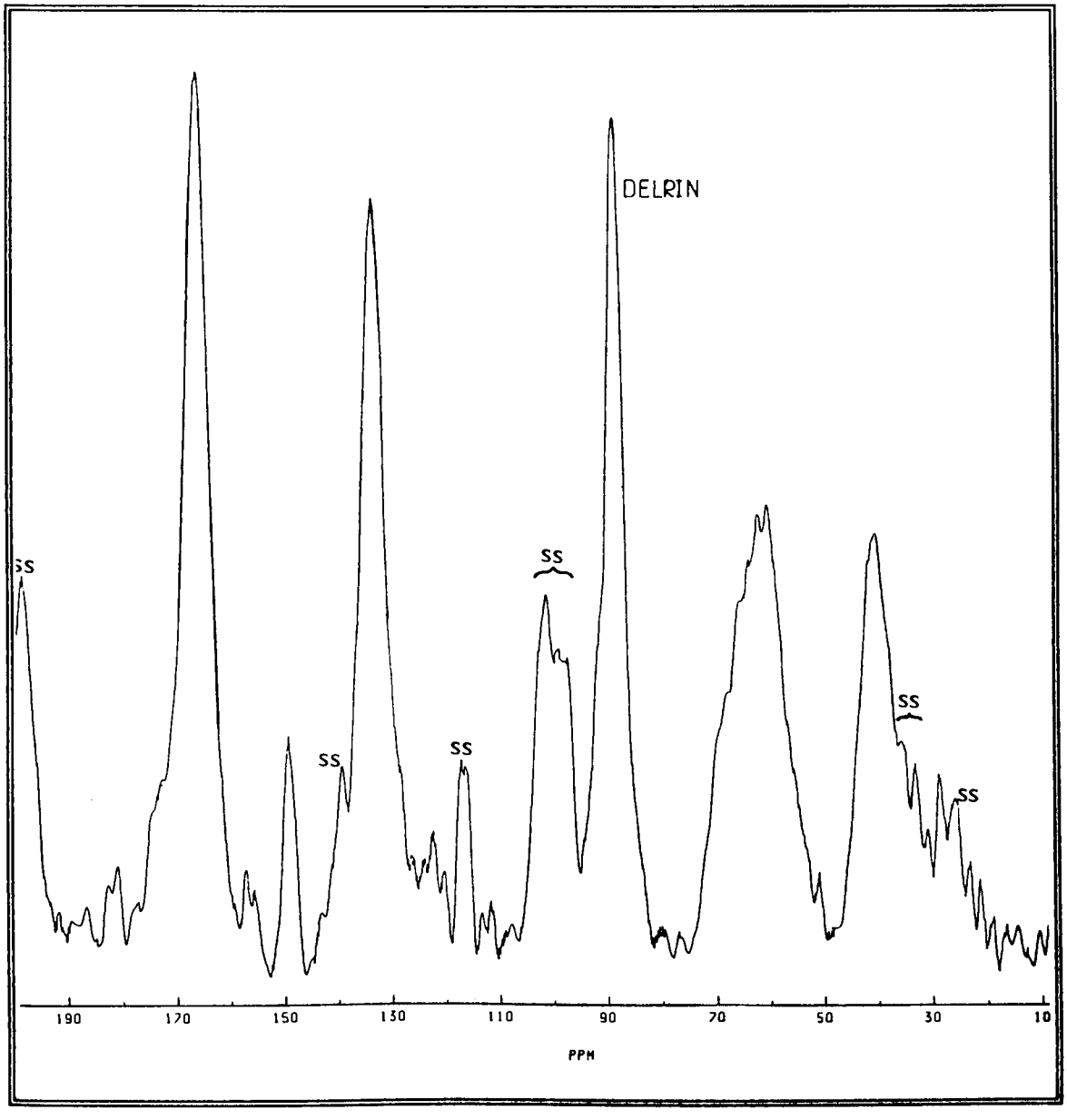

Figure 3.9(b) The PE-MASS ^{13}C-NMR spectrum (delrin; spinning rate: 3010Hz) of the same Terebec enamel scrapings, as used in experiment (a), after being heated to 300^0C for one minute. The effective reduction of the intensities of the extraresin peaks is analogous to the effect of this heat-treatment on Isomid scrapings (cf. figure 3.8(b)).

$\sim\sim CH_2CH_2^+$), occurring by an $A_{AL}1$ esterification mechanism (cf. scheme 2, §1.1.1.1). Alkylation is expected to produce signals at about 137ppm,[148] and again, no NMR evidence for these products is observed. Hence, aromatic by-products are not likely causes of the extraresin peaks.

Having considered reactions with the aromatic rings of the polymer network, there are three alternative possible sources of extraresin radicals in Isomid wire-varnish. The formulation of resin-SC, given in §1.5.2, indicates the presence of three reactive components: Phenolic 709,* Mondur SH,** and the cresylic acid solvent system, all of which contain aromatic groups. The first two are resinous modifiers which are capable of polymerising with resin-SC, in the wire-enamel. Therefore, to test the likelihood of these resins accounting for the extraresin peaks, two model varnishes were formulated (cf. tables 3.8 and 3.9). The proportion of each modifier was chosen to be similar to that used in the Isomid formulation, and m-cresol was chosen to simulate the action of cresylic acid; if any residues of this solvent in the cured film can be detected by solid-state NMR, the methyl carbon resonance, expected at about 15ppm, indicates its presence. The model varnishes were designated #EM709 and #EMSH, indicating the formulation of an enamel ("E") in m-cresol ("M") with one of the resin modifiers (either "709" for Phenolic 709 or "SH" for Mondur SH).

Each of the model varnishes were cast into pyrex dishes

---

* Phenolic 709™ is a m,p-cresol/formaldehyde resin manufactured by Schenectady Chemicals Australia Pty.Ltd.

** Mondur SH™ is a phenol blocked triisocyanate resin made by the cyclisation of toluene diisocyanate; marketed by Mobay Chemicals, Inc.

as thin films of approximately 50μm in thickness, and cured at 300^{0}C in an electric furnace. The model varnishes were stoved for 15 seconds, which is similar to the curing-times (i.e., the oven-residence times) encountered in the wire-enamelling industry. The cured films were rendered into scrapings using a steel blade, and these were examined by PE-MASS NMR spectrometry. The spectra are presented in figures 3.10 and 3.11.

Table 3.8 The formulation for the model-varnish #EM709 which contains the proprietary phenolic resin modifier, Phenolic 709. The quantity of additive was used in the same proportion as used in Isomid wire-varnish (cf. §1.5.2).

Component	Mass (g)	Ratio (wt.%)
Resin-SC	19.58	38.9
m-cresol	28.04	55.8
Catalyst, "Tyzor TBT"	0.47	0.9
Phenolic 709	2.17	4.3

Table 3.9 The formulation for the model-varnish #EMSH which contains the polyisocyanurate resin modifier, Mondur SH. The amount of additive was used in the same proportion as in Isomid (cf. §1.5.2).

Component	Mass (g)	Ratio (wt.%)
Resin-SC	20.06	39.6
m-cresol	28.74	56.7
Catalyst, "Tyzor TBT"	0.48	0.9
Mondur SH	1.38	2.7

The PE-MASS spectra show no evidence of residual **m**-cresol, and only the spectrum of #EM709 exhibits additional aromatic-peaks; two peaks at 131.2 and 132.6ppm. These peaks may be due to the alkyl substituted aromatic-carbons of the phenolic resin, Phenolic 709, but do not simulate the extra-resin peaks, in question. Therefore, since no peaks were

observed in the range 115-129ppm, for either of the model varnishes, neither the resin modifiers nor the catalyst ("Tyzor TBT" was also used in the model varnishes, in accordance with the Isomid wire-varnish formulation; cf. table 1.5) are considered to cause these peaks.

Heat-treatment of the Isomid wire-enamel scrapings produced a reduction in the intensities of the extraresin peaks (cf. the TOSS/PE-MASS ^{13}C-NMR spectrum in figure 3.8(c)), leaving small peaks at 116.8, 123.1, and 130.0ppm. Similar peaks are evident in the TOSS/PE-MASS spectrum of Terebec (cf. figure 3.9(a)), which are seen at 115.9-117.8, 123.5-125.3, and 130.0ppm. These peaks correspond to the aromatic peaks of Phenolic 709 (cf. figure 3.10(b)) at 113-117, 121.6, and 129-131ppm. However, the PE-MASS spectrum of unheated Isomid scrapings (cf. figure 3.8(a)) is notable for the absence of a peak at 116ppm of significant intensity, and so again, Phenolic 709 is not the probable cause of the extraresin peaks since the great reduction in the intensities of the extraresin peaks is not likely to be due to loss by vaporisation of such copolymerised material.

Having eliminated these possibilities, the remaining reactive component of Isomid wire-varnish is the cresylic acid, implying the presence of solvent residues which are detectable by solid-state NMR. As explained in §2.1.2, highly mobile solvent molecules are not detected by MASS NMR techniques by virtue of cross-polarisation which requires substantially immobilised species to occur effectively. Therefore, residual solvents, remaining in the PEI film after thermal curing, cannot be observed unless they are chemically bound to the polymer network, severely inhibiting

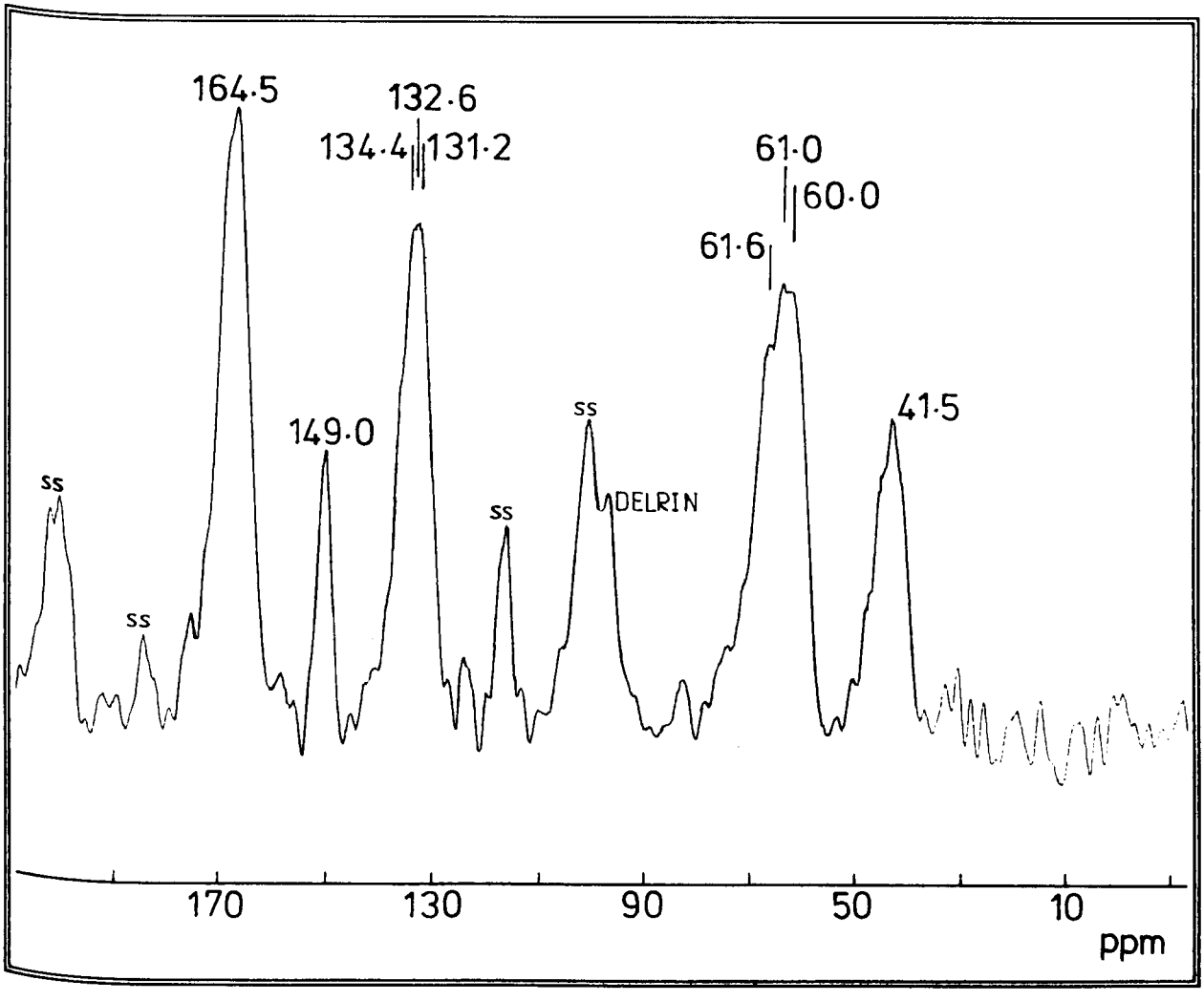

Figure 3.10(a) The PE-MASS ^{13}C-NMR spectrum (delrin; spinning rate: 2470Hz) of scrapings from the cured film (≈50μm in thickness) of the model-varnish #EM709 (cured at 300^{0}C for 15 seconds).

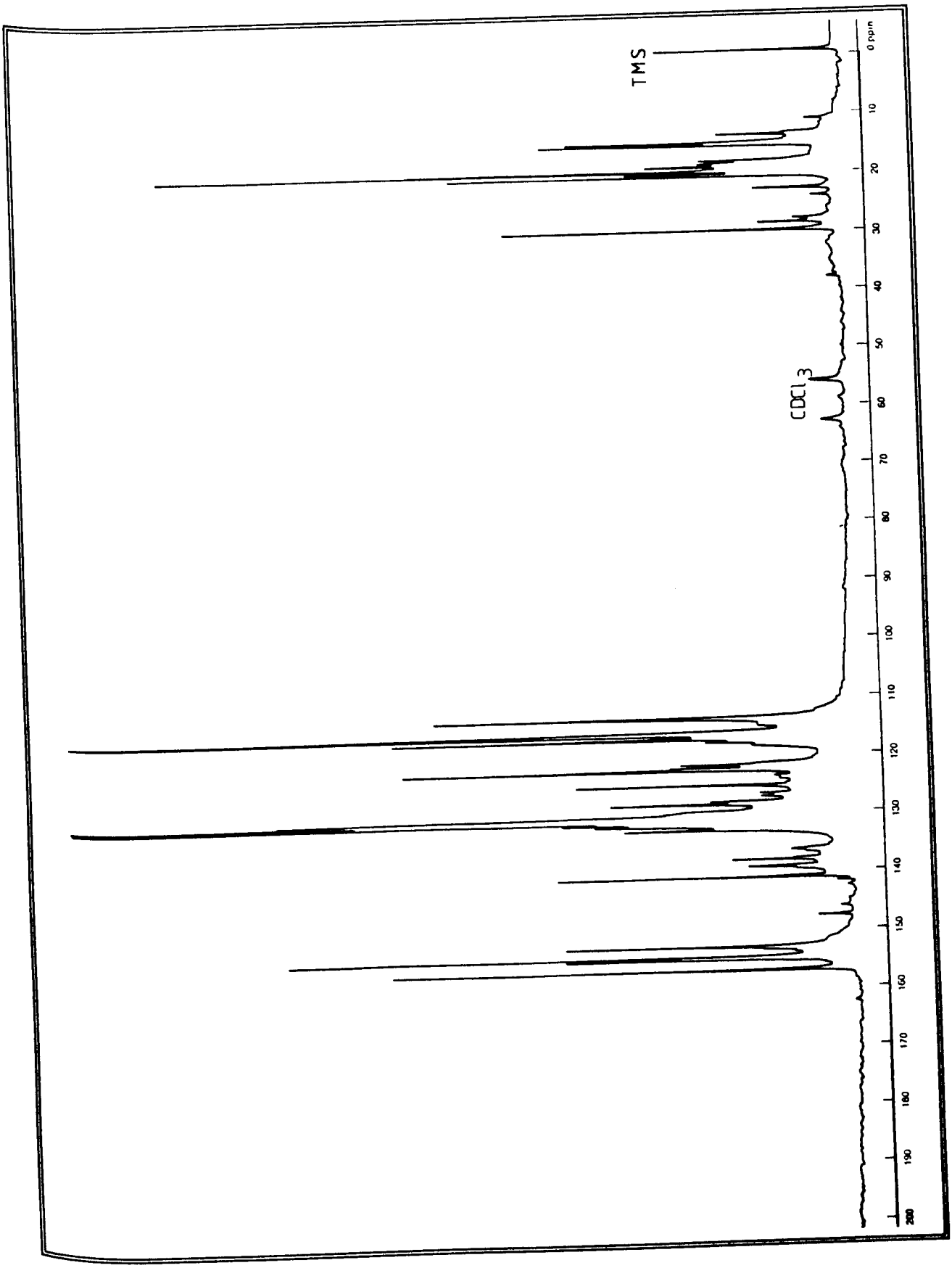

Figure 3.10(b) The BB^{13}C-NMR spectrum (20.1MHz, $CDCl_3$, TMS) of the resin modifier, Phenolic 709.

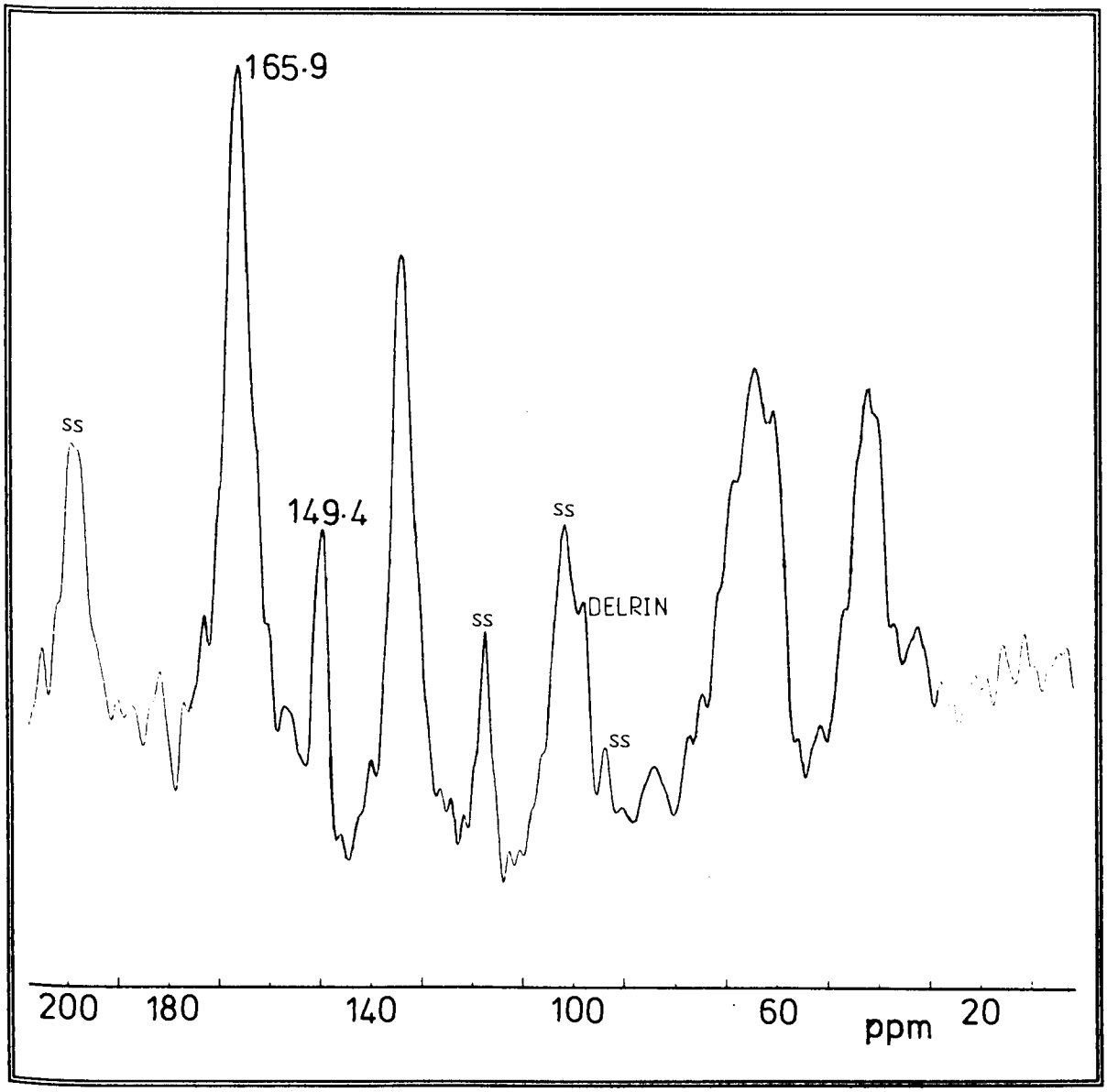

Figure 3.11(a) The PE-MASS ^{13}C-NMR spectrum (delrin; spinning rate: 2470Hz) of scrapings from a cured film (≈50μm in thickness) of model-varnish #EMSH (cured at 300^{0}C for 15 seconds). Note that no aromatic peaks, attributable to the diisocyanate resin, Mondur SH, were detected. The peaks at 121.9, 125.4, and 129.7ppm which are present in the BB^{13}C-NMR spectrum of Mondur SH (cf. figure 3.11(b)), are absent from this solid-state spectrum. The latter is similar to the PE-MASS spectrum of heat-treated Isomid scrapings, shown in figure 3.8(b).

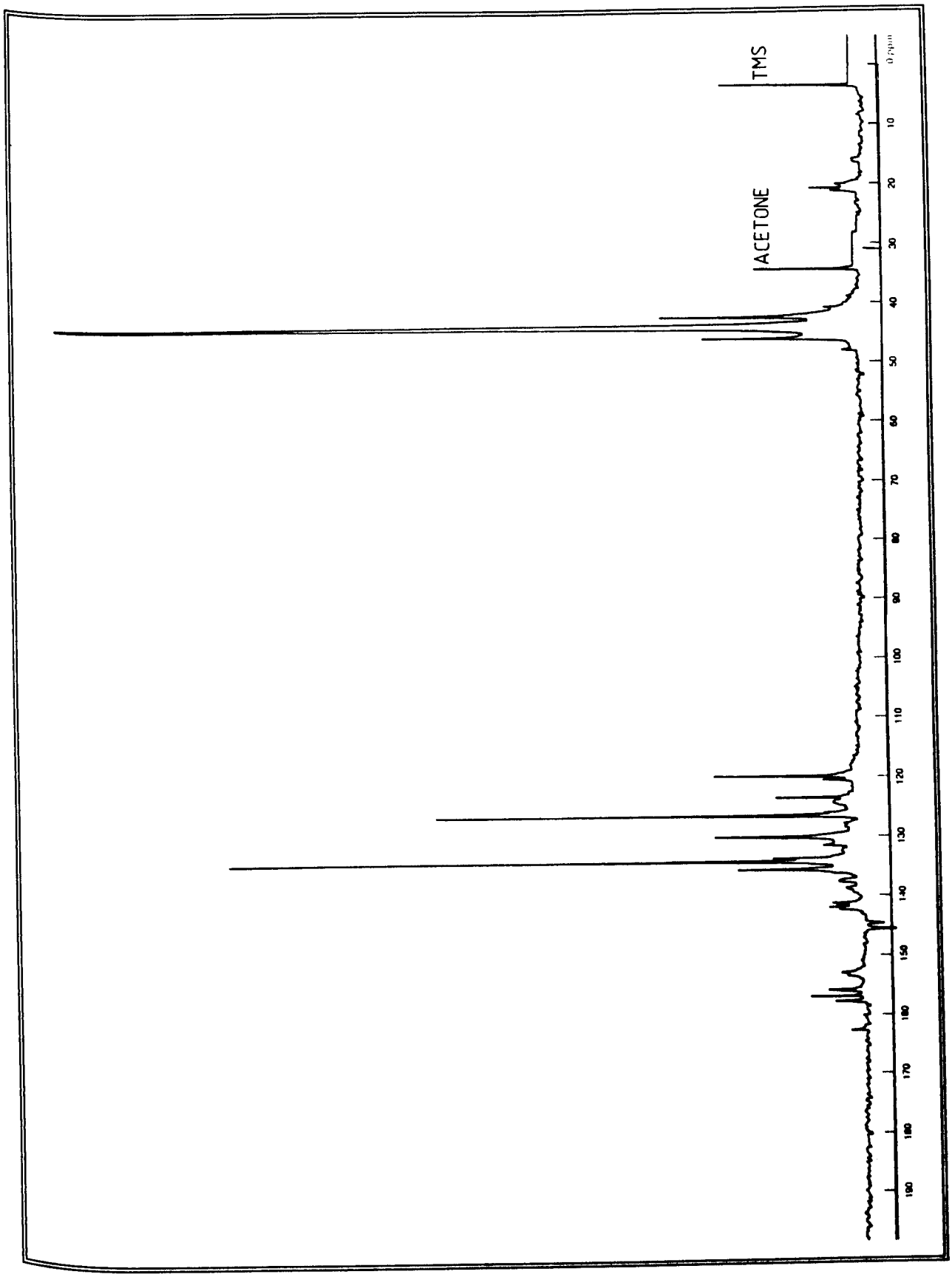

Figure 3.11(b) The BB^{13}C-NMR spectrum (20.1MHz, acetone(d6), TMS) of the resin modifier, Mondur SH.

random motion. As a reminder, cresylic acid is a blend of the homologues of phenol (see §1.5.2.1; table 1.7), primarily phenol and **o**,**m**, and **p**-cresols, with approximately 20wt.% being made up of xylenols.

The presence of residual solvents (i.e, those left behind during the curing process through insufficient stoving) in wire-enamel films is an accepted problem in the wire-enamelling industry, and is subjected to standardisation; for instance, weight-losses from cured enamel-films are specified by Tycan Australia Pty.Ltd. to be less than 0.3 wt.% after stoving at 260^{0}C for 30 minutes. Fukushima et al.[179] have identified such residues in samples of enamelled wire by pyrolytic gas chromatography (PGC), finding them to be very persistent when measured against the enamelling-speed at which the wire sample had been manufactured. Enamelling-speed refers to the speed of the passage of varnish-coated wire through the enamelling-oven. Residues, at levels of ≈200 ppm, were detected even at 6.3meters/minute, which is very slow in industrial terms.

Solvent residues can conceivably be present as either **unreacted** molecules (i.e., effectively acting as a plasticiser) or as reaction-derivatives of the PEI network. The former possibility intimates that solvent molecules which are trapped within the polymer matrix would slowly leach out, however, the extraresin peaks were detected in a three year old sample of Isomid wire-enamel, suggesting that this had not transpired. Furthermore, solid-state NMR of two samples of resin, one with 12wt.% phenol and the other with 12wt.% **p**-cresol added to them by mulling, (cf. figure 3.12) showed no indication of the presence of the aryl alcohols,

establishing that the presence of highly mobile solvent molecules cannot be detected by the PE-MASS NMR techniques used in this investigation. The extraresin peaks are thus unlikely to be due to residues of unreacted aromatic solvents remaining after the thermal curing of the wire-varnish.

The esterification products of the solvents with the resin, on the other hand, are aryl esters, that is,

$$\underset{\text{(carboxyl end-groups)}}{\sim\!\!\sim C(O)\text{—}OH} + \underset{\text{(cresylic acid)}}{ArOH} \longrightarrow \underset{\text{(aryl ester)}}{\sim\!\!\sim C(O)\text{—}OAr} + H_2O\uparrow ,$$

which are more reactive with respect to nucleophilic substitution than either the carboxyl or HE end-groups;[32,33] the aryloxy anion is a better leaving group than either water or EG. The relative reactivities of chain end-groups has been discussed in §1.1. Aryloxy radicals are easily cleaved at temperatures $\geq 150^0C$,[1] allowing substitution by HE end-groups. Cleavage of these radicals regenerates the phenolic solvent which then leaves the curing polymer film.

The persistence of the residual solvents, as found by Fukushima et al.,[179] and the failure of MASS NMR techniques to detect either unreacted phenol or p-cresol which was introduced into powdered resin-SC (cf. figure 3.12), lead to the conclusion that the extraresin peaks arise from the products of esterification and ester exchange reactions of phenolic solvents with the functional groups of the polymer network. The nature of the extraresin peaks requires that the structural units responsible break-off (viz., degrade) readily upon exposure to significant thermal energy; the extraresin peaks were found to disappear after the Isomid wire-enamel scrapings were heated to 300^0C for one minute (cf. figure 3.8). The TOSS/PE-MASS spectrum of these heat-

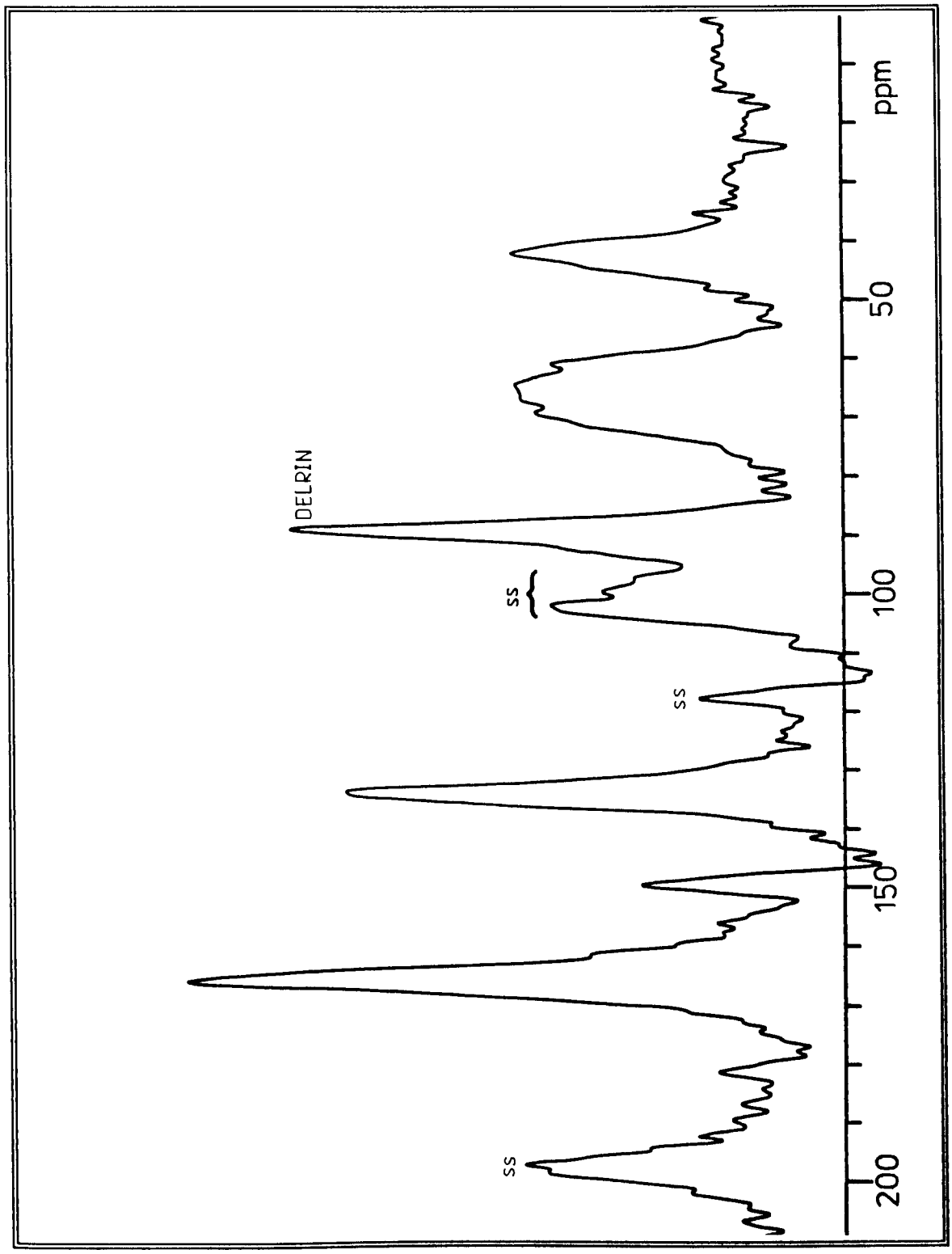

Figure 3.12(a) The PE-MASS ^{13}C-NMR spectrum (delrin; spinning rate: 2460Hz) of powdered resin-SC with 12wt.% phenol added.

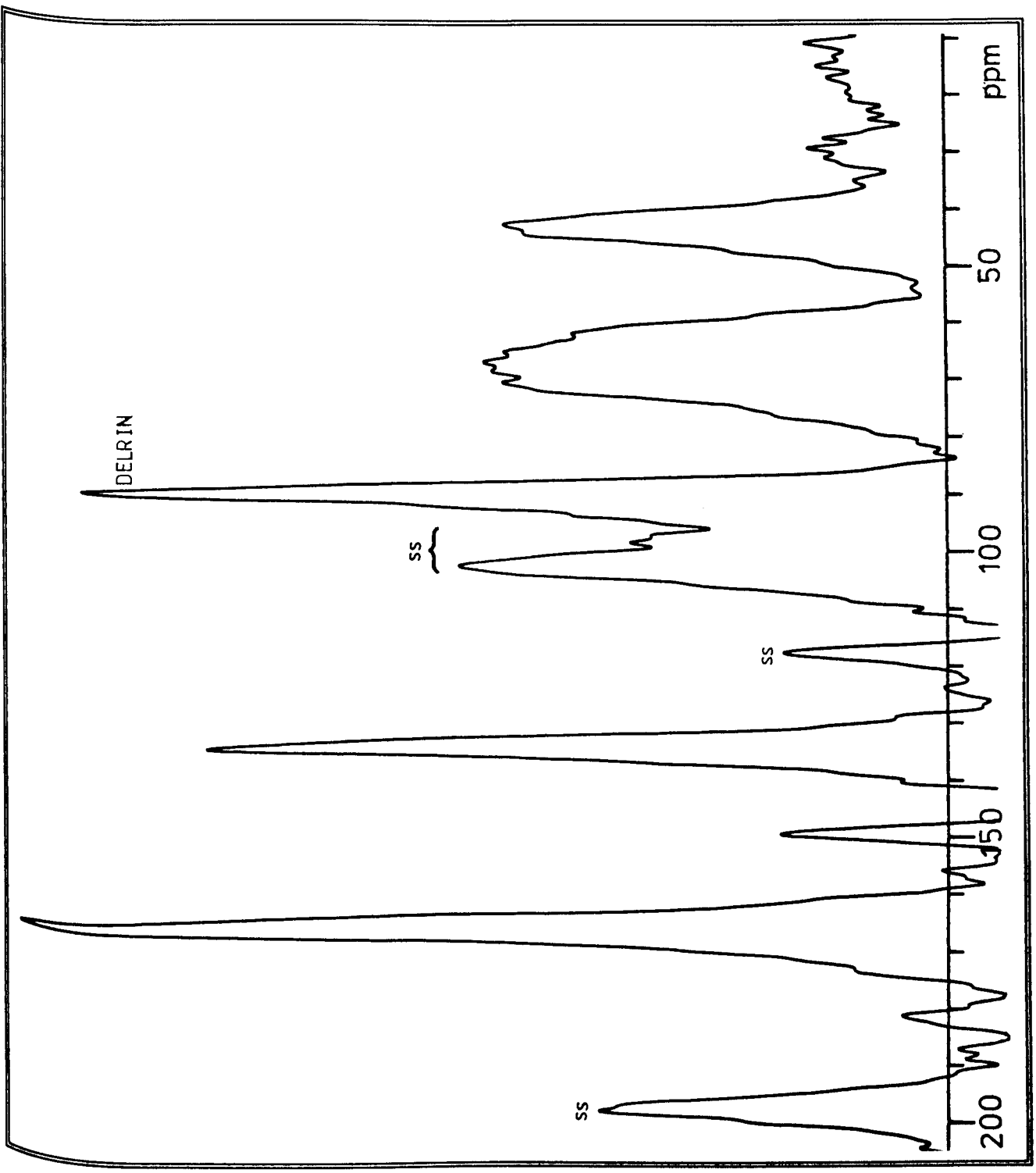

Figure 3.12(b) The PESOLIQ/PE-MASS ^{13}C-NMR spectrum (delrin; spinning rate: 2425Hz) of the resin sample used to generate the spectrum depicted in part (a). The "solid-like" spectrum is identical to the PE-MASS spectrum in (a), and the "liquid-like" spectrum showed no sample signals.

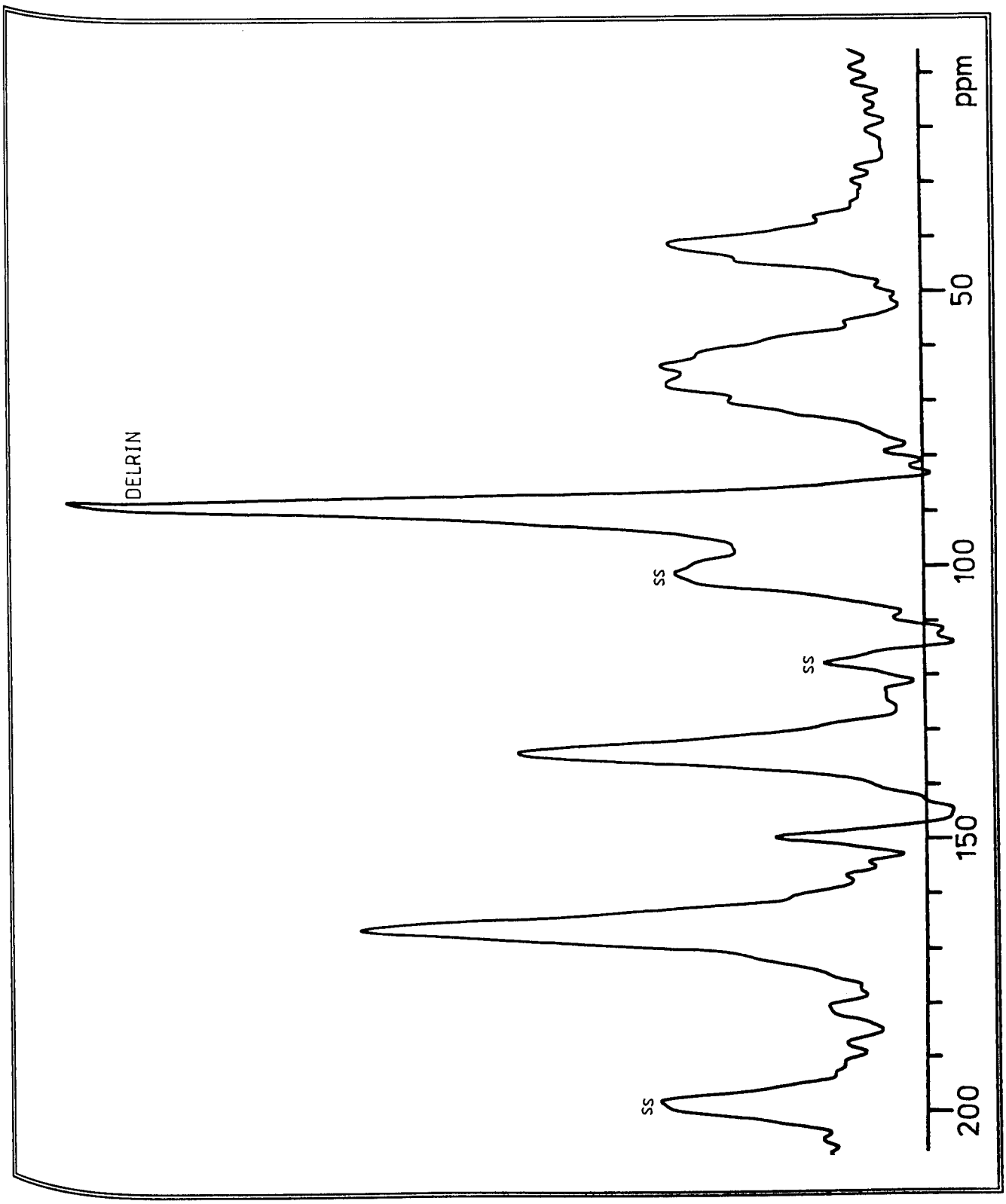

Figure 3.12(c) The PE-MASS ^{13}C-NMR spectrum (delrin; spinning rate: 2460Hz) of powdered resin-SC with 12wt.% **p**-cresol added. Note the conspicuous absence of a methyl carbon signal.

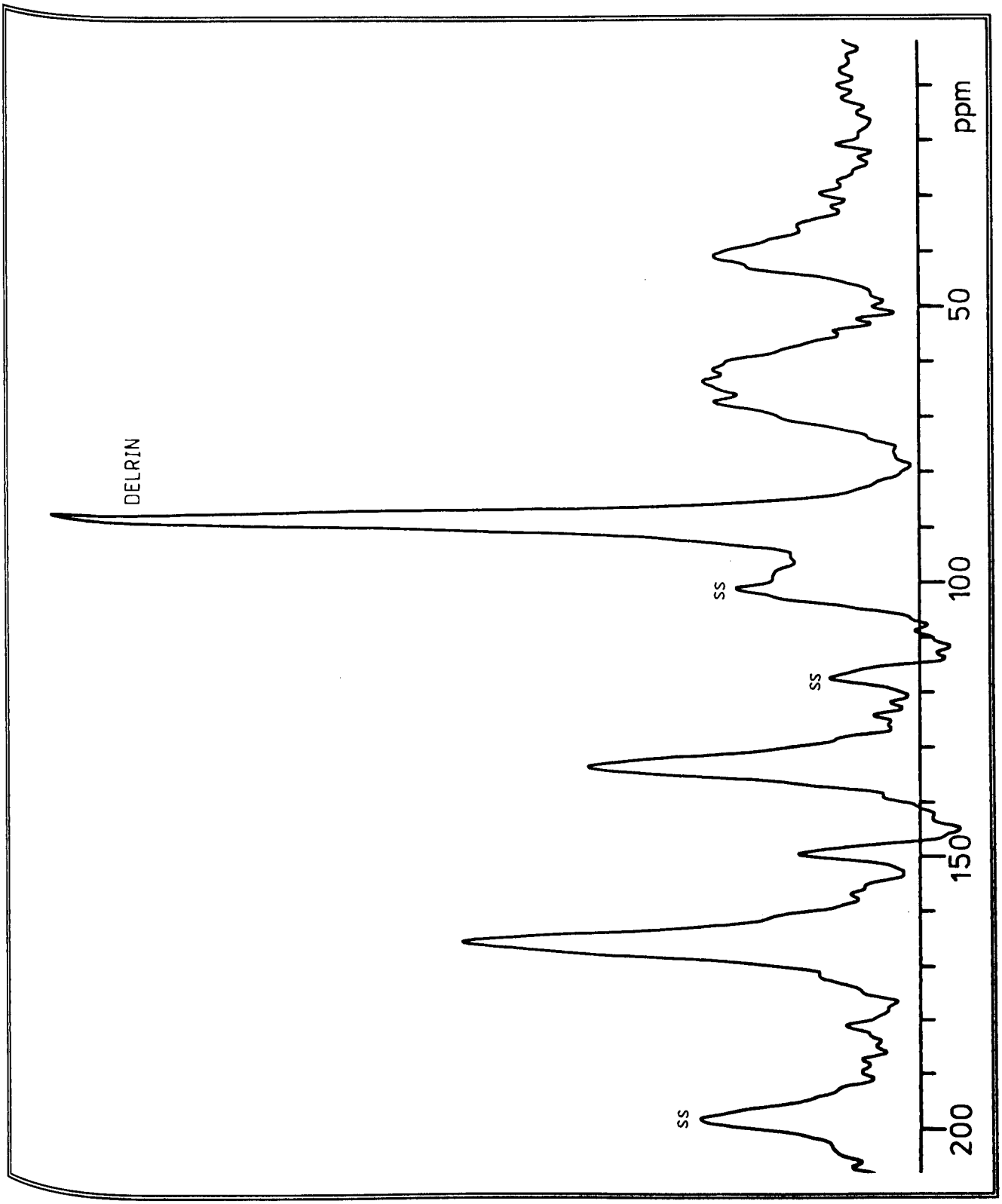

Figure 3.12(d) The PESOLIQ/PE-MASS ^{13}C-NMR spectrum (delrin; spinning rate: 2415Hz) of the sample used to generate the spectrum in part (c). Again, the "solid-like" spectrum is similar to the PE-MASS spectrum.

treated scrapings (cf. figure 3.8(c)) showed extraresin peaks at 29, 116.8, 123.1, 130.0, and 131.9ppm, which are similar to the calculated chemical shifts for the 3,4-xylenol ester derivative of BA (see appendix X, table A.15, for the calculated chemical shifts). Similarly, the TOSS/PE-MASS NMR spectrum of Terebec wire-enamel (cf. figure 3.9(a)) exhibits peaks at 29 and 125ppm which can be attributed to the aryl ester of 2,4,6-trimethylphenol (see appendix X, table A.15). These possibilities are likely since the two phenols named are common components of those commercial cresylic acids separated from natural sources such as coal tar (cf. §1.5.2.1; table 1.9).

The "solid-like" nature of the extraresin materials is also suggested by the PESOLIQ/PE-MASS NMR spectrum of the Isomid scrapings (cf. figure 3.13) where the extraresin peaks are present in the "solid-like" spectrum, but are absent in the "liquid-like" portion of the solid-state spectrum. Note that the significant extraresin peak at 124.9ppm is absent in the latter.

The absence of unreacted solvent molecules was further tested by washing samples of Isomid scrapings in polar solvents and scanning for the presence of aromatic solutes, extracted from the enamel, by UV/visble spectrometry; this technique is highly sensitive to π-electron transitions, and is capable of detecting aromatic compounds at very low concentrations. The range of extraction-solvents included DMSO, dimethyl formamide, EG, $CHCl_3$, ethanol, and acetone. These were used for immersion times of 150 hours at atmospheric pressure and room temperature. The trials failed to detect the presence of any aromatic substances in any of the ex-

traction-solvents. However, upon repeating the procedure with heating of the solvents above a temperature of 145±2^{0}C (a **threshold** temperature), for only a few minutes, UV spectra similar to that of phenol were obtained, showing clear π-electron absorption-bands. Thus, extraresin material was found to be released at a temperature near that needed to break aryl ester bonds[1] (see §3.1.3 for further discussion).

The threshold temperature for the extraction of extraresin material was determined, in the first instance, by slowly heating the extraction-solvents (only for those of high boiling points). Above 100^{0}C, steps of 2^{0}C were achieved by careful application of heat (by a hot-plate). The solvents were maintained at each step for 5-10 minutes, allowing equilibration. After cooling, the UV/visible spectrum of the extraction-solvent was obtained, and aromatic absorption-bands were observed to appear at 143, 146, and 147^{0}C, for three iterations (the average is 145±2^{0}C).

The evidence presented thus far leads to the postulate: the extraresin peaks arise from condensation reactions of the phenolic solvents (i.e., cresylic acid) with the PEI resin (i.e., resin-SC), during thermal curing.

Further work was undertaken in an attempt to model the aryl esters of resin-SC. Two model resins were synthesised on the basis of the formulation for resin-SC, one with all ingredients except EG, replaced with phenol to give a molar equivalence of hydroxyl groups (cf. §2.3.10), and in the other both EG and THEIC were replaced with phenol to give a molar equivalence of hydroxyl groups (cf. §2.3.11). The PE-MASS spectra of these model resins yielded no peaks which could be construed to be the extraresin peaks (cf. figure

3.14), indicating that phenol is not present in the resins, either as derivatives or as **free** (i.e., unreacted) molecules. However, the high synthetic temperatures (>220^{0}C) used tend to degrade any phenyl esters which are formed, and readily vaporise the condensed phenol (boiling point: 181.7^{0}C). Therefore, these experiments were not conclusive.

Another experiment was conducted in an attempt to reproduce the enamelling process and its effects on the polymer film. A model wire-varnish, designated #R/P/TBT (where "P" stands for phenol, used as the solvent) was mixed (see the formulation given in table 3.10), and cast into a thin film (≈3mm in thickness) which was baked in an electric furnace at 300(±10)^{0}C for 15 seconds.

Table 3.10 The formulation for the model wire-varnish, #R/P/TBT.

Component	Quantity (wt.%)
Resin-SC	39.8
Phenol	60.0
"Tyzor TBT"	0.2

The resulting solid film was scraped from the glass surface and examined by PE-MASS NMR spectrometry (cf. figure 3.15). The broad aromatic signal exhibits an upfield shoulder-peak which is consistent with the aromatic peak-structure observed in Isomid and Terebec wire-enamel scrapings. Hence, the extraresin peaks could indeed be caused by the cresylic acid solvents, which was modelled by phenol.

The aryl-ester, polymer/solvent adduct, postulated to be present in Isomid wire-enamel, was further modelled by diphenyl terephthalate (DPT) (cf. §2.3.8). If such aryl

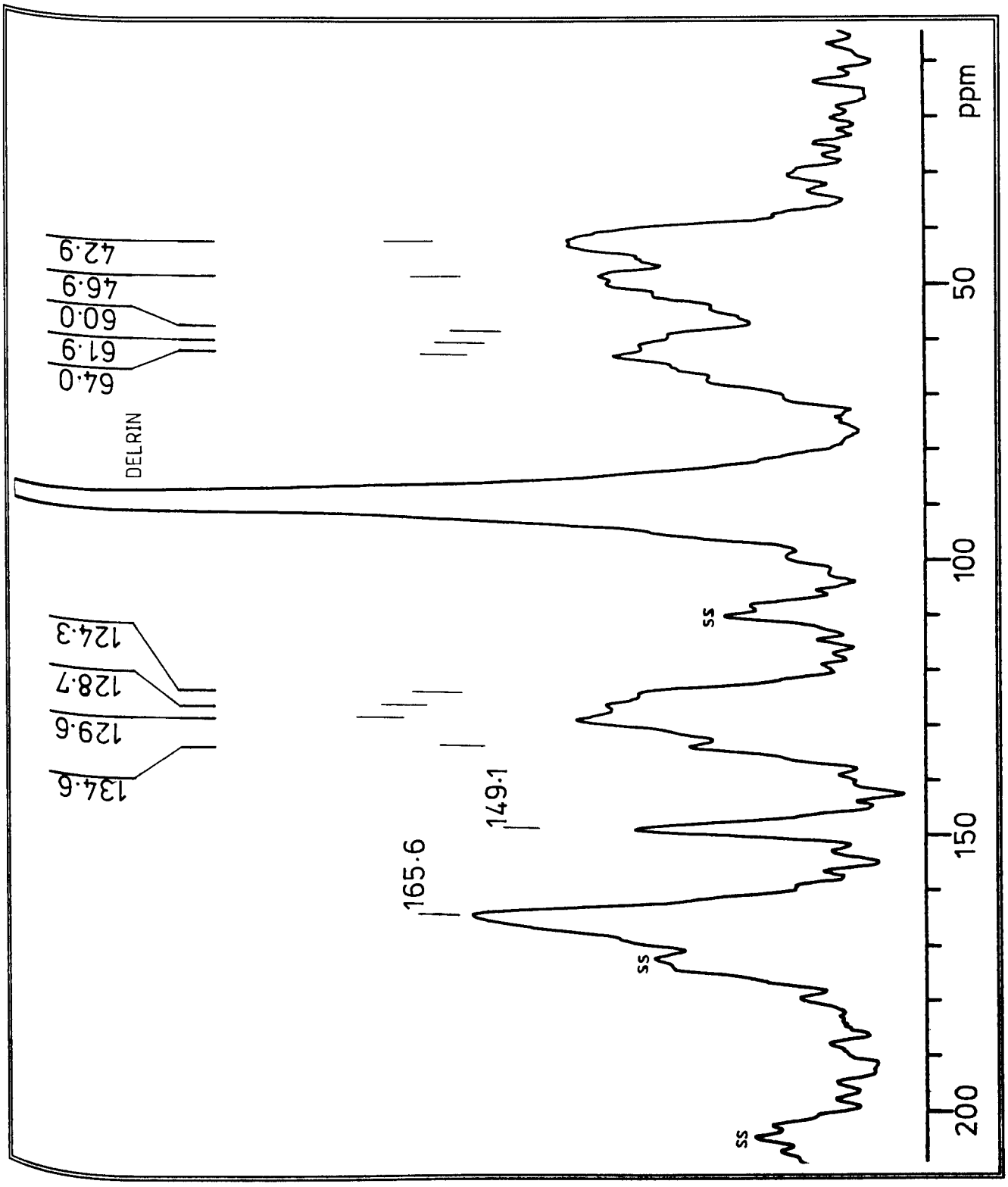

Figure 3.13 The PESOLIQ/PE-MASS ^{13}C-NMR spectrum (delrin; spinning rate: 3000Hz) of scrapings from Isomid wire-enamel. (a) The "solid-like" portion is shown, and is seen to be similar to the PE-MASS spectrum in figure 3.8(a).

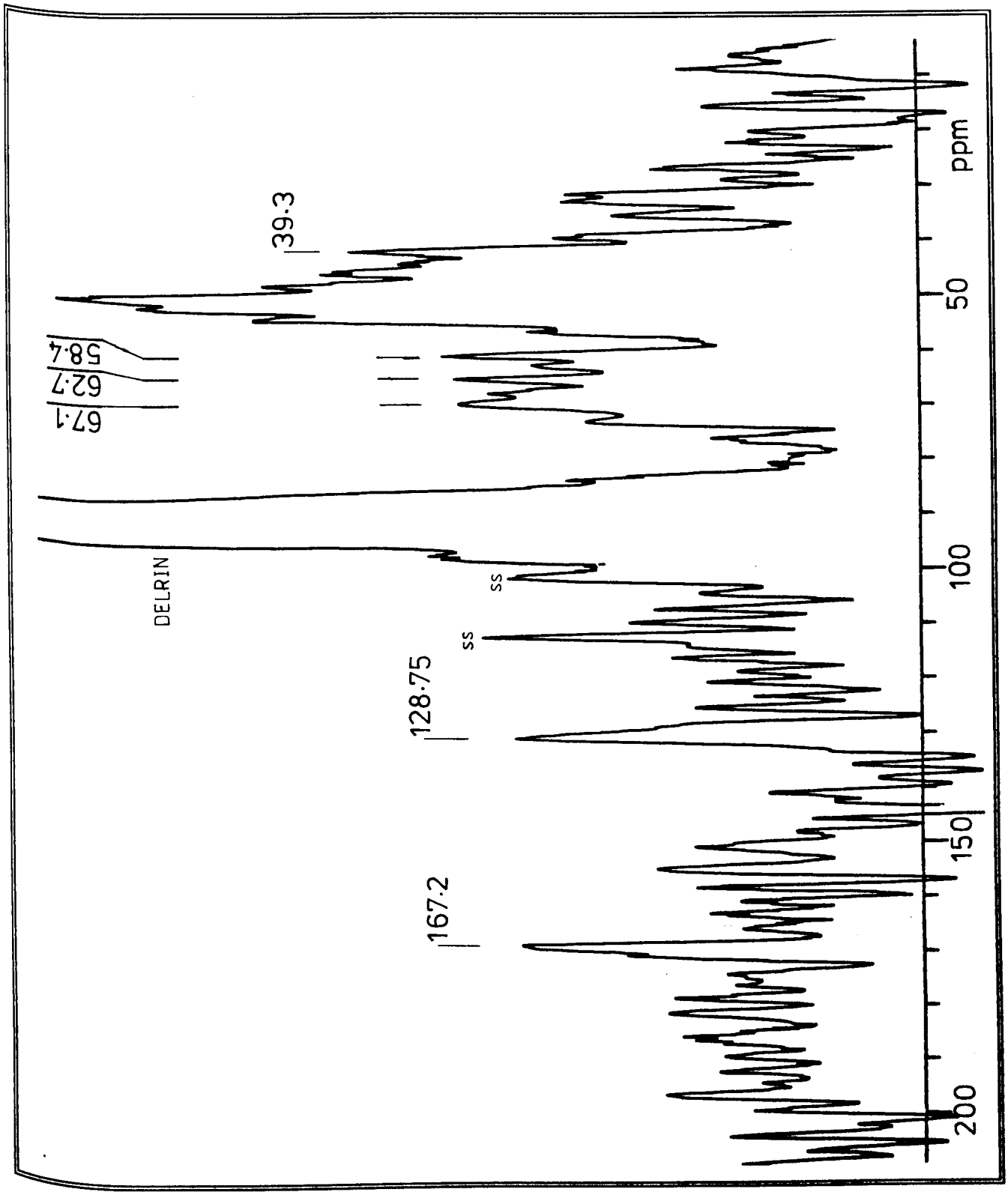

Figure 3.13(b) The "liquid-like" spectrum showing peaks at 167.2ppm (carbonyl carbons), 128.75ppm (aromatic carbons), 58.4ppm (the hydroxylic methylene groups), and 39.3-48.0ppm (diphenyl substituted methylene groups of the MDA radicals and the nitrous methylene groups of the THEIC radicals).

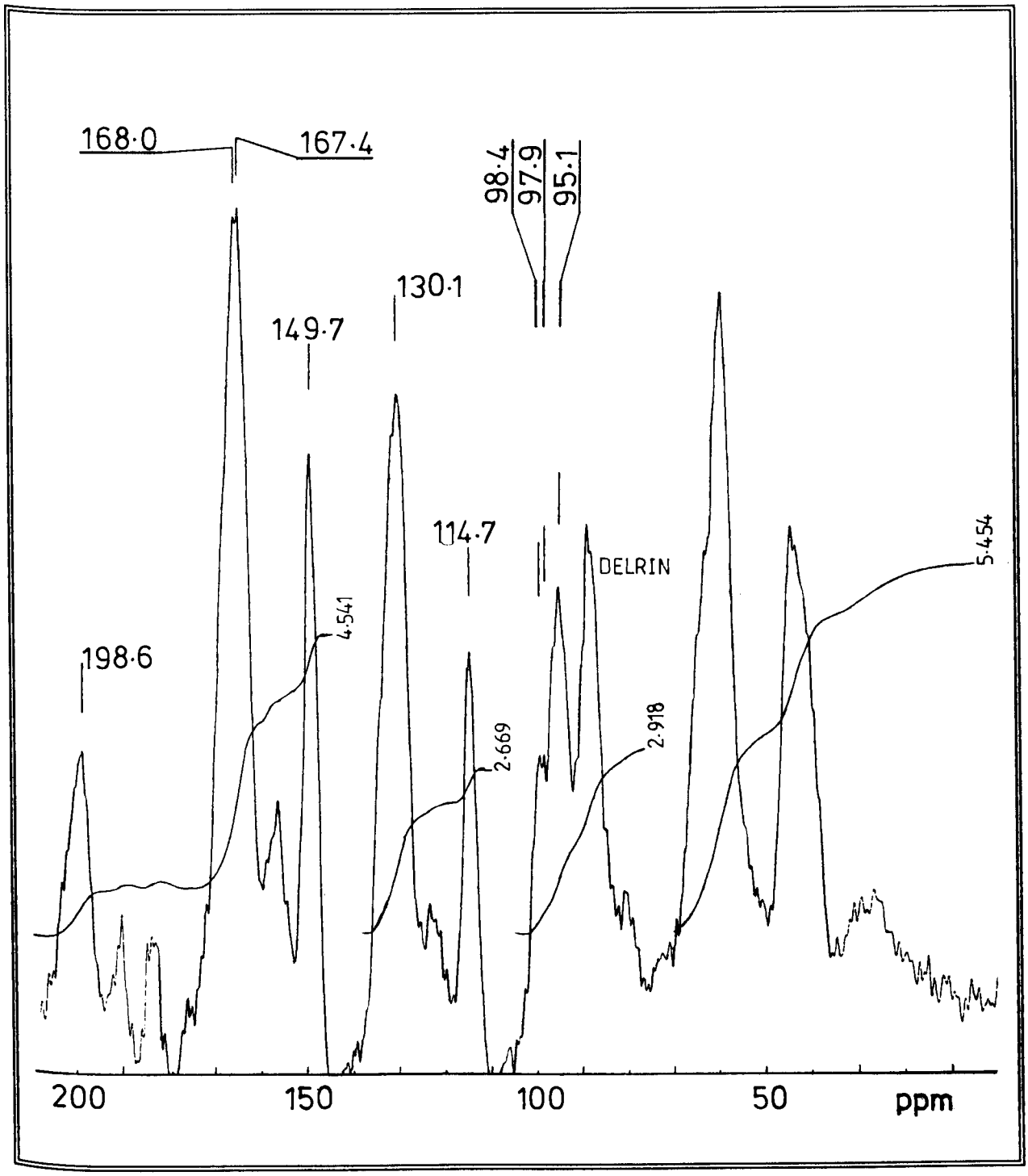

Figure 3.14 The PE-MASS ^{13}C-NMR spectrum (delrin; spinning rate: 2600Hz) of a model-resin made with all the resin-SC ingredients except EG, which was replaced with phenol (molar equivalence of hydroxyl groups). The synthesis of this resin has been described in §2.3.10. Note, §2.3.11 describes the synthesis of a similar model-resin with both EG and THEIC replaced by phenol (molar equivalence of hydroxyl groups), the PE-MASS spectrum of which was found to be similar to that depicted here. Therefore, the latter is not shown.

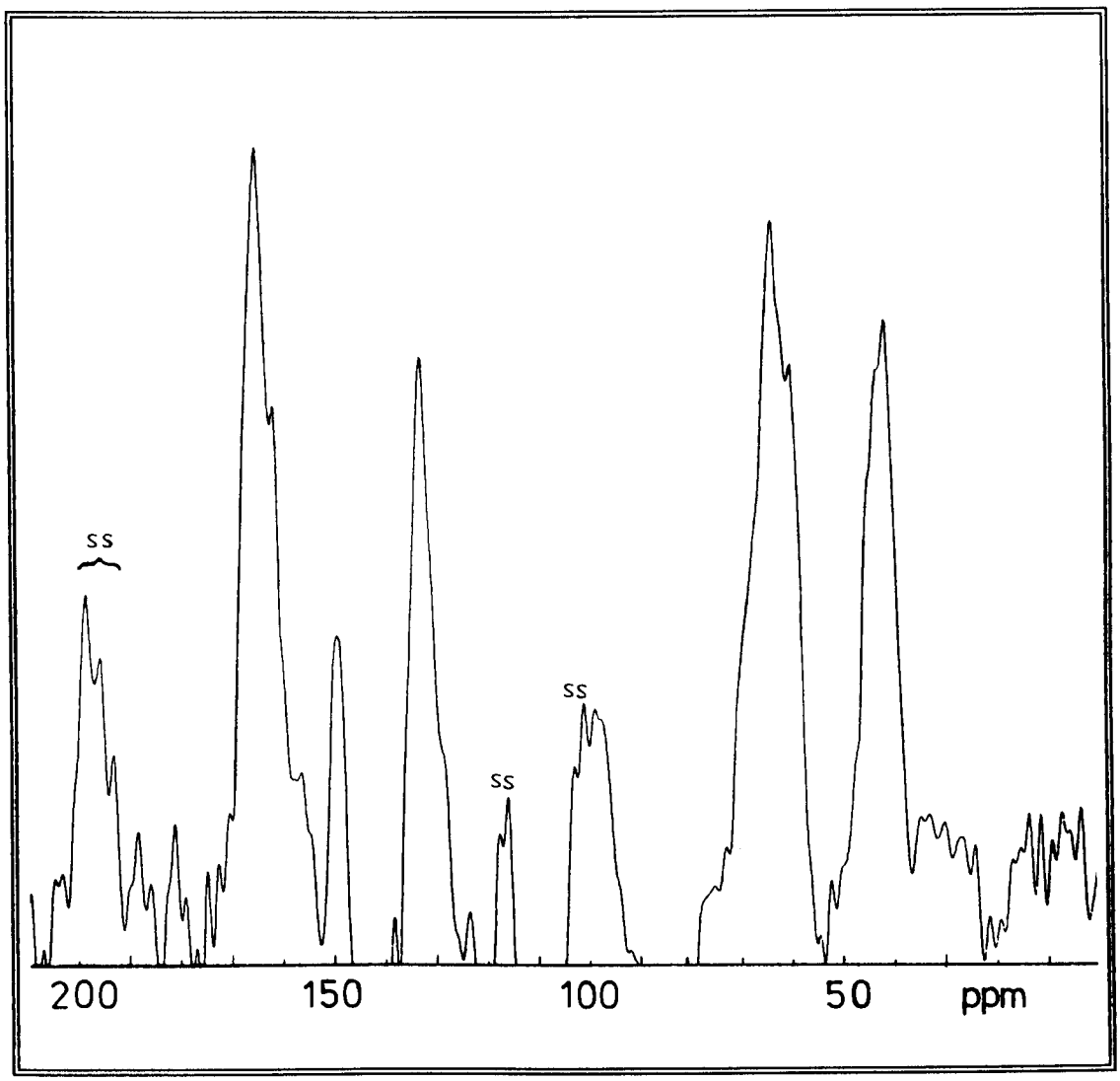

Figure 3.15 The PE-MASS ^{13}C-NMR spectrum (delrin; spinning rate: 2440Hz) of scrapings from the model wire-enamel #R/P/TBT. The recipe is given in table 3.10. A thin film of the model wire-varnish was cured at 300^{0}C for 15 seconds. Note the up-field shoulder-peak on the aromatic signal.

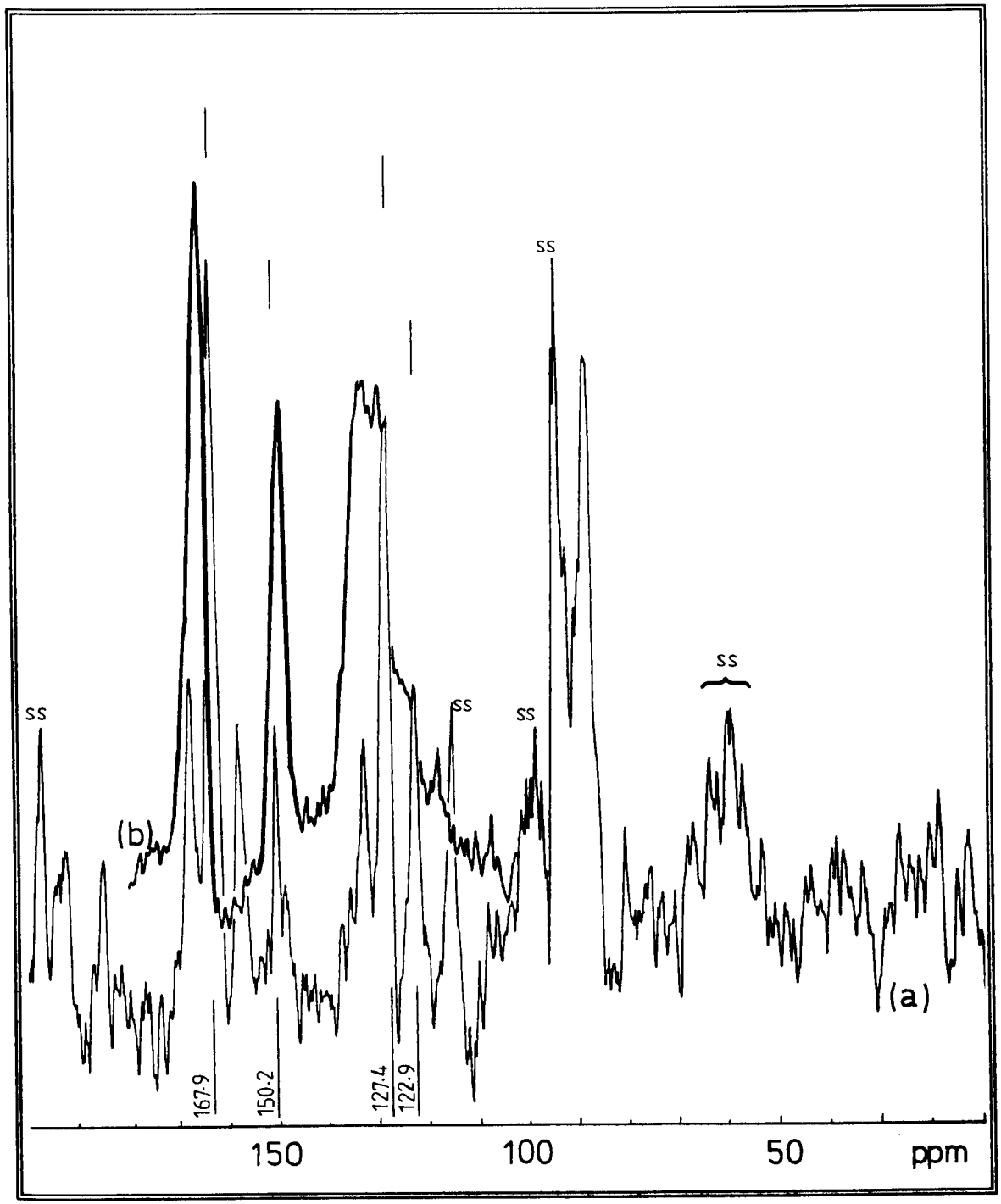

Figure 3.16(a) The PE-MASS ^{13}C-NMR spectrum (delrin; spinning rate: 2640Hz) of the model compound, diphenyl terephthalate (DPT); see §2.3.8 for the synthesis and solution NMR characterisation.
(b) Overlaid, for comparison, is the TOSS/PE-MASS spectrum of the resin-SC cured to a T_g of 102^0C, depicted in figure 3.6(b). Note that the composite aromatic region is similar to that found in the PE-MASS spectrum of Isomid scrapings (cf. figure 3.8(a)).

esters are formed during thermal polycondensation of Isomid wire-varnish, then the solid-state NMR spectrum of DPT is expected to exhibit similar aromatic signals to the extra-resin peaks. The PE-MASS NMR spectrum of DPT is presented in figure 3.16 with an overlaid spectrum of Isomid scrapings (cf. figure 3.6(c)). DPT exhibits two significant peaks at 122.9 and 129.7 ppm which are indeed similar to the extra-resin peaks: 124.9 and 128.9ppm. Therefore, the extraresin peaks could indeed arise from the formation of aryl-ester adducts of resin-SC. Appendix X (cf. table A.15) shows the calculated ^{13}C-NMR resonances for the phenyl radicals in a series of aryl benzoates; a number have chemical shifts which are similar to those of the extraresin peaks. For example, 2-methyl benzoate has calculated phenyl resonances at 130.2 and 125.4ppm, and 2,6-dimethyl benzoate is expected to have peaks at 125.3, 126.1, and 130.1ppm. Apparently, the cresylic acid derivatives (i.e., esters) of the resin-SC could yield the extraresin peaks. In addition, both of the TOSS/PE-MASS NMR spectra for Isomid and Terebec scrapings (cf. figures 3.8(a) and 3.9(a), respectively) exhibit small, but significant peaks at ≈29ppm, consistent with the phenyl-substituted methyl groups of the homologous series of phenol.

3.1.3 **The nature of the extraresin material**

Thus far, the solid-state NMR evidence has suggested that Isomid wire-enamel contains residual phenolic solvents as aryl-ester adducts appending the polymer network.

As mentioned earlier, the residual solvents were found to be extracted from Isomid wire-enamel scrapings only as the temperature of the extraction-solvents was raised above

a threshold of 145±2^{0}C. This process was most effective with those extraction-solvents which had higher boiling points; DMF, DMSO, and EG. The threshold temperature at which the extraresin material is released was verified by mass spectrometry; scrapings were introduced into the ionising chamber at ambient temperature, and as its temperature was gradually increased at ≈20degrees/minute to 287^{0}C, the mass spectrum of any vapours released into the chamber was sampled continuously. No significant vapour was thereby detected until the chamber reached 144^{0}C (see appendix IX for this mass spectrum).

The solvent extractions revealed the presence of aromatic substances since $\pi \rightarrow \pi^*$ electronic transitions were observed by UV/visible spectrometry (cf. figure 3.17). The absorption-bands observed are consistent with those of phenols, corroborating the mass spectrum of the vapours emitted from the Isomid scrapings at 144^{0}C; the spectrum (cf. figure A.5, appendix IX) exhibits significant fragmention peaks at (m/e): 149, 136, 122, 108, and 94, which coincide with the molecular weights of the major components of cresylic acid, those being, dimethylethyl phenol, trimethyl phenol, cresol, and phenol, respectively.

Analysis of the extraresin material was also attempted by PGC, conducted at 600^{0}C. However, a complex chromatographic spectrum resulted which could not be analysed without coupling the column to a mass spectrometer so as to analyse each fraction as it is eluted. Unfortunately, this facility was not available at the time that this work was conducted. Further PGC analyses with pyrolysis temperatures closer to the threshold temperature (e.g., ≈150^{0}C) for the Isomid

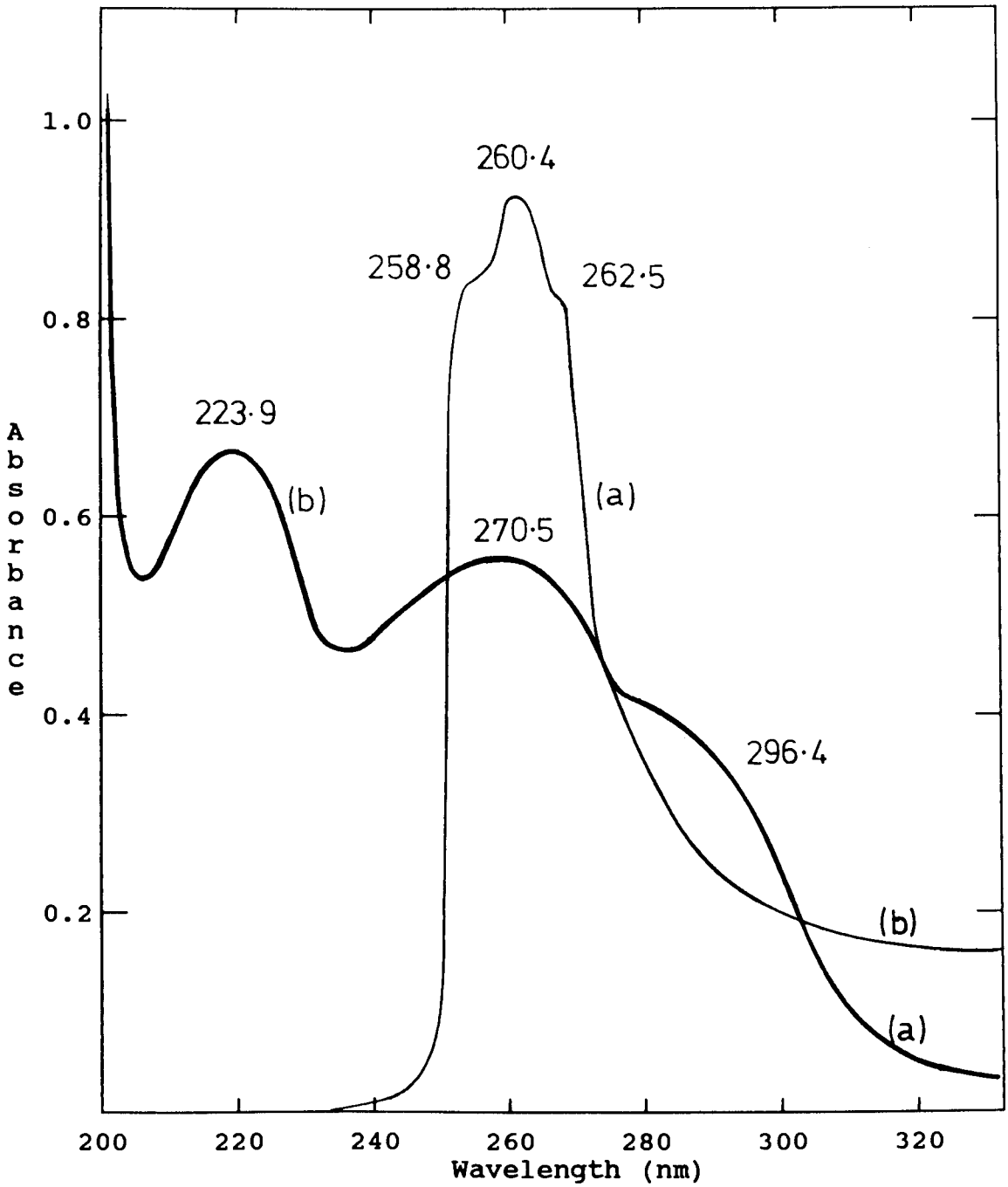

Figure 3.17 The UV/visible spectra of extraresin material extracted from Isomid wire-enamel scrapings. Curve (a) shows the spectrum of DMSO after heating this extraction-solvent to 147^{0}C. Curve (b) shows the result of extraction by refluxing ethanol; the peak at λ_{max}= 223.9 nm is due to ethanol.

Notes. Spectrum (a) was baseline corrected by subtracting the spectrum for pure DMSO. The same ratio of moles of extraction-solvent to mass of enamel scrapings were used in both experiments, and the spectra were obtained at 25^{0}C.

scrapings are needed to preferentially release the extra-resin material; a lower temperature reduces the components due to polymer degradation. When coupled to a suitable, polar column which is heated to a temperature similar to the boiling points of the phenols (i.e., $\approx 200^{0}C$), such an experiment is expected to identify easily the components of the extraresin vapours.

3.1.4 General discussion: aryl-ester curing intermediates

The evidence presented thus far suggests that the phenols of cresylic acid undergo esterification and ester exchange reactions with resin-SC, in particular with the carboxyl and HE end-groups and the glycol ester groups in the chain backbone. The products of these reactions are aryl esters; derivatives which are more reactive to transesterification than the precursory functional groups (viz., carboxyl, HE, and chain-ester groups), and which degrade readily at elevated temperatures, regenerating the phenols. The greater reactivity of the aryl-esters[31,32,33] promotes ester exchange reactions with the HE end-groups, leading to an increase in the propagation-rate for the polycondensation of the polymeric resin, and resulting in the desired glycolic-ester chain units. Hence, cresylic acid is not a passive polymerisation, or delivery, medium for resin-SC in the formation of Isomid wire-enamel coating, but also promotes chain extension through the reactive intermediates; the aryl-ester derivatives.

Scheme 10 (**vide infra**) illustrates the sequence of reversible reactions envisaged to take place during the curing of Isomid wire-varnish. Initially, cresylic acid acts

as a protic acid-catalyst promoting nucleophilic substitution by aryloxy conjugate-anions onto the carboxyl and ester groups of the resin (cf. reactions #1, #2, and #3).

The large initial concentration of cresylic acid (≈60 wt.%), prior to wholesale evaporation as the thin film of varnish is baked, provides that reactions of the phenols with the carboxyl chain end-groups (reaction #1, scheme 10; simple esterification), the chain-ester groups (reaction #2; ester exchange), and HE chain end-groups (reaction #3; ester exchange) predominate. The aryl-ester adducts, thus formed, can then partake of the polymer-extension reaction with the HE end-groups (cf. reaction #4).

In the early stages of curing, the resin is in solution with abundant cresylic acid, providing a relatively high-polarity medium in which the reactive anions and cations (cf. reaction #4(a)) are solvated and stabilised; the cations react with the HE end-groups to extend the polymer network. During the late stages of varnish-curing, that is, where the greater part of the solvents have evaporated, the polymer-film begins to solidify, with viscosity rising rapidly, and the polarity of the reaction-medium tending to decrease. Dropping polarity is expected to reduce solvation of the reactive ions, and replaced with ion-pairs[20] (cf. reaction 4(b)) which may react directly with the HE chain end-groups, without prior cleavage of the C-OAr bond of the aryl-ester polymerisation intermediates.

The early stages of the curing-cycle are characterised by a high concentration of cresylic acid, and reactions #1 to #3 of scheme 10 suggest that the bulk of the condensed EG and water appear early in the cure. The abundance of phen-

ols, both as solvent and polymerisation condensate (by degradation of phenyl-ester intermediates) presents the possibility that EG and water could form azeotropic boiling mixtures with the phenols. Appendix VII gives the azeotropic data for a ternary mixture with phenol, boiling at 101^0C.

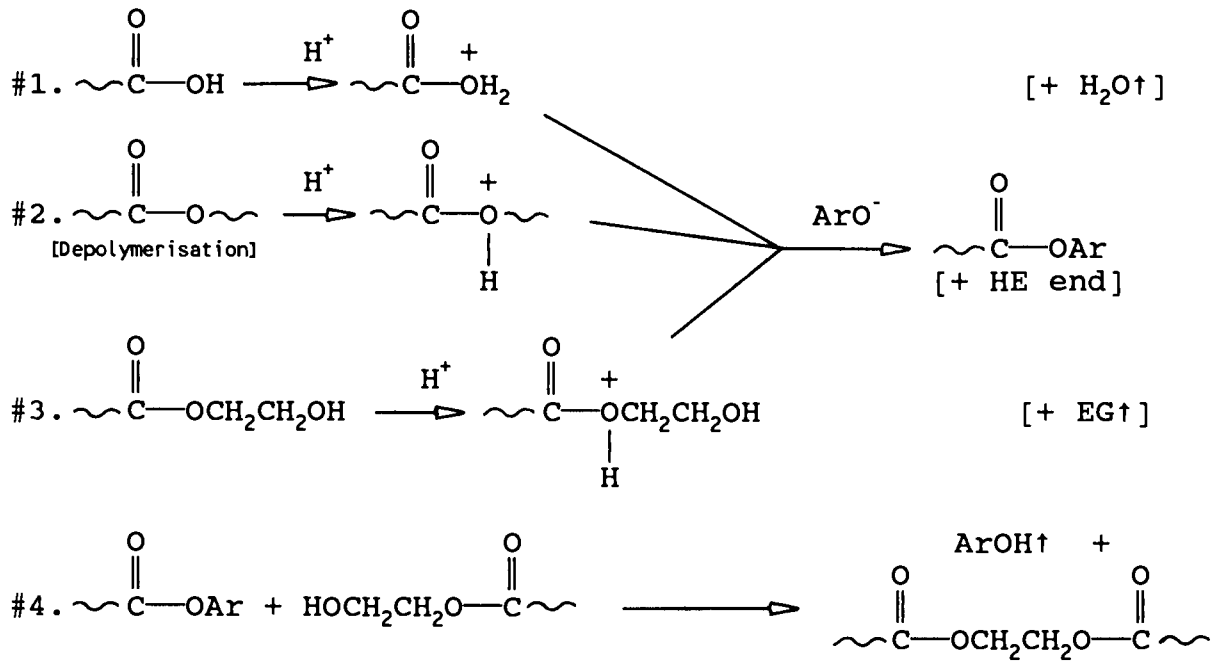

4(a). [in the early stages of curing, and cresylic acid is abundant]

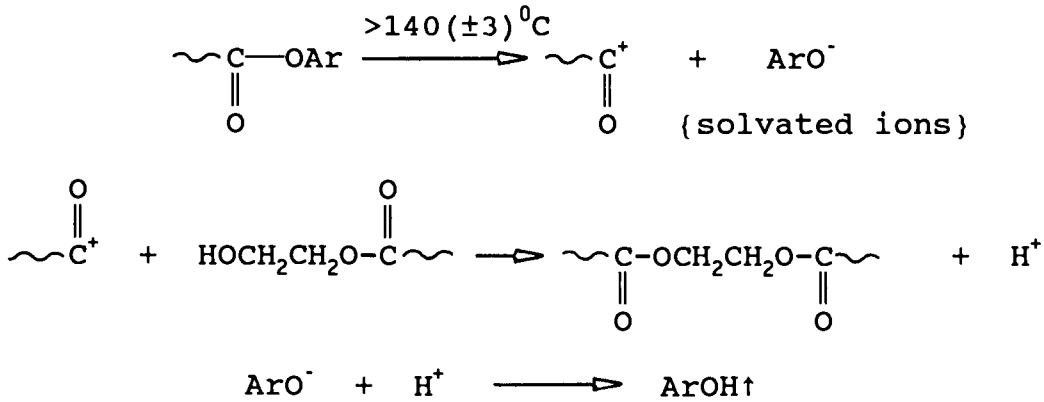

4(b). [in the late stages of curing, where the solvents have substantially evaporated, and the reaction medium has a relatively low polarity]

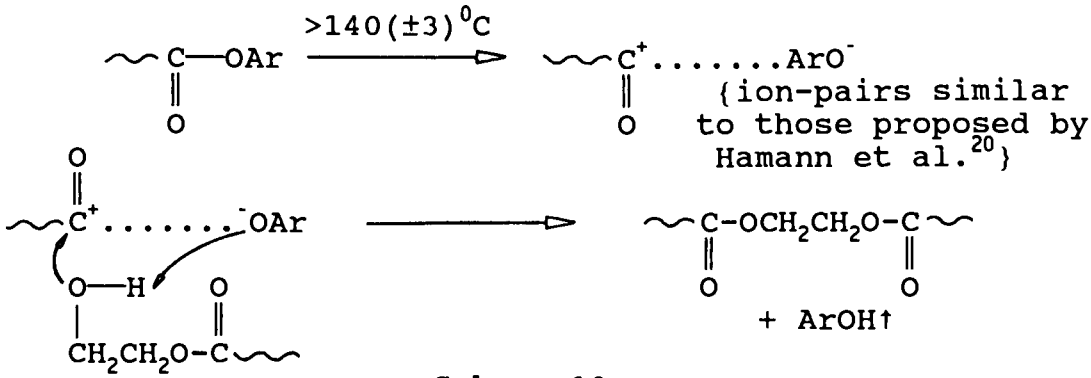

Scheme 10

Therefore, as chain propagation proceeds through aryl-ester intermediates, the major polycondensation byproducts are aryl alcohols which diffuse through the polymer film with greater ease than EG; the diffusion coefficients[28] of small molecules in low molecular weight PET films follow the order: water>>phenol>EG. In this regard, the most desirable solvent is phenol, as it contains no unnecessary substituents (as do its homologues), tending to slow its diffusion. Unhindered movement through the polymer-film reduces the likelihood of nucleate boiling (viz., boiling which occurs at the solvent-polymer interfaces where pools of solvent form deep within the polymerising film) which cause blow-holes and pits over the film-surface (see §1.4.5.2).

The early esterification of the carboxyl end-groups with phenols has the additional advantage of eliminating a potential source of inhibition of the titanate catalyst through the formation of stable Ti(IV)/BA chelates.[69(c),69(e)] Although such chelates tend to be less effective transesterification catalysts at low curing temperatures (viz., $<200^0$C), they are active catalysts at higher temperatures. The alkyl titanate, "Tyzor TBT", is thus freed, allowing it to associate with the carboxylate chain end-groups, and perform its function as a transesterification catalyst.

3.2 **Modelling the wire-enamel curing process**

The complex nature of the curing of Isomid wire-varnish renders it difficult to understand every facet; attempts to model the reactions which instigate curing tend to over-simplify the reaction-conditions. During the early stages of curing, the wire-varnish coating is transformed from a liquid (i.e., a resin in solution) to a solid, highly poly-

merised film as the solvents are removed, either by vaporisation or by reaction with the polymer. Therefore, the polarity of the medium alters continuously. Such changes affect the rates of the curing reactions,[180] and therefore, any modelling of individual reactions must be tempered with this consideration.

3.2.1 Thermogravimetric analysis of thermally cured model wire-varnishes

The experimental method and formulations for the model wire-varnishes adopted for a series of experiments to establish a chemical interaction between resin-SC and the cresylic acid, represented by phenol, are described in §2.4.1.

A **calculated** mass-loss curve was determined from thermogravimetric analyses of the masses lost while the resin and phenol were independently exposed to the stoving regimen. Tables 3.11 and 3.12 record the mass-losses as percentages of the initial sample-masses against stoving-times.

The mass-loss data for phenol and resin-SC were used to construct a calculated percentage-mass-lost versus stoving-time curve (cf. table 3.13 and figure 3.18) for a simulated wire-varnish in which no chemical interaction between the components is possible. The calculations assumed a varnish consisting of 40.00wt.% resin-SC and 60.00wt.% phenol.

Table 3.11 The percentage-mass-lost during the stoving of three matched samples of phenol. The averaged initial mass is 0.68(±0.07)g.

Stoving Time (t, minutes)	Percentage mass-lost sample			Average %mass lost	s.d.
	1	2	3		
0	0	0	0	0	—
10	99.32	99.78	99.72	99.6	0.20
30	99.93	99.93	99.63	99.8	0.14
70	100	100	100	100.0	0.00

Note. s.d. = standard deviation

Table 3.12 The percentage-mass-lost during the stoving of three matched samples of resin-SC. The averaged initial mass is 0.39(±0.01)g.

Stoving Time (t, minutes)	Percentage mass-lost sample 1	2	3	Average %mass lost	s.d.
0	0	0	0	0	--
12	5.17	4.13	6.14	5.14	0.82
33	10.42	9.54	11.59	10.52	0.84
73	14.50	14.03	15.65	14.73	0.68
153	16.99	16.60	18.34	17.31	0.75
313	18.59	18.38	20.34	19.10	0.89

Table 3.13 The **calculated** percentage-mass-losses for a simulated, uncatalysed model wire-varnish consisting of 60.00wt.% of phenol and 40.00 wt.% of resin-SC. The calculations were based on the data presented in tables 3.11 and 3.12.

Stoving Time (t, minutes)	Percentage mass-lost phenol A	resin-SC B	**calculated** wire-varnish A + B
0	0	0	0
10	59.7±0.12	2.1±0.33	61.8±0.45
30	59.89±0.09	4.2±0.34	64.1±0.43
70	59.99±0.00	5.9±0.27	65.9±0.27
150	59.99±0.00	6.9±0.30	67.2±0.30
310	59.99±0.00	7.6±0.36	67.6±0.36

Note. The data for phenol and resin-SC given in tables 3.11 and 3.12 were used to determined the proportions of these in the **calculated** varnish formulation.

Table 3.14 The percentage-mass-lost during the stoving of an uncatalysed model wire-varnish.

Stoving Time (t, minutes)	Sample mass (g)	Percentage of the mass lost (wt.%)
0	0.527±0.008	0
12	0.205±0.009	61.8±1.2
32	0.194±0.005	63.8±0.4
72	0.191±0.004	64.5±0.2
157	0.186±0.004	65.4±0.3
317	0.178±0.005	66.9±0.5

Two model wire-varnishes were mixed using phenol according to the recipes given in §2.4.1; one with catalyst, and the other without. These model varnishes were stoved using the same procedure as for phenol and resin-SC, and the

resulting mass-losses were monitored for three matched samples in each case. The data are recorded in tables 3.14 and 3.15.

Table 3.15 The percentage-mass-lost during the stoving of a catalysed model wire-varnish.

Stoving Time (t, minutes)	Sample mass (g)	Percentage of the mass lost (wt.%)
0	0.562±0.01	0
10	0.224±0.009	60.2±1.5
30	0.215±0.01	63.4±0.9
70	0.201±0.006	64.3±0.8
150	0.198±0.005	64.9±0.5
310	0.191±0.007	66.0±0.8

The experimental method employed has not distinguished any difference in the rate of mass-loss from the catalysed and uncatalysed model wire-enamels, but a significant difference is seen between these and the **calculated** mass-loss; the mass-loss curves are depicted with errors in figure 3.18. The difference, therefore, suggests the occurrence of chemical reactions between phenol and resin-SC, during the curing process.

The esterification of phenol (viz., cresylic acid) with resin-SC accounts for the significantly lower than expected rate of mass-loss from both the catalysed and uncatalysed model varnishes. The formation of polymer/solvent adduct (viz., phenyl ester) prevents the complete removal of phenol; of the order of 1wt.% of the initial amount of phenol in the model varnishes (cf. figure 3.18). Assuming the mass-loss from resin-SC is the same as in the **calculated** varnish for a wire-varnish consisting of 60wt.% phenol and 40wt.% resin-SC, then approximately 1.2wt.% phenol is retained in the curing varnish (cf. table 3.16), according to the diff-

erences determined for the uncatalysed model varnish over the time for which it was stoved. Based on the mass of resin-SC used to make-up the uncatalysed model-varnish (i.e., 0.39±0.1g), the amount of phenol remaining in the cured-enamel, after 150 minutes stoving, is $1.90(\pm0.18)\times10^{-4}$moles/$g_{resin}$. Converting this figure into the units of acid number (i.e., $10.6(\pm0.98)$mgKOH/g_{resin}) it is apparent that the amount of phenol combined with resin-SC equals the available carboxyl end-groups (i.e., $10.5(\pm0.5)$mgKOH/g_{resin}; cf.§2.1.6). Therefore, the phenol combined in the model varnishes seems to be as the aryl-ester derivatives of the carboxyl end-groups.

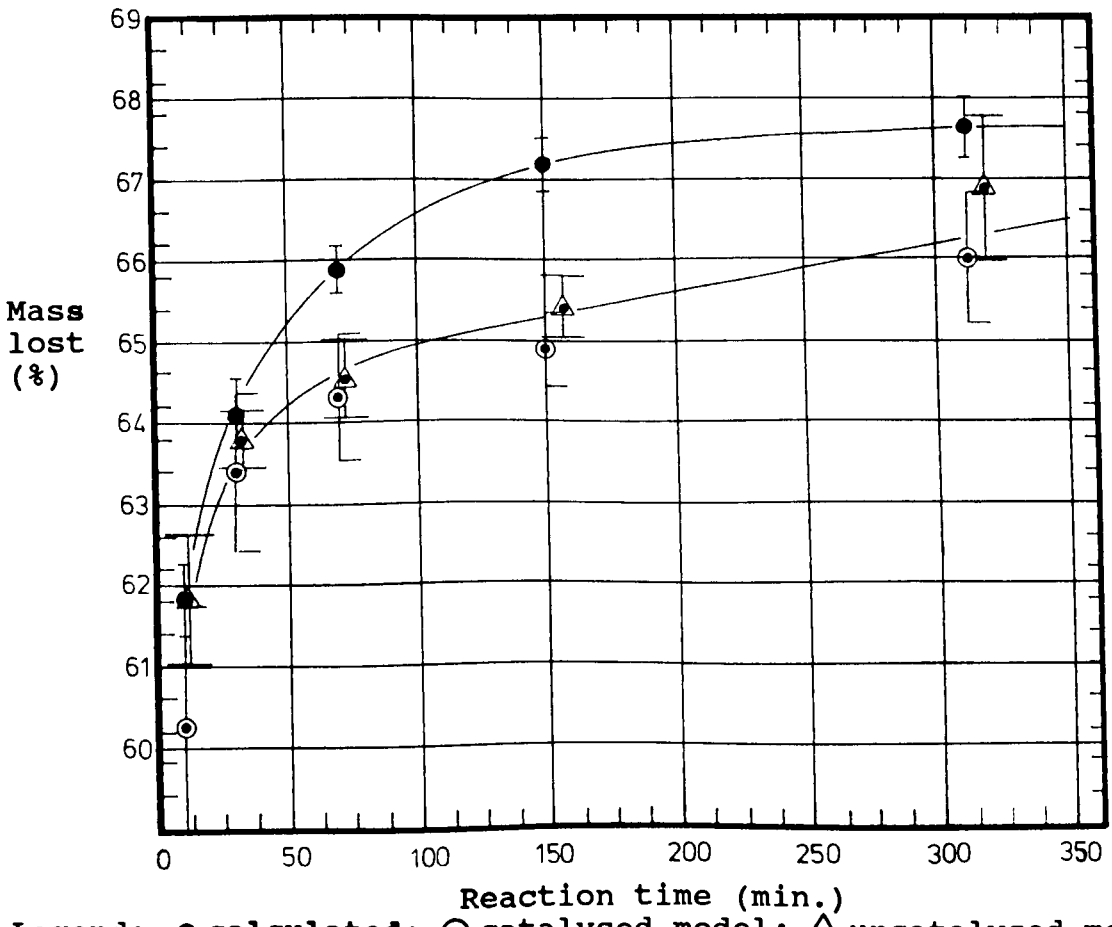

Figure 3.18 The percentage-mass-loss curves, plotted against stoving time (at $300(\pm10)^0$C) for the **calculated** wire-varnish (cf. table 3.12), and the model wire-varnishes (cf. tables 3.14 and 3.15); one catalysed and the other uncatalysed (cf.§2.4.1).

Table 3.16 The difference, factor (Z-W), in the percentage-mass-loss of phenol during stoving between the **calculated** wire-varnish (cf. table 3.13) and the uncatalysed model wire-varnish (cf. table 3.14), assuming that the resin mass-loss for the model varnish is identical to the **calculated** varnish.

Stoving-time (min.)	%mass-loss uncatalysed varnish (X)	%mass-loss of resin only (Y)	X-Y (Z)	%mass-loss of phenol only (W)	Z-W
0	0	0	0	0	0
10	61.8±1.2	2.1±0.33	59.7±10.5	59.7±0.12	0
30	63.8±0.4	4.2±0.34	59.6±5.2	59.89±0.09	0.3±0.03
70	64.5±0.2	5.9±0.27	58.6±2.9	59.99±0.00	1.3±0.06
150	65.4±0.3	6.9±0.30	58.5±2.8	59.99±0.00	1.4±0.07
310	66.9±0.5	7.6±0.36	59.3±3.2	59.99±0.00	1.6±0.09

Notes. The average of (Z-W) = 1.2(±0.06)wt.%.

3.2.2 **Distillate-analysis for model wire-varnishes**

The model wire-varnishes used in the §3.2.1, above (see §2.4.1 for formulations) were also used in these experiments. The model varnishes were cured such that distillates were collected (cf. the procedure is described in §2.4.2); components of the distillate-samples were analysed by GC.

The chemical reaction between phenol and resin-SC, proposed from the thermogravimetric analysis in §3.2.1, is not conclusive. The decreased mass-loss-rate, when compared with the **calculated** mass-loss-rate (cf. figure 3.18), is perhaps a result of slower polymerisation caused by cooling due to the latent heat of vaporisation for phenol (ΔH_{vap}=49.8kJ/(g.mole)). Therefore, it is of interest to know whether all of the phenol is vaporised when the model wire-varnish is cured at well above the boiling point of phenol.

The distillates from the catalysed and uncatalysed model varnishes were compared with those from a sample of

resin only (i.e., 27.70±0.02g; cf. table 3.17). The resin sample was subjected to the same procedure, and heating for 32 minutes resulted in the collection of 0.10±0.02g of distillate (i.e., a mass-loss of 0.4wt.%). A GC analysis showed the components to be EG (0.02g) and water (0.08g).

Generally, heating was continued until vapours were no longer condensed and the distillation still-head temperature dropped below 180^{0}C (i.e., the boiling point of phenol); the catalysed model varnish continued to distill for 63.5 minutes, while the uncatalysed varnish took 79.0 minutes. As well, the silicone oil-bath, used to heat the reaction vessel, provided sufficient energy to quickly heat the varnishes to temperatures between 215 to 243^{0}C, and sufficient energy to vaporise phenol, water, and EG (b.pt., 198^{0}C).

Analysis of the experimental results depends on the masses of reactants and products, therefore weighing errors are important to the discussion; both a top-loading (±0.02g) and an analytical balance (±0.0002g) were used. Apart from weighing errors, the distillate-collection procedure also presented some uncertainty; a small amount of condensed distillate remained uncollected, clinging to the walls of the condenser column. The error in the total mass of distillate was estimated by weighing the condenser column before and after each distillation; the uncollected distillate was consistently of the order of 0.01g. The final source of error was in integrating the GC peaks by the cut-and-weigh method; this integration-method was validated with 6 consecutive analyses of a standard mixture of water, phenol, and EG; the uncertainty was found to be 2wt.%.

Table 3.17 The results of GC analyses of the distillates from the thermal curing of two model wire-varnishes (see §2.4.1) in which the cresylic acid solvent system is represented by phenol.

#	Parameter	Catalysed varnish (g)	Uncatalysed varnish (g)	Resin-SC only (g)
1	Total distillate-mass (D_T)	15.62±0.04	14.76±0.05	0.102±0.05
2	Initial phenol-mass (P_o)	16.57±0.02	16.70±0.02	———
3	Phenol, distilled (P_d)	13.90±0.01	13.82±0.015	———
4	Residual phenol (P_r)	2.688±0.005	2.880±0.006	———
5	Varnish mass (E_o))	27.70±0.02	27.70±0.02	———
6	Enamel mass (E_f)	12.1000±0.0002	13.1880±0.002	———
7	Varnish mass distilled (E_o-E_f)	15.60±0.01	14.51±0.01	———
8	$\alpha = D_T - (E_o - E_f)$	0.0160±0.0003	0.2480±0.0009	———
9	Initial resin mass (R_o)	10.91±0.02	11.00±0.02	27.70±0.02
10	Water, distilled (W_d)	0.68±0.01	0.77±0.015	———
11	EG, distilled (M_d)	0.49±0.01	0.18±0.015	———
12	$C_d = W_d + M_d$	1.17±0.04	0.9±0.11	———
13	$R_r = R_o - C_d$	9.7±0.4	10±1.1	———
14	$\beta = R_r - E_f$	2.36±0.09	3.1±0.3	———
15	Butanol, distilled	0.541±0.01	———	———
16	Reaction time (minutes)	63.5	79.0	58.0

Notes. Some parameters require description: α, embodies the empirical error, the discrepency between the expected distillate-mass, given by weighing the reaction charge before and after "curing", and actual distillate-mass; C_d, the net loss of the polycondensation side-products (i.e., EG and water); R_r, the expected enamel-mass, presuming that no reaction takes place between phenol and resin-SC, and given by the difference between the mass of the resin used in making the model varnish (R_o) and C_d; and β, the amount of phenol that remained undistilled, and given by the difference between the expected residual resin-mass (R_r) and the actual "cured" enamel-mass (E_f) after cessation of distillation.
Row #15 presents the mass of distilled butanol, from the ligand-exchange of "Tyzor TBT".

The results of these experiments are presented in table 3.16, in which row #8 gives the difference between the total distillate-mass (D_T) and the expected distillate-mass; the latter was given by the difference between the mass of "cured" enamel (E_f; i.e., after completion of distillation) and the mass of the initial varnish. The difference is designated as α. The values for α are 0.2480±0.0009g and 0.0160 ±0.0003g for the uncatalysed and catalysed varnishes, representing 1.7wt% and 0.1 wt.% of the total distillate collected (D_T), respectively. These unaccounted complements of the total distillate-masses lay in those droplets of dis-

tillate which remained clinging to the walls of the apparatus, and which were not accounted for by weighing the condenser column after completion of distillation. The magnitudes of α are much smaller than the mass of phenol remaining undistilled (P_r), those being, 19.5wt.% and 17.2 wt.% of D_T, respectively. Hence, a significant proportion of the phenol was not distilled, remaining within the "cured" enamels, as do solvent-residues (≈5wt.%) in wire-enamelling.

Figure 3.19 represents the masses of the various distilled components against reaction time, showing that significantly less EG was generated in the curing of the uncatalysed varnish. Hence, the catalysed model varnish undergoes ester exchange between HE end-groups at a greater rate than the uncatalysed varnish, confirming that "Tyzor TBT" is an effective transesterification catalyst. The similar rate of water distillation, albeit slightly slower for uncatalysed varnish, suggests that this titanate has little activity towards esterification reactions; the total quantities of distilled water (W_d; cf. table 3.17) are similar, although the quantities of distilled EG (M_d) differ greatly (i.e., 2.7 times more EG was evolved from the catalysed model varnish).

The effect of phenol upon the evolution of water and EG (the total of water (W_d) and EG (M_d) distilled; parameter C_d) can be seen clearly when C_d is compard with the initial masses of resin-SC (parameter R_o) for the "resin-SC only" and "uncatalysed varnish" experiments. The 24-fold increase in the distillation of water and EG, for similar reaction times (cf. table 3.18), indicates an increased polycondensation rate; phenol acting as an acid-catalyst, as proposed in reactions #1 and #3 of scheme 10 (cf. p.181).

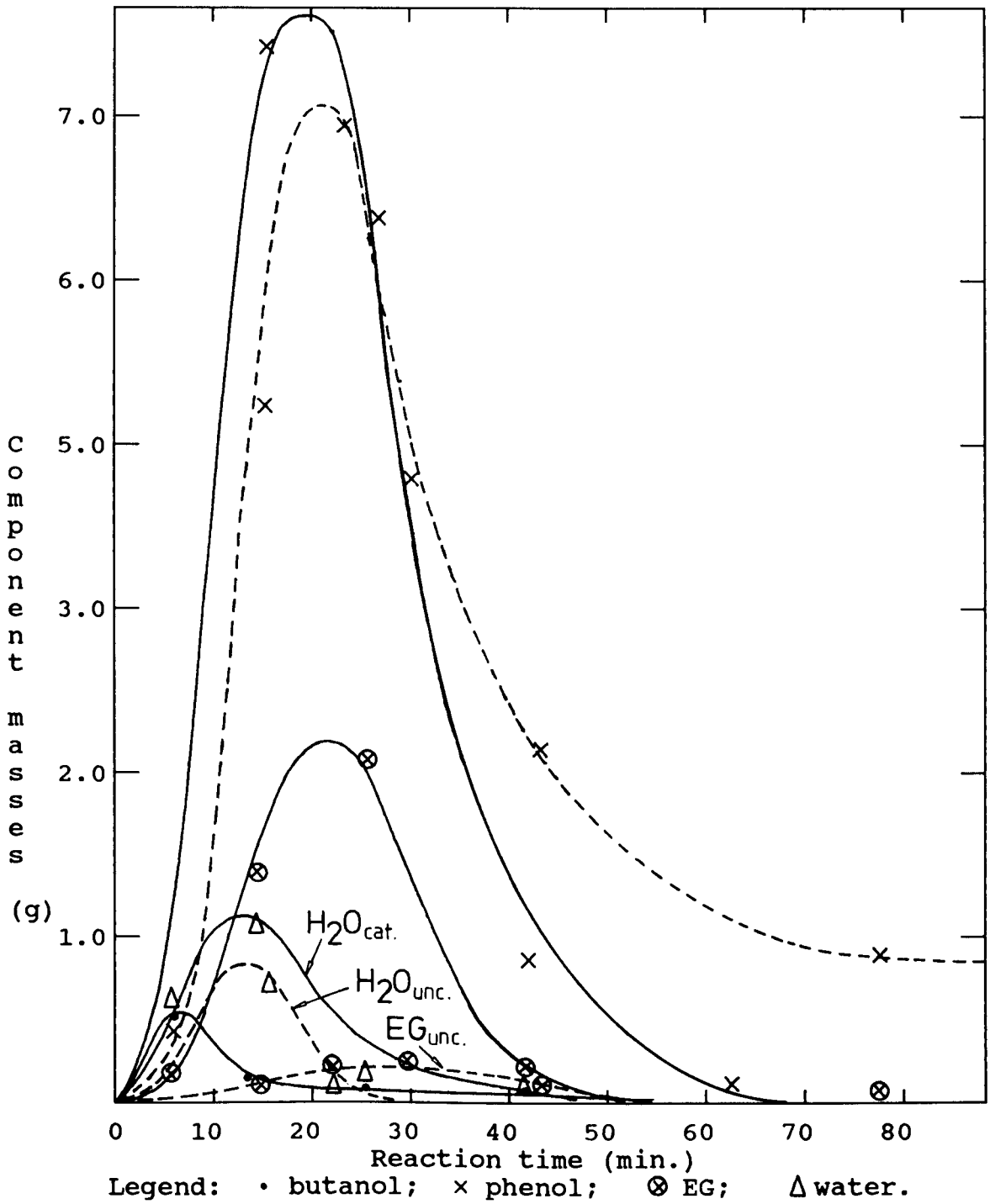

Figure 3.19 The distilled masses of each component from the "catalysed" (solid lines) and the "uncatalysed" (dotted) model varnishes. The distillation of phenol and water is seen to be similar for both samples, in spite of a lower initial reaction temperature for the "uncatalysed" experiment (i.e., at 193°C at 15 minutes of reaction, as opposed to 215°C at 6.3 minutes for the "catalysed" experiment).

The evolution of EG is significantly affected by the presence of "Tyzor TBT", confirming that it is an active transesterification catalyst.

Table 3.18 The ratios of total masses of water and EG distillates (C_d) to the initial masses of resin-SC (R_o) are presented as percentages for the "resin-SC only" and "uncatalysed" experiments.

Distillation Experiment	(C_d/R_o) x 100 (wt.%)
Resin-SC only	0.36±0.08
Uncatalysed varnish	8.64±0.08

Note. The "uncatalysed" experiment demonstrates a 24-fold increase in the amount of water and EG distilled, above that for "resin-SC only".

The amount of phenol remaining after the cessation of distillation (viz., parameter P_r in table 3.16) was found to be 0.031moles for the uncatalysed varnish and 0.029moles for the catalysed varnish. These quantities are much greater than the amounts of carboxyl end-groups available in the uncured resin (i.e., $2.06(\pm0.09)\times10^{-3}$ and $2.04(\pm0.09)\times10^{-3}$ moles, respectively; calculated from the acid number, 10.5 ±0.5 $mgKOH/g_{resin}$ for resin-SC). Given that phenol, and by imputation cresylic acid, esterifies completely the carboxyl end-groups, the surfiet phenol transesterifies the polymeric-ester functions of the resin; reactions #2 and #3 of scheme 10 (cf. p.181).

Curing at ≈300^{0}C (cf. §3.2.1) produced much less residual phenol than at ≈210^{0}C (cf. §3.2.2), suggesting that in the latter, much of the phenol residues may not have reacted. Nevertheless, these experiments indicate a significant proportion has undergone esterification or ester exchange with resin-SC.

3.2.3 Modelling the industrial-curing of Isomid wire-varnish

Comprehensive modelling of the curing of Isomid could not be achieved due to a lack of time and resources required to produce results. However, in an attempt to understand

more fully the effects of catalysts on the curing of resin-SC, the simple esterification reaction of benzoic acid (BA) with EG was chosen to model the polyesterification of the HE with the carboxyl end-groups. Although esterification was chosen, transesterifications are the major polymerisation reactions occurring during the curing of resin-SC.

The polyesterification-rate is similar to simple esterification, provided the reactivities of the chain end-groups are not greatly affected by increasing molecular weight, increasing crosslink-density, or increasing viscosity. Molecular weight has been shown to have little effect[181] for a homologous series of dibasic acids; any differences from the rate constants for monobasic acids vanishing with increasing chain-length. A shift in the rate constant in bulk polyesterification has been noted by Flory[182] for some linear polyesters, but this is an exception rather than the rule; the rate constant **usually** remains unchanged[30] throughout polymerisation or degradation processes. Notwithstanding similarity, the main concern here is with the influence of varnish-solvents and Ti(IV) catalysts on the curing of Isomid.

EG (in 10-fold excess) acted as a reaction-medium as well as providing an impetus to the equilibrium for the formation of 2-hydroxyethyl benzoate (HEB), in preference to the diester, ethylene dibenzoate (EDB). The reaction mixture was heated to a temperature of $220(\pm 10)^{0}C$, and the distillate collected (cf. §2.4.1).

The reaction conditions were conducive (i.e., contained acidic protons) to the formation of ethers, DEG and TEG. However, these products were determined to be minor (<4mol%

of the distillate) by analyses of the distillates with inverse-gated, decoupled ^{13}C-NMR (cf. table 3.19). In any case, etherification is most favoured by the presence of strong dehydrating agents such as concentrated sulphuric acid,[169] of which none were used in the modelling reactions.

Table 3.19 The inverse-gated, decoupled ^{13}C-NMR analyses of the distillate from the titanate-catalysed model esterification (i.e., BA with EG).

Catalyst (cf. §2.3.9)	Reaction time (min.)	Components (±10 mol%) HEB	EDB	EG	DEG(1)	TEG(2)
"Tyzor TBT"	94	13	—	83	3.6	—
TPT	51	20	15	45	——	—
TNPT	35	54	32	12	1.5	0.5
TDNPT	45	25	10	62	0.6	2.4

Notes. (1) DEG = diethylene glycol. (2) TEG = triethylene glycol.
The methylene NMR resonances for the distillate-components were used to estimate the molar ratios of the components (ppm): HEB, 63.3(±0.4) and 66.8(±0.2); EG, 63.7 (±0.3); EDB, 63.0(±0.2); DEG, 61.63(±0.09) and 72.77(±0.05); TEG, 61.63(±0.09), 71.7(±1.4), and 72.95(±0.05). The resonances were determined from BB ^{13}C-NMR (20.1MHz, external DMSO(d6), 25^{0}C) spectra of these compounds.

The rate of distillation of condensed water from the BA/EG esterification is a convenient comparator by which the reaction-rate is reflected. McCaffery[183] has used this method to follow the progress of the esterification reactions of decalin with a series of dibasic acids, and has confirmed by direct titration of the reactant concentrations that the method provides useful kinetic information. However, the aim was not to evaluate the internal order of the esterification reaction, but rather to compare the effects of phenols and titanates on the macroscopic esterification-rate, as reflected by the condensation of water. The masses of water distilled after the first 10 minutes of reaction were determined by GC-analysis of the distillate-samples.

Some comment about the order of the reaction is, however, appropriate. The reaction was performed with excessive EG; a "great-excess-approximation" which allows the rate coefficient to be considered as pseudo-nth-order with respect to BA. Considering only the early stages of reaction (<50% conversion of BA), a plot of ln(moles of H_2O distilled) against reaction time was found to be close to first-order, but somewhat less. The lack of conformity of the data to an integral-order is due to the very nonideal reaction-medium. Nonideality also changed continuously as the concentration of EG decreased as it distilled with H_2O. Hence, the activity coefficients of the reactants (BA and EG) and the transition state ($BA\text{-}EG^{\neq}$) vary continuously. The changing polarity of the medium also contributed to nonideality. Notwithstanding these variations, all the data-points of the first-order plot lie within the 95% confidence limits of a line fitted by linear-least-square-regression, but the deviation was nonrandom, clearly not exactly first-order.

Table 3.20 The moles of water distilled upon the esterification of BA (0.0998±0.004 moles) with EG (0.797±0.03 moles) (see §2.4.2 for the reaction procedure), after 10 minutes, with respect to the catalysts: phenols and tetraaryl titanates (cf. §2.3.9).

Added substance	Quantity[1] of added substance (mole)	Quantity of water distilled (mole, $x10^{-2}$)
———	———	3.0±0.2
phenol	0.0095	6.1±0.3
NP	0.0102	10.4±0.5
DNP	0.0097	7.6±0.4
"Tyzor TBT"	0.0027	3.3±0.2
TPT	0.0023	8.4±0.4
TNPT	0.0027	9.2±0.5
TDNPT	0.0028	>>10[2]

Notes. (1) The amounts of titanates added were 1/4 of the moles of the conjugate phenols also used. (2) The reaction with TDNPT proceeded at a much greater rate than the other reactions; $8.7x10^{-2}$moles of water were distilled in the first 2.9 minutes of reaction. The experimental uncertainty was estimated by averaging the errors found in the collection of distillates; ±0.01g, determined by weighing the apparatus before and after reaction, and the error in the integration of GC-peaks by cutting-and-weighing; ±2wt.%.

Table 3.20 presents the amounts of water distilled within the first 10 minutes of reaction with respect to the presence of catalytic quantities (i.e., ≈1wt.%) of phenol, **p**-nitrophenol (NP), 2,4-dinitrophenol (DNP), and their tetraaryl titanates: TPT, TNPT, and TDNPT. The experimental method and data-treatment were intended to give a comparison of the effect of additives, such that the method can be easily applied in industrial development-laboratories where resources are limited to a gas chromatograph.

The data given in table 3.20 indicate that phenols catalyse the esterification, probably by acid-catalysis (pK_a: phenol, 9.89(20^0C); NP, 7.15(25^0C); DNP, 3.96(15^0C)). Ionisation of the phenols is encouraged by the formation of a mesomerically stablised oxyanion, suggesting that catalytic activity is determined by the acidity of the OH-proton. However, the reaction with NP has condensed more water than DNP or phenol. The intramolecular interaction of the OH and the **o**-NO_2 groups in DNP perhaps hinders the release of acidic protons, inhibiting acid-catalysis.

The molecular dipole moments (see appendix IV, table A.5) of the phenols correlate better with activity (i.e., NP > DNP > phenol). Molecular polarisation reflects the polarisation of each functional group.

"Tyzor TBT" has no appreciable effect on the rate of reaction, possibly due to poisoning by BA.[69(a)] BA was proposed to chelate[69(e)] with the titanium centre, forming an octahedral complex,

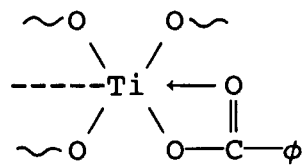

(XI)

and preventing coordination with other reactant molecules. However, tetrabutyl titanate is not completely deactivated by such chelation (i.e., **XI**)[69(c)] since it shows measurable catalytic activity[69(b)] towards esterification,

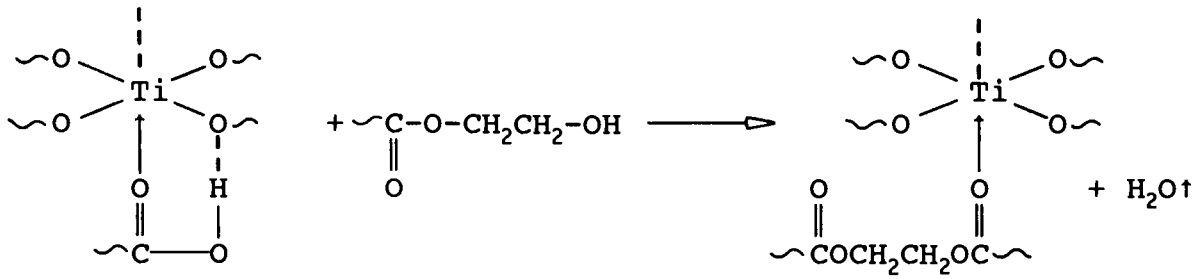

Scheme 11

as well as ester exchange in the polymerisation of poly-(butylene terephthalate) at high reaction temperatures.

TPT and TNPT catalyse esterification to a similar degree as the phenols, suggesting a common rate-determining-step (RDS). However, the absence of a protonating species indicates that protonation of the carboxyl groups, forming activated carbonium ions, is not the RDS. Perhaps a hydrogen bond[69(e)] forms between the carboxyl proton of Ti-coordinated BA molecules and an aryl ligand of the titanate catalyst (adduct **XII**),

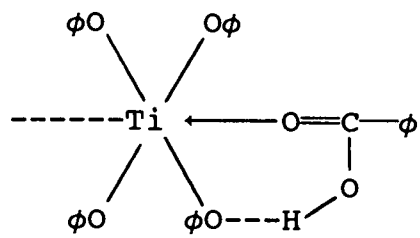

(XII)

which activates the BA-carbonyl group towards nucleophilic attack by EG. However, displacement of aryl ligands by the carboxyl group leads to Ti/BA chelates similar to adduct **XI**, poisoning the catalyst. Hence, the RDS is the attack by EG,

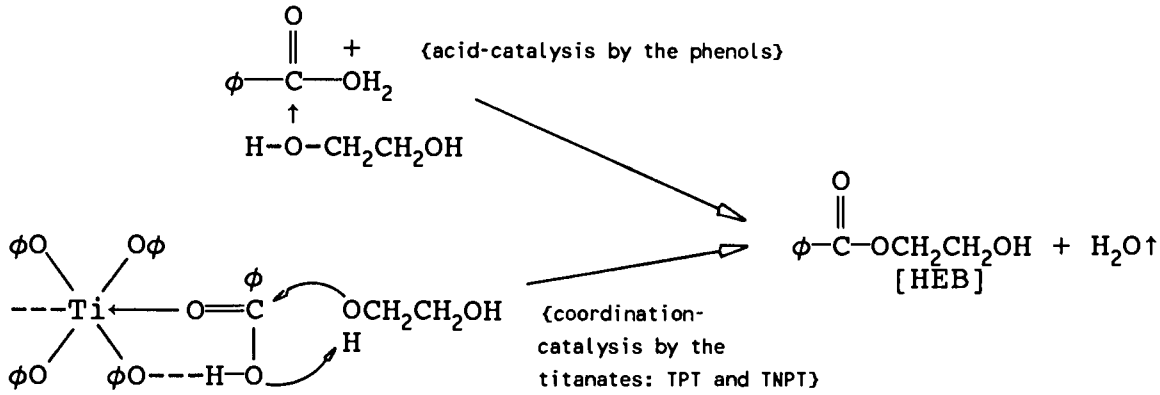

Scheme 12

where the rates of these reactions are similar.

The final phenomenon apparent from table 3.20 is the much greater rate of water-distillation for the esterification catalysed by TDNPT. The cause is not clear without further study of the reaction rate by direct-measurement techniques, that is, titration of the carboxyl groups. Notwithstanding, it appears that the DNP-ligands activate the titanium centre toward catalysis, and in particular, the **o**-NO_2 group has a significant effect upon the central atom. The structural conformation of this titanate is not known; such information is necessary for a detailed understanding of the intramolecular interactions involved. In lieu of a crystallographic analysis, examination of space-filling models suggests a dative bond could form with the titanium centre, producing a six-membered chelate-ring,

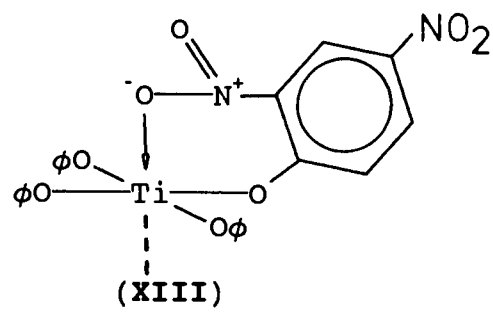

(XIII)

The large difference in the **ipso**-aromatic ^{13}C-NMR signals of DNP and TDNPT (cf. table 3.21) also suggest the chelation model (adduct **XIII**). Complexation of DNP disrupts the

intramolecular hydrogen bond between the hydroxylic proton and the **o**-nitro group, leading to a significant decrease in the electron density at the **ipso**-carbon nucleus. For TPT and TNPT, in which no intramolecular hydrogen bonding can exist, the differences in chemical shifts are much smaller.

The bulky **o**-NO_2 groups are a source of substantial steric repulsion between DNP-ligands, considering the tetrahedral structure postulated in §2.3.9. Reducing the number of ligands is one way of reducing repulsion, but cannot satisfy the valency of titanium(IV). An alternative octahedral conformation is consistent with the known behaviour of the titanates, and it is suggested that two opposing DNP-ligands chelate to the titanium centre through the **o**-NO_2 group, whilst the remaining two are pushed further from the titanium centre by steric repulsion.

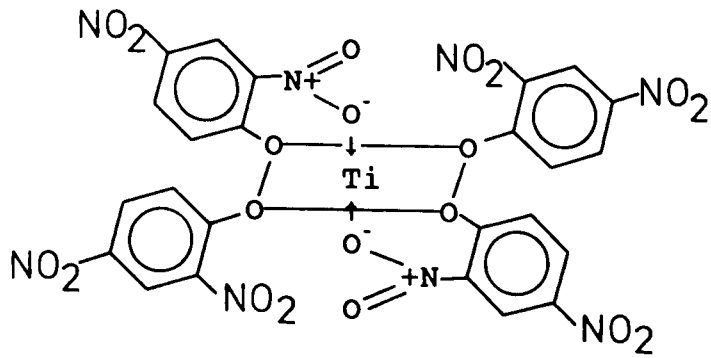

(XIV)

Table 3.21 The BB^{13}C-NMR (20.1MHz, $CDCl_3$) signals for the **ipso**-aromatic carbon nuclei of the phenols and their tetraaryl titanates. The differences ($\Delta\delta$) wrought by complexation are listed for each data-pair.

Basic phenol	Chemical Shift (ppm)	Titanate Complement	Chemical Shift (ppm)	$\Delta\delta$ (ppm)
Phenol	157.8	TPT	156.2	-1.6
NP	163.4	TNPT	164.2	+0.8
DNP	176.5	TDNPT	163.8	-12.7

Note. The direction of movement of the signals is indicated by the sign of the chemical shift difference ($\Delta\delta$); a positive sign indicates a downfield shift from the titanate to the respective phenol.

Occupation of the octahedral positions by dative bonds from the o-nitro groups blocks the approach of reactants (see scheme 7, §1.2). However, with the impetus of steric repulsion, one or both of the more weakly bound DNP-ligands readily cleave, leaving an octahedral cationic complex,

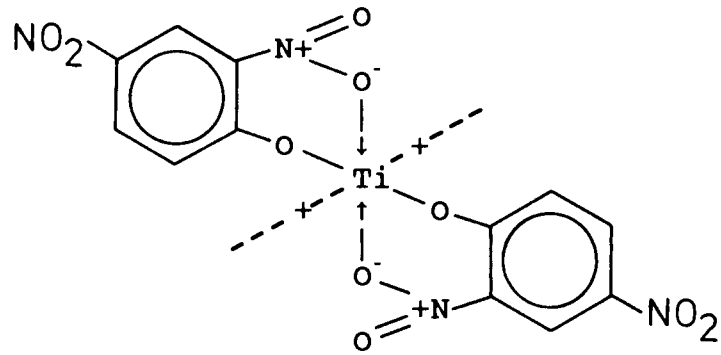

(XV)

The positive character of TDNPT thus enhanced, its Lewis-acidity, and thereby its catalytic activity, is increased; reactants are more strongly attracted into coordination with the titanium. This concept presumes that catalysis is coordinatively controlled, as in the case of the TBT-catalysed condensation of poly(butylene terephthalate).[69(b),69(c)]

Activated complex **XV** contains vacant coordination-sites which could accomodate a BA molecule in such a way as to be activated towards nucleophilic attack by EG,

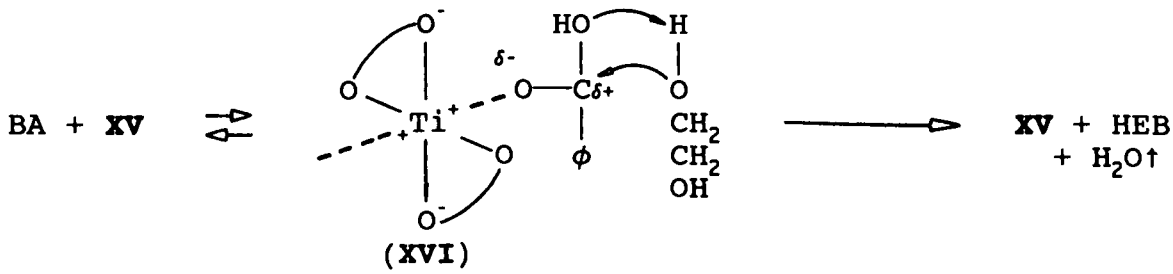

(XVI)

Scheme 13

condensing water and HEB. Coordination increases the positive character of the carbonyl carbon atom, thereby improving the likelihood of nucleophilic attack by EG, the rate of

which then becomes dependent on the size of the positive charge residing on the carbonyl carbon atom.

The possibility of increasing the rate of curing Isomid wire-varnish with a simple change in the titanate catalyst is an attractive proposition to the industrial-market. Hence, SCA has undertaken a curing trial of TDNPT-catalysed Isomid ("Tyzor TBT" being replaced weight-for-weight) against a standard Isomid varnish, but with no significant increase in the maximum enamelling speed, and therefore, no advantage to the wire-enameller, was achieved. The failure of TDNPT to elicit a noticeable increase in the enamelling speed highlights the main shortcoming of the curing model discussed in this section. The Isomid wire-varnish system is oversimplified, that is, only the least important polymerisation reaction was considered. As already established, the predominant class of curing reactions is ester exchange since HE end-groups are ≈15 times more plentiful than are the carboxyl end-groups (see §3.1.1.3, table 3.5).

Although inconclusive of any changes in reaction-rates, on a molecular level, the failure of the trial suggests that the more important consideration in coordinative-catalysis is not the nature of the catalyst-ligands, but rather, the reactive complexes titanium forms with the polymer chain end-groups. Chelated titanate complexes such as titanium lactate (see adduct **IX**; §1.2.2) and the bis(β-ketonato) titanates,[184] partaking of intramolecular, octahedral bis(chelato) complexation similar to the rapidly interconverting stereoisomers of $Ti(acac)_2.X_2$ (where X is a halide), exhibit greater thermodynamic stability. Therefore, in Isomid wire-varnish, titanium is likely to form chelates

with the HE end-groups.

In support of this proposition, it was found that Ti/HEB chelato-adducts are readily formed at room temperature by an exothermic ligand exchange (see appendix VI for a study of the complexation of HEB with Ti(IV)), and it is therefore proposed that in Isomid wire-varnish such chelation with resin-SC occurs with the HE end-groups (cf. scheme 14) during mixing, and before the varnish is thermally cured. Therefore, the catalytic activity of Ti(IV) becomes independent of the type of titanate added to the varnish; the titanate's ligands are likely to be readily substituted in favour of chelation with the end-groups of the resin. Changing the ligands of the parent titanate has, therefore, no bearing on the polycondensation-rate unless they provide greater thermodynamic stability.

The aryl titanates which formed at room temperature by ester exchange of TBT with the phenols of cresylic acid are expected to be, in turn, substituted by HE end-groups through a rapid equilibrium,[69(e)]

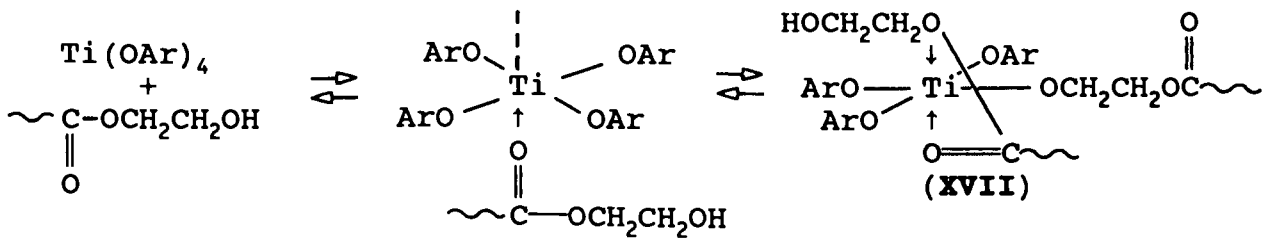

Scheme 14

forming a reactive chelate (**XVII**). The titanium atom acts as a reaction-site, about which polyesterification can take place through the rearrangement of this adduct,

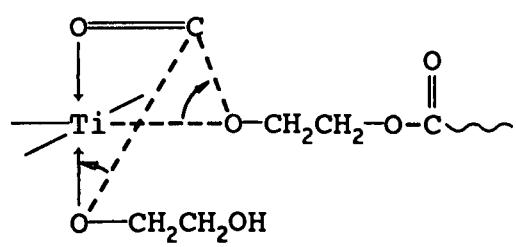

Adduct **XVII** was postulated by Pilati et al.[69(b)] to explain the observed kinetic order for the ester exchange reactions of poly(butylene terephthalate). Under the initial reaction conditions for the model ester exchange of 4-hydroxybutyl benzoate (HBB), the rate was found to be second-order with respect to HBB, and first-order with respect to TBT, leading to the proposition that a complex-adduct similar to **XVII** mediates polymerisation.

Rearrangement of adduct **XVII** condenses EG with the extension of the polymer network,[69(c)]

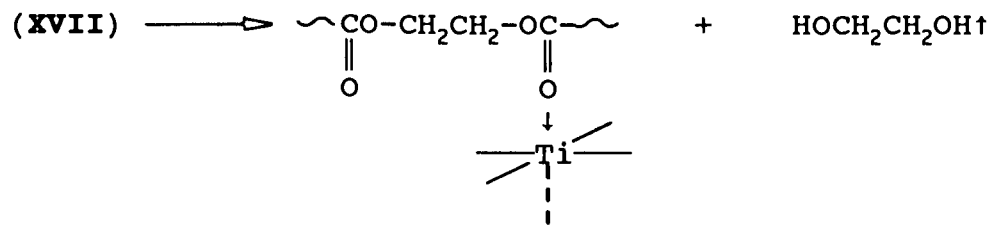

Scheme 17

Apparently, much more work is needed with regard to the kinetics of catalysed ester exchange to enable further discussion concerning the influence of organotitanium complexes on the curing-rate of Isomid.

3.2.4 Future work

The work presented in this thesis does not allow a conclusion to be drawn with respect to the catalytic form of titanium in Isomid wire-varnish. To gain further understanding, the relative thermodynamic stabilities of the aryl titanates and Ti(IV)/HEB adducts can be studied by BB^{13}C-NMR analyses of these when in the same solution. The study can then be extended to proprietary Isomid to determine the presence, or absence of complex-adducts between Ti(IV) and resin-SC. However, since BB^{13}C-NMR is expected to be insufficiently sensitive to produce useful spectra of Isomid with respect to Ti(IV) complexes, a large concentration of "Tyzor

TBT" in $CDCl_3$ can be used as a starting-point, and to which resin-SC and phenol are added in increments of $<\frac{1}{4}$[Ti(IV)], with spectra taken after each addition. It is expected that significant shifts in the OH-methylene peaks (at 3, 4, & 4') and the carboxyl carbonyl peaks (at 28-31, & 31') (cf. table 3.3; figure 3.5(d)), will indicate the ester exchange of TBT, and shifting of the HE-carbonyl peaks (at 24-27) indicate dative-bonding of the carbonyl groups of HE chain end-groups (viz., intramolecular H-bonding). Any observed peak-shifts must be consistent with the model Ti/HEB chelate discussed in appendix VI.

The stability of TDNPT (for a solution in $CDCl_3$) in the presence of HEB (modelling the HE end-groups of resin-SC) can be studied by NMR. Complete substitution of the DNP-ligands would suggest that TDNPT cannot exist in Isomid wire-varnish. However, were it found that TDNPT is not affected, further study of its catalytic activity with respect to the curing-reactions is desirable.

PGC/MS (at column temperatures of $\approx 150^0$C) can be used to identify and quantify the various components of the extraresin vapours, emanating from the model enamels. These vapours are given-off by Isomid wire-enamel above a threshold temperature (viz., 145 ± 2^0C; cf. appendix IX).

The effect of aryl-esters on the rate of industrial curing can be determined by adding phenyl-esters of dibasic acids, for example, DPT or diphenyl adipate, to Isomid prior to thermal curing. Shevchenko et al.[33] have presented evidence for increased polycondensation-rates of PET when small amounts of DPT were added.

An alternative method of introducing aryl-ester groups into Isomid wire-varnish is by the synthesis of a phenyl-esterified analogue of resin-SC. The resin can be treated with $SOCl_2$, in a $CHCl_3$ solution, generating the acid-chloride derivative. The product can then be added to a solution of phenol in $CHCl_3$, to generate the phenyl-ester derivative of resin-SC. The efficacy of the modified resin as a wire-varnish formulated with glycol ester, instead of cresylic acid, can best be tested under industrial-curing conditions. A favourable result would be seen as a marked reduction in the enamelling-speed.

Throughout, attention has focussed on the chemical aspects of the curing, however, the physical properties of a wire-varnish also play a role in its enamelling performance. Paramount is the ability of a solvent to effectively promote wetting of the bare wire-surface, and thereafter the enamel-film. Where wetting is poor, the resulting enamel-film has bare-spots and/or **surface-rippling**. Therefore, in the search for an ideal PEI wire-varnish, the wetting performance of the solvents and how this changes during the course of thermal curing must be considered.

Finally, the carbon NMR analysis of the resin can be improved using various, sophisticated pulse-programs such as INEPT and DEPT.[173] These spectrum editing experiments increase resolution by dividing the spectrum into CH, CH_2, and CH_3 spectra. As well, two-dimensional NMR experiments (e.g., COSY) can also yield useful improvements in sensitivity. Detailed analysis of the chemical structure would be time-consuming, expensive, and not expected to reveal information of use to the varnish manufacturer.

4.0 General conclusions

Spectrometric analyses of the poly(esterimide) (PEI), electromagnet-wire dielectric film-former, resin-SC, suggest the presence of imide functionalities, to the exclusion of the amides. The PEI oligomer therefore contains trimellitic anhydride (TMA) radicals in both the linear imide-units as well as crosslinking ester-units.

As all methylene dianiline (MDA) radicals were found to be in the form of imide-units, the slight excess of TMA with respect to MDA (i.e., 2.2:1.0 molar) indicates that imidisation is favoured above esterification or amidisation. The five-membered heterocylic ring of the imides are mesomerically stabilised by hyperconjugation through the aromatic rings of the MDA and TMA radicals.

Resin-SC was also found to contain carboxyl groups (≈6% of the hyroxyethyl (HE) end-groups), permitting some esterification to take place. The much greater concentration of HE ends than carboxyl end-groups (cf. table 3.5) necessitates that ester exchange is the major curing reaction; between HE ends, and as redistribution reactions between HE ends and polymeric ester functions.

During the thermal curing of Isomid wire-varnish (resin-SC in cresylic acid), the curing-reactions are not limited to those already mentioned. Cresylic acid acts as both a medium for the transportation of resin-SC onto the surface of the electromagnet-wire and as a reaction-medium, during the early stages of curing. Cresylic acid consists of phenols which are capable of both acid-catalysing polycondensation and esterifying the resin. The latter produces aryl-ester derivatives which are remarkable for their greater reactivity

towards ester exchange than the original end-groups; HE and carboxyl functions. Acting as reactive inter-mediates, these derivatives facilitate polymerisation, encouraging the formation of high-quality enamel-film surfaces which are free of blisters, bare-spots, craters, pin-holes, and surface-rippling (see §1.4.5.2).

During the later stages of thermal curing, whereupon much of the solvent has evaporated, some remains in the form of aryl esters. As the last traces of solvent are gradually released by thermal degradation of these esters, nucleation of the volatile vapours is prevented, thereby averting bubbles forming within the plastic enamel-film. Therefore, the reactions of phenols with the polymerising resin both assists polycondensation and provides a mechanism for slowing the release of these solvents after the film has formed. In industry, cresylic acid is considered to be a "good"[108] solvent for the production of electromagnet-wire.

Intramolecular hydrogen-bonding of HE ends was not observed in resin-SC by carbon NMR; the carbonyl signal associated with a bonded OH-proton, expected at ≈175ppm (see appendix II), was not amongst the carbonyl signals detected. The absence of these hydrogen-bonds for resin-SC, in a $CHCl_3$ solution, suggets that the HE ends tend to undergo secondary bonding with proton-accepting groups in the oligomeric resin. However, when dissolved by cresylic acid, the OH groups preferentially bond with the proton-donating phenols.

Isomid wire-varnish contains a substantial proportion of cresylic acid (≈40wt.%), and since the condensation reactions are equilibrium-controlled, the early stages of curing are marked by reactions involving phenols to produce aryl esters

derivatives.

Traces of aryl esters were found in Isomid wire-enamel scrapings by solid-state NMR. The wire-enamelling industry has acknowledged the presence of **residual solvents**, but not the manner in which such materials exist, in enamel-films. Upon heating the scrapings above 145±2^{0}C, free solvent is regenerated and volatilised. This threshold temperature is commonly exceeded in **trickling** and **encapsulating** processes, where coils of enamelled wire are bound by an overcoat of varnish, usually an unsaturated polyester, which is baked at temperatures above 200^{0}C. The residual solvents, thus released into the curing varnish, inhibits polymerisation; an undesirable consequence. The industry has, therefore, limited[108] the maximum permissable level of residual solvents such that a sample of enamelled wire must conform to a 0.3% mass-loss upon stoving at 200^{0}C for 30 minutes.

The phenols can promote polycondensation by acid-catalysis. Such catalysis promotes both esterification and ester exchange reactions, and the effect is dependent upon the acidity of the OH-protons. However, the catalytic effects of **p**-nitrophenol (NP; pK_a=3.41 at 25^{0}C) and 2,4-dinitrophenol (DNP; pK_a =3.96 at 15^{0}C), for instance, are found to be similar to that of phenol (pK_a=9.89, at 20^{0}C), according to the results of the model "industrial-curing" experiments with the esterification of BA with EG (cf. §3.2.3). Since the method did not follow the rate of change of reactant concentrations, the uncertainty of the results is sufficient to obscure a small dependence of proton-donating power between the phenols, although the rate of water-evolution from esterifications catalysed by the phenols followed the order expected, that is, NP > DNP >

phenol.

Another possible chemical interaction of the phenols is that with the proprietary alkyl titanate catalyst, "Tyzor TBT". The aryl titanates are readily formed at room temperature by ester exchange, but the catalytic activity of tetraphenyl titanate on the model esterification, was similar to that of phenol (acid-catalyst). The greater activity of the aryl titanate is a result of an enhanced resistance to inhibition by BA. Their effect on model ester exchange reactions may be greater, but has not been investigated.

Tetra(2,4-dinitrophenyl) titanate (TDNPT) has been found to greatly increase the rate of water-condensation in a model esterification (i.e., benzoic acid with ethylene glycol). However, wire-enamelling trials, conducted at Schenectady Chemicals Australia Pty.Ltd., showed no increase in the enamelling-speed of Isomid wire-varnish with TDNPT over the standard formulation (cf. §1.5), using a tetraalkyl titanate ("Tyzor TBT"; a transesterification catalyst). It is proposed that titanium is more likely to form thermodynamically more stable HE-chelated adducts in the wire-varnish, at room temperature. Such chelation has been observed by carbon NMR for the model HEB/Ti(IV) adduct (cf. appendix VI). However, more study of the Isomid varnish is needed to find evidence for the presence of these chelates.

Chelation has been postulated for the catalysis of the polycondensation reactions, similar to the coordination mechanisms proposed for the polymerisation of poly(butylene terephthalate).[69(b)]

The goal of this work was to provide a greater understanding of the function of cresylic acid in the curing of

Isomid wire-varnish, and specifically, to discover how this solvent facilitates the production of high quality (i.e., smooth) film-surfaces. The work hitherto conducted indicates that phenols serve this end in three ways:

(i) as acid-catalysts, promoting polycondensation;

(ii) as nucleophiles, leading to the formation aryl-ester intermediates which promote polycondensation by facilitating the attack upon the carboxyl carbon by HE ends;

(iii) as a consequence of the formation of aryl esters, these solvents are released slowly during the later stages of curing, thereby avoiding nucleation of the vapours within the polymer-film, preventing blistering.

The formation of a ternary azeotrope between the phenols of cresylic acid, EG, and water is not considered to be a major source of assistance for the removal of EG, except in the early stages of curing where most of the condensed water is evolved. Notwithstanding, the formation of other azeotropes between cresylic acid and EG may occur during this period, when the carboxyl groups are being comprehensively esterified to form the aryl-ester intermediates.

Bearing these facets in mind, the current industrial trend to replacing cresylic acids with "glycol ethers" is considered to result in poorer film quality; glycol ethers are proprietary preparations consisting of either diethers such as methylal ($CH_3OCH_2OCH_3$; b.pt. 42^0C) and ethylene glycol diethyl ether (b.pt. 121^0C), or glycol monoethers such as ethylene glycol monoethyl ether (b.pt. 124^0C) or terpinyl ethylene glycol ether (b.pt. $218-284^0C$). These solvents are chemically similar to EG, and therefore the hydroxylic functions are less reactive nucleophiles than those of cresylic acid;

these solvents are not likely to form reactive intermediates. Therefore, use of these solvents is expected to reduce the maximum achievable wire-enamelling speed, and increase the numbers of surface faults per unit length of enamelled wire.

Simulation of cresylic acid might be achieved by a composite solvent consisting of an acidic component together with an aromatic phenyl ester, such as DPT, in a glycol ether base. However, this approach must be tempered by consideration of the physical requirements for a successful curing-medium. For example, the surface energy (or tension)[216] of a varnish solution may be an important property, underlying successful wetting of the bare wire surface, during the first enamelling-pass, and the PEI film, during subsequent enamelling-passes. Where varnish poorly wets either of these surfaces, it is apparent that beading will occur, producing bare-spots, surface-rippling, and blistering. Hence, both the chemical and physical aspects of the enamelling process must be considered together.

Finally, this study clearly indicates a dynamic curing-medium in which cresylic acid reacts extensively with the oligomeric film-forming resin (viz., resin-SC), facilitating polymerisation, and reducing the likelihood of film-faults. Therefore, cresylic acid is a chemically integral part of Isomid wire-varnish, and the wire-enamel formulator must consider the findings presented herein in making successful alterations to the film-forming system.

APPENDIX I

I.1 TEST METHOD T5-M2-A: DETERMINATION OF ACID NUMBER

{Reproduced with the kind permission of SCA}

Application

This method, using alcoholic potassium hydroxide, is applicable to materials soluble in a 50:50 mixture of isopropyl alcohol and toluol; it defines the acid number required to neutralise the free acids in one gram of sample.

Apparatus

Erlenmeyer Flask, 250ml.

Burette, 50ml, such as Fisher Scientific Co. Catalog No. 3-699.

Graduated Cylinder, 50ml.

Weighing Bottle (for liquid samples), such as Fisher Scientific Co. viscosity tubes (with corks) Catalog No. 13-333.

Mortar and Pestle

Analytical Balance, accurate to at least 1mg.

Chemicals

Isopropyl Alcohol, 99% grade, conforming to ASTM D770-58.

Toluol, nitration grade, conforming to ASTM D841-50.

Phenolphthalein Solution, 1% volumetric indicator in ethanol, such as Fisher Scientific Catalog. No. So-P-62.

0.1N Potassium Hydroxide Solution, alcoholic (methyl), standardised against potassium hydrogen phthalate.

Procedure

(1) Neutralise 50ml of 50:50 alcohol:toluol mixture, by volume, by adding 3-4 drops of phenolphthalein indicator and titrating with 0.1N alcoholic potassium hydroxide to a pink colour that persists for 15 seconds. (Usually only a drop or two is required.)

(2) For liquid samples, use a weighing bottle and add,

directly to the flask containing the solvents, the appropriate weight of sample as tabulated below.

(3) For solid samples, pulverise with a mortar and pestle and weigh into a clean, dry 250ml flask the appropriate weight of sample. Transfer the solvent mixture to the flask containing the weighed sample.

Acid Number	Wt. of Sample
0-30	5.0±0.1g
30-100	2.5±0.1g
100-200	1.0±0.1g
200-500	0.5±0.1g
500-1000	0.25±0.1g

Swirl until the sample is dissolved and homogeneous. If necessary, heat the solution to dissolve the sample, but do not boil, and then cool to room temperature.

In the case of samples that give an indistinct endpoint add an additional 3-4 drops of phenolphthalein indicator to intensify the endpoint.

Titrate with 0.1N alcoholic potassium hydroxide, shaking the flask vigorously, to the appearance of a pink colour which persists for 15 seconds.

(4) Record the volume (in mls) of potassium hydroxide required and calculate as indicated below.

Calculation

Acid Number = (A x F)/(grams of sample)
where A = mls of potassium hydroxide required.
F = Factor: (normality of KOH used) x 56.1

I.2 TEST METHOD T13-M1-A: DETERMINATION OF HYDROXYL NUMBER (Reproduced with permission of SCA)

Theory

Phenolic hydroxyl groups and hydroxyl groups attached to primary and secondary carbon atoms can be esterified. Since direct use of an acid would liberate water and produce an equilibrium short of complete reaction, an acid anhydride is used, with pyridine as the anhydrous reaction medium.

The anhydride consumed can be determined by titration of the unreacted excess with standard KOH.

Since the hydroxyl number is defined as the milligrams of KOH equivalent to one gram of sample, the hydroxyl number of those materials that also exhibit an acid number is calculated by adding the acid number to the hydroxyl value derived from the following procedure. (A separate test method for determining acid number is available.)

Apparatus

Analytical Balance, accurate to 0.1mg.

Mortar and Pestle (for solid samples)

Soil Digestion Flasks, 250ml with 24/40 ground glass joints, with 650mm air condenser tubes attached, such as Fisher Scientific Co. Catalog No.10-102.

Glass Beads

Pipette, 5ml.

Graduate, 50ml and 5ml.

Note: A graduate is a graduated measuring-cylinder.

Hot Plate

Burette, 50ml.

Chemicals

Acetic Anhydride-Pyridine Reagent Prepare by adding 2 parts acetic anhydride to 7 parts 2^0 pyridine, in a clean, dry

graduated cylinder. Mix well and transfer to a clean, dry, dark brown stoppered bottle. The reagent must be prepared fresh daily.

Distilled Water

Phenolphthalein Indicator, 1.0% solution in 20 pyridine by weight. Note: Keep well stoppered.

0.5N Methanolic Potassium Hydroxide, standardised against potassium hydrogen phthalate.

Cresylic Acid (for washing flasks).

Preparation

Note: Moisture causes incomplete acetylation, giving false results. Hence all equipment and reagents must be anhydrous until the acetylation step is completed.

(1) Check all equipment and reagents. They must be free of water and clean.

(2) If sample is solid, crush it with a mortar and pestle.

Procedure

Notes: (A) A blank, omitting only the sample, is run at the same time as the sample. Boiling point of the acetylating reagent is approximately 120^{0}C. (B) Run duplicate samples simultaneously. (C) Work under hood when using pyridine and acetic anhydride. If they come into contact with the skin wash immediately with soap and water.

(1) On an analytical balance, weigh into a flask the proper size sample as indicated in this table:

Approx. Hydroxyl Number	Grams of Sample
40-80	4.0±0.1
80-200	2.0±0.1
200-500	1.0±0.1

Notes: (A) Liqiud samples are weighed by difference from a stoppered weighing bottle. (B) Sample must not be allowed to

touch the neck of the flask.

(2) Add 2 glass beads to the flask and, with a pipette, exactly 5ml of fresh anhydride-pyridine reagent. Grease the ground glass joint of the condenser and attach it to the flask.

(3) Heat the flask and contents an a hot plate, slowly, until sample has dissolved. Then heat to a slow boil and maintain at a slow reflux for 10 minutes.

(4) Measure 50ml of 2^0 pyridine into a graduate and carefully add to the sample through the condenser.

(5) Measure 5ml of distilled water into a graduate and add to the sample through the condenser. Bring the solution to a slow boil for 2 minutes.

(6) Cool flask, momentarily in air then under the tap, before removing condenser.

(7) Remove condenser, add 3-4 drops of indicator (see Reagents) and titrate with 0.5N methanolic potassium hydroxide to a pink endpoint that persists for 15 seconds. Note: Titrate carefully, since 0.1ml may affect hydroxyl number by several units.

(8) Record the ml of potassium hydroxide.

Immediately clean flasks with hot cresylic acid (wear rubber gloves), wash with water and then dry condensers with acetone.

Calculations

Hydroxyl number = ((A-B) x N x 55.228)/grams of sample,

where A = ml of KOH for blank, B = ml of KOH for sample, N = normality of the KOH solution. For samples with an acid number: add the acid number to the hydroxyl value obtained above to obtain the corrected hydroxyl number.

APPENDIX II

HYDROGEN-BONDING IN 2-HYDROXYETHYL BENZOATE

During the late 1950's, Challa[16] found that the **redistribution** reaction (i.e., ester exchange of polymeric esters with HE ends) for the polymerisation of PET,

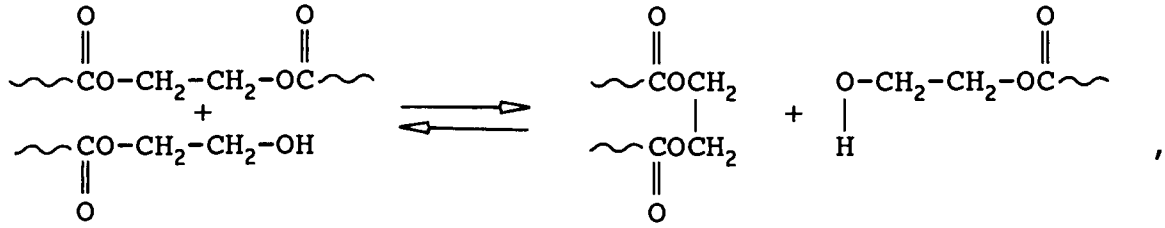

has an activation energy some 33.5kJ/mole greater than the similar chain-scission by EG (i.e., glycolysis). The discrepency was attributed to the energy required to breaking an intramolecular hydrogen-bond (H-bond),

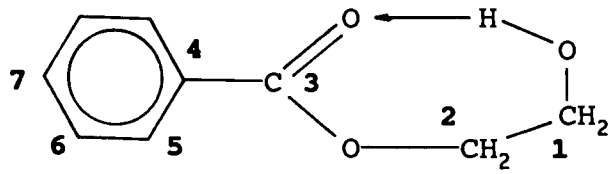

(A.I)

The concept of intramolecular H-bonding led to the tentative proposition that the energy of such a bonding is 29.3 kJ/mole. Interactions of this order are found between carboxylic acids and the stronger Lewis bases, for example, propionic acid with naphthylamine (31.8±3.3kJ/mole) in toluene/water solution,[33] and benzoic acid (BA) with benzyl alcohol (49.4kJ/mole) in benzene.[33] Esterification reactions, by comparison, involve activation energies of the order of 25 kJ/mole.[33]

Shevchenko et al.[32] used this concept to explain differences in the rate constants for esterification reactions of 2-hydroxyethyl benzoate (HEB), when compared with EG. For instance, the difference in the activation energies, derived

from their kinetics results, for the esterification of BA with EG (i.e., 77.0kJ/mole) and BA with HEB (i.e., 40.6kJ/mole) is 36.4kJ/mole. The 2-hydroxyethyl (HE) group was found to be more reactive than EG in the ester exchange of alkyl and aryl benzoates; an enhancement in the nucleophilicity of the hydroxylic oxygen atom by intramolecular complexation (cf. structure **A.I**) was postulated to explain the greater reactivity of HEB.

The strengths of H-bonds are difficult to measure accurately; the nature of a weak secondary bond, in a state of continual flux, renders hydrogen bonds tenuous. However, the energy of such interactions can be estimated by a number of empirical methods, which have been reviewed comprehensively elsewhere.[143,186,187] The HEB H-bond was therefore characterised by IR, NMR and UV spectrometries.

Infra-red spectrophotometry

The IR spectrum of a film of neat, solid HEB on a NaCl window (cast from $CHCl_3$ solution) is summarised in table A.1; from this and IR spectra in $CHCl_3$, the following conclusions have been drawn.

(i) The O-H stretching band is seen at a lower energy than for EG or THEIC (cf. §2.2.1.1 and §2.2.1.2) which exhibit physical properties implying their molecules engage in intermolecular H-bond.[143]

(ii) The two ester C-O stretching bands also show bathochromic shifts to 945 and 1290cm^{-1} from the expected frequency range: 1050-1300cm^{-1}.[188]

(iii) The hydroxyl C-O stretching band shows a bathochromic shift, from 1045/1095cm^{-1}, for EG, to 800/816cm^{-1}.

(iv) The O-H bending bands exhibit hypsochromic shifts

from 860/890 cm^{-1}, for EG, to 1185/1195cm^{-1}.

(v) The C=O stretching frequency is at a lower energy (by ≈20cm^{-1}) than that expected for esters,[188,189] at around 1720cm^{-1}, and the band maximum is found to not change with HEB concentration (which occurs with intermolecular H-bonded systems) in $CHCl_3$. However, the intensity is dramatically affected, increasing with dilution.

(vi) There is no discernible difference between the IR spectra for a CCl_4 solution and for neat HEB.

The presence of H-bonding is indicated by three factors: the unusually low carbonyl band resonance; the broadness of the hydroxyl stretching band is indicative of a fluctuating electrostatic interaction; and the bathochromic shifts of the ester and hydroxyl stretching bands, with the contrasting hypsochromic shifts in the bending resonances, are typical of H-bonded systems.[190]

The lack of a dependence of the absorption band maxima on HEB concentration, and the relatively low melting point (i.e., 44^{0}C) imply that HEB exists as discrete molecules through intramolecular H-bonding. THEIC, by contrast, exhibits the characteristics of intermolecular H-bonding, having a greater melting point (i.e., 139^{0}C; cf. §2.2.1.2).

Estimation of the enthalpy for H-bond formation (ΔH) can be inferred from band-frequency shifts ($\Delta\nu$), using the OH stretching band of benzyl alcohol, at very low dilution (i.e., at 0.0486mol/dm^3) in CCl_4 (i.e., 3130cm^{-1}) as a model to approximate the OH stretching frequency of HEB in the absence of H-bonding. Thus, the magnitude of the bathochromic spectral shift upon intramolecular H-bonding was estimated as 130cm^{-1}. With the empirical relationship for ΔH given

graphically by Pimentel and McClellan,[191] ΔH was estimated from $\Delta\nu$ to be about 25kJ/mole, a value similar to that proposed by Challa.[16]

Table A.1 The IR absorption band assignments for HEB. The sample was cast into a clear film on a NaCl plate from a solution of HEB in $CHCl_3$.

Absorption bands (wavenumbers)		Structural Assignments
2000-3300	S,VB	O-H, stretching
2690	W,sh	C-H (aliphatic), stretching
2570	W,sh	
1700	VS,sh	C=O (halfwidth = 22cm^{-1}), stretching
1610	W,sh	aromatic ring stretching
1590	W,sh	
1460	S,sh	
1440	S,sh	methylenes, bending
1340	S,sh	
1290	S,sh	ester, stretching
1185/1195	W,sh	O-H, bending
1120	W,sh	
1060	W,sh	aromatic ring
1010	W,sh	
1000	VW,sh	C-C (aliphatic), stretching
945	S,B	C-O (ester; halfwidth = 40cm^{-1}), stretching
800/816	W,sh	C-O (hydroxyl), stretching
710	S,sh	C-C (monosubstituted aromatic ring), stretching
702	W,sh	
690	W,sh	C-H, rocking

Proton NMR spectrometry

The proton NMR signals for H-bonded protons are expected to be shifted downfield. Formation of a H-bonding alters[192] the magnetic field around the OH proton because of an inductive change in electron distribution, and where magnetically anisotropic groups act as the base (in the Lewis sense), the magnetic field is influenced by by dipolar interactions as well.

The chemical shift of intermolecularly bonded protons depends on concentration at constant temperature; the signal

shifting dramatically upfield with dilution. For example, upon dilution in CCl_4 which provides a nonpolar solvent-medium, the resonance of the intermolecularly H-bonded OH proton of ethanol exhibits a 5ppm upfield shift,[193] from 5.1 ppm for neat ethanol to 0.9ppm at 0.01mol/dm^3. The resonances of intramolecularly H-bonded protons are much less affected by changes in concentration; o-chlorophenol[192] shows a shift of only 0.9±0.2ppm when extrapolated to infinite dilution, and in salicylaldehyde,[194] the OH proton is shifted by 0.3±0.2ppm upon dilution to 5vol.% in CCl_4.

Table A.2 Proton NMR (solvent is specified, 80MHz, 25^{0}C) assignments for HEB in two solvents of differing H-bonding character: $CDCl_3$ interacts poorly, and acetone is a strong proton-acceptor, by virtue of its carbonyl group.

	Protons (cf. structure **A.I**)						
		methylenes		aromatics			
Parameters	OH	1	2	5	5'	6	7
Chem. Shift in $CDCl_3$ (10mg/ml)	4.672	3.802	4.504	8.146	8.125	7.546&7.565	
multiplicity	1	4	3	2	2	3	3
$^3J_{H,H}$ (Hz)	——	5.2	4.9	8.1	7.5	7.6	7.5
Chem. Shift in $CDCl_3$; (197.9mg/ml)	4.669	——	——	——	——	——	——
multiplicity	1	——	——	——	——	——	——
Chem. Shift in acetone (d6);10mg/ml	4.413	3.677	4.163	——	——	——	——
multiplicity	1	4	3	——	——	——	——

Notes. The integration ratio of peaks 5&5' to 6&7 was calculated from instrumental integrals to be 0.751; the expected ratio is 0.67.

The integral-ratio for peaks 1:2:OH was similarly found to be 2.0:1.8:1.0, where the OH peak is defined as 1.0.

The OH-proton signal showed no tendency to shift with HEB concentration in $CDCl_3$ (viz., 4.627 to 4.669ppm), intimating that intramolecular H-bonding exists in HEB. The signal shifted downfield by H-bonding, as seen from the chemical shift in acetone(d6) (viz., 4.413ppm) which is a strong proton-acceptor, and has the capacity to disrupt the intramolecular H-bond.

The chemical shift of the OH-proton depends on the strength of the intramolecular H-bond, and is thereby dependent on solution-temperature and the proton-accepting character of the solvent.

The behaviour of HEB in $CDCl_3$ at 25^0C was found to be consistent with the presence of intramolecular H-bonding, that is, the chemical shift of the OH proton shifted only slightly, 4.669±0.002ppm at 197.9mg/ml and 4.675±0.002ppm at 32.5mg/ml, amounting to an upfield shift of 0.006ppm, an amount which is of the order of the experimental error.

The chemical shift of intermolecularly H-bonded protons in dilute solution are expected to be dependent[195] on the polarity of the solvent, due to the electrostatic nature of such interactions. However, in the case of intramolecularly H-bonding, the bonding field is expected to be disrupted only by those solvent molecules which possess either a dipole moment greater than the basic half of the H-bond (i.e., proton acceptors), or a highly polarised molecular unit such as an acidic proton (proton donors). Of course, those solvents which contain both attributes also effectively disrupt these H-bonds. The relationship between these characteristics and the carbon NMR signal of the carbonyl carbon atom of HEB, reflecting the presence of the intramolecular H-bond, is discussed in the next subsection.

The NMR chemical shifts of the H-bonded protons for thirty phenol systems in methylene chloride were used by Eyman and Drago[196] to calculate H-bond enthalpies to within 2.1kJ/mole (viz., ±0.38ppm) of ΔH values derived from hypsochromic shifts in the IR bands of the hydroxyl bonds (as described previously). The results gave the relationship

$$\delta_{obsd} = 3.13(\Delta H) - 19.59 \qquad (A.1)$$

which shows a linear trend for ΔH with the observed chemical shift of the OH protons.

Application of equation (A.1) to HEB requires a correc-

tion for the carbonyl group. The carbonyl bond, being magnetically anisotropic, introduces a through-space shielding (σ_D) contribution to the OH proton, in addition to local shielding due to the electrons of the OH σ-bond. The total shielding constant (σ_T) is thus to the sum of the local shielding constant (σ_L) and the shielding due to the molecular charge distribution (σ_D). The contribution of σ_D depends on the magnitude of the magnetic anisotropy (χ) and molecular geometry, including changes in this due to molecular motions. In solution, continual changes in molecular conformation averages out the secondary fields created by induced dipoles. The carbonyl group of HEB is H-bonded to the OH proton, and is therefore a case where a finite shielding is possible; molecular motion cannot average σ_D to zero.

A classically derived expression for σ_D,[197] in which the secondary field is assumed to arise from induced dipoles, is

$$\sigma_D = [1/(3.N_A.R^3)].(2.\chi_1 - \chi_2 - \chi_1.3\cos^2\theta) \qquad (A.2)$$

where N_A is Avogardo's number, and R a radius vector from the weighted centre of the dipole of the carbonyl bond, assumed to be on the oxygen atom, to the bonded proton, lying in either the z-y or z-x planes of a three-dimensional cartesian coordinate system, given that the C=O bond lies in the z-direction. The spatial components of the magnetic anisotropy are defined to be: $\chi_1 = \chi_{zz} - \chi_{yy} = -2.5\text{x}10^{-6}$ and $\chi_2 = \chi_{zz} - \chi_{xx} = 6.6\text{x}10^{-6}$. In equation (A.2), θ is the angle between the z-axis and vector R (see figure A.1 in which the HEB molecule is arranged to conform with the requirements of equation (A.2)) Equation (A.2) is only applicable when the C=O bond is magnetically axially symmetrical (i.e., $\chi_{zz} = \chi_{yy}$

$= \chi_{xx}$), provided the z-axis can be chosen such that R lies within the z-y plane; the plane of the trigonal carboxylate group, or perpendicular to this plane, thereby R lies in the z-x plane.

In the absence of a detailed structural configuration for HEB, defining the position of the H-bonded proton, an assumption is needed. The nonbonding orbitals of the carbonyl-oxygen atom are assumed to lie within the x-z plane, thus placing the H-bonded proton within that plane as well (cf. figure A.1). The H-bond length (R) was estimated from the averaged O(H)-O bond distances[143] for other intramolecularly H-bonded molecules (i.e., R(O-H—O)=2.55Å and R=1.7Å). A **stick-model** for HEB was constructed from these parameters, using bond lengths and angles[198] taken to be the same as those of BA and EG, as measured by X-ray crystallography, and the conformation of the HE group was chosen to approximate, as closely as possible, the gauche arrangement, which Miyake[199] has found to be the most stable in bis-(2-hydroxyethyl) terephthalate crystals and melts. Thus, from the spatial model the angle between C-C-O planes was measured to be 115^0, and gave a Θ of 45^0.

Substituting for Θ in equation (A.2) gives a correction factor (σ_D) of -0.88ppm; the corrected chemical shift for the OH proton (i.e., (4.669 - 0.88)ppm) becomes 3.78ppm, and introducing this value into equation (A.1) for δ_{obsd} yields a ΔH of 40.6kJ/mole. The value is higher than expected, but of the right order; the conformational assumptions provide room for doubt. A decrease in Θ of 5^0 will reduce ΔH by 6.3kJ/mole; an error of 15%, bringing the value of ΔH much closer to that expected (≈30kJ/mole).

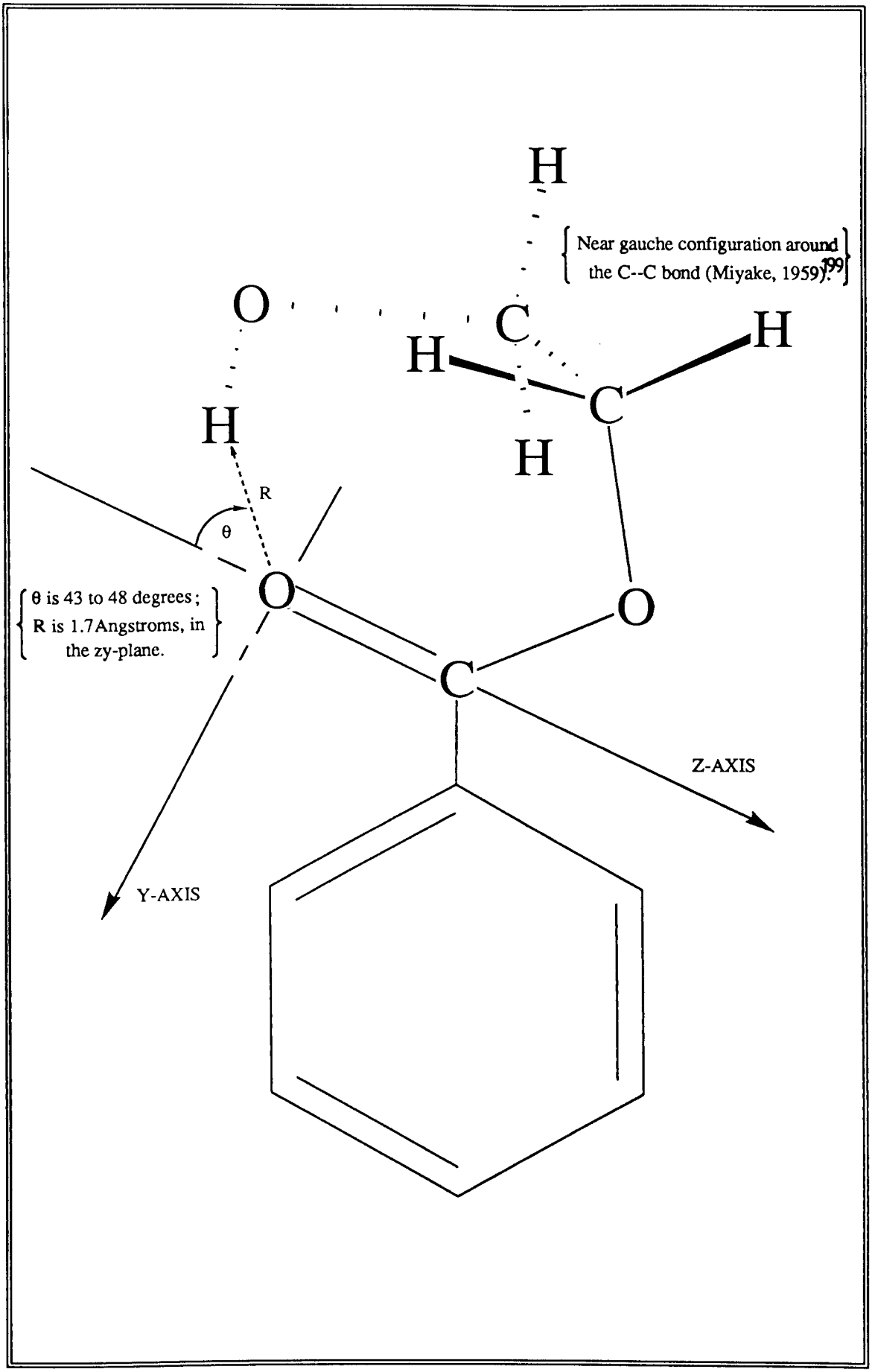

Figure A.1 A diagrammatical representation of the supposed configuration of HEB with intramolecular H-bonding. The cartesian coordinates are shown with the x-y plane through the paper; the origin is at the oxygen atom of the carbonyl group, the assumed site of bonding.

Application of X-ray crystallography to crystals of HEB is needed to more accurately define the bond lengths and angles, given that the difficulty of determining the average location of the H-bonded proton.[187] However, this reservation can be resolved by a relatively simple method for locating the average position of the proton, described by Jackman and Trewella[200] for 1-hydroxyfluorenone. The spin-lattice relaxation times of fully substituted carbon nuclei are related to the relevant proton through the dipole-dipole relaxation term (T_1^{DD}), which is proportional to the sixth power of the internuclear separation ($r_{C,H}$). Generally, three such distances are needed to triangulate the proton's location. The contribution of the H-bonded proton to the relaxation rates of the three carbon nuclei is determined by the differences in the T_1's from the normal molecule and its deuterated analogue (i.e., where the proton of interest is replaced by a deuteron).

Due to financial and time constraints, no attempt was made to apply this method to HEB, however, it remains a promising, elegant approach which is worthy of pursuit.

Carbon NMR spectrometry

The carbon NMR characteristics of HEB in six solvents, ranging in polarity and capacity for H-bonding, were studied. The chemical shifts showed no dependence on concentration, suggesting the absence of intermolecular H-bonding, and in $CHCl_3$, the methylene signals were not detected irrespective of concentration, and remains an unexplained phenomenon. However, the carbonyl signal showed a marked shift in position with changing solvent polarity, and was found be a useful probe for evaluating the interactions of HEB with the

sundry solvents.

Generally, the formation of H-bonds causes a downfield shift of the proton signal indicating a diminution in electron density about the subject proton. As the H-bonding proton interacts with the free electron-pairs of the base-part (viz., carbonyl group), any perturbation of the surrounding electron distribution will also affect the electronic environment of the carbonyl carbon nucleus. Where the electric-dipolar field of the H-bond is considered to be purely an electrostatic attraction, the density of the surrounding electron cloud will depend upon the electronegativity of the species involved (i.e., those acting as proton-acceptor and proton-donor). For example, for a variety of proton-accepting solvents, deshielding of the $CHCl_3$ proton has been shown to increase with the dipole moment of the nonbonding orbital on the proton-acceptor.[195] Strong intramolecular H-bonding increases shielding (i.e., a downfield frequency-shift) at the carbonyl carbon nucleus, and the influence predominates until more favourable alternative electrostatic interactions can disrupt that bonding.

Formation of intermolecular H-bonds between HEB and solvent molecules depends on the ability of the solvent molecule to perturb the intramolecular H-bond; the electrostatic nature of the solvent molecule determines its effectiveness in perturbing that bond. The dipole moment of a molecule is a vectorial representation of the overall distribution of electron density in the molecule, but does not describe completely its ability to either accept (acting as a Lewis base such as the π-bonds of DMSO and acetone) or donate (acting as a Lewis acid such as the hydroxyl protons

of m-cresol and EG) H-bonding protons.

Table A.3 The carbon NMR chemical shift assignments for HEB in a variety of solvent media. The assignments for ethyl benzoate (EB) in $CHCl_3$ are included for comparison. The samples were prepared with excess solvent and the spectra were obtained at 25^0C.

Solvent medium	Molecular dipole moment (debye)	Carbon Atom (cf. structure A.I, p.217)						
		1	2	3	4	5	6	7
Low polarity								
CCl_4	0.00	59.55	66.76	171.99	129.99	130.79	128.10	133.26
$CHCl_3$	1.01	n.d.	n.d.	172.47	130.20	130.26	128.56	133.91
Strong H-bond-donors								
m-cresol	1.45	59.27	66.49	170.77	hid.	130.20	128.50	133.78
EG	2.28	hid.	hid.	169.46	hid.	129.87	128.77	133.63
Strong H-bond-acceptors								
acetone	2.88	59.66	66.83	167.28	129.41	129.44	128.29	132.81
DMSO(d6)	3.96	59.40	66.70	168.10	130.90	129.60	128.40	132.80
EB in $CHCl_3$	1.01	14.4(1)	60.8	166.3	130.9	129.7	128.4	132.8

Notes. Chemical shift data for ethyl benzoate were taken from reference 178.

(1) The carbon designated as "1" for ethyl benzoate (EB) is the methyl carbon analogous to the HEB methylene of the same designation.

Abbreviations: "n.d.", the signal was not detected; "hid.", the signal was hidden by other, more intense signals.

The solvent media are categorised with respect to the most important feature of their interaction with the intramolecular H-bond of HEB. Solvents $CHCl_3$ and CCl_4 do not disrupt the H-bond since they are poor proton-donors and -acceptors; m-cresol and EG are good proton-donors, as well as proton-acceptors; and lastly, acetone and DMSO are highly polar, aprotic substances which are able to disrupt effectively the intramolecular H-bond and accept the proton through the carbonyl and sulphonyl groups, respectively, but cannot strongly donate protons to the carbonyl group of HEB.

The role of the molecular dipole moment of the solvent medium is underscored by the polarisation of individual bonding orbitals. For example, the data given in table A.3 suggests that DMSO and acetone effectively disrupt the intramolecular H-bond of HEB, but do not replace the strong secondary interaction with the carbonyl group (viz., the upfield shift to about 168ppm for the carbonyl carbon nucleus from $CHCl_3$ and CCl_4). Figure A.2 shows graphically the trend in carbonyl carbon chemical shift for the range of

solvent-media studied.

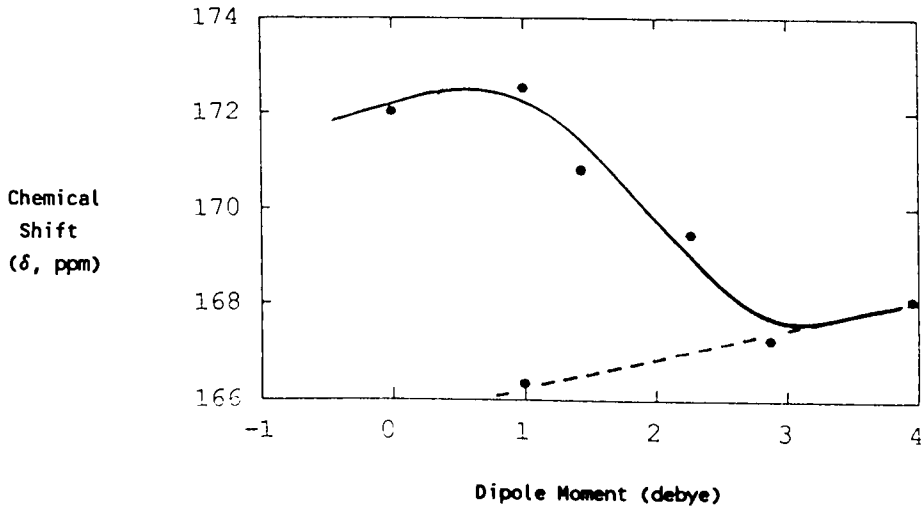

Figure A.2 A plot of the carbonyl carbon chemical shift for HEB against the molecular dipole moment of the solvent medium. The carbonyl carbon shift of EB is included for comparison. The solvents vary in H-bonding ability, qualitatively, according to the functional groups present: CCl_4 and $CHCl_3$ are poor (p); acetone and DMSO are medium (m); and, **m**-cresol and EG are strong (s) hydrogen bond donors.

Hence, the positive poles of the solvent molecules are not effective H-donors. In contrast, the $CHCl_3$ proton, which partakes of H-bonding, is insufficiently polarised to perturb the strong intramolecular H-bond; the carbonyl resonance is similar to that observed in the nonpolar solvent, CCl_4. **M**-cresol, on the other hand, contains a very acidic OH-proton, enabling it to donate a H-bond to the carbonyl group of HEB, disrupting the intramolecular H-bond. EG also disturbs this bond. The basic (or H-accepting) complement for the **m**-cresol and EG donor-protons are the OH-oxygens, which are able to accept H-bonds from HEB, complementing the new H-bonds with intermolecular H-bonding to the OH-protons of HEB. Since the dissociation constant (K_a) of such acidic solvents is dependent on the polarisation of the OH bond;

this property is a measure of the donor-strength of acidic solvents such as cresol.

Interpreting table A.3 and figure A.2 for the carbonyl portion of the intramolecular H-bond of HEB: in $CHCl_3$ and CCl_4, being solvents of low polarity and poor H-donating ability, the H-bond is not disturbed, and the electron density at the carbonyl carbon nucleus is thereby high (i.e., the chemical shift is significantly downfield of the analogous signal for EB in which intramolecular H-bonding cannot occur). In contrast, DMSO and acetone, being highly-polar solvents and poor H-donors, disrupt the bond by accepting a preferred intermolecular H-bond through their sulphoxyl and carbonyl groups, but do not interact strongly with the carbonyl group, leaving the electron density at that carbon nucleus relatively undisturbed, that is, similar to EB. **M**-cresol and EG hold the middle ground; being relatively good H-donors, these media disrupt the intramolecular H-bond to form alternative H-bonds with the carbonyl group of HEB through their hydroxyl protons. Therefore, the chemical shift of the carbonyl carbon is seen to fall between the "non-polar" solvents and the "aprotic-polar" solvents.

The potential energy of the interaction between the H-bond and the solvent-medium can be estimated if we assume that a critical dipole moment for the medium occurs at about 1.0D (cf. figure A.2). That is to say, in a medium containing dipoles of this critical magnitude the intramolecular H-bond of HEB is effectively broken. Therefore, assuming the H-bond polarity also has this magnitude, and that the two interacting species have equivalent permanent electric dipoles (μ_c); the force one exerts on the other (this force is

sufficient to break the intramolecular H-bond) will depend on μ_c, the separation r, and the relative orientation of the dipoles. Since the orientation dependence of the potential energy (**V**) is to be ignored, the **V** must be averaged over all possible orientations. Thus, if the two species are oriented randomly with respect to each other, their average interaction energy would be zero due to repulsion occurring at the same frequency as attraction. However, the Boltzmann factor $e^{-V/kT}$ favours the attractive orientations which have lower energies. The orientation-averaged potential energy of two dipoles species calculated with allowance for the Boltzmann distribution is

$$\mathbf{V}_{d\text{-}d} = -(2/3kT)(\mu_c^4/r^6) \qquad (A.3)$$

where μ_c is the critical dipole moment in cgs gaussian units (statC.cm), and **V** is in ergs. Equation (A.3) yields the **dipole-dipole** contribution to the overall potential energy of interaction.

The values for the variables in equation (A.3) must be estimated for this problem. First, μ_c is assumed to be 1.0D (i.e., 9.999×10^{-19}statC.cm) determined from the inflection in figure A.2; the separation of the dipoles must be of the same order as the intramolecular H-bondlength in order for disruption to take place, therefore, r is taken to be 1.7Å (i.e., 1.7×10^{-8}cm); lastly, the temperature of the interaction was 298K. Hence, substitution into equation (A.3), followed by conversion to SI units gives a value for $\mathbf{V}_{d\text{-}d}$ of 6.71×10^{-20}J or 40.4kJ/mole. This value is an estimate of the energy required to disrupt the intramolecular H-bond of HEB, and therefore reflects the strength of that bond. The value is similar to that estimated by proton NMR (**vide supra**; last

subsection, "Proton NMR spectrometry").

The carbonyl signal of EB in chloroform has been included in figure A.2 for comparison; the EB molecule differs from HEB only by the absence of the terminal hydroxyl group, and the intramolecular H-bond is eliminated. The carbonyl carbon signal is 6.4ppm downfield of the analogous resonance of HEB (in $CHCl_3$). Therefore, the intramolecular H-bond is a strong interaction, causing a significant increase in the electron density about the carbonyl group.

More data is necessary to establish the definite relationships hinted at in figure A.2. The dependence of the carbonyl signal of HEB on the medium could be studied for two series of solvents: first, H-bond donors which provide a range of pK_a's, whilst the other series are poor H-bond acceptors or donors, providing a range of polarities. The latter could be hydrocarbons, and their halo-, nitro-, and cyano-derivatives.

UV/visible spectrophotometry

The electronic transitions of HEB in CCl_4 and in acetone were studied using differential UV spectroscopy. The effect of the intramolecular H-bond was seen by comparing the UV spectra in a nonperturbing solvent (i.e., CCl_4) and in one which provides preferred H-bonds (i.e., acetone), according to the findings presented in figure A.2.

Polar solvents often stabilise the ground state of the $n \rightarrow \pi^*$ transition more than the excited state, giving a bathochromic ("blue") shift in this absorption band. On the other hand, in $\pi \rightarrow \pi^*$ transitions the excited state is more stabilised than the ground state, and give a corresponding hypsochromic ("red") shift. Since $n \rightarrow \pi^*$ transitions have a higher

dipole charge than the $\pi \rightarrow \pi^*$ transition, they are more solvent-dependent and shift to lower frequencies (a "red" shift) in more polarisable solvents; acetone is more so than CCl_4. In addition, the absorption band maxima were found to be independent of solute concentration.

The direction in which they shifted upon disruption of the intramolecular H-bond.[201] The forbidden $n \rightarrow \pi^*$ transition is of lower energy than the $\pi \rightarrow \pi^*$ transition which in turn is of lower energy than a $n \rightarrow \sigma^*$ transition. The last is usually found at wavelengths shorter than 200nm.

The enthalpy of H-bond formation was estimated from the empirical relationship for $n \rightarrow \pi^*$ transitions given by Pimentel.[143] According to this, a shift in the band maximum from 350 to 2500cm^{-1} corresponds monotonically with ΔH values of 1.0 to 29kJ/mole. The value of ΔH for HEB is therefore estimated to be 33.5kJ/mole (cf. table A.4). No relationship is given for the $\pi \rightarrow \pi^*$ transition.

Table A.4 The UV absorption bands for HEB in CCl_4 and acetone. The ΔH for the intramolecular H-bond was estimated from the shift in the band maximum of the $n \rightarrow \pi^*$ transition.

Electronic transition	Assignment	Absorption band max.(2) in CCl_4 (cm^{-1})	Frequency shift(3)	ΔH(1) kJ/mole
$n \longrightarrow \pi^*$	Non-bonding electrons of the carbonyl oxygen	38,900	+2,900	33.5
$\pi \longrightarrow \pi^*$	Electron redistribution; enhanced electron density in antibonding orbitals	35,500	-1,900	——

Notes. (1) The enthaplies of bond formation for the intramolecular H-bond of HEB were estimated using an empirical relationship for the $n \rightarrow \pi^*$ transition, given by Pimental and McClellan[143]; 1.0 to 29kJ/mole corresponds to a band-frequency shift of 350 to 2500cm^{-1}, respectively.
(2) The band maxima for the unperturbed H-bond of HEB was estimated from its UV spectrum in CCl_4.
(3) The shifts in the frequency maxima caused by disruption of the intramolecular H-bond were determined in acetone; known to H-bond in preference to CCl_4, according to figure A.2).

Summary

The HEB molecule forms an intramolecular H-bond through the hydroxylic proton, thereby dissolving easily in a wide spectrum of solvents and having a relatively low melting point. The H-bond is perturbed and broken by either highly polar solvents, forming preferred intermolecular H-bonds, or by acidic solvents, which form new H-bond to the carbonyl oxygen, as well as to the OH proton of HEB.

Enthalpies for intramolecular H-bond formation have been estimated by four methods, giving the following estimations,

Spectrometric Method of Analysis	ΔH kJ/mole
IR	25.1
proton NMR	40.6
carbon NMR	40.4
UV/Visible	33.5

and the average value of ΔH is 34.9±6.3kJ/mole. The average enthalpy of formation is similar to the value postulated by Challa[16] (viz., 29.3kJ/mole), and that derived from the kinetic results of Shevchenko et.al[32] (viz., 36.4 kJ/mole).

APPENDIX III

MEASUREMENT OF THE SPIN-LATTICE RELAXATION TIME (T_1) FOR THE RESIN, RESIN-SC

The method for measurement of the spin-lattice relaxation time (T_1) is described in chapter 2.0. The null method was used to estimate T_1 for the PEI resin (coded resin-SC). For a static field (B_0), the length of the time delay τ_T for the pulse sequence, 180^0-τ-90^0 for which the initial signal intensity (A) becomes zero, is related to T_1 according to $\tau_T = T_1.\ln 2 = 0.69.T_1$ (equation (A.4)).

In the frequency domain, this condition is equivalent to the merging of sample-signal into the baseline. Figure A.3 shows the carbon NMR spectra of the resin, in DMSO(d6), for τ_T between 0.05 and 35 seconds. The spectrum for τ_T = 0.1 seconds shows very little signal, and was therfore used as a rough estimate for the null-spectrum. Substituting the τ_T into equation (A.4) yields a T_1 of 0.14 seconds. This technique gives a very approximate estimation for T_1.

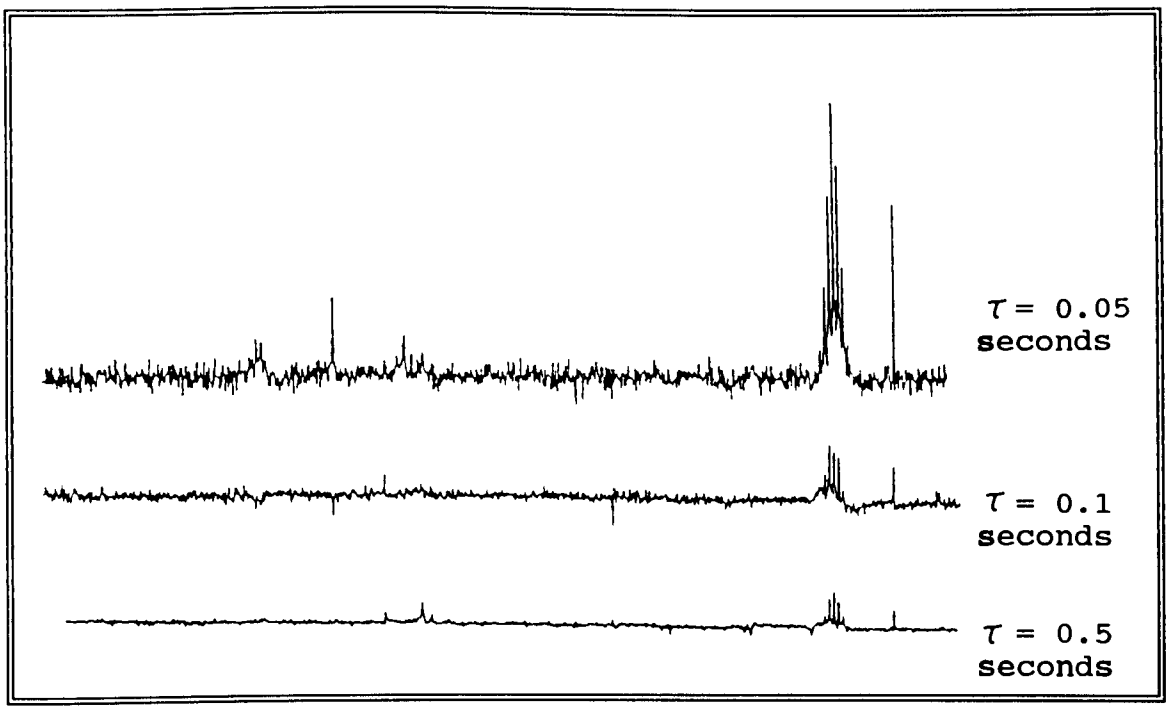

Figure A.3 The inversion-recovery carbon NMR (DMSO(d6), 20.1MHz) spectra for the resin; displayed against the pulse-spacing τ, in seconds.

APPENDIX IV

DIPOLE MOMENTS OF PHENOL, p-NITROPHENOL, AND 2,4-DINITROPHENOL

The dipole moments of polar molecules are directly related to their dielectric constants. When such a molecule is placed into an electric field, the permanent dipole axis tends to align with that field, minimising the potential energy of the interaction, assuming that the molecule is a rigid entity and disregarding any moments induced by the field with intensity **F**.

At the electric field strengths and temperatures commonly used for dielectric measurements, alignment is opposed by thermal agitation, conducing a statistical equilibrium with a slight excess of molecules in an antiparallel orientation. In the case where the molecule is oriented in the direction of **F**, the potential energy **u** is the product of the molecular dipole moment (μ) and the field strength, i.e., $\mathbf{u} = -\mu.\mathbf{F}$. However, dipole orientations are distributed around the field vector.

For an angle θ, from the field vector, the potential energy decreases as the cosine of that angle,

$$\mathbf{u} = -\mu.\mathbf{F}.\cos\theta \qquad (A.5)$$

and the Maxwell-Boltzmann distribution for these dipoles is

$$N_{dipole} = A.\exp(-\mu/kT).d\Omega \quad , \qquad (A.6)$$

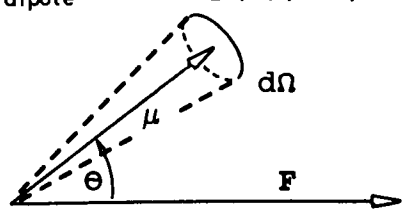

where N_{dipole} is the number of dipoles in the direction of μ, and within an angle of $d\Omega$ from θ; A is a proportionality constant depending on the number of dipoles under consider-

ation; k is the molecular gas constant 1.38×10^{-16}erg.K^{-1}; and T is the absolute temperature.

The moment of each dipole, in the direction of **F**, is $\mu.\cos\theta$, the total moment within the sweep angle ($d\Omega$) is given by $A.\exp(\mu.\mathbf{F}.\cos\theta/kT).\mu.\cos\theta.d\Omega$, and the orientation of all dipoles is accounted by $A.\exp(\mu.\mathbf{F}.\cos\theta/kT).d\Omega$. Hence, the average moment (u) of a molecule in the direction of **F** is

$$u = \frac{A.\exp(\mu.\mathbf{F}.\cos\theta/kT).\mu.\cos\theta.d\Omega}{A.\exp(\mu.\mathbf{F}.\cos\theta/kT).d\Omega}$$

Letting $\mu.\mathbf{F}/kT = \delta$, then $u/\mu = \coth\delta - (1/\delta) = L(\delta)$, where $L(\delta)$ is the Langevin function of δ, expanding as follows,

$$\delta/3 - \delta^2/45 + 2\delta^3/945 - \ldots\text{etc.}$$

For commonly used field strengths and temperatures, δ is small, and $L(\delta)$ may be considered to be adequately approximated by the first term. Thus,

$$u = \mu.\delta/3 = \mu^2.\mathbf{F}/3.kT \qquad (A.7)$$

Induced moments are also present, so the mean molecular moment in the direction of **F** becomes

$$u = \alpha_0.\mathbf{F} + \mu^2.\mathbf{F}/3.kT \qquad (A.8)$$

where α_0 is the molecular polarisability induced by distortion, and the last term represents the polarisability due to orientation. Hence, for a polar molecule, the total (effective) polarisability is given by $\alpha = \alpha_0 + \mu^2/3.kT$.

The expression for the total polarisability can be substituted into the Clausius-Mosotti relationship for the dielectric constant of a molecule,

$$\frac{\epsilon - 1}{\epsilon + 2} + \frac{M}{d} = \frac{4.\pi.N}{3}.\alpha \quad ,$$

where ϵ is the dielectric constant, M the molecular weight,

and d the density, and N is Avogadro's number. That is,

$$\frac{\epsilon - 1}{\epsilon + 2} + \frac{M}{d} = \frac{4.\pi.N}{3}.(\alpha_0 + \mu^2/3.kT) \qquad (A.9)$$

The left-hand side of equation (A.9) is the total molecular polarisability of the molecule, and is equal to the sum of the electronic and atomic polarisations. The right-hand side consists of a molecular distortion term, $4.\pi.N.\alpha_0/3$, and an orientation polarisation term, $4.\pi.N.\mu^2/9.kT$.

Equation (A.9) requires the molecular polarisability by distortion (α_0) to be determined for the calculation of a dipole moment. Osipov[202] proposes a relationship which expresses α_0 in terms of the refractive index (n_d); for measurements made at the same frequency, $\epsilon = n_d^2$. Thus, the total polarisation is identical to the molecular refraction according to the Lorentz-Lorentz relationship,

$$\frac{4.\pi.N}{3} \cdot \frac{\mu^2}{3kT} = \frac{M}{d}\left[\frac{(\epsilon - 1).(\epsilon + 2)}{8.\epsilon} - \frac{(n_d^2 - 1).(n_d^2 + 2)}{8.n_d^2}\right] \qquad \ldots (A.10)$$

Equation (A.10) can be used to calculate the dipole moments of pure polar substances from dielectric constants. The calculation has been demonstrated[202] to yield the dipole moments for many organic compounds with an error less than 0.1 debye.

Alternatively, dipole moments can be determined from a vectorial sum of the moments of the fundamental molecular fragments. For meta- and para-substituted aromatc compounds, this method has been utilised by Minkin et al.,[203] giving good agreement with experimental values, but with the **ortho**-substituted aromatics, a term must be introduced to account

for the induced dipoles caused by the proximity of functional groups. The groups are able to influence one another through mesomerism, London dispersion forces, and perhaps secondary bonding. Minkin et al.[203] improved the correlation of **ortho**-disubstituted benzenes by estimating the induced dipole. A similar approach was used in the calculation of the dipole moment of 2,4-dinitrophenol (DNP).

Estimation of the dipolar interaction moment for the **ortho**-substituents in DNP was achieved by comparison of the dipole moment of **o**-nitrophenol calculated from the static dielectric constant (via equation A.10) and the dipole moment determined from the vectorial sum of the aromatic substituent moments.

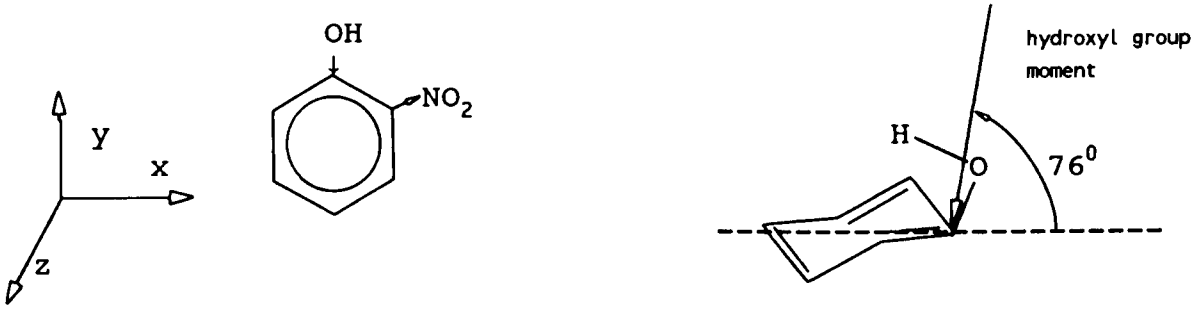

For consistency, the direction of the group moments are designated as positive when pointing toward the aromatic ring.

The hydroxyl group has a dipolar axis lying outside of the plane of the aromatic ring[204] by 76^0 and, from summation of group moments,[205] the molecular dipole moment for phenol is 1.55 debye. Therefore, the three-dimensional spatial vector for the OH group are: $\mu_x = 0$; $\mu_y = -1.55\cos 76^0 = -0.37$; $\mu_z = -1.55 \sin 76^0 = -1.50$.

Similarly, in nitrobenzene, with a molecular dipole moment[204] of 4.01 debye, the vectors for the NO_2 group are: $\mu_x = 4.01\cos 30^0 = 3.47$; $\mu_y = 4.01\sin 30^0 = 2.01$; $\mu_z = 0$.

Therefore, for **o**-nitrophenol: $\Sigma\mu_{xi} = 3.47$; $\Sigma\mu_{yi} = 1.64$; $\Sigma\mu_{zi} = -1.50$, and the vectorial sum gives the molecular dipole moment, $\mu_{vector} = (3.47^2 + 1.64^2 + (-1.50)^2)^{1/2} = 4.12$ debye.

Estimating the dipole moment (μ_{sdc}) from the static dielectric constant (ϵ = 17.3 e.s.u.) for **o**-nitrophenol, using a rearrangement of equation (A.10),

$$\mu_{sdc} = \left[\frac{M.9.k.T}{d.4.\pi.N} \left[\frac{(\epsilon-1).(\epsilon+2)}{8.\epsilon} - \frac{(n_d^2-1).(n_d^2+2)}{8.n_d^2} \right] \right]^{\frac{1}{2}}$$

$$= 3.29 \text{ debye.}$$

Hence, the substituent interaction moment (μ_{int}) is the difference, that is, $\mu_{int} = \mu_{sdc} - \mu_{vector} = 0.83$ debye, which includes contributions from induction, mesomeric effects, and hydrogen bonding between the adjacent groups.

The molecular dipole moment of DNP can be estimated by calculating the vectorial sum of the substituent moments and applying the interaction moment, for the **ortho**-groups, to obtain a corrected value. Applying a similar calculation as for **o**-nitrophenol yields an uncorrected value (μ_{vector}) of 4.46 debye, therefore, $\mu_{DNP} = \mu_{vector} - \mu_{int} = 3.63$ debye.

Table A.5 lists the dipole moments and the dielectric constants for phenol, **p**-nitrophenol, DNP, and butanol.

Table A.5 The dipole moments (μ) and static dielectric constants (ϵ) for the precursor alcohols used to synthesise the aryl titanates described in §2.3.9.

Compound	ϵ (at 25^{0}C	μ (debye)
phenol	9.78(60^{0}C)	1.55[1]
p-nitrophenol	42.12[2]	5.03[1]
2,4-dinitrophenol	22.15[2]	3.63[3]
butanol	17.8(20^{0}C)	1.66[4]

Notes. Values for ϵ were taken from the "Handbook of Chemistry and Physics", 67th edition, CRC Press, (1986). (1) See reference 204. (2) See reference 205. (3) ϵ values were calculated from values of μ, using equation (A.10). (4) The value of μ was calculated from the vectorial sum of the substituent-moments, corrected for the ortho-group interaction moment.

APPENDIX V
NMR CHARACTERISATION OF TETRAPHENYL TITANATE (TPT)

Broadband carbon NMR spectrometry was utilised to follow the synthesis of tetraphenyl titanate (TPT) by the ester exchange of "Tyzor TBT" with an excess of phenol (cf. §2.3.9). The synthetic reaction was spontaneous and exothermic at room temperature, so the reaction was conducted in a test-tube into which was placed 16.94g of "Tyzor TBT" (i.e., 0.04 mole of titanium) and 21.60g (0.23mol) of phenol in the following increments,

#	Increment of phenol added (in moles)	Molar ratio of phenol to titanium
1.	0.038	1.0
2.	0.076	3.0
3.	0.076	5.0
4.	0.057	6.5

An orange precipitate formed after the addition of the third increment. The elemental analysis is given in table A.6.

Table A.6 The elemental analysis of the orange precipitate, compared with published analyses[58,65] for TPT.

Compound	Elemental Analysis (mass%) Ti	C	H	Calculated Analysis (mass%) Ti	C	H
Reaction	-	68.29	5.15	-	68.58	4.80
TPT[(1)]	-	56.3	4.4	-	55.9	3.9
TPT[(2)]	11.45	68.6	4.9	11.40	68.58	4.80

Notes. (1) Data from reference 207. (2) Data from reference 208.

The elemental analysis confirms that TPT is substantially monomeric, as suggested by Dijgraaf and Rousseau.[208]

The progressive exchange of the butoxyl ligands in "Tyzor TBT" by phenol produces marked downfield shifts of the **ipso**-phenyl carbon nucleus (i.e., by 7.9ppm) and the **ortho**-phenyl carbon (i.e., by 3.8ppm). Esterification with

the titanium(IV) atom centre increases the electron density at these nuclei.

Notably, the downfield shifts of the phenyl ligands retrogress with increasing butoxyl ligand displacement, and as the orange TPT begins to precipitate. The phenyl chemical shifts approach those of the analogous carbon nuclei of phenol.

Table A.7 The BB^{13}C-NMR chemical shifts of the phenoxyl ligands in TPT as the extent of ligand exchange with "Tyzor TBT" increases according to the increments of phenol added. The reaction was performed in a 10mm NMR sample-tube used to obtain the spectra.

Molar Ratio phenol/Ti	Phenyl carbon chemical shifts (δ, ppm) ipso-	ortho-	meta-	para-
1.0	165.7	119.5	129.4	120.5
3.0	160.7	117.4	129.9	121.2
5.0	157.2	116.8	130.7	121.8
6.5	156.4	115.7	129.7	120.9
phenol(1)	157.8	115.7	129.6	119.7

Note. (1) The phenol sample was measured as a neat liquid at 305K.

The concept of dative, secondary bonding between the titanium centre and the phenoxyl oxygen atom, proposed by Haslam,[161] explains these observations. In the early stages of ester exchange, the strong dative bonding is in mesomeric resonance with the phenyl ring, producing increased electron density at the **ipso-**, **ortho-**, and **para**-carbon nuclei. As the number of phenoxyl ligands about the titanium centre grows to three and four, the Ti-O bond lengthens under the strain of interligand steric repulsion. Lengthening reduces the strength of the dative bond, which requires distortion of the lone-pair orbitals on the oxygen, reducing the electronic redistribution.

APPENDIX VI

COMPLEXATION OF TITANIUM(IV) WITH 2-HYDROXYETHYL BENZOATE

A benzene solution of $TiCl_4$ was added to 2-hydroxyethyl benzoate (HEB) (0.07mol, in benzene), and the BB ^{13}C-NMR spectrum obtained for each increment of addition (viz., $7.3x10^{-3}$moles). Table A.8 lists the chemical shifts for HEB against the increments of $TiCl_4$ added, and selections from the spectra are presented in figure A.4, grouped together into the methylene, aromatic, and carbonyl chemical shift regions.

Table A.8 The carbon NMR chemical shifts of HEB with $TiCl_4$ (in benzene) added in increments of $7.3x10^{-3}$mole. (cf. figure A.1 for carbon atom labelling)

Increment	Carbon Chemical Shifts for HEB (δ, ppm)						
	1	2	3	7	4	5	6
0	60.5	66.6	166.9	133.1	130.9	129.7	128.5
1	60.5	66.6	166.8	133.1	130.2	129.7	128.5
2	61.7	66.2	166.9	133.2	hid.	129.7	128.5
3	62.4	66.1	167.1	133.2	hid.	129.8	128.5
4	hid.	65.9	167.2	133.2	hid.	129.8	128.5
5	hid.	65.5	167.6	133.2	hid.	129.8	128.5
6	69.5	65.4	167.5	133.3	hid.	129.9	128.5
7	70.3	65.4	167.7	133.1	hid.	129.6	128.2
8	72.4	64.4	167.7	133.2	hid.	129.8	128.3
9	73.0	64.4	167.8	133.3	129.8	129.6	128.2

Note. Abbreviation: "hid.", the signal was hidden or indistinguishable due to peaks overlapping.

The induced shifts of the peaks for HEB with increasing amounts of $TiCl_4$ indicate the formation of a HEB/Ti(IV) complex adduct. The greatest induced shifts tell of the strongest interactions; the OH-methylene (atom **1**) and the carbonyl (atom **3**) carbon nuclei are seen to shift substantially downfield. The former exhibits significant signal broadening as well, suggesting the formation of a covalent Ti-O bond which exchanges with the Ti-Cl bond of the precursor titanium compound.

The induced peak shifts were found to be linearly dependent on the amount of $TiCl_4$ added (see table A.9 for the linear parameters), as is suggested by the results of Bose et al.[209] for the proton chemical shifts of a range of alcohols, ketones, carboxylic acids, esters, and cyanohydrocarbons, where the induced proton NMR chemical shifts were found to be linearly related to the molar ratio of $TiCl_4$ to substrate. The magnitude of the induced shifts were observed to decrease with the distance from the interacting functional groups, and the "sensitivity" of the functional groups of HEB to $TiCl_4$ are expected to be: alcohol >> ester.

Table A.9 The slopes (K) of each set of induced ^{13}C-NMR chemical shifts for HEB. The data was fitted by linear regression to the linear equation-form: Chemical Shift = K(Increment of $TiCl_4$ added) + constant.

Carbon Atom	Slope (K)	Constant
1	215.9	59.1
2	-34.6	66.8
3	16.6	166.8
4	-9.38	130.4
5	-0.33	129.8
6	-4.65	128.6
7	1.91	133.1

Note. The sign of K indicates the direction of the induced peak shift: +ve signs represent downfield shifts, and -ve signs are upfield shifts.

The magnitudes of the linear slopes (K) for the induced shifts of the HEB carbon peaks against the amount of $TiCl_4$ added indicate the strengths of the interactions between the titanium centre and the carbon nuclei. The values of K confirm that the hydroxyl group interacts most strongly, the magnitude of the interaction suggesting that it forms a covalent Ti-O bond, and the carbonyl carbon shows the next strongest interaction. Therefore, the structure of the HEB/Ti adduct is considered to involve the coordination of the carbonyl group, chelating the HEB ligand,

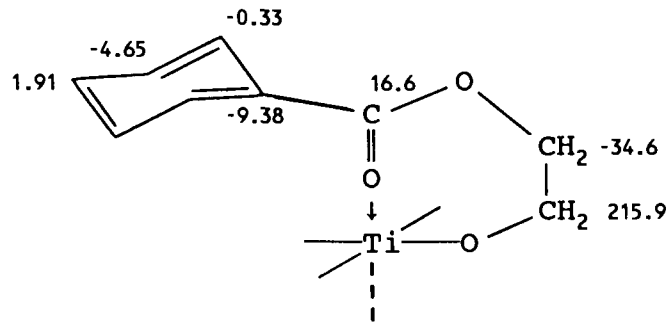

where the carbon nuclei have been labelled with the corresponding value of K from table A.9. The most apparent feature is the rapid attenuation of the induced shifts, along the HEB-ligand, with the distance from the titanium centre. Titanium(IV), being a Lewis acid, draws electron density toward itself, and without any intramolecular interactions the induced charges, residing at each carbon nucleus, ought to decrease constantly with the distance from titanium. However, the carbonyl carbon atom (four bonds from the titanium atom) exhibits a greater interaction than expected. The anomolous trend is explained by a secondary intramolecular interaction between the carbonyl group and the titanium atom, accomodated through the octahedral site, and leading to chelation.

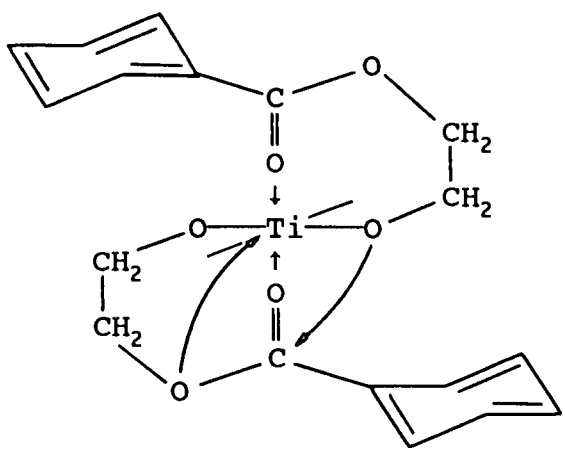

Chelation renders the titanium centre unreactive to ester exchange with the phenols of cresylic acid, used in Isomid wire-varnish, due to greater stability. The chelate was noticed to be very stable in benzene solution at room temperature when in the presence of phenol.

The chelation postulated suggests the structure of the intermediate complexes of titanium(IV) in the catalysis of the transesterification reactions between hydroxyethyl chain end-groups, involved in the curing of the PEI resin (viz., resin-SC). The following possible transition-state may mediate these polycondensation reactions,

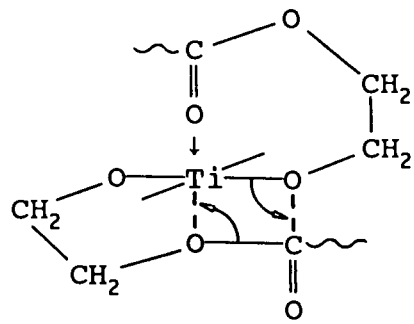

wherein ester exchange proceeds by a structural rearrangement about the titanium centre

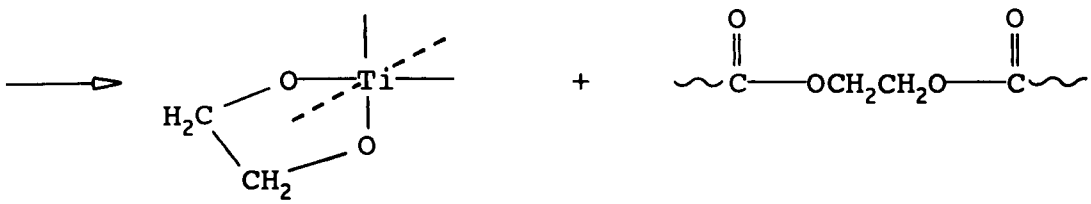

producing an extended polymer chain and a stable glycoxy-chelato titanate.

Habib and Malek[210] and Nondek and Malek[211] have found tetraalkyl titanates to be good polycondensation catalysts for PET, with the rate of polyesterification depending on the concentrations of carboxylic acid, glycol, and titanate,

suggesting that all are involved in a reactive intermediate complex.

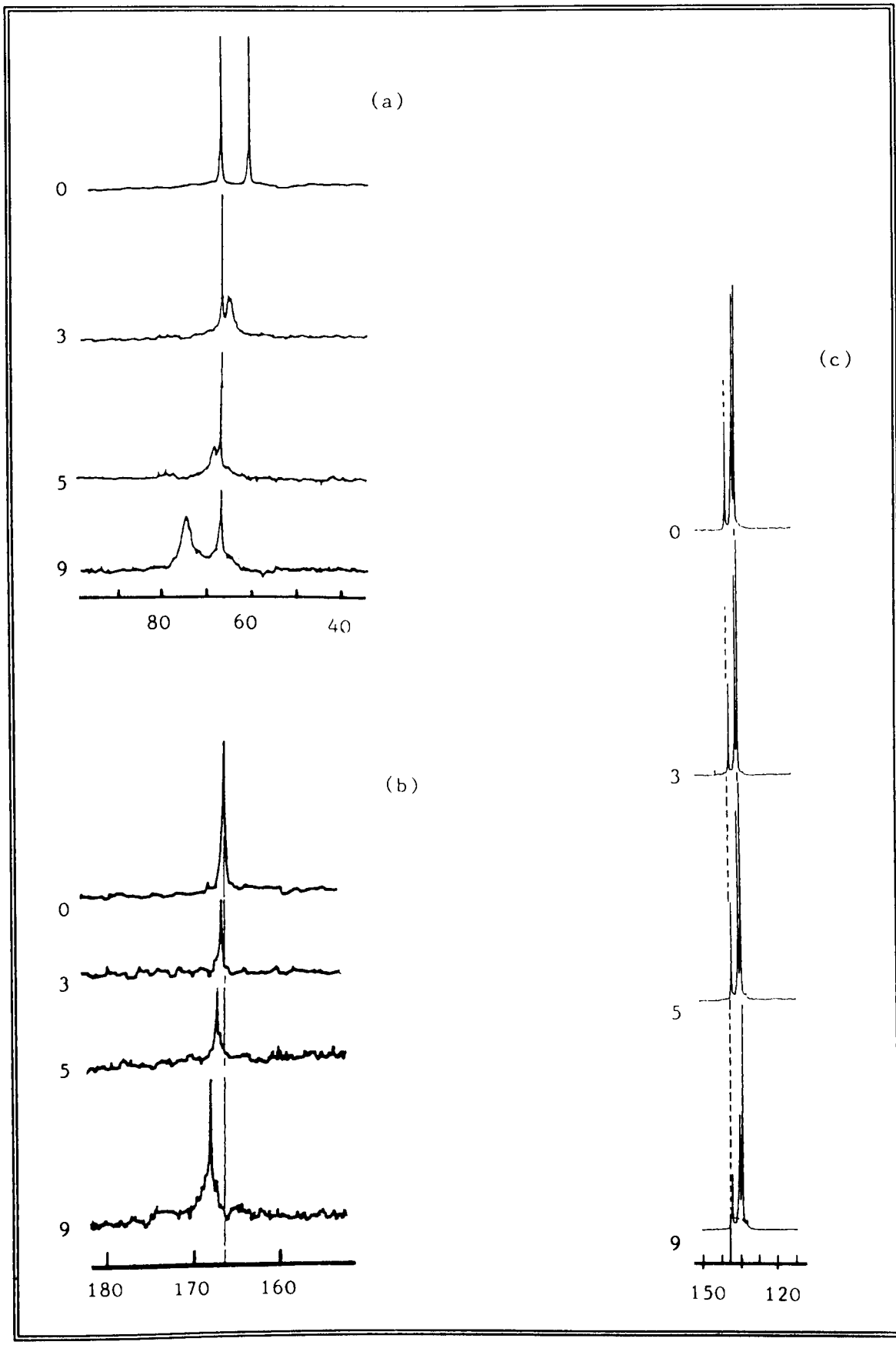

Figure A.4 A selection from the broadband, decoupled carbon NMR spectra of the HEB/Ti(IV) complexation reaction. (a) The methylene chemical shift region. (b) The carbonyl region. (c) The aromatic region. The spectra shown are for the 0, third, fifth, and ninth increments of $TiCl_4$ addition (cf. table A.8).

APPENDIX VII

TERNARY AZEOTROPE OF PHENOL, WATER, AND ETHYLENE GLYCOL

The formation of an azeotrope of cresylic acid with the condensation products (i.e., water and EG), of polyesterification reactions in the curing of Isomid wire-varnish, can lower the boiling points of the less volatile substances. Thus, the removal of the solvent and the condensed reaction products is affected by the existence of azeotropic mixtures.

Phenol was used to represent the cresylic acid solvent system.

Azoetropic data for phenol, water, and EG mixtures was not found in the literature,[212] therefore, the distillate from a boiling mixture (i.e., 10.05 moles of phenol, 74.96 moles of water, and 14.99 moles of EG, heated in an oil bath at 200^{0}C) was analysed by gas chromatography.

The distillate was found to boil at 101^{0}C, and consist of 8.02wt.% phenol, 91.4wt.% water, and 0.617wt.% EG.

APPENDIX VIII

SELF-CONSISTENT FIELD, LINEAR COMBINATION OF ATOMIC ORBITALS APPROXIMATION FOR THE ELECTRONIC DISTRIBUTION IN N-(4-METHYLPHENYL) MALEIMIDE

The approximate molecular orbital theory of Pople and Beveridge[155] was used to estimate the electronic distribution in a model molecule, N-(4-methylphenyl) maleimide (MPM)

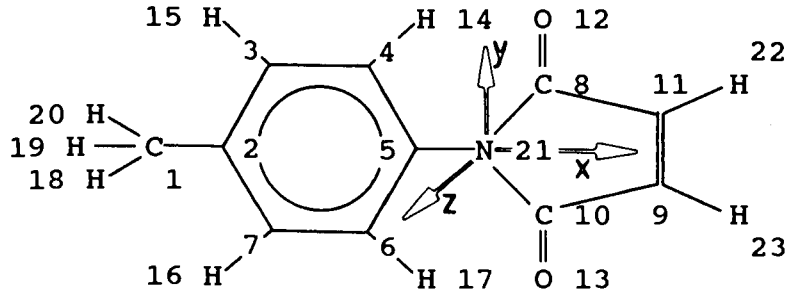

(The molecule is defined to lie in the x-y plane)

The molecule modelled the fundamental structure of the trimellitimide portion of the molecular structure of the PEI resin, resin-SC. The distribution of electrons around the nitrous phenyl ring indicates the order of the NMR chemical shifts of the carbon nuclei, thereby assisting their assignments in the model compound MBPT (cf. §2.3.1).

The FORTRAN IV computer program, given by Polpe and Beveridge[155], for the complete-neglect-of-differential-overlap (CNDO) and intermediate-neglect-of-differential-overlap (INDO) calculations were utilised in the calculations of electronic distributions. The calculation considers the molecular geometry, electronic charge distribution, electron-spin-nuclear-spin interactions, and nuclear-spin-nuclear-spin interactions, and is capable of computing CNDO wavefunctions for open and closed-shell molecules containing the elements hydrogen to fluorine.

The CNDO/INDO computations are semiempirical approaches in the calculation of electronic distribution in polyatomic

molecules, using general molecular orbital theory based on LCAO (viz., linear combination of atomic orbitals).[156] Experimental data for atoms and model molecular systems are used to estimate values for quantities entering the calculations. The CNDO method assumes a zero-differential overlap in which the main features of electron repulsion are retained (only valence electrons are explicitly considered) whilst the inner shells are assumed to be a part of a rigid core of electrons. The INDO modification accomodates the different interactions that take place between two electrons of parallel or antiparallel spins, particularly for those on the same atom. In the computation of electron densities, the INDO method was preferred since CNDO theory does not account for σ-π echange integrals[213] which give rise to non-zero π spin density in the aromatic prototype molecule (viz., MPM). These exchange integrals model the long-range coupling of π-electron spin polarisation, transmitted through σ and π molecular orbitals.

The program-matrices are only large enough to allow molecules containing up to 35 atoms or 80 basis functions, whichever is smaller. One atomic basis function is allowed for hydrogen (1s), four for both carbon and nitrogen (2s, $2p_x$, $2p_y$, $2p_z$).

In the absence of an X-ray crystallographic structure for MPM, the molecular geometry was assumed from the known[214] structures of **p**-toluidine (**vide infra**) and succinimide. With the origin of a 3-D cartesian coordinate system at the centre of the nitrogen atom, the coordinates of each carbon and hydrogen atom were determined for MPM (see table A.10), and for **p**-toluidine (see table A.10). The coordinates defined

the molecular geometry and were used to compute the eigenvector matrix.

Table A.10 The 3-D coordinates for each carbon and hydrogen atom in the supposed structure of the model molecule, MPM. The origin of the coordinate system is defined to be at the centre of the nitrogen atom. The atom numbering is given in the MPM structure (**vide supra**).

Atom	Number of Valence Electrons	Coordinates		
		x	y	z
1	4	-5.6199	1.1000	0.0000
2	4	-4.1700	0.9300	0.0000
3	4	-3.4800	1.2100	0.0000
4	4	-2.0699	1.1900	0.0000
5	4	-1.3900	0.0000	0.0000
6	4	-2.0699	-1.1700	0.0000
7	4	-3.4500	-1.1400	0.0000
8	4	0.8200	1.1799	0.0000
9	4	2.2300	-0.7000	0.0000
0	4	0.7950	-1.1700	0.0000
11	4	2.2400	0.7000	0.0000
12	6	0.4450	2.2700	0.0000
13	6	0.4200	-2.2400	0.0000
14	1	-1.5100	2.1400	0.0000
15	1	-4.0100	2.1600	0.0000
16	1	-4.0700	-2.0899	0.0000
17	1	-1.5200	-2.1099	0.0000
18	1	-5.9699	-0.7850	-0.9000
19	1	-5.9699	1.2000	1.0400
20	1	-5.9699	1.0000	-0.9000
21	5	0.0000	0.0000	0.0000
22	1	3.1800	1.2400	0.0000
23	1	3.1800	-1.2500	0.0000

Note. The total number of valence electrons is 70 with 65 valence orbitals. Therefore, there are 35 electron pairs, and the CNDO/INDO computation has yielded a 35x65 eigenvectore matrix.

The resulting matrix of eigenvalues (a_i) and eigenvectors was used to calculate the distribution of electronic charge. The share of electrons for each atom was determined according to equation (A.11),

$$\text{Number of electrons} = 2. \sum_{i=1}^{35} a_i^2 \qquad \text{(A.11)}$$

The values so derived are presented in table A.9. Note that the electron share of atom **5** is less than that of atom **2**, indicating that the carbon NMR chemical shift of the former

is expected to be greater than the latter.

Table A.11 The electronic charge distribution calculated from the approximated molecular orbitals, with CNDO/INDO. The values, listed against atoms, are the numbers of electrons.

Atom Number	Share of Molecular Electrons
1	7.9998
2	7.9997
3	7.9159
4	7.9990
5	7.9574
6	7.9984
7	7.9719
8	0.0036
9	0.0001
10	0.0040
11	0.0001
12	0.0017
13	0.0020
14	1.9987
15	1.9998
16	1.9998
17	1.9984
18	1.9998
19	1.9998
20	2.0002
21	0.0518
22	0.0000
23	0.0000
total	69.9022

Application of the CNDO/INDO calculations to p-toluidine, for which the molecular geometry is known[214] (see table A.12 for the atomic coordinates, assuming the origin of space to be at the centre of the nitrogen atom),

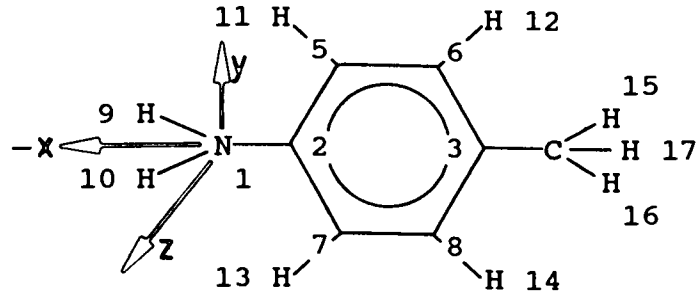

gave a similar disposition of molecular electrons (cf. table A.12). The nitrous aromatic-carbon (2) has a lesser share of

the molecular electrons than atom 3, suggesting the disposition of the carbon NMR signal of the former to be downfield from the latter.

Table A.12 The electronic distribution for the p-toluidine molecule, computed using the CNDO/INDO program and equation (A.11), for the given atomic coordinates.

Atom Number	Share of Molecular Electrons	Coordinates		
		x	y	z
1	5.2706	0.0000	0.0000	0.0000
2	3.8543	1.4700	0.0000	0.0000
3	3.9710	4.2300	0.0000	0.0000
4	4.0388	5.8299	0.0000	0.0000
5	4.0387	2.1600	1.1600	0.0000
6	3.9804	3.5599	1.1400	0.0000
7	4.0377	2.1600	-1.1500	0.0000
8	3.9849	3.5699	-1.1600	0.0000
9	0.8964	-0.5000	0.9000	0.0000
10	0.8962	-0.5000	-0.9000	0.0000
11	1.0080	1.6200	2.1199	0.0000
12	1.0188	4.0900	2.1099	0.0000
13	1.0112	1.6100	-2.1099	0.0000
14	1.0148	4.0799	-2.1500	0.0000
15	0.9931	6.1999	0.8100	-0.5150
16	0.9909	6.1999	0.0000	1.0270
17	0.9941	6.1999	0.8200	-0.5150
total	50.0180			

APPENDIX IX

MASS SPECTRUM OF VAPORS EMINATING FROM INDUSTRIALLY CURED ISOMID WIRE-ENAMEL UPON HEATING ABOVE 140^{0}C.

The 70eV mass spectrum of heated scrapings from Isomid PEI wire-enamel, cured by SCA onto copper wire, is presented in figure A.5. No evidence of ionisation was detected until the ionisation chamber was heated to 144^{0}C.

Clusters of peaks are seen at molecular weights corresponding to the phenol homologues which are usual components of cresylic acid solvent systems (cf. §1.5.2.1 for a description of these).

The fragmentation patterns of phenol and the isomers of cresol are presented in figure A.6 for the same ambient conditions, of the ionisation chamber, as used to examine the enamel-scrapings.

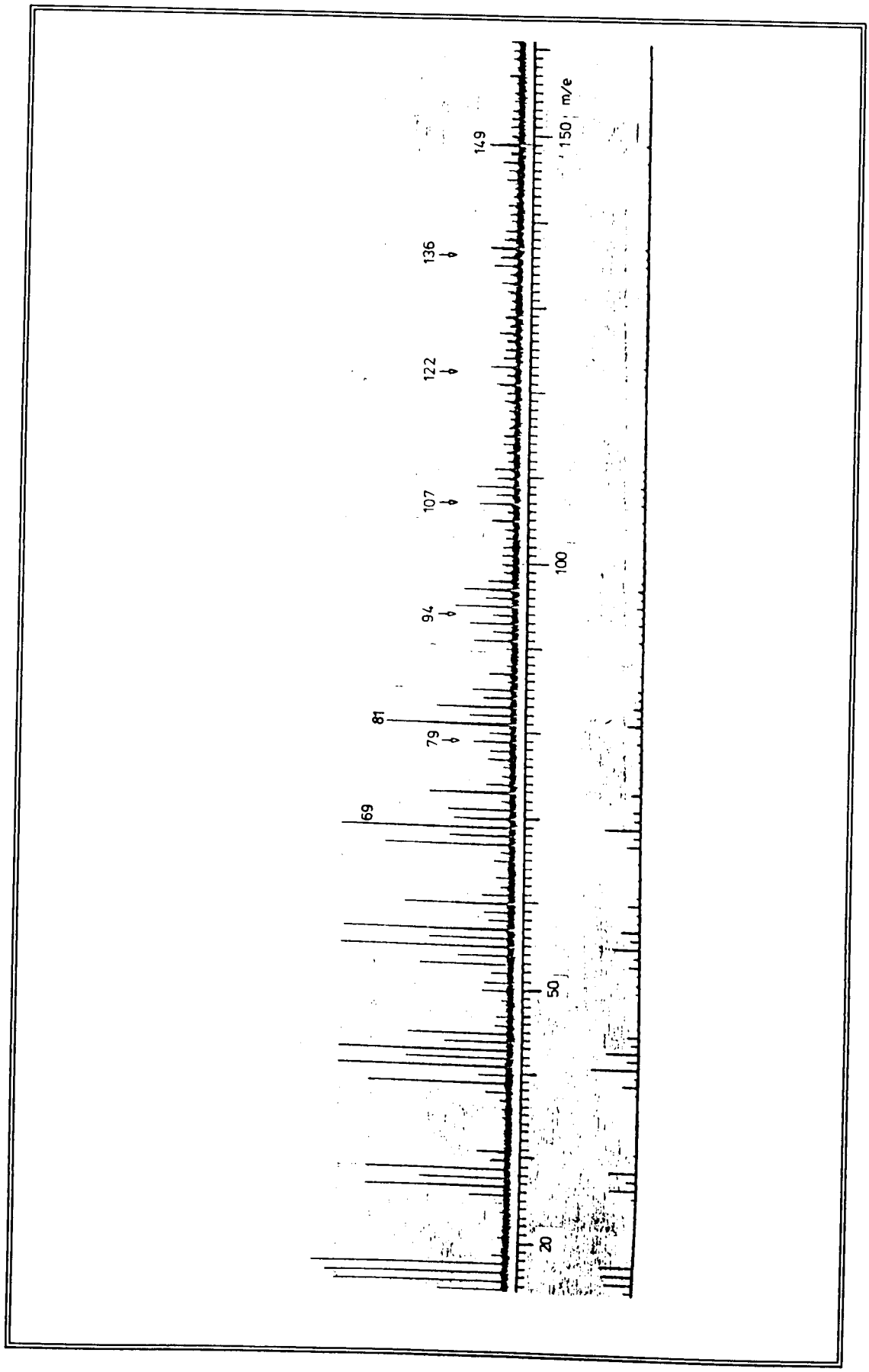

Figure A.5 The 70eV mass spectrum of Isomid wire-enamel scrapings heated to 144^{0}C.

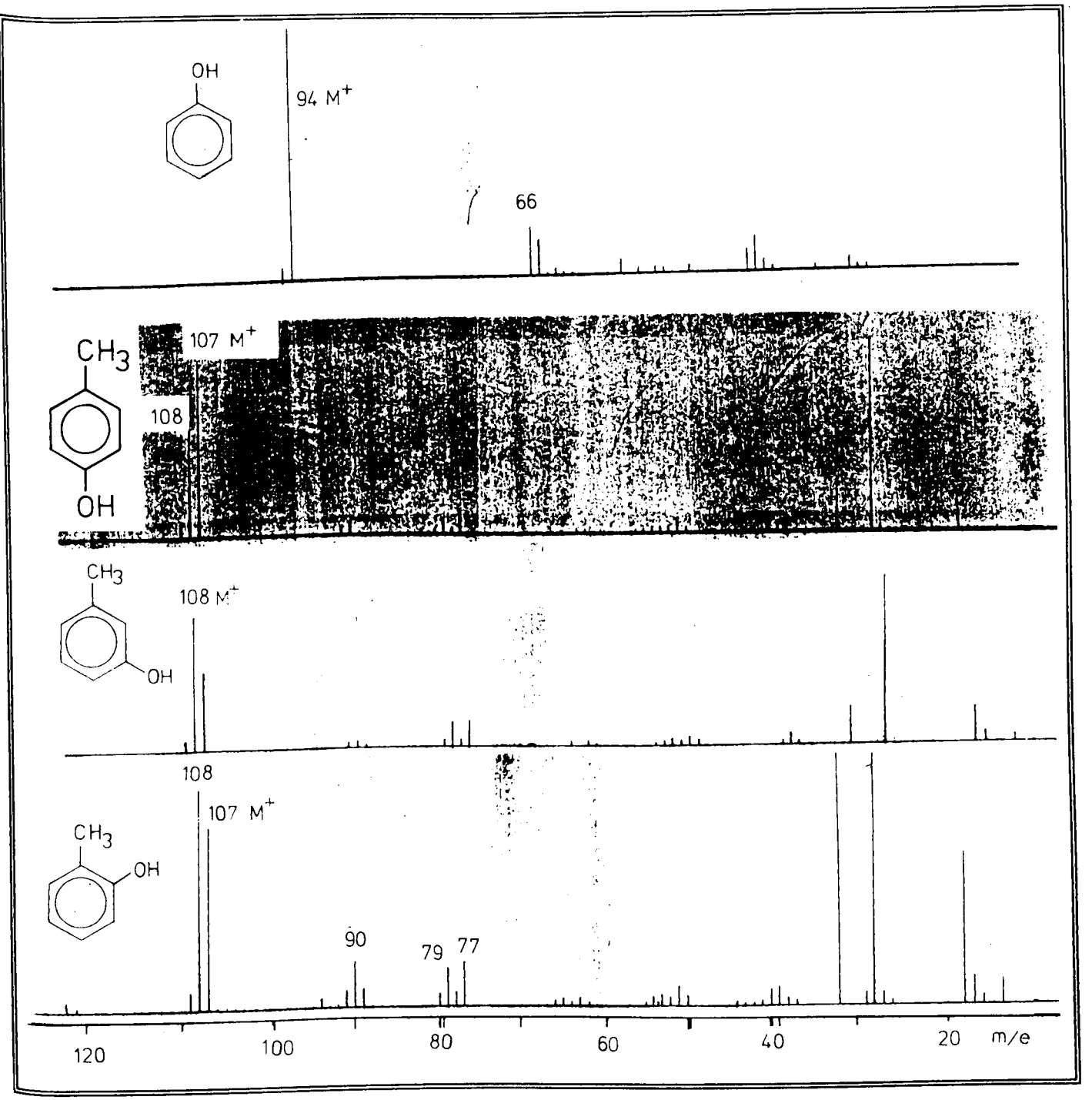

Figure A.6 The 70eV mass spectrum of the isomers of cresol.

APPENDIX X

AROMATIC CARBON NMR CHEMICAL SHIFTS OF COMPONENTS IN CRESYLIC ACID

The carbon NMR chemical shifts for the phenol-homologue components of cresylic acid (cf. §1.5.2.1) were calculated by the addition substituent shifts, given by Levy et al.[215] The calculated values were compared with experimental and literature values wherever possible. The results are presented in table A.14.

The calculated chemical shifts of a number of benzoate-ester analogues of the phenol-homologues are also given (cf. table A.15). The experimental chemical shifts for phenyl benzoate (cf. §2.3.7) yielded the substituent effects for the phenol aromatic ring.

Table A.13 The ^{13}C substituent effects of mono-substituted benzene, relative to benzene as standard (chemical shift = 128.5ppm).

Substituent	Aromatic Carbon			
	ipso	ortho	meta	para
-OC(O)Ph	+22.4	-7.2	-0.2	-3.0

Table A.14 The calculated aromatic ^{13}C NMR chemical shifts for the phenol-homologues in the cresylic acid solvent system.

Compound (φ=phenol)	Aromatic Carbon Chemical Shifts 1	2	3	4	5	6
φ	155.4	115.8	129.9	121.2	-	-
exptl.	156.0	116.3	130.2	121.7	-	-
lit.	157.8	115.7	129.6	119.7	-	-
2-methylφ	158.5	124.6	130.3	119.6	126.7	115.6
exptl.	153.9	124.9	131.8	121.6	127.6	115.8
lit.	155.7	124.1	130.8	119.0	126.8	114.9
3-methylφ	157.7	116.4	138.5	120.4	129.5	112.8
exptl.	155.5	116.8	140.4	122.6	130.0	113.1
lit.	157.1	116.1	138.9	119.8	129.3	112.6
4-methylφ	154.9	115.6	130.3	128.6	-	-
exptl.	153.3	115.9	130.8	128.8	-	-
lit.	155.4	115.4	129.1	127.4	-	-
2,4-dimethylφ	155.6	124.5	131.0	128.5	127.4	115.5
2,6-dimethylφ	159.2	124.5	127.4	119.5	-	-
3,5-dimethylφ	157.6	113.5	138.4	122.1	-	-
3,4-dimethylφ	154.8	116.3	139.2	129.3	130.2	112.7
exptl.	153.0	116.9	139.8	131.3	130.8	113.3
2,3-dimethylφ	158.4	125.3	139.2	120.3	126.6	112.7
2,5-dimethylφ	156.6	122.3	130.8	122.3	136.2	116.9
2,4,6-trimethylφ	156.3	124.4	128.1	128.4	128.1	124.4

Notes. Experimental values were obtained with a Brüker WP80 spectrometer and neat liquid samples at room temperature.
Literature values were obtained from reference 178.

Table A.15 The calculated aromatic ^{13}C chemical shifts for the benzoate-ester analogues of the phenol-homologues, using the substituent constants given in table A.13 for the phenyl substituent.

Ester (-benzoate)	Aromatic Carbon-13 Chemical Shifts 1	2	3	4	5	6
2-methyl	151.6	130.2	129.0	125.4	-	-
3-methyl	150.8	122.0	137.2	126.2	128.2	118.4
4-methyl	148.0	121.2	129.0	134.4	-	-
2,3-dimethyl	151.5	130.9	136.5	126.1	125.3	118.3
2,4-dimethyl	148.7	130.1	129.7	134.3	126.1	121.1
2,6-dimethyl	152.3	130.1	126.1	125.3	-	-
3,4-dimethyl	147.9	121.9	137.9	135.1	128.9	118.3
3,5-dimethyl	150.7	119.1	137.1	126.9	-	-
3,6-dimethyl	151.5	121.9	134.3	126.1	128.9	127.3
2,4,6-trimethyl	149.4	130.0	126.8	134.2	126.8	130.0

Note. The substituent-effects of the methyl groups were taken from reference 215.

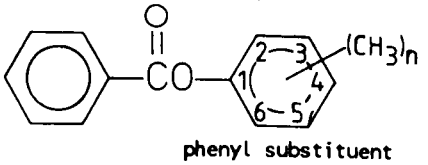

phenyl substituent

Glossary of abbreviations and terms

Ar ...denotes the presence of an aromatic ring

bare spots ...spots on the surface of enamelled wire which are devoid of enamel, and is due to inadequate wetting of the metal-substrate

BB ...broadband decoupling in carbon NMR, used for the suppression of heteronuclear (i.e., C-H) coupling, leading to NOE (**vide infra**)

beaking ...failure of wire-enamel to withstand thermal shock (**vide infra**) after 15% elongation, followed by a 1x mandrel-wrap and stoving at 200^{0}C for 30 minutes, producing peripheral coaxial breaks in the enamel film which are similar in appearance to beaks

blistering ...the formation of bubbles on the surface of enamelled magnet-wire

blowholes ...broken enamel blisters

build ...the thickness of enamel applied to the metal-substrate

burn-out ...the voltage at which the wire-enamel chars and allows short-circuit for a twisted-pair (**vide infra**) sample

catalytic-oven ...a curing-oven designed to allow the hot vapours eminating from the curing wire-varnish to be oxidised to carbon dioxide and water by contact with a heated (to ≈600^{0}C) solid catalyst (tantalum mesh); the hot products are channelled to the oven-inlet (recirculated), providing additional heat for curing. This oven-type is both much more energy-efficient, and is more environmentally favourable

concen-tricity ...the ratio of the thickest and thinnest builds for an enamelled wire cross-section

cratering ...small depressions seen at the wire-enamel's surface, and due to a lack of wetting of the wire-varnish for the underlying substrate, either metal or polymer film

curing-oven ...a thermal oven open at two ends to allow the passage of varnished wire; it can be either vertical or horizontal in configuration

DET ...diethyl terephthalate

diluent ...aromatic hydrocarbons added to reduce the cost of wire-varnish solvents, but which are nonsolvents for the resins

DNP ...2,4-dinitrophenol

DPT ...diphenyl terephthalate

EB ...ethyl benzoate

EDB ...ethylene dibenzoate

EG ...1,2-ethanediol

electro-magnet-wire ...metallic wire, commonly copper, coated with a high-quality dielectric such as PEI, and which is used to wind magnet-coils

enamelling-pass ...one passage of varnish-coated wire through an enamelling-oven

encapsulating varnish ...a varnish used to cover an electromagnetic winding, to provide greater protection

extraresin ...that in the enamel film which is derived from a source other than the resins employed to make-up the PEI wire-varnish

HBB ...4-(hydroxybutyl) benzoate

HEB ...2-(hydroxyethyl) benzoate

Isomid ...registered trade mark of Schenectady Chemicals, Inc. and referring to the wire-varnish made with resin-SC.

jerk-test ...a quick test used by wire-enamellers to judge the extent of cure where a length of wire is rapidly elongated by hand to breakage; a well cured enamel exhibits a single coaxial break with no loss of adhesion to the metal-substrate

knee-point ...the intersection of the projections from the baseline and the riser of an inflection of a graphical trace

mandrel-wrap ...winding of wire into a tight coil onto a diameter identical (1x) with or twice (2x) that of the wire

magnet-coils ...coils wound with electromagnet-wire, used to produce an electric field, e.g., stator and armature windings in electrical motors

magnet-wire ...see electromagnet-wire

MBPA ...4,4'-methylene bis-(N-phenylterephthalamic acid)

MBPT ...4,4'-methylene bis-(N-phenyltrimellitimide)

MDA ...methylene dianiline

MPM ...N-(4-methylphenyl) maleimide

NOE ...nuclear Overhauser effect, a consequence of

BB (**vide supra**) giving enhancement of peak intensities in carbon NMR spectra; can be eliminated with inverse-gated, decoupling of the spectrum (cf. §2.1.1)

NMR ...nuclear magnetic resonance

PB ...phenyl benzoate

PDIV ...potential-discharge inception-voltage; also known as the **breakdown voltage** at which coronal discharge occurs over the wire-enamel surface when a potential stress is applied across the dielectric film

PEI ...poly(esterimide)

PEI-T ...a PEI containing THEIC (**vide infra**), similar to resin-SC, and used by the Inst.Chem.Przem. (Warsaw, Poland) group of researchers,including P.Penczek, G.Cynkowska, and E.Wardzińska (cf. references 104 and 105). The resin contains 45wt.% imide based on the structure, hydroxyl number is 165-225mgKOH/g_{resin}, acid number is 3.4-13.1mgKOH/g_{resin}

PET ...poly(ethylene terephthalate)

phenols ...the components of the solvent used in wire-varnish, and is synonymous with cresylic acid in the work presented in this thesis

pinholes ...small blowholes (**vide supra**) caused when the solvent leaves before the diluents, leading to resin precipitation

PGC/MS ...pyrolytic gas chromatography with the elution column attached to a mass spectrometer

oven-residence time ...the time spent by the varnished wire in the curing-oven; of the order of a few seconds

rectangular ...wire drawn into a rectangular cross-section

resin-SC ...the PEI resin made according to Schenectady Chemicals, Inc. (cf. reference 107(a)), and is the subject of this thesis. The resin is consists of THEIC, EG, TA, MDA, and TMA precursors

round ...wire drawn into a circular cross-section

SCA ...Schenectady Chemicals Australia Pty.Ltd.

solids content ...the mass left behind after a 2g sample of wire-varnish has been heated at 200^{0}C to remove the volatile components; the property is quoted as the wt.%, and is similar to the amount of resins in the varnish formulation

solvent-crazing ...crazing of the wire-enamel film caused by

polar solvents in the industrial environment

surface-ripples ...waviness on the surface of wire-coatings which is caused by unfavourable changes viscosity of the wire-varnish during thermal-curing or by inadequate wetting of the wire-substrate

TA ...terephthalic acid

TBT ...tetrabutyl titanate

TDNPT ...tetra(2,4-dinitrophenyl) titanate

THEIC ...tris-(2-hydroxyethyl) isocyanurate

thermal shock ...or **heat shock**, the resistance of the wire-enamel to 15% elongation, followed by 1x mandrel-wrap and stoving at 200^{0}C for 0.5 hours; failure is evidenced by the appearance of beaks (**vide supra**)

THET ...tris-(2-hydroxyethyl) trimellitate

TMA ...trimellitic anhydride

TNPT ...tetra-(**p**-nitrophenyl) titanate

TPT ...tetraphenyl titanate

twisted-pair ...two lengths of enamelled wire lightly twisted together

"Tyzor TBT" ...proprietary tetra-**n**-butyl titanate

wire-enamel ...the hard, cured clear polymer coating lining electromagnet wires

wire-varnish...the resin solution used to coat electromagnet-wires

References

1. J.B.Hendrickson, D.J.Cram and G.S.Hammond, "Organic Chemistry", McGraw-Hill, N.Y. (1970), 3rd edition, p.501-515.

2. P.J.Flory, "Principles of Polymer Chemistry", Cornell University Press, N.Y. (1953), pp.69-74.

3. P.E.M.Allen and C.R.Patrick, "Kinetics and Mechanisms of Polymerization Reactions: Applications of Physico-chemical Principles", Ellis Horwood Ltd., England (1974), p.246.

4. H.G.Elias, "Macromolecules.2: Synthesis, Materials and Technology", 2nd edition, Plenum Press, N.Y. (1984), chapter 17.

5. G.V.Schultz and G.Harborth, Makromol.Chem., **1**, 106 (1947).

6. R.G.W.Norrish and R.R.Smith, Nature, **150**, 336 (1942).

7. E.Trommsdorf, H.Köhle and P.Lagally, Makromol.Chem., **1**, 169 (1948).

8. P.J.Hoftyzer, Appl.Polym.Symp., **26**, 349-363 (1975).

9. Tang Au-Chin and Yao Kuo-Sui, J.Poly.Sci., **35**, 219-233 (1959).

10. C.Y.Huang, Y.Simono and T.Onizuka, Polymer Previews, **2**, 307 (1966).

11. P.J.Flory, J.Amer.Chem.Soc., **59**, 466-470 (1937).

12. S.D.Harmann, D.H.Solomon and J.D.Swift, J.Macromol.Sci.-Chem., **A2**(1), 153-174 (1968).

13. F.Mares, V.Bazant and K.Krupicka, Collect.Czech.Chem. Commun., **34**, 2208-2222 (1969).

14. C.M.Fontana, J.Poly.Sci.:Pt.A1, **6**, 2343-2358 (1968).

15. H.G.Elias, "New Commercial Polymers 2", Gordon & Breach Science Publishers, N.Y. (1986), p.331.

16. G.Challa, Makromol.Chem., **38**, 105-122 (1960).

17. ibid., **38**, 123-137 (1960).

18. G.Challa, Rec.trav.chim., Pays-Bas., **79**, 90-100 (1960).

19. C.K.Ingold, "Structure and Mechanism in Organic Chemistry", Cornell University Press, Ithaca, N.Y. (1953), chapter XIV.

20. S.D.Hamann, D.H.Solomon and J.D.Swift, Macromol.Sci.-Chem., **A2**(1), 153-174 (1968). 21. K.Yoda, K.Kimoto and T.Toda, Kogyo Kagaku Zasshi, **67**, 909-914 (1964).

22. S.G.Hovenkamp, J.Poly.Sci.:Pt.A1, **9**, 3617-3625 (1971).

23. S.A.Motov, L.I.Danilina and A.N.Pravednikov, Poly.Sci. USSR, **22**(10), 1558-2565 (1980).

24. R.W.Stevenson and H.R.Nettleton, J.Poly.Sci.:Pt.A1, **6**, 889-900 (1968).

25. G.Challa, Makromol.Chem., **38**, 138-146 (1960).

26. R.W.Stevenson, J.Poly.Sci.:Pt.A1, **7**, 395-407 (1969).

27. M.Murano and R.Yamadera, Poly.J., **2**(1), 8-12 (1971).

28. T.Shima, T.Yrasaki, I.Oka, Polymer Preprints, **13**(1), 578-582 (1972).

29. G.A.Campbell, Diss.Abstr.-Eng., 3617-B (1970).

30. P.J.Flory, J.Amer.Chem.Soc., **61**, 3334-3340 (1939).

31. V.V.Shevchenko, G.D.Mikhailov, A.S.Chegolya, T.A. Polyakova, Khim.Volokna, **1977**(5), 55-59.

32. V.V.Shevchenko, G.D.Mikhailov, A.S.Chegolya and T.A. Polyakova, Kinetica i Kataliz, **20**, 600-605 (1979).

33. V.V.Shevchenko, L.P.Repina, E.M.Aizenshtein, T.A. Polyakova, Khim.Volokna, **1977**(1), 22-24.

34. P.J.Flory, J.Amer.Chem.Soc., **62**, 1057-1070 (1940).

35. C.H.Hofrichter,Jnr., U.S.Pat. 2,641,592 (E.I.DuPont de Nemours and Co., Inc.) (1967).

36. S.Maiti and S.Das, J.Appl.Poly.Sci., **26**, 957-978 (1981).

37. W.H.Carothers, J.Am.Chem.Soc., **51**, 2548-2559 (1929).

38. S.V.Vinogradova, V.V.Korshak and Yu.I.Korzeneva, Poly.Sci.USSR, 7, 2242-2246 (1965).

39. H.Dostal and R.Raff, Montash., **68**, 188-201 (1936).

40. D.H.Solomon, Proc.Roy.Aust.Chem.Inst., **1969**, 50-52.

41. A.C.Rolfe and C.N.Hinshelwood, Trans.Farad.Soc., **30**, 935-944 (1934). [C.A. 29:20603]

42. R.H.Kienle and A.G.Hovey, J.Amer.Chem.Soc., **51**, 509-519 (1929).

43. T.Katsuki and K.B.Sharpless, J.Am.Chem.Soc., **102**, 5974-5976 (1980).

44. D.C.Bradley and M.J.Hillyer, Trans.Faraday Soc., **62**(9), 2374-2381 (1966).

45. M.F.Lappert, D.S.Patil and J.B.Pedley, J.Chem.Soc., Chem.Comm., **1975**, 830-831.

46. J.K.Kochi, Pure Appl.Chem., **52**, 571-605 (1980).

47. K.B.Sharpless, S.S.Woodward and M.G.Finn, Pure Appl. Chem., **55**, 1823-1836 (1983).

48. T.Boyd, J.Poly.Sci., **7**(6), 591-602 (1951).

49. E.Bis an and I.Gömöry, Chem.Zvesti., **10**, 91-95 (1956).

50. (a) S.Minami and T.Iishino, J.Chem.Soc.Japan, Ind.Chem. Sect., **58**, 32-34 (1955); (b)S.Minami, T.Akiyama and T. Ishino, J.Chem.Soc.Japan, Ind.Chem.Sect., **58**, 34-36 (1955).

51. D.C.Bradley, "Metal-Organic Compounds", Adv.Chem.Series, vol.23, edited by ACS Applied Publications, ACS, Washington, D.C. (1959), p.29.

52. D.C.Bradley, F.M.Ab-del Halim and W.Wardlaw, Chem.Ind., **1951**, 310-311.

53. A.F.D'Adamo and R.H.Kienle, J.Am.Chem.Soc., **77**, 4408 (1955).

54. G.Winter, Aust.Dept.Supply, Defense Standards Labs., **191**, 10, 20 (1953); ibid., Can.Varnish Mag., **25**, 14, 17, 19 (1951).

55. A.Ley, Z.Elektrochem., **10**, 954-957 (1904).

56. J.Böeseken, Ber., **46**, 2612-2628 (1913).

57. (a) A.Rosenheim and I.Baruttschisky, Ber., **58B**, 891-893 (1925); (b) A.Rosenheim and W.Plato, Ber., **58B**, 2000-2009 (1925).

58. R.F.Weinland and K.Binder, Ber., **47**, 977-985 (1914).

59. C.M.Langkammerer, U.S.Pat. 2,453,520, E.I.du Pont de Nemours & Co. (1948).

60. J.E.Booge and H.C.Gulledge, U.S.Pat. 2,468,916, to E.I. du Pont de Nemours & Co. (1949).

61. (a) T.Poll, G.Helmchen and B.Bauer, Tetra.Lett., **25**(21), 2191-2194 (1984); (b) T.Poll, J.O.Metter and G. Helmchen, Angew.Chem.Int.Ed.Engl., **24**(2), 112-114 (1985).

62. Z.Dawoodi, M.L.H.Green, V.S.B.Mtetwa and K.Prout, J. Chem.Soc., Chem.Commun., **1982**, 1410-1411.

63. A.L.Suvorov and I.V.Emel'yanova, Tr.Inst.Khim., Akad. Nauk SSSR, Ural Filial, **1971**(21), 23-32.

64. A.L.Suvorov, I.V.Emel'yanova and S.S.Spasskii, Tr.Inst. Khim., Akad.Nauk SSSR, Ural Filial, **1966**(13), 57-63.

65. J.H.Haslam, U.S.Pat. 2,732,799, to E.I. du Pont de Nemours & Co. (1956).

66. I.Kraitzer, K.McTaggart and G.Winter, Paint Notes, **2**(9), 304-309 (1947).

67. J.R.Caldwell, U.S.Pat. 2,720,502, to Eastman Kodak Co. (1955).

68. A.Fradet and E.Marechal, Eur.Poly.J., **14**, 761-767 (1978)

69. (a) F.Pilati, P.Manaresi, B.Fortunato, A.Munari and V. Passalacqua, Polymer, **22**, 1566-1570 (1981); see the following related articles: (b) ibid., **22**, 799-802(1981); (c) F.Pilati, P.Manaresi, B.Fortunato, A.Munari and P.Monari, Polymer, **24**, 1479-1483 (1983); (d) F.Pilati, A.Munari and P.Manaresi, Polymer Comm., **25**, 187-189 (1984); (e) F.Pilati, A.Munari, P.Manaresi and V.Bonora, Polymer, **26**, 1745-1748 (1985); (f) B.Fortunato, P.Manaresi, A.Munari and F.Pilati, Polymer Commun., **27**, 29-31 (1986).

70. R.S.Barshtein and I.A.Sorokina, Kinetica & Catalysis, **20**(6), 1217-1221 (1980); translated from Kinetika i Kataliz (Akad.Nauk SSSR), **20**(6), 1472-1477 (1979).

71. M.I.Siling, V.V.Kuznetsov, Yu.E.Nosovskii, S.A.Osintseva and A.N.Kharrasova, Kinetics & Catalysis, **27**(1), 88-92 (1986); translated from Kinetika i Kataliz (Akad.Nauk SSSR), **27**(1), 98-102 (1986).

72. N.Yoshino and T.Yoshino, J.Soc.Chem.Ind.Japan, **74**(8), 1673-1676 (1971).

73. C.M.Fontana and R.J.Osborne, J.Poly.Sci., **47**(149), 522-525 (1960).

74. (a) C.M.Fontana, J.Poly.Sci.:Pt.A-1, **6**, 2343-2358(1968); (b) C.E.Holloway, J.Chem.Soc., Dalton, **1976**, 1050-1054.

75. K.Tomita and H.Ida, Polymer, **16**, 185-190 (1975).

76. K.C.Malhotra, N.Sharma and S.C.Chaudhry, Prac.Indian natn.Soc.Acad., **48A**(3), 244-247 (1982).

77. J.H.Haslam, U.S.Pat. 2,708,205, to E.I.du Pont de Nemours & Co. (1955).

78. C.Dijkgraaf and J.P.G.Rousseau, Spectrochimica Acta, **25A**, 1831-1839 (1969).

79. J.H.Haslam, "Chemistry and Uses of Titanium Organic Compounds", Advances in Chemistry Series, vol.23, ACS Applied Publications, Washington (1959), p.274.

80. D.C.Bradley, R.C.Mehrota, D.P.Gaur, "Metal Alkoxides", Academic Press, London (1978).

81. R.J.H.Clark, "The Chemistry of Titanium and Vanadium", Elsevier, N.Y. (1968), p.298.

82. M.Nowakowska, K.Czaja, M.Makowski, K.Marcinkiewicz and L.Maizner, Poly.Sci.USSR, **20**(10), 2523-2532 (1979); translated from Vysokomol.soyed., **A20**(10), 2243-2251

(1978).

83. K.Scczegot, M.Nowakowska and A.Kruger, Poly.Sci.USSR, **23**(11), 2766-2776 (1981); translated from Vysokomol. soyed., **A23**(11), 2551-2559 (1981).

84. U.Zucchini, I.Cuffiani and G.Pennini, Makromol.Chem., Rapid Comm., **5**, 567-571 (1984).

85. R.W.Taft, J.Amer.Chem.Soc., **74**, 3120-3128 (1952).

86. Yu.A.Sangalov, A.I.Il'Yasova and K.S.Minsker, Poly. Sci.USSR, **18**(4), 876-882 (1976); translated from Vysokomol.soyed., **A18**(4), 772-777 (1976).

87. Reference 51, p.14.

88. J.J.Melchiore and I.W.Mills, IEEE Trans.Elect.Insul., **EI-2**(3), 150-155 (1967).

89. D.A.Rogers, Jr., Proc.7th EIC, IEEE pub.no. 32C79 (1976), pp.100-102.

90. (a) L.Pauling, Proc.Roy.Soc., **A196**, 343-362 (1949); (b) L.Pauling, Proc.Intern.Congr.Pure and Applied Chem. (London), **11**, 249-257 (1947).

91. N.B.Hannay(ed.), "Treatise on Solid State Chemistry", vol.6B, Plenum Press, N.Y. (1976), p.60.

92. D.O.Hayward and B.M.W.Trapnell, "Chemisorption", Butterworths, London (1964).

93. G.C.Bond, "Catalysis by Metals", Academic Press, N.Y. (1962).

94. G.Turner, U.S.Pat. 3,161,710, to E.I. du Pont de Nemours & Co. (1964).

95. R.W.Stevenson, J.Poly.Sci.:Pt.A-1, **7**, 395-407 (1969).

96. R.W.Stevenson and H.R.Nettleton, J.Poly.Sci.:Pt.A-1, **6**, 889-900 (1968).

97. Clement, Hack & Co., Aust.Pat. 12,661,017, to Schenectady Chemicals, Inc. (1966).

98. P.E.Alexander, Proc.12th Elec.Insul.Conf., IEEE Pub., 114-118 (1979).

99. D.F.Loncrini, J.Poly.Sci.:Pt.A-1, **4**, 1532-1541 (1966).

100. C.L.Maros and J.DeAbajo, Angew.Makromol.Chem., **55**(808), 73-83 (1976).

101. S.Yamada and T.Ikeda, Fr.Demande FR 2,475,052 (Cl. C08G81/00), 07 Aug., 1981; JP Appl. 80/9,322,31 Jan. 1980; 22pp.

102. H.Ishida, S.T.Wellinghoff, E.Baer and J.L.Koenig, Macromolecules., **13**(4), 826-834 (1980).

103. D.O.Hummel, Farbe und Lack, **74**, 11-13 (1968).

104. P.Penczek, G.Cynkowska and E.Wardzińska, Farbe und Lack, **88**(1), 20-22 (1982).

105. G.Cynkowska, P.Penczek and E.Wardzińska, Polimery (Warsaw), **27**(6-7), 253-256 (1982).

106. M.I.Karyakina, Khim.Teknol.Khim., **1973**(1), 121-123.

107. (a) J.T.Keating, "Solutions of Polyesterimides", Aust. Patent Appl. AU-A-25 234/77, 18 May 1977 (USA, 22 Feb 1977), to Schenectady Chemicals, Inc.; (b) D.C.Shen, "Polyesterimides", Aust.Patent Appl. AU-A1-78 609/81, 17 Dec. 1981 (USA, 23 Dec. 1980), to Schenectady Chemicals, Inc.

108. M.F.Bray (magnet-wire enamelling consultant to Tycan Aust. P/L) private communication (1983).

109. M.H.Strunk, Jr., Proc.16th Elect.Insul.Conf., IEEE Pub., 305-308 (1983).

110. (a) J.D.Roberts, F.J.Weigert, J.I.Kroschwitz and H.J. Reich, J.Amer.Chem.Soc., **92**(5), 1338-1347 (1970); (b) C.E.Holloway, J.Chem.Soc., Dalton, **1976**, 1050-1054.

111. F.Bloch, Phys.Rev., **70**, 460 (1946).

112. N.Bloembergen, E.M.Purcell, and R.V.Pound, Phys.Rev., **73**, 679-712 (1948).

113. H.Günther, "NMR Spectroscopy: An Introduction", p.360, translated by R.W.Gleason, John Wiley & Sons (1980).

114. J.Schaefer and E.O.Stejskal, "Topics in C-13 NMR Spectroscopy", G.C.Levy(editor), Wiley-Interscience, N.Y. (1979), pp.284-324.

115. J.R.Havens and J.L.Koenig, Appl.Spectrosc., **37**(3), 226-249 (1983).

116. D.J.O'Donnell, "NMR and Macromolecules", ACS Symposium Series, no.247, Chapt. 2, J.C.Randall(editor), American Chemical Society, Washington (1984).

117. N.Bloembergen and T.J.Rowland, Acta Metall., **1**, 731-746 (1953).

118. I.J.Lowe, Phys.Rev.Lett., **2**(7), 285-287 (1959).

119. E.R.Andrew, A.Bradbury, and R.G.Eades, Nature, **182**, 1659 (1958).

120. E.R.Andrew, Prog.Nucl.Magn.Reson.Specrosc., **8**, 1 (1971).

121. J.Schaefer, E.O.Stejskal, and R.Buchdahl, Macromolecules, **8**(3), 291-296 (1975).

122. E.R.Andrew and R.G.Eades, Proc.Roy.Soc.Lond., **A216**, 398-412 (1953).

123. E.R.Andrew, S.Clough, L.F.Farnell, T.D.Gledhill, and I.Roberts, Phys.Letters, **21**(5), 505-506 (1966).

124. A.Pines, M.G.Gibby, and J.S.Waugh, J.Chem.Phys., **59**, 569-590 (1973).

125. S.R.Hartmann and E.L.Hahn, Phys.Rev., **128**, 2042-2053 (1962).

126. J.C.Randall and E.T.Hsieh, "Carbon 13 NMR in Polymer Qualitative Analysis", ACS Symposium Series, no.247, Chapt. 9, ACS, Washington (1984).

127. S.Kaplan, H.A.Resing, and J.S.Waugh, J.Chem.Phys., **59**, 5861-5867 (1973).

128. J.Urbina and J.S.Waugh, Ann.N.Y.Acad.Sci., **222**, 733-739 (1973).

129. J.Urbina and J.S.Waugh, Proc.Natl.Acad.Sci., U.S.A., **71**(12), 5062-5067 (1974).

130. A.Pines and J.J.Chang, Phys.Rev., **A10**(3), 946-949 (1974).

131. W.T.Dixon, J.Schaefer, M.D.Sefcik, E.O.Stejskal, and R.A.McKay, J.Mag.Res., **49**, 341-345 (1982).

132. J.W.Beams, Rev.Sci.Instrum., **1**, 667-671 (1930).

133. R.K.Harris, "Nuclear Magnetic Resonance Spectroscopy: A Physicochemical View", Longman Scientific and Technical, UK (1986), p.159.

134. H.M.McNair, "Basic Gas Chromatography", Varian Aerograph, Walnut Creek, Calif., U.S.A. (1971).

135. D.F.Loncrini, J.Polym.Sci.: Pt.A-1, **4**, 1531-1541 (1966).

136. Reference 3, chapter III.

137. Reference 3, p.91.

138. A.Sadle, US Pat.3,660,392(Cl.260,248NS;C07d), 02 May 1972, Appl.89067, 12 Nov. 1970; 2pp.

139. N.Sawa and N.Kano, Japan Kokai 7,873,574 (Cl.C07D251/34), 30 June 1978, Appl. 76/149.274, 11 Dec.1976; 4pp.

140. V.D.Vorotyntseva, Ts.N.Roginskaya, V.P.Moleva, T.N. Tikhonova, A.I.Finkelstein, and V.I.Zagranichnyi, Zh.Prikl.Spektrosk., **17**(4), 661-665 (1972).

141. T.C.Frazier, E.D.Little, and B.E.Lloyd, J.Org.Chem., **25**, 1944-1946 (1960).

142. C.Shimasaki, T.Nakayama, and Y.Iino, Nippon Kagaku

Kaishi, **3**, 375-382 (1979).

143. G.C.Pimentel and A.I.McClellan,"The Hydrogen Bond", W.H.Freeman and Co., San Francisco (1960).

144. C.J.Pouchert, "The Aldrich Library of Infrared Spectra", 2nd edition, Aldrich Chem. Co., Inc. (1975).

145. C.N.R.Rao, "Chemical Application of Infrared Spectroscopy", 225-236, Academic Press, London (1963).

146. M.Windholz(editor), "The Merck Index", Merck & Co., Inc., N.J., U.S.A. (1983).

147. D.Bruck and M.Rabinovitz, Tetrahed.Lett., **47**, 4121-4124 (1977).

148. G.C.Levy, R.L.Lichter, and G.L.Nelson, "Carbon-13 Nuclear Magnetic Resonance Spectroscopy", 2nd edition, Wiley-Interscience, N.Y. (1980).

149. J.R.Havens, I.Hatsuo, and J.L.Koenig, Macromolecules, **14**(5), 1327-1333 (1981).

150. P.A.Martinez, V.Cadiz, A.Serra, and A.Mantecon, Die Angew.Makro.Chem., **136**, 2204, 159-175 (1985).

151. G.M.Bower and L.W.Frost, J.Polym.Sci.,Pt.A, **1**(10), 3135-3150 (1963).

152. S.Das, S.Maiti, and M.Maiti, J.Macromol.Sci.-Chem., **A17**(8), 1177-1192 (1982).

153. C.L.Maros and J.DeAbajo, Die Angew.Makro.Chem., **55** (808), 73-83 (1976).

154. D.M.White, T.Takekoshi, F.J.Williams, H.M.Relles, P.E.Donahue, H.J.Klopfer, G.R.Loucks, J.S.Manello, R.O.Matthews, and R.W.Schluenz, J.Poly.Sci., Polym. Chem.Ed., **19**, 1635-1658 (1981).

155. Pople and D.L.Beveridge, "Approximate Molecular Orbital Theory", McGraw-Hill Series in Advanced Chemistry (1970), pp.158 & 163.

156. C.C.J.Roothaan, Rev.Modern Phys., **23**, 69-89 (1951).

157. G.Serboli, Brown Boveri Rev., **49**(11/12), 576-590 (1962).

158. A.Miyake, J.Poly.Sci., **38**, 479-495 (1959).

159. A.Vogel, "Textbook of Practical Organic Chemistry", 4th edition, Longman (1978), p.844.

160. V.P.Kuceski, US Pat. 4,020,099(Cl.260-475PN; C07C69/80), 26 Apr.1977, Appl. 269,120, 10 Oct.1972; 8pp.

161. J.H.Haslam, Symposium on Metal-Organic Compounds, 131st. National Meeting of the Amer.Chem.Soc., Miami, Florida, April (1957). ACS Applied Publications (1959).

162. H.Kriegsmann and K.Licht, Z.Elektrochem., **62**, 1163-1174 (1958).

163. M.J.Frazer and Z.Goffer, J.inorg.nucl.Chem., **28**, 2410 (1966).

164. W.M.Alvino and L.W.Frost, J.Poly.Sci.:Pt.A-1, **9**, 2209-2224 (1971).

165. A.Ray, Y.V.Rao, V.K.Bhattacharya and S.Maiti, Polymer J., **15**(2), 169-173 (1983).

166. K.Ohm, Ger.Offen. 2,747,456(Cl.C09D5/25), 26 Apr. 1979, Appl. 22 Oct. 1977; 11pp.

167. K.Kurita, H.Itoh and Y.Iwakura, J.Poly.Sci., Polym. Chem.Ed., **16**, 779-789 (1978).

168. S.E.Sroog, A.L.Endrey, S.V.Abramo, C.E.Berr, W.M. Edwards and K.L.Oliver, J.Poly.Sci.:Pt.A, **3**, 1373-1390 (1965).

169. R.T.Morrison and R.N.Boyd, "Organic Chemistry", 3rd edition, Allyn and Bacon, Inc., Boston (1973), p.554.

170. Reference 113, p.21.

171. ibid., pp.90 and 91.

172. ibid., p.227.

173. A.E.Derome, "Modern NMR Techniques for Chemistry Research", Pergamon Press, Oxford (1987), chapters 8 and 9.

174. V.V.Shevchenko, Prepr.-Mezhdunar.Simp.Khim. Voloknam (2nd), **1**, 201-203 (1977).

175. R.M.Lum, J.Poly.Sci.:Poly.Chem.Ed., **17**, 203-213 (1979).

176. V.Passalacqua, F.Pilati, V.Zambroni, B.Fortunato and P.Manaresi, Polymer, **17**, 1044-1048 (1976).

177. J.Devaux, P.Goddard and J.P.Mercier, Makromol.Chem., **179**, 2201-2209 (1978).

178. "Brüker Carbon-13 Data Book", vol.1, copyright to Brüker Physik, Switzerland (1979); compiler uncredited.

179. M.F.Fukushima, T.Hoshino and A.Kondo, Proc.Inst. Electrical and Electronic Engineers, 154-158 (1981).

180. S.G.Entelis and R.P.Tiger, "Reaction Kinetics in the Liquid Phase", translated by R.Kondor, J.Wiley & Sons, N.Y. (1976).

181. A.Skrabal and E.Singer, Monatsh., **41**, 339-400 (1920).

182. Reference 2, chapter III, p.103.

183. E.L.McCaffery, J.Chem.Ed., **46**(1), 59-60 (1969).

184. (a) R.C.Fay and A.F.Lindmark, J.Amer.Chem.Soc., **105**(8), 2118-2127 (1983); see also the following related articles: (b) D.C.Bradley and C.E.Holloway, J.Chem.Soc., A **1969**(2), 282-285; (c) J.F.Harrod and K.Taylor, J.Chem. Soc., Chem.Commun., **1971**(13), 696-697; (d) D.G.Bickley and N.Serpone, Inorg.Chim. Acta, **43**(2), 185-189 (1980); (e) G.D.Byrd, R.C.Burnier and B.S.Freiser, J.Amer.Chem. Soc., **104**(13), 3565-3569 (1982).

185. P.Sykes, "A Guidebook to Mechanism in Organic Chemistry", 5th edition (3rd impression), Longman Inc., N.Y. (1983), p.97.

186. P.Schuster, G.Zundel and C.Sandorfy(editors), "The Hydrogen Bond. Recent Developments in Theory and Experiments", North-Holland Pub. Co., Amsterdam (1976).

187. S.N.Vinogradov and R.H.Linnell, "Hydrogen Bonding", Van Nostrand Reinhold Co., N.Y. (1971).

188. Reference 169, p.689.

189. A.Miyake, Bull.Chem.Soc.Japan, **30**, 361-363 (1957).

190. Reference 143, p.172.

191. ibid., p.83.

192. C.M.Huggins, G.C.Pimentel and J.N.Shoolery, J.Phys. Chem., **60**, 1311-1314 (1956).

193. Reference 143, p.146.

194. Reference 113, p.91.

195. ibid., p.89; graph from H.J.Friedrich, Z.Naturforsch., **20**b(11), 1021-1032 (1965).

196. D.P.Eyman and R.S.Drago, J.Amer.Chem.Soc., **88**(8), 1617-1620 (1966).

197. P.T.Narisimhan and M.T.Rogers, J.Phys.Chem., **63**, 1388-1394 (1959).

198. H.J.M.Bowen, J.Donohue, D.G.Jenkin, O.Kennard, P.J. Wheatley and D.H.Whiffen, "Tables of Interatomic Distances and Configuration in Molecules and Ions", The Chemical Society, London (1958).

199. A.Miyake, J.Poly.Sci., **38**, 479-495 (1959).

200. L.M.Jackman and J.C.Trewella, J.Amer.Chem.Soc., **98**(18), 5713-5714 (1976).

201. Reference 143, pp.160-162.

202. O.A.Osipov, Zhur.Fiz.Khim., **31**, 1542-1546 (1957).

203. V.I.Minkin, O.A.Osipov and Y.A.Zhdanov, "Dipole Moments in Organic Chemistry", translated by B.J.Hazzard, Plen-

um Press, N.Y. (1970).

204. C.P.Smyth, "Dielectric Behaviour and Structure", McGraw-Hill, Inc., N.Y. (1955).

205. R.J.W.LeFevre, "Dipole Moments", 3rd edition, Methuen and Co., Ltd., London (1953).

206. J.W.Smith, "Electric Dipole Moments", Butterworths Sci. Pub., London (1955).

207. A.Flamini, D.J.Cole-Hamilton and G.Wilkinson, J.Chem. Soc., Dalton, **1978**, 454-459.

208. C.Dijkgraaf and J.P.Rousseau, Spectrochimica Acta, **24A**, 1213-1217 (1968).

209. A.K.Bose, P.R.Srinivasan and G.Trainor, J.Amer.Chem. Soc., **96**(11), 3670-3671 (1974).

210. O.M.O.Habib and J.Malek, Collect.Czech.Chem.Commun., **41**(9), 2543-2555 (1976).

211. L.Nondek and J.Malek, Makromol.Chem., **178**(8), 2211-2221 (1977).

212. L.H.Horsley(ed.), "Azeotropic Data-III", ACS Pub., Washington (1973).

213. M.Brookhart and M.L.H.Green, J.Organomet.Chem., **250**, 395-408 (1983).

214. Reference 198, pp.M214 and M108s.

215. G.C.Levy, R.L.Lichter and G.L.Nelson, "Carbon-13 Nuclear Magnetic Resonance Spectroscopy", 2nd edition, J. Wiley & Sons, N.Y. (1980), chapter 4.0.

216. J.E.Pound (Technical Manager, Schenectady Chemicals Australia Pty.Ltd.), private communication (1989).